

~~UNCLASSIFIED~~

AD **242 586**

*Reproduced  
by the*

ARMED SERVICES TECHNICAL INFORMATION AGENCY  
ARLINGTON HALL STATION  
ARLINGTON 12, VIRGINIA



---

**UNCLASSIFIED**

NOTICE: When government or other drawings, specifications or other data are used for any purpose other than in connection with a definitely related government procurement operation, the U. S. Government thereby incurs no responsibility, nor any obligation whatsoever; and the fact that the Government may have formulated, furnished, or in any way supplied the said drawings, specifications, or other data is not to be regarded by implication or otherwise as in any manner licensing the holder or any other person or corporation, or conveying any rights or permission to manufacture, use or sell any patented invention that may in any way be related thereto.

third  
symposium on  
**DETONATION**

**JAMES FORRESTAL  
RESEARCH CENTER  
PRINCETON UNIVERSITY  
SEPTEMBER 26-28, 1960**

cosponsored by

**NAVAL ORDNANCE LABORATORY  
WHITE OAK  
and  
OFFICE OF NAVAL RESEARCH**



**Office of Naval Research • Department of the Navy**

preprints

586  
242  
ASTIA  
AS AD No

ONR Symposium Report  
ACR-52  
Vol. 2

**third  
symposium on  
DETONATION**

**JAMES FORRESTAL  
RESEARCH CENTER  
PRINCETON UNIVERSITY  
SEPTEMBER 26-28, 1960**

**sponsored by**

**NAVAL ORDNANCE LABORATORY  
WHITE OAK**

**and**

**OFFICE OF NAVAL RESEARCH**

**Office of Naval Research • Department of the Navy**



# CONTENTS

## VOLUME 2

The Detonation Velocity of Pressed TNT . . . . .	327
M. J. Urizar, E. James, Jr., and L. C. Smith	
Measurements of Detonation, Shock, and Impact Pressures . .	357
R. T. Keyes and W. O. Ursenbach	
Low Pressure Points on the Isentropes of Several High Explosives . . . . .	386
W. E. Deal	
Strong Shocks in Porous Media . . . . .	396
J. L. Austing, H. S. Napadensky, R. H. Stresau, and J. Savitt	
The Behavior of Explosives at Impulsively Induced High Rates of Strain . . . . .	420
H. S. Napadensky, R. H. Stresau, and J. Savitt	
Initiation and Growth of Detonation in Liquid Explosives . . .	436
F. C. Gibson, C. R. Summers, C. M. Mason, and R. W. Van Delah	
Initiation Characteristics of Mildly Confined, Bubble-Free Nitroglycerin . . . . .	455
C. H. Winning and E. I. du Pont	
Shock Initiation of Detonation in Liquid Explosives . . . . .	469
A. W. Campbell, W. C. Davis, and J. R. Travis	
Shock Initiation of Solid Explosives . . . . .	499
A. W. Campbell, W. C. Davis, J. B. Ramsay, and J. R. Travis	
Shock Induced Sympathetic Detonation in Solid Explosive Charges. . . . .	520
M. Sultanoff, V. M. Boyle, and J. Paszek	
Growth of Detonation from an Initiating Shock . . . . .	534
J. W. Enig	

Initiation of a Low-Density PETN pressing by a Plane Shock Wave . . . . .	562
G. E. Seay and L. B. Seely, Jr.	
The Transition from Shock Wave to Detonation in 60/40 RDX/TNT . . . . .	574
R. L. Kendrew and E. G. Whitbread	
Determination of the Shock Pressure Required to Initiate Detonation of an Acceptor in the Shock Sensitivity Test . . .	584
I. Jaffe, R. Beauregard, and A. Amster	
A Computational Treatment of the Transition from Deflagration to Detonation in Solids. . . . .	606
C. T. Zovko and A. Macek	
A Method for Determination of Detonability of Propellants and Explosives . . . . .	635
S. Wachtell and C. E. McKnight	
Author Index . . . . .	659

## THE DETONATION VELOCITY OF PRESSED TNT\*

M. J. Urizar, E. James, Jr., and L. C. Smith  
Los Alamos Scientific Laboratory  
University of California  
Los Alamos, New Mexico

### ABSTRACT

The detonation velocity of pressed TNT has been determined as a function of charge diameter at each of a series of loading densities. Current theories of the diameter effect are discussed and used to compute infinite diameter detonation velocities ( $D_\infty$ ) and detonation reaction zone lengths from the experimental data. The results for the velocity-density dependence may be summarized as follows:

$$\begin{aligned} D_\infty &= 1872.7 + 3187.2 \rho & (0.9 \leq \rho \leq 1.5342 \text{ gm/cc}) \\ D_\infty &= 6762.5 + 3187.2 (\rho - 1.5342) - 25,102 (\rho - 1.5342)^2 \\ &\quad + 115,056 (\rho - 1.5342)^3 & (1.5342 \leq \rho \leq 1.636 \text{ gm/cc}) \end{aligned}$$

The reaction zone lengths computed from the data are a decreasing function of the charge density and are in good agreement with predictions based on the grain-burning model of the reaction zone.

### I. INTRODUCTION

The velocity of detonation is a fundamental and readily measured characteristic property of a high explosive, and it has received considerable study, both experimental and theoretical. Phenomenologically, the detonation velocity of a given explosive depends most importantly on the loading density, the size, and the amount and type of lateral confinement of the charge. Theoretical studies of the detonation process have shown that the density dependence has a thermodynamic origin -- specifically, in the nonideality of the equation of state of the detonation products at the temperatures

---

\* This work was performed under the auspices of the U. S. Atomic Energy Commission.

and pressures involved. The remaining two factors have similarly been shown to be related to the kinetics of the reaction which converts the unburned explosive to its detonation products.

The detonation process is most simply studied theoretically on the basis of an idealized, one-dimensional hydrodynamic model. The detonation properties deduced from such a model are independent of both the size and confinement of the system (of its kinetics, in fact), and the detonation velocity, in particular, is customarily referred to as the infinite diameter, plane-wave velocity. It is of importance in such studies to have available accurate experimental data on the infinite diameter velocities of various explosives, and in this paper we present the results of an experimental program whose principal objective was to obtain such data on pressed TNT over the accessible range of loading densities.

It is obvious that to achieve this objective requires some sort of an extrapolation from finite charge data. Our work is based on the assumption that the detonation velocity of a finite charge is related to the infinite diameter velocity by the equation (1)

$$D = D_{\infty} \left( 1 - \frac{a}{2R} \right) . \quad (1)$$

Here  $D$  is the detonation velocity of a cylindrical charge of radius  $R$ ,  $a$  is assumed independent of  $R$  (but a function of the explosive, loading density, and confinement), and  $D_{\infty}$ , as the notation suggests, is the infinite diameter velocity. This equation accurately represents our results over the range of charge diameters included in this study. Other work done at this Laboratory, both by others and by us<sup>(2)</sup>, indicates that the equation does not necessarily hold in the region of very small charge diameters, and this has recently been verified in the case of TNT, in particular, in a contemporary study of this explosive by Stesik and Akimova.<sup>(3)</sup>

The procedure, then, was to determine the detonation velocity as a function of charge diameter at each of a series of loading densities. The corresponding values of  $D_{\infty}$  are then estimated from least square fits of equation (1) to the experimental data. It is obvious that this procedure simultaneously provides estimates of the quantity  $a$  under various conditions, and in the discussion the significance of this quantity is discussed in terms of current theories of the diameter effect.

## II. EXPERIMENTAL

### A. Explosive

All the data reported here were obtained with a single lot of commercial TNT (2,4,6-trinitrotoluene) manufactured in August 1944 by the Atlas Powder Company. Its melting point, as determined from a cooling curve, was 80.55°C, and its purity was estimated as 99.6 mole percent. The principal impurities are presumed to be the other

TNT isomers and the dinitrotoluenes, as these are usually found in the typical commercial product. The results of a sieve analysis of the granular material, before pressing, are given in Table I.

TABLE I  
TNT PARTICLE SIZE ANALYSIS

<u>U.S. Std Sieve No.</u>	<u>Sieve Opening (microns)</u>	<u>Cumulative (% Retained on)</u>	<u>Differential (%)</u>
40	420	0.4	
50	300	1.6	1.2
70	210	11.2	9.6
100	149	60.0	48.8
120	125	73.8	13.8
140	105	88.6	14.8
200	74	96.4	7.8
230	62	97.2	0.8
325	44	98.4	1.2

#### B. Charge Preparation

All the low-density charges (below 1.4 gm/cc) were prepared and fired in 0.2" wall brass tubes, primarily to contain, and prevent damage to, the more fragile low-density pressings, but these tubes also provided confinement in the detonation velocity measurements, reducing the magnitude of the diameter effect and thereby permitting a more accurate estimate of  $D_{\infty}$ . Unpublished measurements made at this Laboratory indicate that the limiting effectiveness of brass in reducing the diameter effect in Composition B is reached at a wall thickness of less than 0.1",<sup>(4)</sup> while, for 60/40 Amatol, Copp and Ubbelohde<sup>(5)</sup> found that limiting effectiveness of steel was reached with a wall thickness of less than 0.2". Confinement by 0.2" of brass is thought to be more than adequate for pressed TNT, and the use of thicker tubes in any event would have created difficulties in obtaining accurate weights on the loaded tubes with the balances which were available.

It is important to note in this connection that the shock velocity in the confining medium must not exceed the detonation velocity of the explosive, as the explosive will otherwise be compressed at the wall by the shock in the tube, and the velocity obtained will not be that corresponding to the initial charge density. Roughly speaking, brass is a satisfactory confining medium for velocity measurements down to about 4000 m/sec.

Most of the data reported here on high-density TNT were obtained with unconfined charges, although in a few cases confined high-density charges were fired to verify that the value of  $D_{\infty}$  obtained was independent of the technique used.

The brass tubes were prepared and measured by professional machinists, starting with extruded tubing of convenient size. The nominal inside diameters and lengths of the finished tubes were as follows:

<u>ID (in.)</u>	<u>Length (in.)</u>
0.7683	3.000
1.0250	3.000
1.5385	3.000
3.077	6.000

A 0.5" wide by 0.005" deep notch was milled in one end of each tube to provide space for the pin foils in the shot assembly.

Each tube was carefully weighed on an analytical balance of the appropriate capacity before and after loading to obtain the total weight of explosive in the finished charge. The tubes were loaded to the desired density, one inch at a time, by pressing the explosive directly into them. For the last increment or two, an auxiliary loading sleeve which meshed with the notch on the upper end of the tube was used to contain the loose explosive and to serve as a guide for the punch. The loading was done in increments to minimize density variations along the length of the charge. Radial density variations were controlled by carefully distributing the loose powder in the tube before pressing the increment. The desired finished height of each loading increment was obtained by using punches of different lengths, together with spacers of the appropriate heights inserted between the upper flange of the punch and the end of the tube or loading sleeve.

During the pressing, the bottom end of the tube rested on a flat Lucite plate, and at this end the face of the charge after pressing was flat and flush with the end of the tube to within 0.001" or better. At the top the situation was somewhat different. In the first place, to provide space for the pin foils without introducing gaps between successive tubes in the shot assembly, the finished height of the explosive was held at  $+0.000$ " relative to the end of the tube. In addition, in the case  $-0.003$ " of the larger diameter, medium-density charges, there was a tendency for this end of the charge to bow out as a result of reexpansion. This could be corrected by placing a 1/2" thick Lucite plate on the end of the charge and pressing on its center with an undersized punch. With some experience this could be done in such a way that after reexpansion had occurred, the charge was flat and of the desired length.

The high-density unconfined charges were made by pressing 6" diameter by 4" high stock pieces in a locally available die, and machining from these cylindrical charges of the desired sizes. The same diameters and lengths were used as before in most cases, except that the 6" long pieces were made up of two 3" long cylinders. Only those parts of the stock pieces were used which were reasonably

uniform in density. The finished cylinders were quite rigid and could be measured and handled without difficulty.

The high-density confined charges were prepared in the same way, except that after machining, the cylinders of explosive were cooled slightly and slipped into the confining tubes. Upon rewarming to room temperature, the explosive expanded, giving a snug fit in the tube.

### C. Velocity Measurements

The detonation velocity measurements were made by a group working under the supervision of A. W. Campbell, using a technique which has already been described in detail elsewhere.<sup>(6)</sup> Only a few special features of the shot assembly, as it evolved after considerable experimentation, will be described here.

Each shot was made up of approximately nine increments, with transit-time pin foils inserted at the end of each increment (see Fig. 6 of ref. 6). Thus the 3" diameter charges were (generally) 54" long, the others 27" long. The charges were initiated by means of a detonator, a small tetryl pellet, and a 1" thick pad of Composition B. With this type of initiation the detonation velocity of the charge had become stable after it had traveled through two, or at most three, of the nine increments, so that six or seven data points were normally obtained from each shot. The whole assembly was held together by clamps to insure good contact between successive components of the train. In the case of small-diameter unconfined charges this must be done carefully, for if excessive clamping pressure is used, the charge will be shortened significantly and the velocity obtained will be too high. It is necessary to check the total length of the charge, after clamping, against the sum of the lengths of the individual increments to insure that the proper amount of pressure is being applied.

After each shot had been assembled, it was placed in an insulated box and its temperature was adjusted to  $75 \pm 5^\circ\text{F}$  before it was fired.

### D. Sources of Error

The velocity measuring technique described above and in ref. 6 has been developed to such an extent that charge quality has become the determining factor in the over-all precision of the data. Accordingly, our discussion here will be largely devoted to the problem of measuring charge density, and to the control and effects of density variations within the charge.

From the data presented later it can be seen that an error of 0.001 gm/cc in determining the density of a charge corresponds to an error of about 3 m/sec in the detonation velocity. It is therefore essential that the charge density be determined with considerable accuracy. In our experiments this problem was most serious in the

case of the smallest diameter charges. Therefore only these will be discussed, and it will be left as understood that the errors are proportionately smaller for the larger charges.

The densities of all confined charges prepared by pressing the explosive directly into the confining tubes were derived from measurements of the inside diameters and lengths of the tubes, and from their weights before and after loading. Our best estimates for the uncertainties in these quantities are as follows:

<u>Measurement</u>	<u>Uncertainty</u>
Weight of explosive (corrected for buoyancy)	< 1/10,000
Length	2/10,000
Diameter	7/10,000

It follows that the maximum uncertainty in the density is somewhat less than 0.003 gm/cc. We believe that the errors in these measurements are primarily random, and hence their effect would be expected to appear as a loss of precision rather than accuracy.

It will be recalled that in pressing the final increment into the tube, the finished surface of the explosive was allowed to be as much as 0.003" below the end of the tube. The reason the length of the tube, rather than the actual height of the explosive, is the dimension used in the volume calculations is that compensating effects are present. If the actual height of explosive in a particular increment were 2.997" instead of 3.000", the actual density of that increment would be higher than our recorded density by one part in a thousand. As a result, the transit time through the column of explosive would be 0.02 - 0.03  $\mu$ sec less than it would be if the actual height of explosive were 3.000". However, we estimate that this is just about the time required for the product gases to move across the 0.003" gap and initiate the next increment, so that the two effects should cancel very closely. Since the size of the gap between various increments of the charge varied from zero to three mils, the over-all error in the measurements from this source is probably negligible. The variation in the length of the gap, and in the position of the pin foils within the gaps, will contribute slightly to the standard deviation of the data.

The densities of the high-density charges were determined directly from measurements of the weights and dimensions of the pieces and were corrected for buoyancy. The reported densities are estimated to be accurate to  $\pm 0.002$  gm/cc for the 3/4" diameter charges. The water displacement method was used to check the results in some cases, and the densities determined by the two methods of measurement agreed to within the assigned experimental error.



Density variations within the charge also are a problem in precise detonation velocity measurements on pressed explosives, and two types are recognizable in charges such as we are describing here. The first, which we refer to as axial, is a periodic variation in density along the length of the charge which is an unavoidable consequence of the incremental loading procedure. As each loading increment is pressed, the material next to the punch is compressed to a higher density than the material at the bottom of the increment. The result is a sawtooth variation in density along the charge whose wavelength and amplitude are direct functions of the length of the loading increment (one inch in our work). The shorter the increment, the lower the amplitude, and, of course, the shorter the wavelength. The second type, referred to as radial, is a nonuniformity in density in any plane perpendicular to the axis of the charge. Careful distribution of the powder in the tube or die before pressing will decrease the radial density variations, but it will not eliminate them entirely unless the bulk explosive is very uniform. Radial density variations become worse when very short increments are pressed, since a slight unevenness in the distribution or packing of the loose powder will produce a proportionately larger variation in density.

We attempted to evaluate the effect of axial density variations by deliberately introducing large variations in an experimental charge. First, a 3" ID x 4" OD x 6" long polystyrene tube was loaded in one-inch increments. The increments were weighed out to give alternating densities of 1.35 and 1.25 gm/cc. After the tube was loaded, the densities of the successive increments were determined by X-ray absorption technique.<sup>(7)</sup> The results were as follows:

<u>Increment</u>	<u>Intended Density (gm/cc)</u>	<u>Measured Density (gm/cc)</u>
Top	1.25	1.25
5	1.35	1.29
4	1.25	1.30
3	1.35	1.31
2	1.25	1.31
Bottom	1.35	1.36

The precision of the X-ray method used is about 1% in density, and it is obvious that only the top and bottom increments are significantly different from the average. Nevertheless, this loading procedure would be expected to exaggerate whatever axial density spreads are present in our rate sticks, so a 3" diameter rate stick was prepared in brass tubes by this method, and a second was prepared at the same time using our usual loading procedure. The velocities of the two charges were measured with the following results:

<u>Loading Method</u>	<u>Ave Over-all Density(gm/cc)</u>	<u>No. Velocity Increments</u>	<u>Average Velocity</u>	<u><math>\pm L_{95}</math></u>
Nonuniform	1.300	7	5987.9	6.1
Uniform	1.300	7	5985.3	6.4

Our conclusion is that axial density fluctuations of this wavelength are not a limiting factor in the over-all precision of our results.

This is not entirely unexpected, since the detonation wave does not respond instantaneously to changes in local conditions,<sup>(1)</sup> and hence there is a significant damping out of the effects of density variations providing these are commensurable in size with the build-up (or build-down) distance of the detonation wave. This is true both for axial and radial inhomogeneities in density.

We have also attempted to use the X-ray absorption method to estimate the magnitude of the radial density variations in a single increment. These appear to amount to about  $\pm 0.010$  gm/cc in typical charges. It is important to avoid systematic radial density variations. For example, if the loose explosive is simply poured into the tube in such a manner as to assume a cone shape, and the increment is then pressed without redistributing the explosive, the central core of the whole charge will be above average density, and this high-density core will control the rate of propagation of the wave. In other words, the observed velocity will correspond to the density of the core, rather than to the average density of the charge. We have verified this statement experimentally with other explosives, but the results are not sufficiently novel to merit detailed reporting here.

Density variations as large as  $0.010$  gm/cc are known to be present in the lower density pieces cut from the  $6'' \times 4''$  stock charges. An attempt was made to minimize systematic errors from this source by cutting the rate sticks from selected regions of the stock charge.

At densities near crystal density, such problems as internal density spreads, errors in the measurement of over-all density, and gaps in the shot assembly, are eliminated or greatly reduced in magnitude, and generally somewhat better statistics were obtained in the velocity measurements on the highest density charges.

### III. DATA AND ANALYSIS

The rate stick data were analyzed by the difference method, which has been shown to be the correct procedure for cumulative straight-line data such as we obtain.<sup>(8)</sup> After discarding the first two or three observations (representing the booster section), we compute the detonation velocities over the remaining individual increments, and then obtain the average velocity, and its variance and 95% confidence limit ( $\pm L_{95}$ ), in the usual way.

In some cases this procedure had to be modified to correct for nontrivial variations in the densities of the individual increments within the charge. The correction is made by adjusting the incremental velocities by an amount

$$(\bar{\rho} - \rho) \left( \frac{\partial D}{\partial \rho} \right)_{\bar{\rho}}$$

where  $\bar{\rho}$  is the average density of the rate section,  $\rho$  is the density of the increment in question, and  $\left( \frac{\partial D}{\partial \rho} \right)_{\bar{\rho}}$  is the slope of the velocity-density curve at  $\bar{\rho}$ . For reasons already mentioned, this probably represents an over-correction, but it is usually small, and in any event its only effect is on the variance and confidence limit.

One additional adjustment is usually necessary before proceeding to the next step in the analysis. In fitting equation (1) we require that the velocities corresponding to the various diameters be obtained at a common density. In practice this could not always be achieved, and hence in each diameter series it was usually necessary to adjust one or more of the velocities, using the same correction factor as before. The corrections in this case can be made with considerable confidence.

The data analysis of a typical shot is displayed in Table II. A summary of the charge data and final velocities is given in Table III. We attach little significance to the individual  $\pm L_{95}$ 's appearing in this table since the sampling errors in estimating such a statistic in a single experiment are large. They do provide an indication of the dispersion of the incremental velocities observed in the various shots. However, in making the least squares fits to equation (1) we have elected to treat each shot as a single independent observation of weight unity, and no further use is made of these particular  $\pm L_{95}$ 's in the subsequent discussion.

The remainder of the analysis is carried out in two steps, the first of which involves obtaining the least squares fits of equation (1) to the experimental data. This is straightforward, and the results are summarized in Table IV. From each fit we obtain an independent estimate of the variance of the underlying population,  $s^2$ . These were tested and found to be homogeneous by Bartlett's test, (9)<sup>1</sup>, implying that the true variance,  $\sigma^2$ , is independent of  $\rho$  (the test also was made on the confined and unconfined shots separately, with the same result). The variances were therefore pooled and a value of 19.1, with 42 degrees of freedom, was obtained.

The second step is somewhat more complicated and involves obtaining a least squares fit of a suitable equation to the velocity-density data ( $D_{\infty}$  vs  $\rho$ ). Preliminary computation indicated that, with considerable accuracy,  $D_{\infty}$  is a linear function of  $\rho$  up to a density of about 1.53 gm/cc, but that at higher densities a polynomial fit would be required. The fitting procedure finally adopted was as

TABLE II - TYPICAL SHOT DATA ANALYSIS  
 Nominal Density 1.5127 gm/cc - Diameter 2.603 cm - Unconfined

Increment No.	Uncorrected Density (gm/cc)	Increment Length (cm)	Average Incremental Transit Time (μsec)	Uncorrected Det Vel (m/sec)	$\bar{\rho} - \rho$ (gm/cc)	$\left(\frac{\partial D}{\partial \rho}\right) (\bar{\rho} - \rho)$ (m/sec)	Corrected Det Vel (m/sec)
1	1.516	7.6225	(Booster)				
2	1.498	7.6200	(Booster)				
3	1.515	7.6200	11.4579	6650.4	-0.009	-28.5	6621.9
4	1.502	7.6200	11.5204	6614.3	0.004	12.7	6627.0
5	1.504	7.6197	11.5129	6618.4	0.002	6.3	6624.7
6	1.506	7.6208	11.5031	6625.0	0.000	0.0	6625.0
7	1.505	7.6200	11.5054	6623.0	0.001	3.2	6626.2
8	1.505	7.5692	11.4305	6621.9	0.001	3.2	6625.1
9	1.505	7.6200	11.4997	6626.2	0.001	3.2	6629.4
Averages (Incr. 3 - 9)	1.5069 <sup>a</sup>			6625.6			6625.6
Variance				135.9			5.3
Std Dev				11.6			2.3
95% Conf. Interval				+ 10.7			+ 2.1
Adjustment of D to Nominal Density	1.5127				0.0058	18.4	6644.0

<sup>a</sup> After buoyancy correction.

TABLE III - SUMMARY OF SHOT DATA

<u>Confined Charges</u>						
Density (gm/cc)	Dia (cm)	Length of Increment (cm)	No. of Increments Booster Section	Rate Section	D(m/sec)	$\pm L_{95}$
0.9009	1.951	7.620	3	6	4587.2	3.2
0.9009	2.603	7.620	2	7	4632.3	6.8
0.9009	3.906	7.620	2	7	4663.6	5.7
0.9009	7.816	15.240	2	7	4713.4	5.1
1.0511	1.951	7.620	2	7	5052.4	13.1
1.0511	2.603	7.620	2	7	5103.0	4.6
1.0511	3.906	7.620	2	7	5133.7	9.7
1.0511	7.816	15.240	2	7	5180.8	6.8
1.2008	1.954	7.620	2	7	5568.8	8.0
1.2008	2.605	7.620	2	7	5598.3	4.7
1.2008	3.908	7.620	2	7	5623.6	3.1
1.2008	7.815	15.240	2	7	5662.1	5.6
1.3005	1.905	7.620	2	7	5900.0	7.7
1.3005	2.605	7.620	3	6	5926.9	10.7
1.3005	2.605	7.620	2	7	5925.7	5.6
1.3005	3.908	7.620	2	7	5951.9	6.6
1.3005	3.908	7.620	2	7	5955.4	8.6
1.3005	7.815	15.240	2	7	5990.0	4.8
1.3005	7.816	15.240	2	7	5982.2	6.0
1.4470	1.951	7.620	3	6	6401.2	10.4
1.4470	1.951	7.620	2	7	6398.9	11.6
1.4470	2.603	7.620	2	7	6417.7	2.7
1.4470	2.603	7.620	2	7	6425.9	11.9
1.4470	3.908	7.620	2	7	6442.1	11.1
1.4470	3.906	7.620	2	6	6443.9	7.0
1.4470	7.816	15.240	2	6	6466.9	2.1
1.4470	7.823	15.240	2	7	6469.8	5.4
1.5342	1.951	7.620	2	7	6732.9	6.3
1.5342	2.603	7.620	2	7	6722.0	11.7
1.5342	3.906	7.620	3	6	6742.2	10.4
1.5342	7.813	15.240	2	7	6743.6	5.9
1.5695	1.951	7.620	2	7	6816.5	4.0
1.5695	2.603	7.620	2	7	6824.9	2.4
1.5695	3.906	7.620	2	7	6833.8	0.8
1.5695	7.816	15.240	2	7	6831.6	1.8

TABLE III - Continued

SUMMARY OF SHOT DATAConfined Charges

Density (gm/cc)	Dia (cm)	Length of Increment (cm)	No. of Increments		D(m/sec)	$\pm L_{95}$
			Booster Section	Rate Section		
1.6359	1.951	7.620	2	7	6933.0	2.1
1.6359	2.603	7.620	2	7	6934.6	1.6
1.6359	3.909	7.620	2	7	6938.5	4.0
1.6359	7.823	15.240	2	7	6941.4	3.1

Unconfined Charges

1.4407	1.951	7.620	2	6	6372.1	8.6
1.4407	3.906	7.620	2	7	6423.3	5.2
1.4407	7.823	12.700	3	6	6447.5	5.4
1.5127	1.951	7.620	1	8	6624.9	1.7
1.5127	2.603	7.620	2	7	6644.0	2.1
1.5127	3.906	7.620	3	6	6661.7	7.6
1.5127	7.818	7.620	4	5	6684.5	9.4
1.5127	7.818	7.620	4	5	6681.1	23.9
1.5627	1.951	7.620	1	8	6802.7	3.4
1.5627	2.603	7.620	2	7	6812.9	2.3
1.5627	3.906	7.620	3	6	6831.9	30.3
1.5627	7.818	7.620	4	5	6823.2	8.6
1.5627	7.818	7.620	4	5	6832.1	14.7
1.6094	1.951	7.620	1	8	6901.8	3.5
1.6094	2.603	7.620	2	7	6907.4	21.3
1.6094	3.906	7.620	2	7	6902.9	16.9
1.6094	7.816	7.620	4	5	6909.7	3.0
1.6094	7.816	7.620	4	5	6907.4	5.2
1.6238	1.951	7.620	2	6	6933.3	3.2
1.6238	2.603	7.620	2	7	6929.1	5.4
1.6238	3.909	7.620	2	5	6926.8	6.3
1.6238	7.823	15.240	5	4	6930.3	1.9
1.6251	0.693	5.080	2	7	6906.4	10.8
1.6251	0.846	5.080	1	3	6905.3	5.7
1.6251	1.090	5.080	2	7	6922.1	2.3
1.6251	1.524	5.080	2	7	6923.6	1.3
1.6251	2.540	5.080	2	7	6926.4	5.2
1.6251	7.620	5.080	2	7	6928.3	4.1

TABLE III - Continued

SUMMARY OF SHOT DATAUnconfined Charges

<u>Density</u> <u>(gm/cc)</u>	<u>Dia (cm)</u>	<u>Length of</u> <u>Increment</u> <u>(cm)</u>	<u>No. of Increments</u>		<u>D(m/sec)</u>	<u>+ L<sub>95</sub></u>
			<u>Booster</u> <u>Section</u>	<u>Rate</u> <u>Section</u>		
1.6324	1.951	7.620	1	8	6936.6	2.3
1.6324	2.606	7.620	1	7	6941.1	7.9
1.6324	3.909	7.620	2	7	6943.6	9.0
1.6324	7.818	7.620	4	5	6941.2	3.7
1.6324	7.818	7.620	4	5	6941.9	5.2

TABLE IV - ANALYSIS OF DATA

Density Index 1	Density (gm/cc)	No of Shots at 1 <sup>th</sup> Dens N <sub>1</sub>	First Stage of Analysis			Second Stage of Analysis	
			D <sub>∞</sub> (m/sec)	S <sub>1</sub> <sup>2</sup>	a (mm)	D <sub>∞</sub> (m/sec) <sup>b</sup>	± L <sub>95</sub>
	Confined Charges						
1	0.9009	4	4751.5	28.8	0.673	4,744.3	15.1
2	1.0511	4	5221.3	34.3	0.621	5,222.9	11.0
3	1.2008	4	5689.5	17.7	0.419	5,700.0	7.7
4	1.3005	7	6012.2	14.1	0.366	6,017.8	6.3
5	1.4470	8	6489.8	8.5	0.272	6,484.7	6.9
6	1.5342	4	6748.2	31.2	0.060	6,762.6	8.5
7	1.5695	4	6840.2	17.4	0.062	6,848.9	8.5
8	1.6359	4	6944.1	0.5	0.033	6,948.2	13.4
	Unconfined Charges						
9	1.4407	3	6473.0	00.7	0.304	6,464.6	6.8
10	1.5127	5	6701.6	2.7	0.224	6,694.1	8.0
11	1.5627	5	6839.2	53.0	0.097	6,835.7	7.6
12	1.6094	5	6909.7	7.9	0.020	6,909.3	12.1
13	1.6238	4	6927.0	7.8	-0.013	6,929.4	8.0
14	1.6251	6	6933.6	20.8	0.027	6,931.3	7.9
15	1.6324	5	6944.0	4.4	0.016	6,942.5	10.2

<sup>a</sup> Computed from S<sub>1</sub><sup>2</sup><sup>b</sup> Detonation velocity predicted by equation (3).



follows: (10) We define a step function

$$F(\rho, \rho^*) = 0 \quad \rho \leq \rho^* \\ = 1 \quad \rho > \rho^*$$

and write

$$D_\infty = a_0 + a_1 \rho + F(\rho, \rho^*) \left[ a_2 (\rho - \rho^*)^2 + a_3 (\rho - \rho^*)^3 \right] \quad (2)$$

The least squares normal equations are readily obtained for this function in the usual way. However, since the experimental design was not symmetrical (i.e., the diameters and numbers of shots fired are not the same for all densities), the correct procedure is a weighted least squares analysis with weight factors

$$w_i = \frac{N_i \sum_{j=1}^{N_i} (\delta_{ij} - \bar{\delta}_i)^2}{\sum_{j=1}^{N_i} \delta_{ij}^2}$$

where  $\delta = 1/2R$ , and  $i$  and  $N_i$  are as in Table IV. By a trial and error method it was determined that an appropriate value for  $\rho^*$  was 1.5342 gm/cc; that is, values of  $D_\infty$  for densities greater than this exhibit significant departure from the linear part of equation (2). The final result of the analysis is as follows:

$$D_\infty = 1872.7 \pm 37.2 + (3187.2 \pm 27.1) \rho + F(\rho, 1.5342) \left[ (-25,102 \pm 10,212) (\rho - 1.5342)^2 + (115,056 \pm 103,667) (\rho - 1.5342)^3 \right] \quad (3)$$

The  $\pm$  values in this equation are the 95% confidence limits of the coefficients.

This part of the analysis also provides an independent estimate,  $S_2^2$ , of the variance of the underlying population. We find  $S_2^2 = 47.3$  with 11 degrees of freedom. The ratio  $S_2^2/S_1^2$  is 2.48, from which it is concluded by the  $\chi^2$  test (11) that the two variances are from different populations. The observed ratio only slightly exceeds the critical ratio, 2.32 (5% level), and it is quite possible that this conclusion is the result of a small fitting error introduced into the analysis by our assumption as to the form of equation (2). However, the use of a more complicated expression hardly seems justifiable.

The last two columns of Table IV contain the values of  $D_\infty$  computed from equation (3) and their 95% confidence intervals. The confidence intervals are obtained from the equation.

$$\pm L_{95} \text{ of } D_\infty = \sqrt{s^2 \left[ \frac{1}{15} + \sum_{k=1}^3 (X_k - \bar{X}_k)^2 C_{kk} + \sum_{l \neq k} \sum_l (X_k - \bar{X}_k)(X_l - \bar{X}_l) C_{kl} \right]}^{1/2}$$

"t" (0.95, 11)

where  $X_1 = \rho$ ,  $X_2 = (\rho - \rho^*)^2$ , and  $X_3 = (\rho - \rho^*)^3$ . The  $C_{kl}$  are the elements of the covariance matrix. Their values are

$$\begin{aligned} C_{11} &= 3.2232 & C_{12} &= -4.846 \times 10^2 \\ C_{22} &= 4.564 \times 10^5 & C_{13} &= 4.036 \times 10^3 \\ C_{33} &= 4.674 \times 10^7 & C_{23} &= -4.582 \times 10^6 \end{aligned}$$

Figures 1 and 2 are deviation plots for the reciprocal diameter fits. They indicate quite clearly that our diameter effect data do not depart from the form of equation (1) in any systematic way. In Fig. 3, the upper curve is a deviation plot for the whole of equation (3), while the lower curve illustrates the manner in which the high-density data depart from the extrapolated linear portion of that equation.

#### IV. DISCUSSION

We have seen that equation (1) accurately represents our data over the range of diameters studied by us, but its use for extrapolation purposes needs to be justified. To this end we will want to make use of the observation that in our experiments we have

$$\frac{D}{D_\infty} \geq 0.985 \text{ (unconfined charges)} \quad \frac{D}{D_\infty} \geq 0.965 \text{ (confined charges)}$$

where these relations hold for all diameters and densities.

Two theories of the diameter effect have been proposed, the curved-front theory of Eyring and coworkers<sup>(1)</sup> and the nozzle theory of H. Jones.<sup>(12)</sup> In both cases the theory was developed for three types of confinement -- no confinement, light confinement, and heavy confinement. We are here concerned only with the first and last of these.

In both theories the existence of a detonation reaction zone of finite length  $x$  is assumed, and we need only replace  $a$  by  $x$  in equation (1) to obtain the result given by the curved-front theory

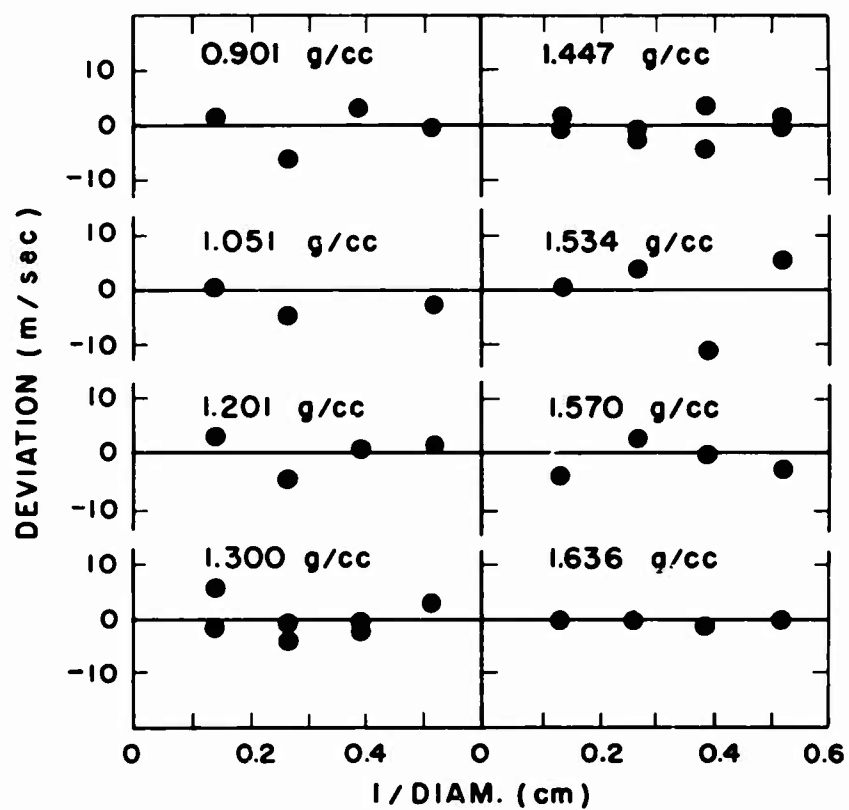


Figure 1

Deviation plots (experimental-calculated)  
for reciprocal diameter fits -- confined  
charges.

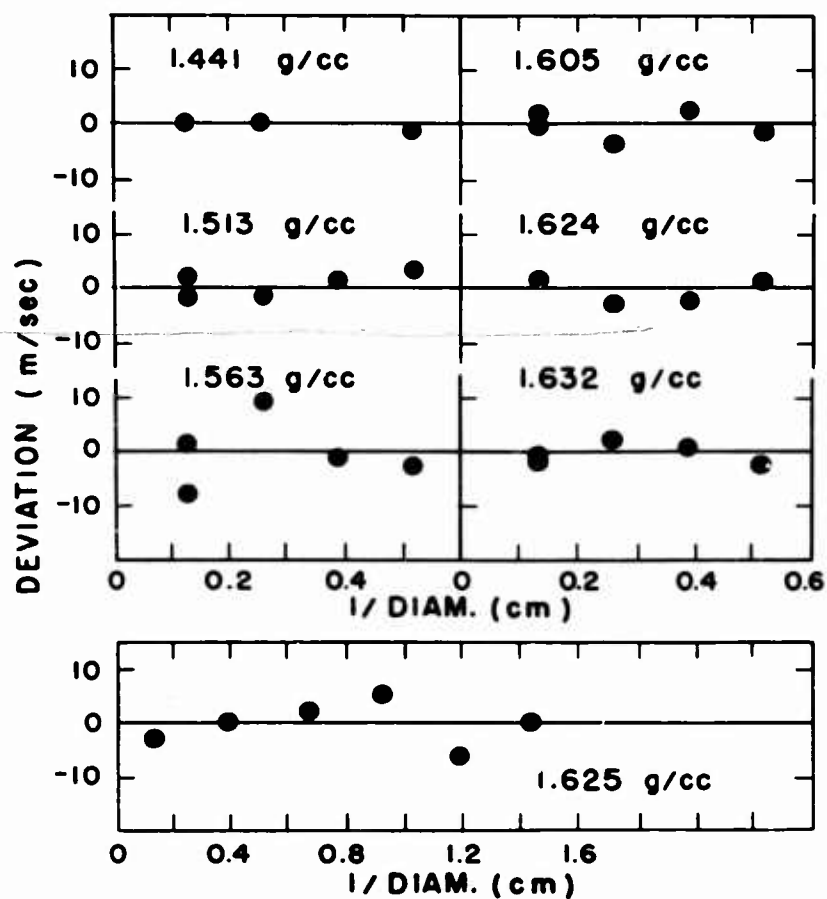


Figure 2

Deviation plots (experimental-calculated)  
for reciprocal diameter fits -- unconfined  
charges.

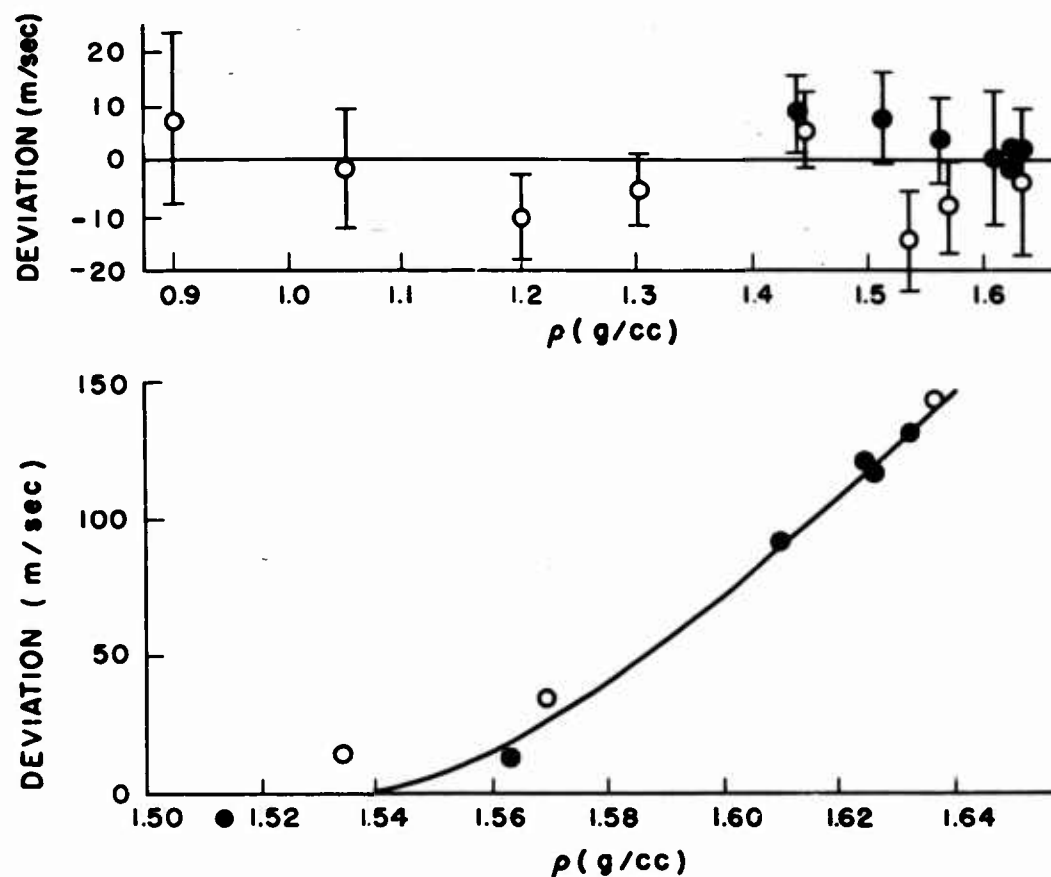


Figure 3

Deviation plots (experimental-predicted) for the  $D_{\infty}$  vs  $\rho$  data. Open circles: Confined charges. Full circles: Unconfined charges. The upper graph is for the whole density range and shows the deviation of the experimental points from the velocities predicted by equation (3). The error flags (where shown) are the 95% confidence intervals calculated from  $S_2^2$  (see text). In the lower graph, the high-density region has been expanded to emphasize the departure from linearity (first two terms of equation (3)) in this region. The curved line represents the contribution of the higher order terms of equation (3).

for unconfined charges (we assume that  $x$  is not sensibly dependent on  $R$ ). The corresponding result for heavily cased charges is

$$\frac{D}{D_{\infty}} = 1 - 0.88 \frac{x}{R} \sin \phi$$

with  $\phi$  given by

$$\tan \phi = \frac{\rho}{\rho_c} \sqrt{\frac{D_c^2}{D^2} - 1}.$$

Here  $\rho_c$  and  $D_c$  are the initial density and shock velocity in the confining material, respectively, and the other symbols have already been defined. Upon inserting reasonable values for  $D_c$  in the last equation, we find that in our experiments  $\tan \phi < 0.25$ , and hence to a sufficiently good approximation  $\sin \phi \cong \tan \phi$ . Furthermore, at a given density  $\rho$ , the expression under the radical sign varies by about twenty percent or less, while  $R$  varies by a factor of four. Hence well within the precision of our data we may set

$$1.76 \sin \phi \cong 1.76 \frac{\rho}{\rho_c} \sqrt{\frac{D_c^2}{D^2} - 1} \cong C(\rho) \quad (4)$$

and we then have

$$\frac{D}{D_{\infty}} = 1 - \frac{C}{2} \frac{x}{R}$$

which is of the desired form. Our estimates of the values of  $C$  at the densities of interest, obtained from equation (4), are as follows:

$\rho$	$C$
0.9	0.12
1.05	0.18
1.2	0.24
1.3	0.28
1.45	0.34
1.53	0.38
1.57	0.40
1.64	0.43

An approximate form of Jones' equation for heavily cased charges is

$$\frac{1}{D^2} = \frac{1}{D_{\infty}^2} \left( 1 + \frac{9 x \tan \phi}{R} \right).$$

Here  $\phi$  is the expansion angle of the case, and the other symbols have the meanings already assigned. It is assumed that  $\frac{x}{R} \tan \phi$  is small, and indeed we have  $\frac{x}{R} \tan \phi < 0.01$  for  $D/D_\infty > 0.96$ . Under these conditions we can equally well write

$$D = D_\infty \left( 1 - \frac{4.5 x \tan \phi}{R} \right)$$

which is of the desired form providing the expansion angle is constant at a given loading density. This would appear to be an entirely reasonable assumption. We note in passing that, to within about a factor of two,  $x = 4a$  for heavily cased charges by both theories.

The Jones theory for unconfined charges is a quite different matter. For  $D/D_\infty \approx 1$  these equations can be written

$$D = D_\infty \sqrt{1 - 4.5 (r - 1)}$$

where  $r$  is defined parametrically by

$$r = 1.85 \left( 1 - \frac{x}{R} \cot \theta \right)$$

$$\frac{x}{R} = 0.919 \frac{\sin \theta}{1 + \cos \sqrt{2} \theta}$$

If in this case we assume that  $x$  is independent of  $R$ , we find that a plot of  $D/D_\infty$  vs  $x/R$  curves rather sharply as  $D/D_\infty \rightarrow 1$ , so that it is not possible to obtain a reasonable representation of our results by means of these equations unless  $x$  is allowed to vary with  $R$ . The functional form which such a dependence might assume is not contained in either theory, and hence a unique solution for  $D_\infty$  cannot be obtained.

To summarize, then, for  $x$  independent of  $R$ , and for  $D/D_\infty \approx 1$ , equation (1) is of the form predicted by both theories for heavily confined charges, and by the curved-front theory for unconfined charges. It is, under these same conditions, inconsistent with the results of the nozzle theory for unconfined charges. Nevertheless, we feel that its use in estimating infinite diameter velocities from our finite charge data has been adequately justified on both experimental and theoretical grounds.

Corresponding to the reaction zone length  $x$  which appeared in the foregoing discussion, there is a reaction time  $\tau$ . These are quantities of considerable physico-chemical interest which are difficult to measure by any direct method. From elementary conservation of mass considerations, they are related by the equation

$$\tau = \frac{x}{D} \frac{\bar{\rho}}{\rho}$$

where  $\rho$  is the initial density of the explosive and  $\bar{\rho}$  is the average density (unburned explosive plus products) in the reaction zone. The value of the ratio  $\bar{\rho}/\rho$  is not known, but from the presumed structure of the reaction zone (1) we can assert that  $\rho_{CJ}/\rho$  is a lower bound where  $\rho_{CJ}$  is the density at the Chapman-Jouguet plane. For many explosives  $\rho_{CJ}/\rho \cong \frac{4}{3}$ . With this in mind, but otherwise quite arbitrarily, we set  $\tau = \frac{1.5x}{D}$ , and, in Table V, we have summarized the values of  $x$  and  $\tau$  computed from our data, using the results of the curved-front theory. In Fig. 4,  $x$  is plotted as a function of  $\rho$ . From this figure we see that  $x$  is a smoothly decreasing function of  $\rho$  over the whole density range, becoming quite small as crystal density (1.654 gm/cc) is approached. Similar results were obtained by Stesik and Akimova, although these investigators used a quite different, empirically calibrated relationship between  $D/D_\infty$  and  $x/R$ . The dashed line in Fig. 4 represents the dependence of  $x$  on  $\rho$  according to the data of their paper. The differences in the two curves are readily explainable, qualitatively at least, if the TNT used by Stesik and Akimova was of a smaller average particle size (around 40 microns) than that used by us. It is not unlikely that this was the case, as they state that their TNT had been ball milled.

These results must be interpreted with some reserve, since the theories of the diameter effect are imprecise, and also because little is known about the actual kinetic structure of the reaction zone. Regarding the latter, one reaction mechanism which appears consistent with much of the available experimental data is surface ignition, followed by inward burning, of the individual grains.<sup>(13)</sup> This mechanism is generally referred to as the grain-burning theory. A decrease in  $x$  with  $\rho$  would be expected on the basis of this theory, and may be viewed as the result of two effects -- a decrease in grain size due to crushing of the grains in the pressing operation, and an increase in burning rate with increasing pressure in the reaction zone. It is of some interest to compare the data of Table V with corresponding estimates made on the basis of the grain-burning theory. The comparison is most readily made using the reaction times  $\tau$ . If the explosive grains are assumed to be uniform spheres of radius  $r$ , and if  $\dot{r}$  is their linear (radial) burning rate, then we have  $\tau = r/\dot{r}$ . In practice the explosive grains are neither spherical nor uniform in size; furthermore, many of them are agglomerates of smaller crystals, and even the individual crystals may have internal fissures and voids. Finally, some attrition of the grains must occur during their passage through the shock front (by spalling, for example). The data of Table I cannot, therefore, be used in any straightforward way to estimate an average effective grain radius for the reaction time calculations. For this reason, to make the comparison we have turned the calculation around, and from the values of  $\tau$  given in Table V and estimated values of  $\dot{r}$  we have calculated  $r$ . The values of  $r$  so obtained are then to be compared with the data of Table I, keeping



TABLE V

Reaction Zone Length  $x$  and Reaction Time  $\tau$  - Curved-Front Theory

$\rho$	Confined		Unconfined	
	$x$ (mm)	$\tau^a$ ( $\mu$ sec)	$x$ (mm)	$\tau^a$ ( $\mu$ sec)
0.901	$5.61 \pm 0.85$	1.78		
1.051	$3.45 \pm 0.52$	0.99		
1.201	$1.75 \pm 0.35$	0.46		
1.300	$1.31 \pm 0.19$	0.33		
1.441			$0.30 \pm 0.08$	0.07
1.447	$0.80 \pm 0.14$	0.19		
1.513			$0.22 \pm 0.06$	0.05
1.534	$0.16 \pm 0.19$	0.04		
1.563			$0.10 \pm 0.06$	0.02
1.570	$0.15 \pm 0.18$	0.04		
1.609			$0.02 \pm 0.06$	<0.01
1.624			$0.01 \pm 0.03$	<0.01
1.625			$0.03 \pm 0.02$	<0.01
1.632			$0.02 \pm 0.06$	<0.01
1.636	$0.08 \pm 0.16$	0.02		

<sup>a</sup> Computed from  $\tau = 1.5 \frac{x}{D}$ . See text.

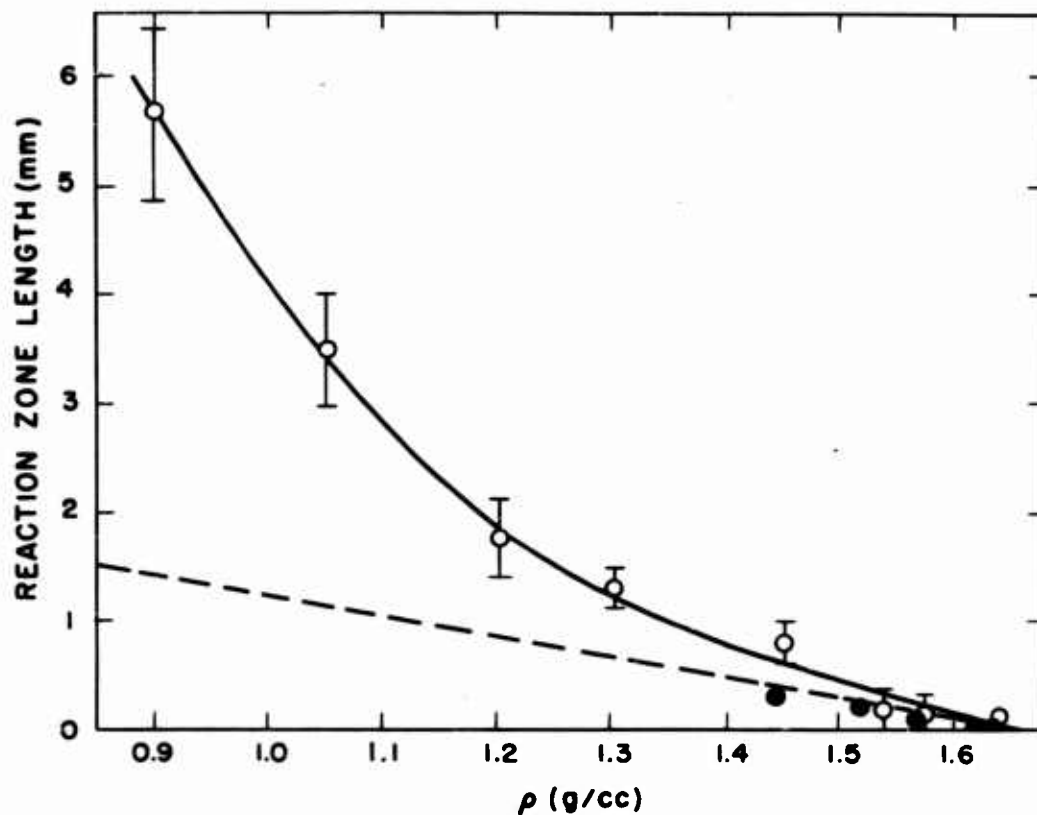


Figure 4

Detonation reaction zone length as a function of loading density.

Open circles: Confined charges.

Full circles: Unconfined charges.

Error flags shown are 95% confidence intervals.

The dashed line represents data by Stesik and Akimova, (see text).

in mind the above comments regarding the expected relative magnitudes of the two sets of data.

The linear burning rate of TNT crystals has been measured by Jacobs as a function of pressure up to about 3000 atm. The details of this investigation have never been published in the open literature,<sup>(14)</sup> but the burning rate of TNT was found to follow an equation of the form

$$\dot{r} = k P^n .$$

The coefficient  $k$  is temperature dependent, increasing at the rate of about 2% for each 10°C rise in temperature. At room temperature,  $k = 0.53 \times 10^{-6}$  for  $\dot{r}$  in mm/μsec and  $P$  in atmospheres. If we assume that the temperature of the shocked (but unreacted) explosive is 900°C (vide infra), then  $k$  has the value  $3.0 \times 10^{-6}$ . The exponent  $n$  was found by Jacobs to be equal to 0.81. Therefore, for the burning rate we use the equation

$$\dot{r} = 3.0 \times 10^{-6} P^{0.81}$$

and hopefully extrapolate this into the range of detonation pressures. The latter also must be estimated in the density range of interest. For this purpose we have used the equation

$$P_{CJ} = 2.75 \times 10^{-3} \rho D^2 \quad (5)$$

where  $P$  is given in atmospheres for  $D$  in m/sec. This choice is based in part on the results of hydrodynamic calculations<sup>(15)</sup> and in part on an experimental value at  $\rho = 1.455$  gm/cc.<sup>(16)</sup> The pressure varies considerably throughout the reaction zone, perhaps by as much as a factor of two,<sup>(1)</sup> being higher at the front of the zone. For this reason we have computed the burning rates using a pressure (assumed constant throughout the reaction zone) 20% higher than that given by equation (5). The results of these calculations may be summarized as follows:

TABLE VI

$\rho$ (gm/cc)	$P \times 10^{-3}$ (atm)	$\dot{r} \times 10^3$ (mm/μsec)	$r \times 10^3$ (mm)	Grain Dia (microns)
0.90	67	24.4	43.5	87
1.05	94	32.4	32.1	64
1.20	128	41.3	19.0	38
1.30	155	47.6	15.7	31
1.45	201	59.2	11.3	23

The agreement between the numbers appearing in the last column of this table and the numbers which might have been predicted from the sieve analysis data is surprisingly good, particularly in view of the impressive extrapolation of Jacobs' burning rate equation which was involved in the calculations.

An alternative model for the detonation reaction is the homogeneous adiabatic decomposition of the shock-heated explosive, assuming an Arrhenius rate law. Under these conditions the reaction time is given by the equation (17)

$$\tau = \frac{cRT_0^2}{ZQE} e^{E/RT_0}$$

where  $c$  is the heat capacity,  $Q$  is the heat of reaction,  $T_0$  is the temperature of the shocked explosive,  $R$  is the gas constant, and  $Z$  and  $E$  are the preexponential factor and activation energy, respectively, in the Arrhenius law. In this equation everything but  $R$  is uncertain in the regime of interest here. We begin by setting  $c = 0.5 \text{ cal/gm/}^\circ\text{C}$  and  $Q = 1000 \text{ cal/gm}$ . Temperatures on the Hugoniot of unreacted TNT have been computed (15) for two assumed equations of state, one of the Mie-Grüneisen form, and the other of the form cited by Cowan and Fickett for graphite. (18) In both cases the parameters in the equation of state were adjusted to fit experimental Hugoniot data for unreacted TNT. (19) Similar temperatures were obtained with both equations of state, and, for the pressures and densities listed in Table VI, we have  $T_0 \approx 1200^\circ\text{K}$ . It is of interest to note that, in this range, a  $100^\circ$  change in  $T_0$  changes  $\tau$  by about a factor of three.

The greatest uncertainty arises in the values to be assigned to  $E$  and  $Z$ . From studies of the thermal decomposition of liquid TNT, Robertson (20) obtained  $Z = 10^{11.4} \text{ sec}^{-1}$  and  $E = 34.4 \text{ kcal/mole}$ , while Cook and Abegg (21) obtained  $Z = 10^{12.2} \text{ sec}^{-1}$  and  $E = 43.4 \text{ kcal/mole}$ . Inserted in the above equation, with the previously assigned values of  $c$ ,  $Q$ , and  $T_0$ , these rate laws lead to the following estimates of the reaction time:

$$\begin{aligned} &0.3 \text{ } \mu\text{sec (Robertson)} \\ &1.5 \text{ } \mu\text{sec (Cook and Abegg)} \end{aligned}$$

Thus these estimates also are in good agreement with the "experimental" values. On the other hand, we view them as even less reliable, and by a considerable margin, than the burning rate calculations summarized in Table VI.

We conclude this discussion of reaction zone lengths with a few general comments. First of all, while the interpretation of our data in terms of the combined curved-front/grain-burning theories has led to surprisingly good agreement in the computed reaction zone lengths, this agreement cannot be cited as proof of any part of the theory. The agreement could be accidental, and the only justifiable

conclusion to be drawn from these results is that this interpretation of the data has not led to any gross inconsistencies.

Secondly, and in spite of this agreement, we feel that some modification of the grain-burning theory might be profitable. The argument is as follows: When a soft granular material is shocked to a density well above its crystal density, it would seem reasonable to expect that the individual grains would completely lose their identity, so that the model of inward burning grains becomes somewhat implausible. On the other hand, the discontinuities in the material (voids and intergranular contact points) are likely places for burning to start -- by spalling, intercrystalline friction, or adiabatic compression as the material passes through the shock front. These considerations suggest that the reaction may proceed through the outward burning of numerous small hot spots (holes) more or less randomly distributed throughout the compressed material. Both the number and size distribution of such hot spots presumably would depend on the strength of the shock in such a manner that a decrease in reaction zone length with increasing charge density would result from this effect as well as from the increase in burning rate. Reaction zone lengths deduced from this "hole burning" model would not be expected to be grossly different from those computed from the grain burning model. Its principal advantage, aside from plausibility considerations, is that it can explain a wider range of reaction times. Unfortunately, this same flexibility, which is an inherent feature of the model, makes simple calculations of reaction zone lengths somewhat more difficult to justify in terms of the conditions assumed to hold initially behind the shock front. Some of the consequences of the model are currently being explored at this Laboratory.

The literature abounds in detonation velocity data on TNT, but most of it was obtained before the development of accurate instrumental methods and also before the importance of charge geometry and confinement was fully appreciated. We will here consider only the more recent studies.

Cybulski, Payman, and Woodhead,<sup>(22)</sup> using a rotating mirror camera, made a number of measurements, mostly on cast TNT, in which they studied the effect of purity, crystal size, charge diameter, and confinement. From their data they deduce a limiting velocity of 6950 m/sec for cast TNT at a density of 1.624 gm/cc. This is some 25 m/sec above our curve. As a check on the reproducibility of the method they also determined the detonation velocity of pressed TNT at a density of 1.00 gm/cc in 1.25" diameter unconfined charges, using a TNT having a particle size two to three times larger than that of the TNT we used. Their velocity of 4650 m/sec is over 300 m/sec below what we would predict from our results for confined charges of this diameter and density. This emphasizes the importance of the effects of confinement and particle size on detonation velocities determined at low loading densities.

Copp and Ubbelohde<sup>(23)</sup> used a careful application of the Dautriche method to obtain detonation velocity data on confined charges of cast TNT at a density of 1.60 gm/cc with various charge diameters. From their results they deduce a limiting velocity of 6970 m/sec. This is some 70 m/sec above our curve and indeed lies very close to the extrapolation of our least squares line. We believe the discrepancy lies in the method used by Copp and Ubbelohde to extrapolate their experimental points to obtain an infinite diameter velocity. The velocity actually reported by them for 3" diameter charges is 6850 m/sec, and the correlation between velocity and diameter is not statistically significant in the case of their data.

The wartime work of the Explosives Research Laboratory at Bruceton has never been published in the open literature but has been summarized in an OSRD report.<sup>(24)</sup> Over a hundred velocity measurements were made on TNT at a variety of densities, charge diameters, particle sizes, and degrees of confinement. The data are difficult to analyze in a systematic way, but a limiting velocity curve deduced by the investigators is given as

$$D = 1785 + 3225 \rho$$

which is in good agreement with our results.

Stesik and Akimova's work most nearly parallels ours in plan and objective, although it differs considerably from ours in experimental details and in the treatment of the data. Their infinite diameter velocities are a linear function of  $\rho$  up to 1.55 gm/cc and are described by the equation

$$D_{\infty} = 1669 + 3342 \rho .$$

This is only in fair agreement with our equation (3). Their infinite diameter velocities are some 70 m/sec below ours in the low-density region and are higher than ours by a similar amount at high density. We can only speculate as to the reasons for this. The difference at low density may be a consequence of their extrapolation procedure and, more directly, of the method they used to calibrate it. The situation at high density is more obscure, as many of their experimental velocities are higher than our infinite diameter velocities.

It is interesting to note that their highest density point, at 1.62 gm/cc, lies some 83 m/sec below the straight line determined by their other four experimental points. Thus their data also contain evidence of the downward curvature of the  $D_{\infty}$ - $\rho$  line observed by us in the high-density region.

#### ACKNOWLEDGMENTS

This work was made possible only through the cooperation of many members of GMX Division of the Los Alamos Scientific Laboratory.

We especially wish to acknowledge the valuable contributions of W. W. Wood and A. W. Campbell of this Laboratory, and of R. J. Hader of the Institute of Statistics at the University of North Carolina. We also are indebted to W. H. Rogers, now deceased, who determined the cooling curve of the TNT used in this investigation, and to R. G. Shreffler for helpful discussions and criticisms.

#### REFERENCES

- (1) Eyring, Powell, Duffey, and Parlin, Chem. Rev. 45, 69 (1949).
- (2) Malin, Campbell, and Mautz, J. Appl. Phys. 28, 63 (1957).
- (3) Stesik and Akimova, Zhur. Fiz. Khim. 33, 1762 (1959).
- (4) Private communication from A. W. Campbell of this Laboratory.
- (5) Copp and Ubbelohde, Trans. Faraday Soc. 44, 646 (1948).
- (6) Campbell, Malin, Boyd, and Hull, Rev. Sci. Instru. 27, 567 (1956).
- (7) We are indebted to Grover Taylor for these measurements.
- (8) Mandel, J. Amer. Stat. Assoc. 52, 552 (1957).
- (9) A. Hald, Statistical Theory with Engineering Applications, (John Wiley and Sons, Inc., New York, 1952), p 291.
- (10) We are greatly indebted to R. J. Hader and W. W. Wood, who suggested this method of analysis.
- (11) Ref 9, p 379.
- (12) Jones, Proc. Roy. Soc. A189, 415 (1947). See also ref 1.
- (13) Kistiakowsky, Third Symposium on Combustion, Flame, and Explosion Phenomena, p 560. Williams and Wilkins Co., Baltimore.
- (14) The work is briefly described in Science in World War II, Chemistry volume. Little, Brown and Co., 1948. See also ref 13.
- (15) By C. L. Mader of this Laboratory.
- (16) W. Garn, J. Chem. Phys. 32, 653 (1960).
- (17) This is, for example, readily obtained from equation (6), p 174 of ref 1, after correcting an error in sign in the two exponentials.

- (18) Cowan and Fickett, J. Chem. Phys. 24, 932 (1956).
- (19) Unpublished data by W. Garn of this Laboratory.
- (20) Robertson, Trans. Faraday Soc. 44, 977 (1948).
- (21) Cook and Abegg, Ind. Eng. Chem. 48, 1090 (1956).
- (22) Cybulski, Payman, and Woodhead, Proc. Roy. Soc. A197, 51 (1949).
- (23) Copp and Ubbelohde, Trans. Faraday Soc. 44, 658 (1948).
- (24) MacDougall, Messerly, Hurwitz, et al, OSRD-5611, "The Rate of Detonation of Various Explosive Compounds and Mixtures".



## MEASUREMENTS OF DETONATION, SHOCK, AND IMPACT PRESSURES\*

M. A. Cook, R. T. Keyes, W. O. Ursenbach  
Institute of Metals and Explosives Research, University of Utah  
Salt Lake City, Utah

### ABSTRACT

An "aquarium technique" for the measurement of detonation, shock, and impact pressures is described which is capable of measuring accurately pressures over a range extending from roughly one to several hundred kilobars. An experimental determination of the equation of state for water, upon which use of the aquarium technique relies, is presented and compared with results obtained by other investigators. Similar data are presented for lucite. Measurements of pressures for a variety of explosives including both ideal and non-ideal ones are presented for various charge diameters and lengths using explosives of widely different reaction zone lengths. These pressures were found to correspond to the Chapman-Jouguet value of the detonation pressure calculated from thermohydrodynamic theory.

---

\*This investigation was supported by the U.S. Navy Bureau of Ordnance under Contract Number NOrd-17371.

## Introduction

When a shock wave propagates through an undisturbed medium of density  $\rho_1$ , all the remaining shock wave parameters may be expressed uniquely in terms of any one chosen parameter. For example, pressure, temperature, and particle velocity may each be expressed uniquely in terms of the velocity of the shock wave. The fact that disturbances, even of relatively low pressure, propagate in water as shocks, coupled with the fact that water is transparent, thereby permitting convenient and continuous observation of shock velocity by a streak or framing camera, suggest that water can be used as a pressure gauge for measuring transient pressures. For instance, it may be used to measure the peak pressures in detonation waves of condensed explosives, in impact-generated shocks produced by the collision of a moving plate with a fixed plate, or, for that matter, it may be used to measure the peak pressures of shocks in various other media irrespective of the mode of shock generation.

Before water can be used as a pressure measuring medium its shock parameters must be known. The Rankine Hugoniot curves for water have been derived by a number of investigators including Kirkwood and Montrall,<sup>(1)</sup> Kirkwood and Richardson,<sup>(2)</sup> Richardson, Arons and Halverson,<sup>(3)</sup> Arons and Halverson,<sup>(4)</sup> and Doering and Burkhardt.<sup>(5)</sup> In these treatments systematic extrapolations of Bridgman's<sup>(6,7)</sup> PVT data for water were made. Probably the most comprehensive extrapolation of Bridgman's PVT data, however, was carried out by Snay and Rosenbaum<sup>(8)</sup> who used more recent data of Bridgman<sup>(9,10)</sup> which for water extended to 36,500 kg/cm<sup>2</sup> and for ice VII to 50,000 kg/cm<sup>2</sup>.

A different approach was used in a later study by Walsh and Rice.<sup>(11)</sup> In their method an intense plane shock wave was generated in an aluminum plate by the detonation of a slab of Composition B in contact with one side of the plate. The shock through a portion of the plate was then transmitted into water. Higher pressures in the aluminum plate were reported by "slapping" the aluminum plate with a thin, high velocity, explosively driven plate rather than detonating the charge directly in contact with the test aluminum. By application of a special streak camera technique pioneered by Walsh and co-workers and through use of a previously derived equation of state for aluminum the shock velocity in water as a function of the corresponding shock pressure in the aluminum at the interface was determined. Continuity conditions of pressure and particle velocity across the interface between the aluminum and water were then applied to determine the Hugoniot curves for water.

In determining shock parameters for water a factor which should be considered is the possibility of a phase change of the medium within the shock wave. This possibility was investigated by Snay and Rosenbaum<sup>(8)</sup> and by Walsh and Rice.<sup>(11)</sup> According to Snay and Rosenbaum the Rankine Hugoniot curve for supercooled water and the Rankine Hugoniot curve for partially frozen water are never far

apart, and thus the shock velocity would not be materially affected if freezing did occur. Since partial freezing of a liquid should lead to reduced transparency, because of differences in indices of refraction of water and ice, Walsh and Rice carried out some transparency experiments of water being traversed by a shock wave in the pressure range of 30 to 100 kilobars. No sign of opacity due to freezing was observed. They concluded therefore that even though P,T conditions might be proper for freezing under static conditions, the time the liquid was under the correct conditions within the shock wave apparently was too short for freezing to occur.

In using water as a pressure gauge (by observing the transmission of the shock into it) one must calculate from the measured shock pressure in water the pressure in the adjacent medium of interest from which the water shock was transmitted. In a previous application of the "aquarium technique" for the measurement of pressure, two procedures were used to perform such a calculation.<sup>(12)</sup> The first method, which was considered the more exact one, was patterned after a treatment given by Riemann for a shock propagating across a boundary into a medium of lower impedance. The second method utilized the shock "impedance mismatch" equation

$$p_i = \frac{p_t (\rho_t V_t + \rho_i V_i)}{2\rho_t V_t} \quad (1)$$

where  $p$  is pressure,  $\rho$  is initial density of the medium before being traversed by a shock,  $V$  is the velocity of the shock, and subscripts  $i$  and  $t$  designate the incident medium and the transmitting medium, respectively. Although the shock impedance mismatch equation theoretically should only be accurate when the wave reflected at the interface is a weak shock, in the investigations covered by Ref. 12 where the reflected wave was a rarefaction, equation (1) was found to yield results in very good agreement with the first method. Consequently, in the present study equation (1) was used to calculate  $p_i$  from measured values irrespective of whether the reflected wave was a release wave or a shock wave.

This paper presents results obtained by application of the aquarium method for the measurement of detonation pressures of a number of explosives.

Furthermore, since the results of Snay and Rosenbaum were derived from an extrapolation of low pressure PVT data, and since the curve of Walsh and Rice is dependent upon the equation of state of aluminum and application of continuity conditions across the aluminum-water interface, results of a shock parameter study for water by a third, independent method are described. Less comprehensive results are also presented for lucite which, like water, possesses desirable characteristics for use as the transmitting medium of a pressure gauge.

Experimental(a) Shock parameter determinations

The shock parameters which are of interest in this study are related by the familiar hydrodynamic equations

$$p - p_0 = \rho_1 V W \quad (2a)$$

$$W/V = [1 - (\rho_1/\rho)] \quad (2b)$$

and the approximate relation

$$W \approx V_{fs}/2 \quad (3)$$

where  $p$  is the pressure,  $\rho$  is the density,  $V$  is the shock velocity,  $V_{fs}$  the free surface velocity, and  $W$  is the particle velocity, the subscript 1 indicating initial conditions before passage of the shock wave. Equation (3) expresses the fact that the particle velocity in the shock at a free surface is approximately twice the particle velocity in the shock in the medium in question.

The method used for determining the shock-parameter data for water and some of the data for lucite consisted of simultaneous measurements of the shock velocity immediately inside the free surface and the free surface velocity as the shock emerged from the water or lucite. Observations of the shock and free surface velocities were made with a rotating mirror streak camera using diffuse backlighting from an explosive flash bomb to show the propagation of the shock wave and the free surface. Fig. 1 illustrates the aquarium setup. Note that point-initiated charges were used. For this reason it was necessary that the slit view of the streak camera lie along the charge axis in order to obtain the correct values of shock velocity and the corresponding free surface velocity. Care was also taken in the alignment for the free surface in the cases of both the water and the lucite to lie on the optic axis of the system so that the view of the camera was flush with the free surface.

Two sizes of aquaria were used, the smaller being 6" x 6" x 6" and the larger 12" x 12" x 8", the size of the aquarium being dictated by the height,  $h$ , of water above the receptor charge. As  $h$  was increased above a certain limit the dimensions of the aquarium had to be increased due to the fact that the shattering of the glass propagated with a velocity which exceeded the shock velocity in the liquid. Increasing the size of the aquarium, of course, resulted in an increased path length for fracture which permitted the events of interest at the water-air interface to be photographed before they were obscured.

The pressure or velocity of the shock wave when it reached the air surface was varied primarily by one of two methods: (1) By

varying the height,  $h$ , of the liquid above the surface of the generator charge, and (2) by varying the size of the shock-generator charge, since use of smaller diameter generator charges resulted in a greater attenuation of the shock in water. With 3" diameter x 3" length shock-generator charges and 2" diameter x 2" length donor charges of Composition B the pressure of the shock wave, when it reached the water-air interface, could be varied conveniently between an upper limit of about 130 kb when the height of the liquid was 0.5 cm and a lower limit of about 30 kb using a liquid height of about 7 cm. For lower pressure, rather than employing further increases of water height, it was more convenient to reduce the size of the charge. Consequently, for pressures below roughly 30 kb and down to as low as 1 kb, 1" diameter x 1" length Composition B shock-generator charges and 1" diameter x 3" length donor charges were used. The calibration curve was extended to 155 kb by using a charge based on

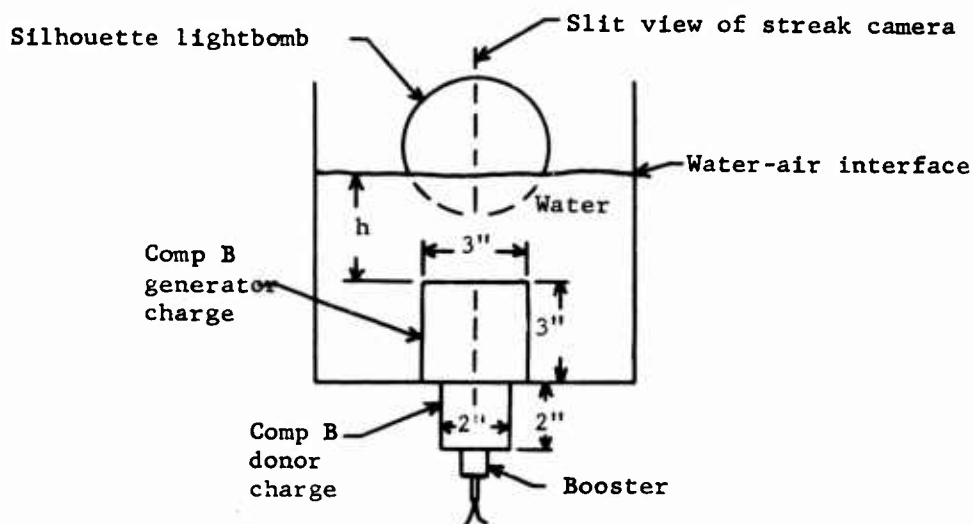


Fig. 1: Aquarium setup for measuring velocity of water shock along the charge axis and free surface velocity.

HMX as the shock-generator charge. This value was sufficiently high for measurements of detonation pressures of the explosives of interest. Walsh and Rice reported, however, extending shock parameter data to above 300 kb by hurling an explosively driven, thin, flat plate across a short air gap.

The silhouette-type lightbomb comprised a 4" diameter x 3" length 50/50 TNT/Composition B charge inserted in a 4" x 30" paste-board tube of about 1/16" wall thickness. A sheet of translucent polyethylene plastic was taped to the front of the tube which served as a diffusing screen. The height of the lightbomb was

adjusted so that the surface of the water in the aquarium was approximately in line with the center of the front of the lightbomb as viewed by the camera. The aquarium assembly and the streak camera were arranged such that the slit view of the streak camera was as shown in Fig. 1, i.e., perpendicular to the water-air interface and lying along the axis of the generator charge. Consequently, with proper synchronization of the lightbomb, a streak camera trace was obtained of the shock propagating through the liquid to the water-air interface. When the shock front reached the surface of the water the trace showed a rarefaction wave propagating back into the water and the spalling of the water surface. This spall apparently is in the form of a very fine spray because it is relatively opaque and permits photographing the motion of its front and thus the direct recording of the free surface velocity.

Fig. 2 reproduces a typical streak camera trace showing the attenuating shock wave, the release wave, and spall. Note that the spall velocity is very constant. The results of interest obtained from the films are the shock velocity just as the shock reached the interface and the free surface or spall velocity. Both these measurements were obtained from the slopes of the traces at the interface through application of the proper magnification factors and camera writing speed. The writing speed of the camera in general was chosen such that the slopes of the shock wave trace and the free surface trace about equally bracketed the slope corresponding to a  $45^\circ$  angle.

The water used in this investigation was ordinary tap water rather than distilled water because the amounts required were rather large (some aquaria holding seven gallons) and the difference between the compressibility of distilled water and tap water is small. The temperature of the water was  $20^\circ\text{C} \pm 5^\circ$ .

A few shock-parameter determinations for lucite were made in the same manner as those for water, i.e., by simultaneous measurements of shock velocity at the free surface and the free surface velocity. However, a greater number of determinations were made by transmitting the shock from lucite into water, measuring the final velocity of the shock in lucite and the initial velocity of the shock in water by means of a streak camera (utilizing a silhouette backlight bomb to render the shocks visible), and then by means of the previously obtained equation of state for water and equation (1), calculating the shock pressure in lucite immediately inside the lucite-water interface. The shocks in lucite were generated by the detonation of 4.8 cm diameter x 18 cm length, point initiated, cylindrical Composition B charges. As in the aquarium method the assemblies were carefully aligned in order that the slit view of the streak camera fell along the charge axis which made the use of expensive plane wave initiators unnecessary. The strength of the shock in lucite at the lucite-water interface was regulated by varying the thickness of lucite between the charge and the water.

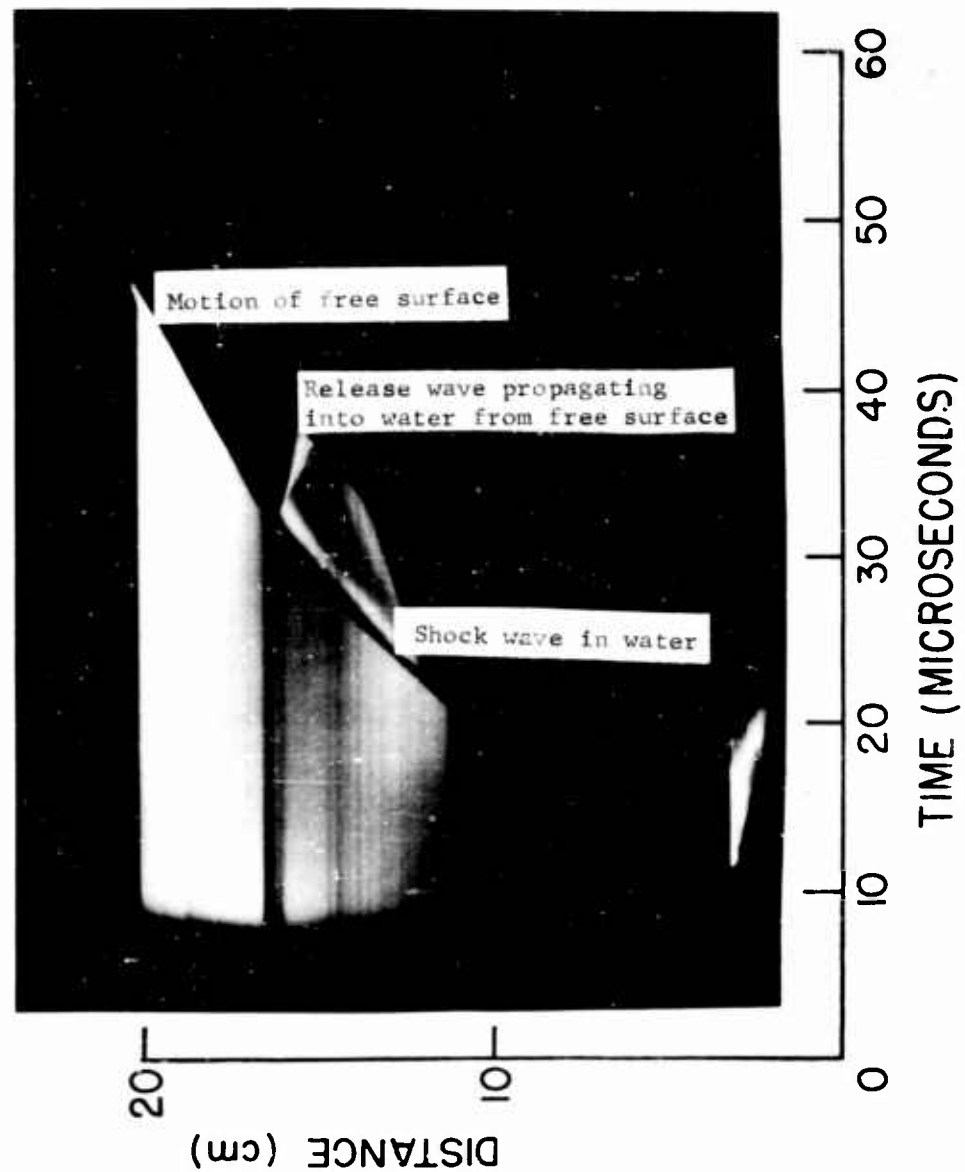


Fig. 2: Typical streak camera trace obtained using the arrangement of Fig. 1 (shock parameter determination for water).

The diameter of the lucite was in all cases sufficiently large to shield the detonation products from the region where the motion of the shock wave was observed.

(b) Detonation pressure determinations

Fig. 3 illustrates the aquarium assembly used for measuring the initial velocity of the shock (and pressure) in water transmitted directly from a detonation wave. As in the previous cases the assembly was aligned such that the streak camera observations were made along the charge axis, the height and tilt of the assembly being such that the bottom face of the charge in this case was coincident with (and parallel) to the optical axis of the camera. The streak camera at this installation viewed upward through a periscope in which the line of sight was reflected to a horizontal direction by a front surface mirror. The camera was mounted on a turntable and three supporting casters, permitting rotation of the camera about its optic axis. Thus the slit view of the camera could conveniently be adjusted to either the horizontal or vertical direction or to any position between them simply by rotation of the turntable. This method of mounting the camera therefore permitted the proper alignment to be made with ease.

The cast charges were detonated with the bare end immersed in the aquarium. However, in cases where there existed the possibility of absorption of water or solution of some of the charge components the charges were sprayed with Krylon for waterproofing. Charges made up from granular or loose material were vibrator-packed in thin-walled (approximately 1/16" thick) cardboard tubes. The ends of the charges which were immersed in water in these cases were "closed off" with a layer of polyethylene 3 mils thick which was too thin to affect appreciably the shock transmitted into the water.

The average densities of all charges were determined just prior to firing. In addition to the determination of the initial velocity of the shock transmitted into water the detonation rate of the charge was measured, and thus all variables were evaluated whose magnitudes were required in the impedance mismatch equation for calculation of pressure in the incident medium in terms of that in the transmission medium. Detonation velocities as well as the initial shock velocities were calculated from the slopes of the traces. This procedure when carefully applied was found to yield satisfactory results even for the initial shock velocity determinations because care was taken to obtain traces of approximately 45° slope but more importantly because in many cases (with the primary exception of short charges) the attenuation of the water shock during the initial stages proved not to be rapid.

Numerous measurements of the peak pressure in the detonation wave to detect pressures higher than the C-J pressure have been carried out previously.<sup>(13,14)</sup> However, these experiments utilized



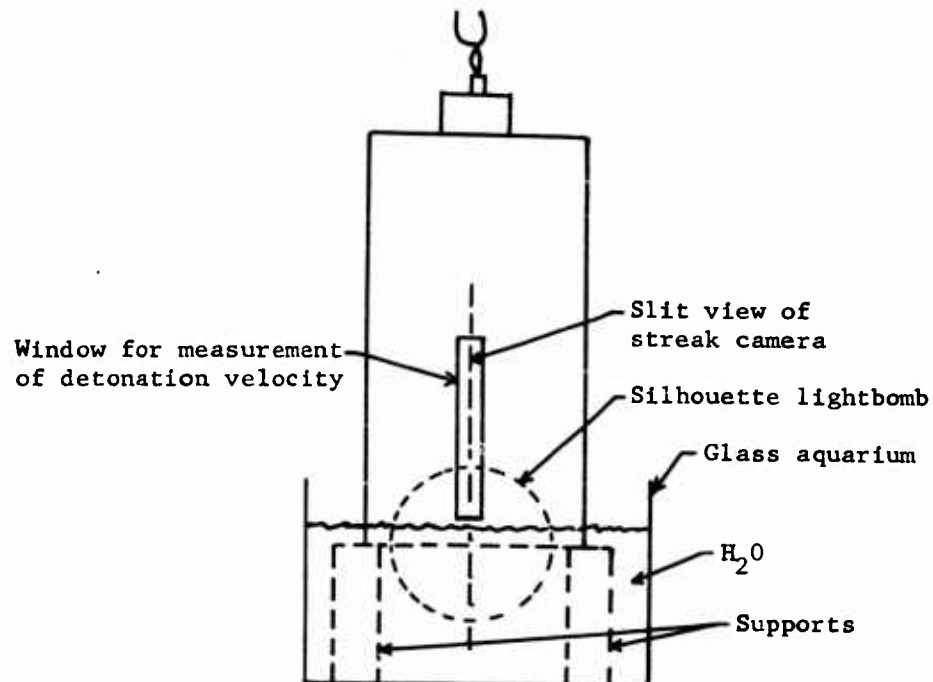


Fig. 3: Aquarium assembly for measurement of velocity along the axis (and pressure) of the transmitted shock in water from a detonation wave.

measurements of free surface velocity from aluminum acting as the transmission medium for shocks generated by detonation of the explosive in contact with the test sample. Since the observations were carried out on the free surface or exit side of the aluminum rather than at the explosive-metal interface, questionable measurements with very thin plates were required, <sup>(15,16)</sup> requiring also extrapolations to zero thickness to determine the pressure or particle velocity at the detonation front.

The difficulties in using excessively thin plates in the method of Ref. 13 and 14 were amplified by the fact that experiments were devoted mainly to explosives of short reaction zone length, such as Composition B, cast TNT, and fine, granular TNT for which the detonation "spike" would be "erased" quickly as it propagated into the aluminum. In the aquarium method, however, where a continuous observation of the shock wave velocity from the explosive-water interface outward into the liquid is possible, one does not need to use thin layers of the transmitting medium. Admittedly a streak camera may not be able to resolve very rapid changes in velocity

(or pressure) in a short distance near the explosive-water interface. Consequently, in this study emphasis was placed upon the use of explosives known to possess long reaction zone lengths and especially those whose characteristic impedances very nearly equalled the shock impedance of water, thus assuring that the impedance mismatch equation represented a good approximation for the pressure in the explosive.

The explosives included in this study were pelleted TNT of standard Tyler mesh sizes, -4+6, -6+8, -8+10; -48+65 granular TNT; and cast 50/50 amatol. Also included here are measurements made by Bauer<sup>(17)</sup> for the "blasting agents", 94/6 AN/fuel oil and the coarse TNT and Composition B "slurries"<sup>(18)</sup>, because the reaction zone lengths of blasting agents are quite likely among the greatest of all detonating explosives. Also additional measurements are included for explosives of much shorter reaction zone length, namely granular RDX, granular RDX-salt, cast TNT, cast 65/35 baratol, 50/50 pentolite, Composition B, HBX-1, and a special explosive X. Measurements of this sort have been presented previously for pentolite, Composition B, TNT and tetryl by Cook, Pack and McEwan.<sup>(16)</sup>

Except for a study with Composition B and one with a special explosive X where charge length was varied to observe transient effects of pressure vs charge length the charge lengths used in this investigation were all at least four charge diameters in order to insure that the detonation velocity was constant before the detonation front reached the end of the charge. In the case of the pelleted TNT and the blasting agents, all of which possessed long reaction zone lengths, the charge diameters were varied between values extending in some cases from the critical diameter to a diameter sufficiently large for the detonation velocity to be nearly ideal.

## Results

### (a) Shock parameter determinations

Table I presents the experimental shock velocity, free surface velocity, particle velocity ( $W = V_{fs}/2$ ) and pressure results for water. In Fig. 4 are plotted the experimental points with pressure as the ordinate and shock velocity as the abscissa. Fig. 5 presents a similar plot in which the low pressure part of the curve of Fig. 4 has been expanded to a larger scale. On both figures the smooth curve through the points represents an approximate best fit as "drawn by eye" to the data. Velocity-pressure values from this curve of best fit are given in Table II and represent the most reliable values.

Results of Snay and Rosenbaum,<sup>(8)</sup> and Walsh and Rice<sup>(11)</sup> also are plotted in Fig. 4. Note that Snay and Rosenbaum's results agree with the results of the present study at pressures up to about

Table I: Experimental shock parameter data for water  
(20°C ± 5C°)

Shot No.*	Shock Velocity (m/sec)	Free Surface Velocity (m/sec)	Particle Velocity (m/sec)	Shock Pressure (kilobars)
170	1630	143	72	1.16
182	1710	229	115	1.96
167	1810	355	178	3.21
168	1890	377	189	3.57
178	1780	360	180	3.20
179	1820	368	184	3.35
169	2050	556	278	5.70
177	2070	550	275	5.69
176	2110	605	303	6.38
29	2410	940	470	11.3
40	2260	900	450	10.2
41	2300	920	460	10.6
174	2800	1010	505	14.1
175	2760	1020	510	14.1
171	3540	1600	800	28.3
199	3510	1780	890	31.2
21	3680	1740	870	32.0
187	4000	2150	1080	43.0
6	4330	2750	1380	59.8
19	4240	2830	1420	60.0
193	4250	3160	1580	67.2
195	4490	3080	1540	69.1
194	4750	3130	1570	74.3
196	4720	3040	1520	71.7
5	4650	3160	1580	73.5
13	4810	3310	1660	79.6
32	4610	3080	1540	70.9
201	4930	3230	1620	79.6
202	4750	3230	1620	77.8
203	4750	3280	1640	77.9
17	4680	3420	1710	80.0
30	4900	3290	1650	80.6
204	5070	3540	1770	89.7
205	4900	3560	1780	87.2
206	4900	3570	1790	87.5
207	4870	3540	1770	86.2
200	4810	3380	1690	81.2
12	4960	3800	1900	94.2
	5070	3840	1920	97.3

\* Note: Shot number has been included for convenience of the writers.

Table I: Continued

Shot No.*	Shock Velocity (m/sec)	Free Surface Velocity (m/sec)	Particle Velocity (m/sec)	Shock Pressure (kilobars)
4	5080	3850	1930	98.0
190	5070	4200	2100	106
11	5470	4100	2050	112
189	5380	4210	2110	113
192	5530	4120	2060	114
213	5570	4110	2060	114
1	5480	4690	2350	128
2	5580	4440	2220	124
3	5320	4500	2250	120
10	5610	4400	2200	123
36	5420	4440	2220	120
37	5330	4490	2250	120
38	5410	4530	2270	122
34	5660	4730	2370	134
9	6050	4720	2360	143
183	6010	5040	2520	151
181	6130	4980	2490	153
184	6270	5090	2550	160
185	6200	5150	2580	160
186	6290	4980	2490	157

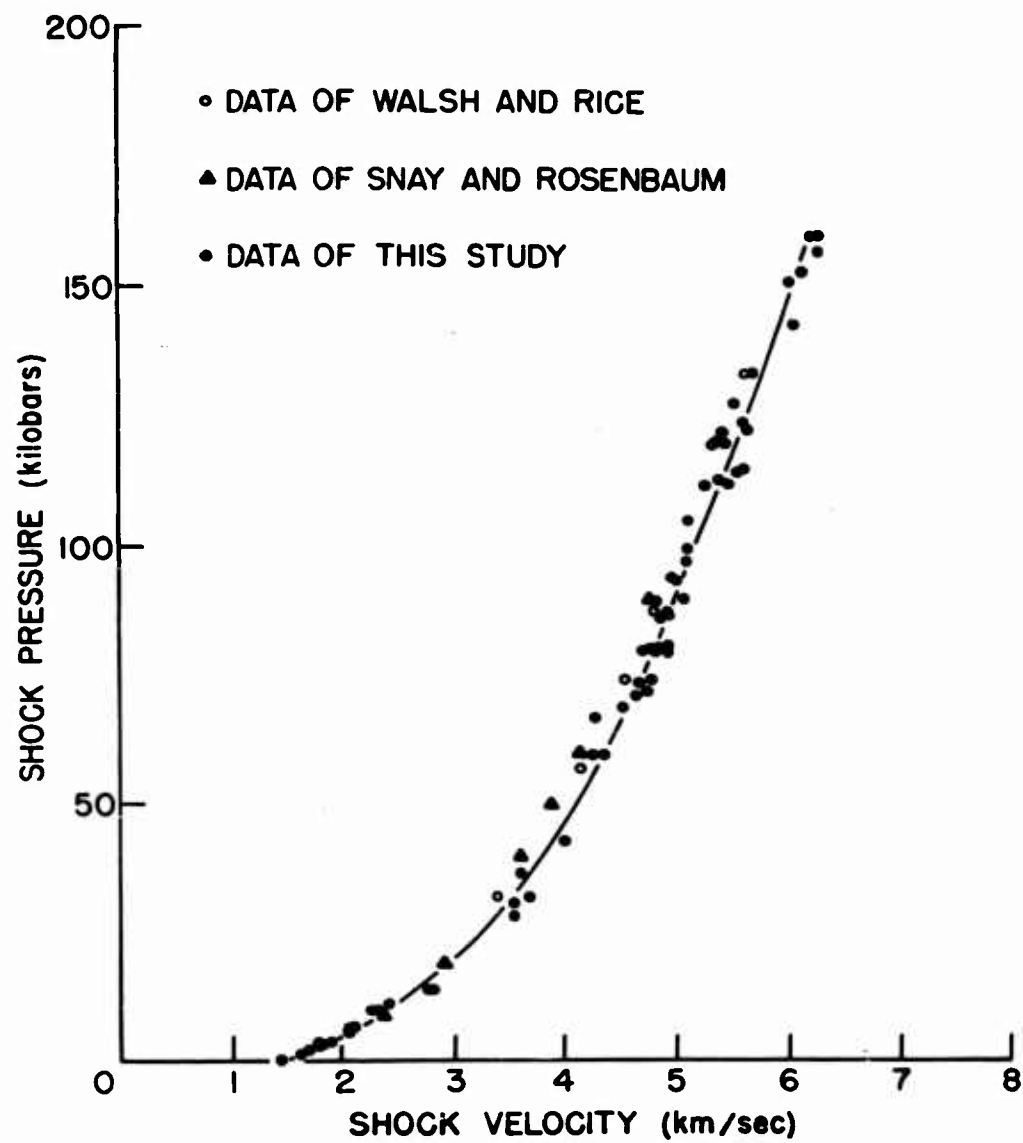


Fig. 4: Experimental shock velocity vs pressure data for water.

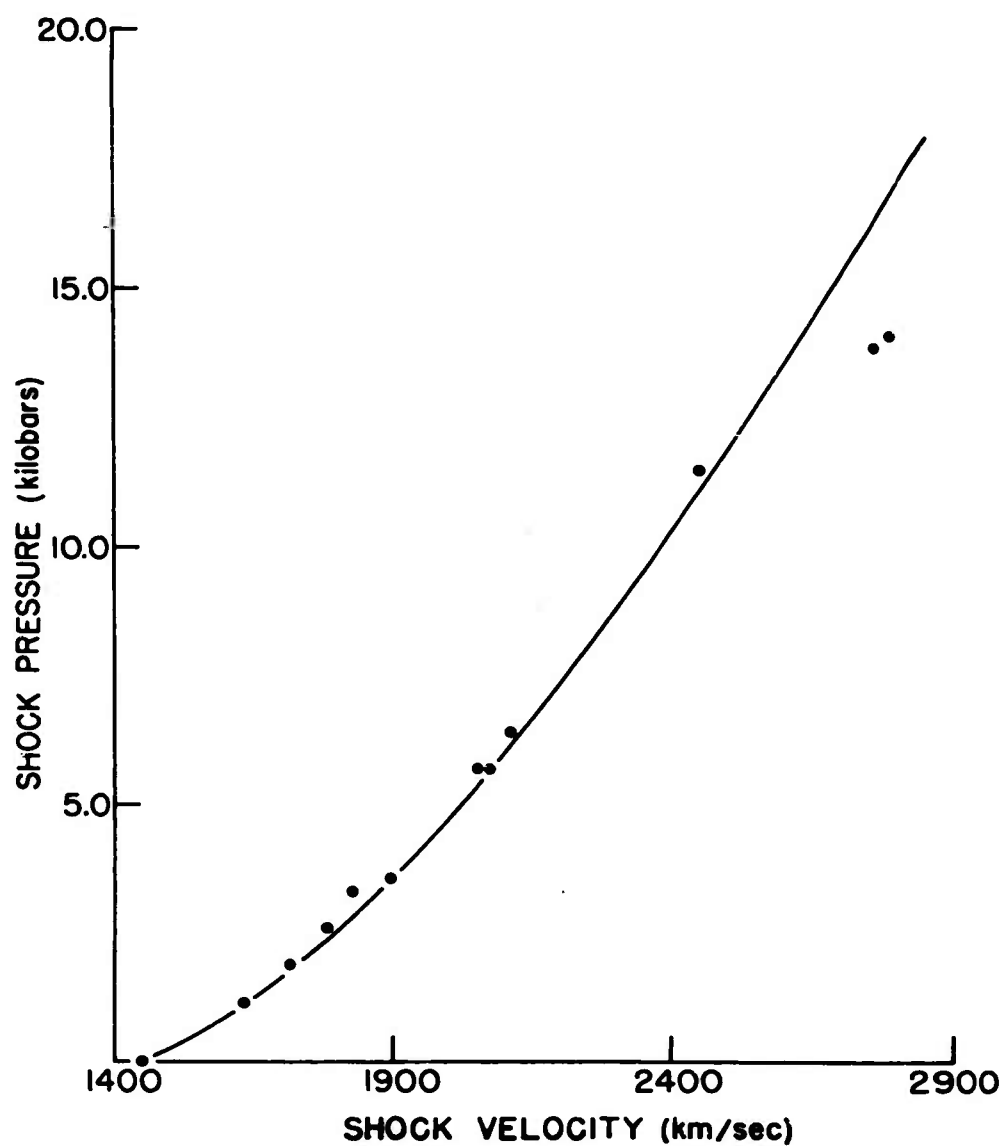


Fig. 5: Experimental shock velocity vs pressure data for water (low pressures).

Table II: Smoothed shock parameter results for water  
(20°C ± 5C°)

Shock Velocity (m/sec)	Shock Pressure (kilobars)	Shock Velocity (m/sec)	Shock Pressure (kilobars)
1450	Sonic	3450	30.0
1620	1.0	3820	40.0
1740	2.0	4120	50.0
1840	3.0	4350	60.0
1940	4.0	4570	70.0
2020	5.0	4780	80.0
2100	6.0	4980	90.0
2170	7.0	5170	100.0
2240	8.0	5350	110.0
2310	9.0	5530	120.0
2380	10.0	5700	130.0
2680	15.0	5870	140.0
2980	20.0	6040	150.0
		6200	160.0

10 kb, and from thence there is a tendency for their data to bear to the left showing that their results indicate a greater compressibility. The results of Walsh and Rice fall about midway between those of Snay and Rosenbaum and this study. The differences in compression between the results of Walsh and Rice, which should be more comprehensive than Snay and Rosenbaum's data, and the data of this study were 3.2% for a shock velocity in water of 3500 m/sec and 2.8% for a shock velocity of 5500 m/sec, corresponding to pressures of 31 kb and 125 kb, respectively. The disagreement in pressures at these two velocities amounts to 9.7% for the lower velocity and 4.2% for the higher one.

The agreement between the shock parameter data for water obtained by Walsh and Rice and the data of this investigation is reasonably good. One may conclude, therefore, that the Rankine Hugoniot curves for water are now known with sufficient accuracy that water may reliably be used as the transmission medium for the measurement of pressures in shock and detonation waves.

In Table III are listed shock-parameter results for lucite in the form of shock velocity vs shock pressure, the data being portrayed graphically in Fig. 6. No differentiation was made in either case as to which of the two methods was used to obtain a given  $p(V)$  point because the results of the two methods were indistinguishable within the limits of the experimental error involved. The smoothed results representing the most reliable values are given in Table IV. Note that in Fig. 6 the curve was not extended to the sonic velocity because it was found that considerable variation existed in values of sonic velocity available for lucite, and thus the true value was uncertain.

#### (b) Detonation pressure measurements

Results obtained for the military-type explosives in which the charge length was maintained at approximately 4 diameters to assure that the detonation wave was steady are listed in Table V. All the charges in this case may be considered to be unconfined, the cast charges being bare and the loose charges being contained in 1/16" thick pasteboard tubing. In Table V are listed the type explosive, the charge density, the charge diameter, the measured detonation velocity ( $D$ ), the initial velocity of the shock transmitted into water ( $V_t$ ), the initial pressure of the shock front in water ( $p_t$ ), the ideal or hydrodynamic velocity  $D^*$  corresponding to the given density, the pressure of the detonation wave or incident wave ( $p_i$ ) calculated through application of equation (1) (the impedance mismatch equation), the ideal detonation pressure calculated by means of thermohydrodynamic theory as outlined in Ref. 19, the ratio of pressure of the incident wave or detonation wave to ideal detonation pressure, and the  $(D/D^*)^2$  ratio.



Table III: Experimental shock parameter data for lucite.

Shock Velocity (m/sec)	Shock Pressure (kilobars)	Shock Velocity (m/sec)	Shock Pressure (kilobars)
3300	19	4000	33
3400	23	4000	35
3520	23	4400	48
3700	27	4620	59
3740	29	5370	105
3800	30	6040	134
3800	31	6200	166
3950	32	6360	169

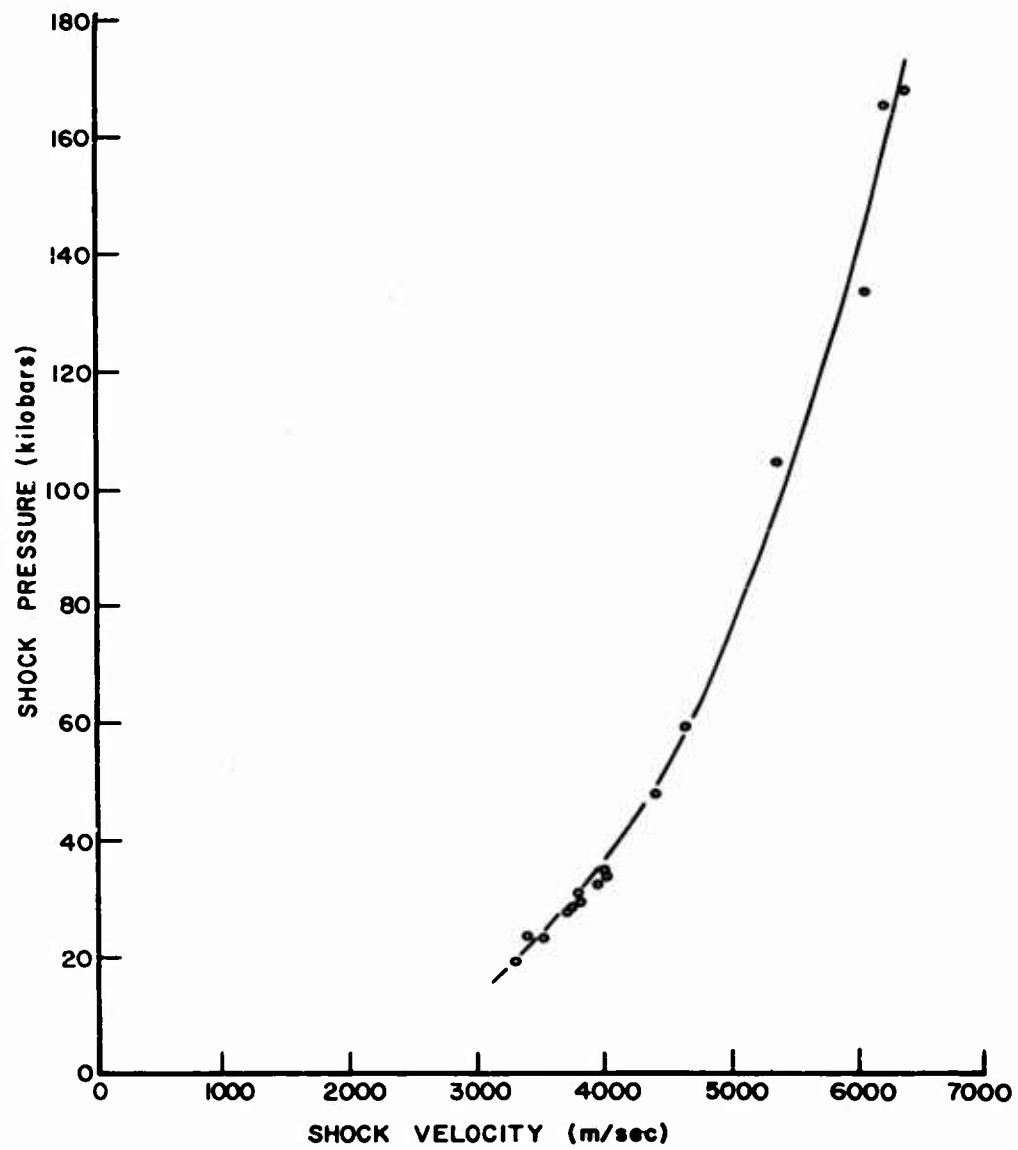


Fig. 6: Experimental shock velocity vs pressure data for lucite.

Table IV: Smoothed shock parameter data for lucite.

Shock Velocity (m/sec)	Shock Pressure (kilobars)	Shock Velocity (m/sec)	Shock Pressure (kilobars)
3350	20	5410	100
3820	30	5560	110
4160	40	5700	120
4430	50	5840	130
4670	60	5960	140
4880	70	6100	150
5070	80	6210	160
5250	90	6330	170

Table V: Experimental pressure measurement results for military type explosives

Explosive	$\rho_1$ (gm/cm <sup>3</sup> )	d <sub>exp</sub> (cm)	D (m/sec)	V <sub>t</sub> (m/sec)	P <sub>t</sub> (kb)	D* (m/sec)	P <sub>t</sub> (kb)	P <sub>1</sub> (kb)	P <sub>2</sub> (kb)	P <sub>1</sub> /P <sub>2</sub> <sup>*</sup>	(D/D*) <sup>2</sup>
RDX	1.10	1.25	5830	4640	75	6400	89	115	115	.78	.91
RDX	1.23	2.53	6410	5250	108	6850	135	145	145	.93	.90
RDX	1.17	2.53	6360	4760	80	6660	103	130	130	.79	.90
RDX	1.22	2.53	6535	5520	120	6830	147	142	142	1.02	.98
RDX	1.21	2.53	6610	5470	115	6800	141	139	139	1.01	.94
RDX	1.18	3.77	6750	4920	89	6730	118	130	130	.91	1.00
RDX	1.21	4.40	6665	5010	94	6800	123	139	139	.90	.96
RDX	1.21	5.05	6825	5325	113	6800	143	139	139	1.04	1.01
RDX	1.17	5.05	6750	5270	105	6670	131	130	130	1.01	1.00
RDX	1.17	5.05	6730	5400	112	6670	138	130	130	1.07	1.02
RDX	1.10	6.30	6400	5085	94	6370	112	115	115	.98	1.00
RDX	1.13	7.62	6620	5115	97	6550	119	122	122	.98	1.02
65/35 Ba(NO <sub>3</sub> ) <sub>2</sub> TNT	2.35	5.00	5150	4420	62	5600	116	156*	156*	.74	.85
HMX-1	1.75	5.00	7160	5485	116	7400	190	190*	190*	1.00	.94
50/50 NH <sub>4</sub> NO <sub>3</sub> TNT	1.58	4.80	5720	4860	84	6600	120	144	144	.84	.76
(AN #1)**											
50/50 NH <sub>4</sub> NO <sub>3</sub> TNT	1.53	4.80	5550	4610	72	6450	102	136	136	.75	.74
(AN #2)**											
50/50 NH <sub>4</sub> NO <sub>3</sub> TNT	1.58	7.62	6230	5160	100	6600	145	144	144	1.00	.89
(AN #1)**											
50/50 NH <sub>4</sub> NO <sub>3</sub> TNT	1.53	7.62	6040	4850	85	6450	121	136	136	.89	.94
(AN #2)**											
80/20 RDX Salt	1.32	2.53	5790	4850	85	6310	110	125	125	.88	.85
80/20 RDX Salt	1.30	4.40	6198	4925	87	6240	115	121	121	.95	.98
80/20 RDX Salt	1.28	5.00	6198	5000	92	6180	119	118	118	1.01	1.01
TNT -8+10 mesh	.95	5.05	3670	3810	40	4850	38	62	62	.61	.58
TNT -8+10 mesh	.95	5.05	3790	3906	43	4850	41.5	62	62	.67	.61
TNT -8+10 mesh	.97	7.62	4630	4080	49	4920	52	64	64	.81	.69

Table V: Continued

Explosive	$\rho_1$ (gm/cm <sup>3</sup> )	d <sub>exp</sub> (cm)	D (m/sec)	V <sub>t</sub> (m/sec)	P <sub>t</sub> (kb)	D* (m/sec)	P <sub>i</sub> (kb)	P <sub>2</sub> * (kb)	P <sub>i</sub> /P <sub>2</sub> *	(D/D*) <sup>2</sup>
TNT -8+10 mesh	1.01	7.62	4660	4395	62	5050	64	70	.91	.85
TNT -8+10 mesh	1.00	7.62	4711	4220	56	5010	59	68	.87	.88
TNT -8+10 mesh	.99	10.00	4765	4410	63	4960	65	66	.98	.92
TNT -8+10 mesh	1.01	10.00	4835	4272	58	5060	62.5	70	.88	.92
TNT -6+8 mesh	1.00	7.62	4505	4410	63	5010	64	68	.94	.81
TNT -6+8 mesh	.99	7.62	4507	4000	47	4980	50	67	.75	.82
TNT -6+8 mesh	1.01	10.00	4675	4420	63	5060	65	70	.93	.85
TNT -6+8 mesh	1.02	10.00	4966	4362	61	5100	66	72	.92	.96
TNT -6+8 mesh	.97	16.10	4880	4350	60	4880	63	63	1.00	1.00
TNT -4+6 mesh	1.00	7.62	4414	3865	43	5010	45.5	68	.67	.77
TNT -4+6 mesh	1.02	10.00	4669	4206	55	5090	59	72	.82	.85
TNT -4+6 mesh	1.01	10.00	4645	4365	60	5030	62	68	.91	.85
TNT -4+6 mesh	1.06	12.35	4995	4410	63	5200	69	77	.90	.92
TNT -4+6 mesh	1.00	15.9	4800	4480	65	5010	66	68	.96	.92
TNT -4+6 mesh	.99	25.3	4600	4425	64	4980	65	67	.97	.97
TNT -48+65 mesh	.80	2.53	3840	4075	49	4350	43	46	.93	.77
TNT -48+65 mesh	.87	2.53	3870	4080	49	4600	45	52	.86	.72
TNT -48+65 mesh	.86	3.77	4550	4045	47.5	4550	47	51	.92	.93
TNT -48+65 mesh	.87	3.80	4445	4225	54	4650	52	52	1.00	.93
TNT -48+65 mesh	.86	4.40	4385	4080	49.0	4550	47	51	.92	.93
TNT -48+65 mesh	.87	5.05	4550	4385	62	4550	59	52	1.00	1.10
TNT -48+65 mesh	.87	5.05	4580	4262	56	4600	54	52	1.00	1.04
TNT -48+65 mesh	.91	5.05	4430	3910	45	4750	46	57	.81	.86
TNT -48+65 mesh	.91	5.05	4680	3910	45	4750	47	57	.82	.96
TNT -48+65 mesh	.81	7.62	4400	3915	43	4350	41	46	.89	1.00
TNT -48+65 mesh	.86	7.60	4525	4400	62	4540	57	51	1.11	.99
Composition B***	1.71			5800	140		230	230	1.00	
50/50 pentolite**	1.65			5680	134		214	215	.995	

Table V: Concluded

Explosive	$\rho_1$ (gm/cm <sup>3</sup> )	$d_{exp}$ (cm)	D (m/sec)	$V_t$ (m/sec)	P (kb)	$P_t$ (kb)	D* (m/sec)	$P_i$ (kb)	$P_2^*$ (kb)	$P_i/P_2^*$	$(D/D^*)^2$
Tetryl***	1.50			5400	115			172	175	.982	
TNT***	1.58			5100	96			159	160	.994	
TNT***	.87			3600	34			37	42	.881	

\* Computed from  $P_2^* = (\rho D^2)/4$

\*\* AN #2 = 35 mesh

AN #1 was somewhat finer

\*\*\* Data from Ref. 16. (Detonation velocities were not measured. However, Composition B, 50/50 pentolite, pressed tetryl, and cast TNT should have propagated at ideal velocity.)

$\rho$  = average density of the explosive

D = measured detonation velocity

D\* = ideal or hydrodynamic value of detonation velocity

$V_t$  = initial velocity of shock wave in the transmitted medium (water)

$P_t$  = initial pressure of the shock wave in the transmitted medium (water)

$P_i$  = pressure of the wave in the incident medium (the explosive) calculated from the impedance mismatch equation in terms of  $P_t$

$P_2^*$  = Chapman-Jouguet value of the detonation pressure at ideal detonation velocity calculated from thermohydrodynamics.

Fig. 7 presents results for special explosive X in 5 cm diameter and Composition B in 4.8 cm diameter for which the charge length was varied from 1 cm to 6 cm to determine if a pressure-buildup effect existed in explosives of very short reaction zone lengths where one would expect no detonation velocity transient. These charges were all boosted with identical 1/2" x 1" pressed RDX boosters. With such short charges, however, difficulty was encountered in measuring the initial velocity of the shock wave in water because of a rapid attenuation in velocity of the shock in the aquarium. The plot of the results indicates, despite of the observed scatter, a small pickup in detonation pressure as the charge length was increased. Whether or not the detonation velocity increased slightly over this region in order to produce the pressure pickup could not be determined.

Data for the commercial blasting agents are given in Table VI through the courtesy of the Intermountain Research and Engineering Company, Salt Lake City, Utah. These results are given both for unconfined charges and charges confined in 3/8" thick or 1/4" thick steel tubing. One will note that the detonation velocity and pressure of the low density AN/fuel oil mix was very sensitive to confinement. In 5" diameter unconfined charges the detonation velocity was only 2770 m/sec which corresponded to a  $D/D^*$  ratio of only 0.66 while with 3/8" steel confinement in the same diameter the detonation velocity was 3930 m/sec corresponding to a  $D/D^*$  ratio of 0.94. The DBA series of coarse TNT or Composition B "slurries" were much less sensitive to confinement probably because their detonation pressure is much higher.

In comparing the measured values for pressure in the explosive, that is, pressures of the incident waves ( $p_i$ ) obtained by the aquarium technique, one will note that in every case where the detonation wave propagated at ideal velocity,  $p_i$  was found to agree within experimental error with the Chapman-Jouguet pressure  $p_2^*$ , i.e., to the detonation pressure calculated from thermohydrodynamic theory. A similar result was found in the study of Ref. 12. It should also be stressed that in most of the loose packed explosives the impedance match between the explosive and water was very good. Therefore, calculations of pressure in the incident medium in terms of pressure of the transmitted medium, through applications of the shock impedance mismatch equation, should be very reliable.

Since the pressure through a detonation wave is given by the relation  $p = \rho_1 DW$  one would expect that in non-ideal detonations the Chapman-Jouguet pressure, which is defined as the pressure at the surface in the wave ahead of which chemical reaction supports propagation and behind which chemical reaction lends no support, should be given by

$$p = (D/D^*)^2 p_2^* \quad (4)$$

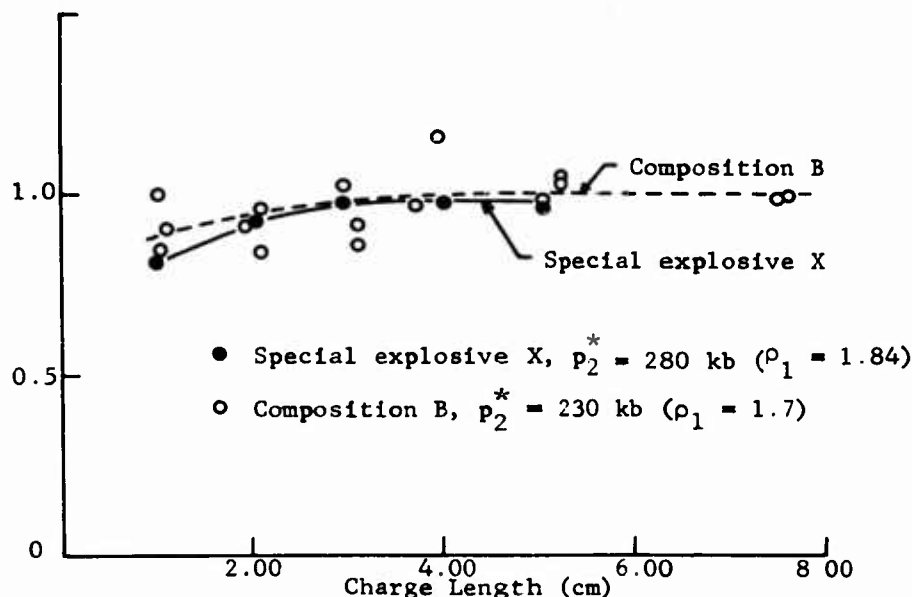


Fig. 7: Pressure of the detonation wave (measured by the aquarium technique) as a function of charge length for 5 cm diameter special explosive X and 4.8 cm diameter Composition B boosted with 1/2" x 1" pressed RDX.

where asterisks signify ideal values,  $p_2^*$  being the ideal detonation pressure. Equation (4) assumes that  $W/D$  depends only on  $\rho_1$  and not on  $D/D^*$ , an assumption well justified by the generality of the covolume-specific volume ( $\alpha[v]$  curve for high explosives)<sup>(19)</sup> Comparisons of  $(D/D^*)^2$  with  $p/p_2^*$  given in Tables V and VI indeed show a striking agreement in most cases.

Some very important information regarding the pressure or particle velocity profiles of detonation waves are also apparent from this study. According to the Zeldovich-von Neumann concept, which is based upon transport phenomena being negligible in a detonation wave, the pressure at the detonation front should be approximately twice the Chapman-Jouguet pressure. Then as chemical reaction proceeds the pressure decays along the Rayleigh line to the Chapman Jouguet value at the end of the reaction zone. For explosives of reaction zone length of the order of a few mm or less, e.g., Composition B, the presence of the von Neumann spike would be very difficult to detect. As mentioned earlier previous experiments to determine the pressure profiles through reaction zones by means of the aluminum free surface velocity technique were devoted primarily to explosives of very short reaction zone length, i.e., Composition B.



Table VI: Experimental pressure measurement results for commercial blasting agents

Blasting Agent	$\rho$ (g/cm <sup>3</sup> )	d (in)	Confine-ment	No. Measurements	D (m/sec)	V <sub>t</sub> (m/sec)	P <sub>t</sub> (kb)	D* (m/sec)	P <sub>i</sub> (kb)	P <sub>2</sub> * (kb)	P <sub>1</sub> /P <sub>2</sub> * (D/D*) <sup>2</sup>
94/6 AN/FO	0.82	5	None	3	2770±50	2550±70	12±.5	4200	13.5±1.0	40	0.34 0.43
94/6 AN/FO	0.82	5	Steel*	2	3930±20	3900±170	42.5±3	4200	37.5±1.5	40	0.93 0.88
DBA-1	1.52	5	None	5	4900±100	4000±100	46±3	6400	85±3	150	0.57 0.59
DBA-1	1.52	5	Steel*	1	5120	4720	77	6400	103	150	0.69 0.64
DBA-2	1.68	5	None	2	5500±100	4480±120	64±4	6800	97±5	180	0.54 0.66
DBA-2	1.60	5	Steel*	2	5270±70	4800±100	80±5	6500	111±10	155	0.71 0.66
DBA-3	1.58	5	None	4	5800±80	4600±200	71±10	6800	126±8	180	0.70 0.72
DBA-3	1.58	5	Steel*	2	6180±80	5530±190	125±10	6800	172±11	180	0.95 0.83
DBA-3	1.58	2	None	3	5300±100	4700±100	74±5	6800	101±5	180	0.56 0.63
DBA-3	1.58	2	Steel*	2	5885±15	5050±150	94±7	6800	134±6	180	0.75 0.75

\* Steel confinement was 3/8" tubing for 5" diameter and 1/4" tubing for 2" diameter

$\rho$  = average density of the explosive

D = measured detonation velocity

D\* = ideal or hydrodynamic value of detonation velocity

V<sub>t</sub> = initial velocity of shock wave in the transmitted medium (water)

P<sub>t</sub> = initial pressure of the shock wave in the transmitted medium (water)

P<sub>i</sub> = pressure of the wave in the incident medium (the explosive) calculated from the impedance mismatch equation in terms of P<sub>t</sub>

P<sub>2</sub> = Chapman-Jouguet value of the detonation pressure at ideal detonation velocity calculated from thermohydrodynamics.

Note: The plus and minus variations cover the spread in the experimental data.

This choice of explosive necessitated the use of very thin plates for which the free surface velocity measurements were in question. Since there is no reason to believe that an overpressure, if present, would exist in a rapidly reacting explosive and not in a slowly reacting one, it would seem prudent to look for evidence of a spike in slowly reacting explosives. The blasting agents listed in Table VI represent a class of explosives known to possess the longest reaction zones of the detonating type explosives and, according to any published theory, possess reaction zone lengths sufficiently great that a spike could easily be detected by the aquarium technique, but no evidence of a spike was observed. The coarse TNT series, especially -4+6 mesh TNT, also have reaction zone lengths which are ample for easy detection of a spike by the aquarium technique. And yet with -4+6 mesh TNT in 25.3 cm diameter, where the detonation velocity was in close agreement with the ideal value, and the impedance match was very good, the pressure of the incident wave corresponding to the initial velocity of the transmitted wave was found to equal the Chapman-Jouguet value.

Fig. 8 shows a streak camera trace illustrating the aquarium technique for measuring detonation pressures by transmitted shock waves in water. In this case the charge consisted of a slurry explosive detonated in a 5" I.D. steel tube. Note the slow attenuation of the velocity of the shock wave in water. This is typical of large charges which permits an accurate measurement of the initial velocity of the shock.

In conclusion, therefore, since even with explosives possessing the longest known reaction zone lengths, the aquarium technique measured the Chapman-Jouguet value of the detonation pressure, it appears that the highest pressure in the detonation wave is the Chapman-Jouguet pressure. This conclusion is strengthened by the fact that such results have been obtained in those cases where the characteristic impedance of the explosive very nearly equalled the shock impedance of the water under which condition computations from the impedance mismatch equation would be expected to be very reliable.

#### Acknowledgment

Appreciation is extended to Carl H. Christensen who assisted in experimental work and reduction of data for the studies of coarse TNT.

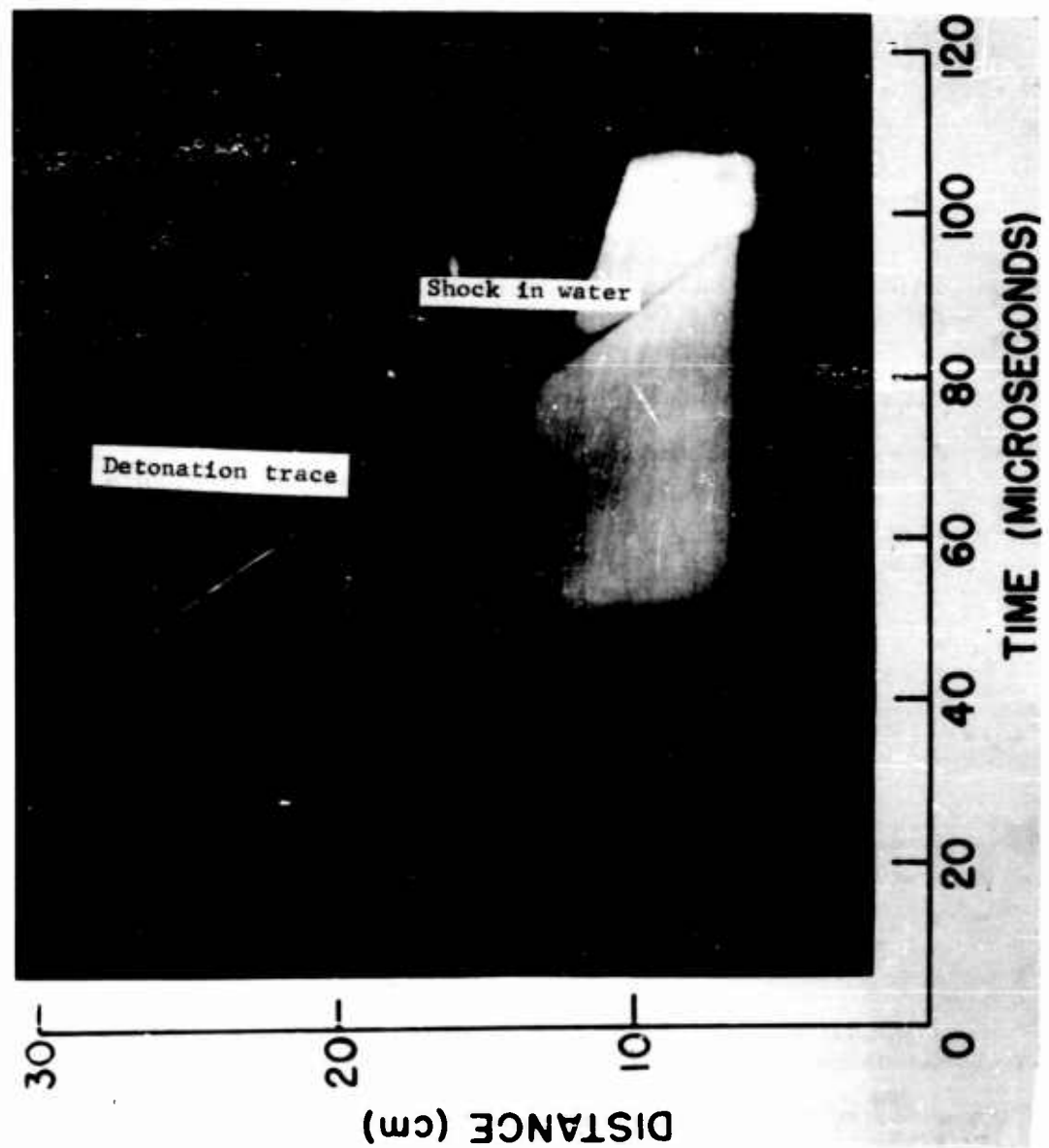


Fig. 8: Streak camera trace illustrating the aquarium technique for measurement of detonation pressure (explosive, slurry in 5" I.D. steel tube).

BIBLIOGRAPHY

1. J. G. Kirkwood and E. W. Montrall, "The Pressure Wave Produced by an Underwater Explosion II," OSRD No. 670, June 1942.
2. J. G. Kirkwood and J. M. Richardson, "The Pressure Wave Produced by an Underwater Explosion III," OSRD No. 813, August 1942.
3. J. M. Richardson, J. M. Arons, and R. R. Halverson, "Hydrodynamic Properties of Sea Water at the Front of a Shock Wave," J. Chem. Phys. 15, 785-794 (1947).
4. A. B. Arons and R. R. Halverson, "Calculations for Sea Water at the Shock Front," OSRD No. 6577, March 1946.
5. W. Doering and G. Burkhardt, "Contribution to the Theory of Detonation," HEC Accession List No. 60, Page 4, Bias Group.
6. P. W. Bridgman, "Water in the Liquid and Five Solid Forms under Pressure," Proc. American Academy of Arts and Sciences, 47, 441-558 (1912).
7. P. W. Bridgman, "The Phase Diagram of Water to 45,000 kg/cm<sup>2</sup>," J. Chem. Phys. 5, 964-966 (1937).
8. H. G. Snay and J. H. Rosenbaum, "Shockwave Parameters in Fresh Water for Pressures up to 95 Kilobars", NAVORD Report 2383, U.S. Naval Ordnance Laboratory, White Oak, Maryland, April 1952.
9. P. W. Bridgman, "Freezing and Compressions to 50,000 kg/cm<sup>2</sup>", J. Chem. Phys. 9, 794-797 (1941).
10. P. W. Bridgman, "Freezing Parameters and Compression of Twenty-One Substances to 50,000 kg/cm<sup>2</sup>," Proc. American Academy of Arts and Sciences, 74, 399-424 (1942).
11. J. M. Walsh and M. H. Rice, "Dynamic Compression of Liquids from Measurements in Strong Shockwaves", J. Chem. Phys. 26 (1957).
12. W. C. Holton, "The Detonation Pressures in Explosives as Measured by Transmitted Shocks in Water," NAVORD 3968, U.S. Naval Ordnance Laboratory, White Oak, Maryland, 1 Dec 1954.
13. R. E. Duff and E. Houston, "Measurement of the Chapman-Jouguet Pressure and Reaction Zone Length in a Detonating High Explosive," Second ONR Symposium on Detonation, Washington, D.C., February 9-11 (1955), page 225.

14. H. D. Mallory and S. J. Jacobs, "The Detonation Zone in Condensed Explosives," Second ONR Symposium on Detonation, Washington, D.C. February 9-11 (1955), page 240.
15. R. B. Clay, M. A. Cook, and R. T. Keyes, "Plate Velocities in the Impulse Loading by Detonation Waves," Preprint 9, Symposium on Shock Waves in Process Equipment, Annual Meeting, Chicago, Illinois, American Institute of Chemical Engineers, Dec 8-11, 1957.
16. M. A. Cook, D. H. Pack and W. S. McEwan, "Promotion of Shock Initiation of Detonation by Metallic Surfaces", Trans. Fara. Soc. No. 451, Vol. 56, Part 7, July 1960.
17. A. Bauer and M. A. Cook, "Observed Detonation Pressures of Blasting Agents", Submitted for publication in the Canadian Mining Journal.
18. M. A. Cook and H. E. Farnam, U.S. Patent No. 2,930,685, March 29, 1960.
19. M. A. Cook, "The Science of High Explosives," Reinhold Publishing Corporation, New York (1958).

## LOW PRESSURE POINTS ON THE ISENTROPES OF SEVERAL HIGH EXPLOSIVES

W. E. Deal  
University of California  
Los Alamos Scientific Laboratory  
Los Alamos, New Mexico

### Basic Principles

When a plane detonation wave travelling perpendicular to a plane explosive-air interface arrives at that interface, a shock is driven forward into the air by the expanding explosive reaction products and a rarefaction is reflected back through these reaction products. Assuming the detonation wave to be a shock followed by a reaction zone of rapidly decreasing pressure (von Neumann spike) terminating at the Chapman-Jouguet (C-J) plane which in turn is followed by the rarefaction wave from the rear of the explosive (Taylor wave), one might expect the air shock velocity to exhibit an initial value which decays rapidly\* followed by a region of more gradual decay. The state behind the air shock after decay of the von Neumann spike effect and before appreciable Taylor wave decay would correspond to expansion of the explosive reaction products from the C-J state\*\*. The interaction at the interface between the air and reaction products after decay of spike effects is shown in the pressure-particle velocity plane in Fig. 1. The coordinates of the intersection between the air shock Hugoniot and the reaction products isentrope in this plane are the pressure and particle velocity behind both the forward moving air shock and the backward

---

\* If, however, the rarefaction reflected into the explosive quenches the reaction, there will be a thin layer of unreacted explosive carried ahead of the reaction products. The interaction of this thin layer of unreacted or partially reacted explosive with the reaction products from the C-J state is analogous to the problem of a thin foil on the free surface of a moving thick plate of lower shock impedance. The thin layer equilibrates rapidly to the velocity of the thick pushing medium.

\*\* The C-J state may not be clearly defined for charges of finite length and diameter in which case the state at the terminus of the reaction zone is intended.

moving rarefaction wave into the reaction products (i.e., these two quantities are continuous across the interface). Determination of the pressure and particle velocity for the air shock thus gives a point on the reaction products isentrope from the C-J state.

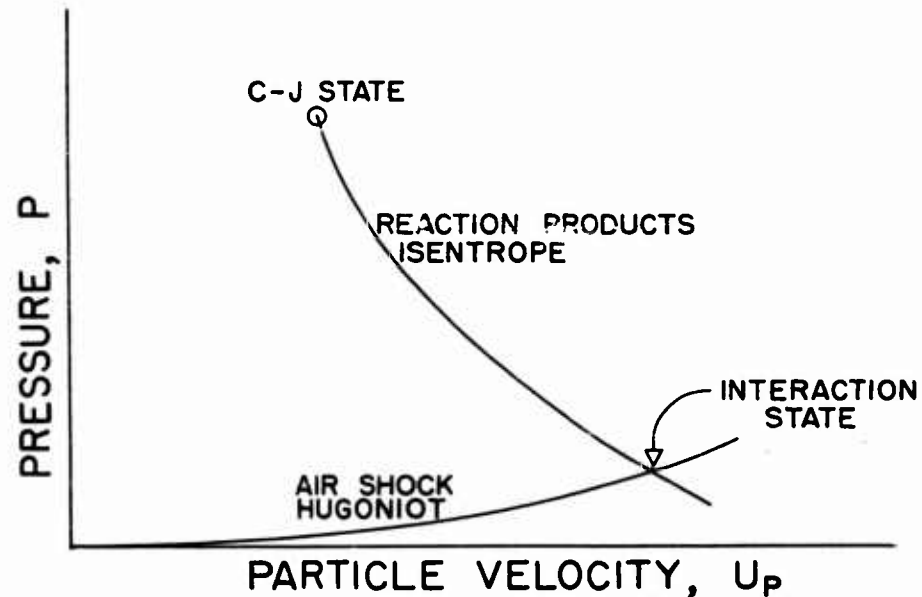


Fig. 1 - Interaction at Air-Reaction Products Interface

C-J pressures are of the order of 300 kilobars and the air shock pressures are of the order of one kilobar, consequently such determinations allow checking of an equation of state at two widely separated pressures. For a gamma-law equation of state (i.e.,  $P/\rho^\gamma = \text{const.}$ ), the  $P$ - $U_p$  isentrope from the C-J state is given by (1):

$$U_p = [P_{CJ}/(\alpha \rho_0 D)] [1 + \alpha - (P/P_{CJ})^\alpha], \quad 1$$

$$\text{where } \alpha = (\gamma - 1)/2\gamma, \quad 2$$

$$\text{and } \gamma = (\rho_0 D^2/P_{CJ}) - 1. \quad 3$$

Insertion of known values for explosive initial density  $\rho_0$  and detonation velocity  $D$  as well as pressure  $P$  and particle velocity  $U_p$  from air shock determinations yields gamma and C-J pressure  $P_{CJ}$  by successive iteration. These quantities may then be compared to values obtained from measurements in metals (2). Error analysis of these equations shows that a 1% error in  $U_p$  corresponds to very nearly 1% change in the calculated  $\gamma$  and 3/4% change in the calculated  $P_{CJ}$ .

### Experimental Technique

The explosive system for these experiments consisted of an explosive plane wave lens of 8-in. aperture which detonated a cylinder of the explosive to be studied on one end. The expansion of the reaction products from the opposite end of the cylinder after complete detonation then acted as the piston which drove the air shock. A schematic of the shot arrangement is shown in Fig. 2.

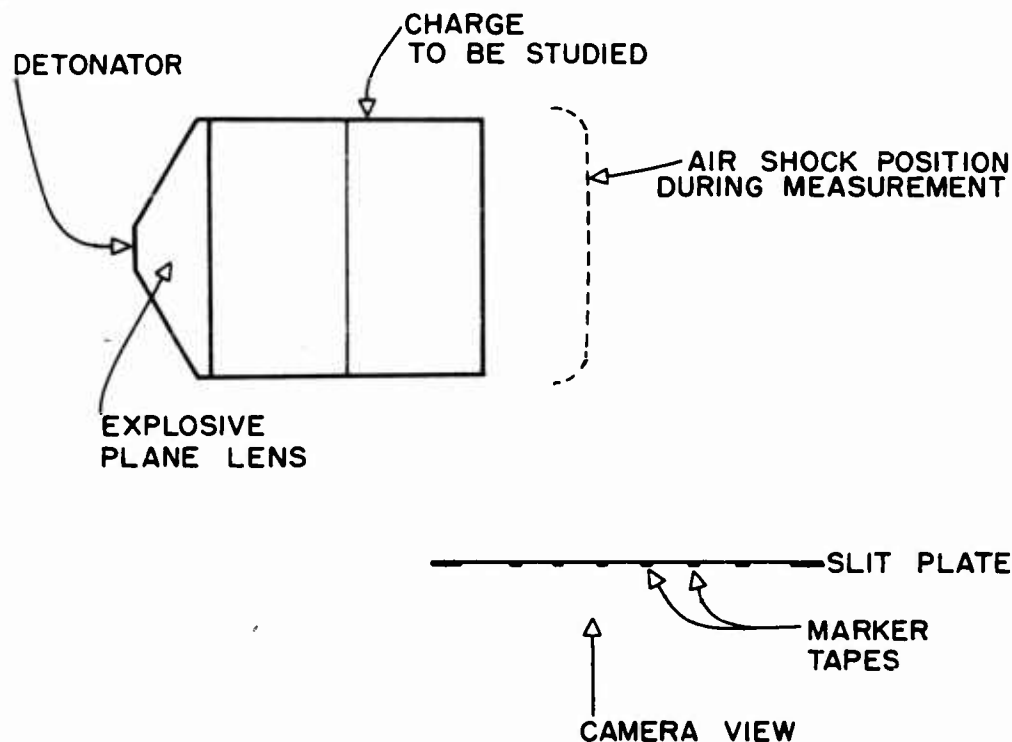


Fig. 2 - Schematic of Shot Arrangement

The velocity of this air shock was determined using a sweeping image camera to view the luminous\* shock through a slit

\* The use of the self-luminosity of the shock introduces uncertainties in measurements of rapidly varying shock velocity because of possible emission relaxation times long compared to the period of shock velocity change; however, results quoted here are for essentially steady state shocks as can be seen from the typical record shown in Fig. 3.



parallel to the direction of shock travel. An image of the slit with its scaling markers was swept on the film perpendicular to its length. The writing speed of the camera was adjusted to yield a trace angle of about  $45^\circ$ . A typical good quality record is shown in Fig. 3. The slope of the leading edge of luminosity along with camera demagnification and writing speed yield a value for the air shock velocity.

It is possible to deduce particle velocity from the shot record by use of the slope of the line of extinction of luminosity; however, because of effects at the explosive periphery, this edge is so much more diffuse than the leading edge that attempts to measure it were abandoned in favor of calculating it using an IBM 704 program (3) developed by Dr. R. E. Duff of this laboratory. The program was used to calculate shock parameters for an air mixture of 78.11, 20.96 and 0.93 mole percent of  $N_2$ ,  $O_2$ , and A respectively. Species  $N_2$ ,  $O_2$ , A, NO, N, O,  $N_2^+$ ,  $O_2^+$ ,  $A^+$ ,  $NO^+$ ,  $N^+$ ,  $O^+$ ,  $O^-$ , and electrons were included in the calculation. Thermodynamic functions given by F. R. Gilmore (4) were used. An individual calculation was performed for each shot; thus initial air temperature and pressure needed only to be measured for each experiment, not controlled.

Charges of 8-in. diameter and 8-in. thickness made up of two 4-in. layers were used in all experiments reported here. Three shots each were fired for charges of pressed TNT, Composition B, 77/23 Cyclotol, and Octol. Charge densities were obtained for the pieces fired; composition analysis, composition spread and density spread within a charge were obtained by sectioning charges prepared in an identical manner. These quantities are listed in Table I along with the other data.

Camera demagnification was obtained for each shot from a photograph of the slit plate by the shot camera with the image stationary. A correction was then applied to this demagnification value because the point of origin of the light in the shock front was behind the slit a small distance. Careful alignment of the axis of the charge relative to the optical axis of the camera was necessary such that these axes were perpendicular at the point in front of the charge where the precise measurement was desired. With an object distance of about 400 inches, variation of the point of light emission across the face of a 4-in. radius charge could cause as much as  $\pm 1\%$  variation in the demagnification factor. In fact, the air shock is not perfectly plane as is seen in the framing camera pictures of Fig. 4 and except for the very first motion this error could not be greater than  $\pm 0.5\%$ .

#### Data and Results

The coordinates of the leading edge of luminosity of the camera record were read with a two-axis comparator after first aligning the time direction with one axis. The slope of this edge was then determined by a linear least squares fit to the coordinates

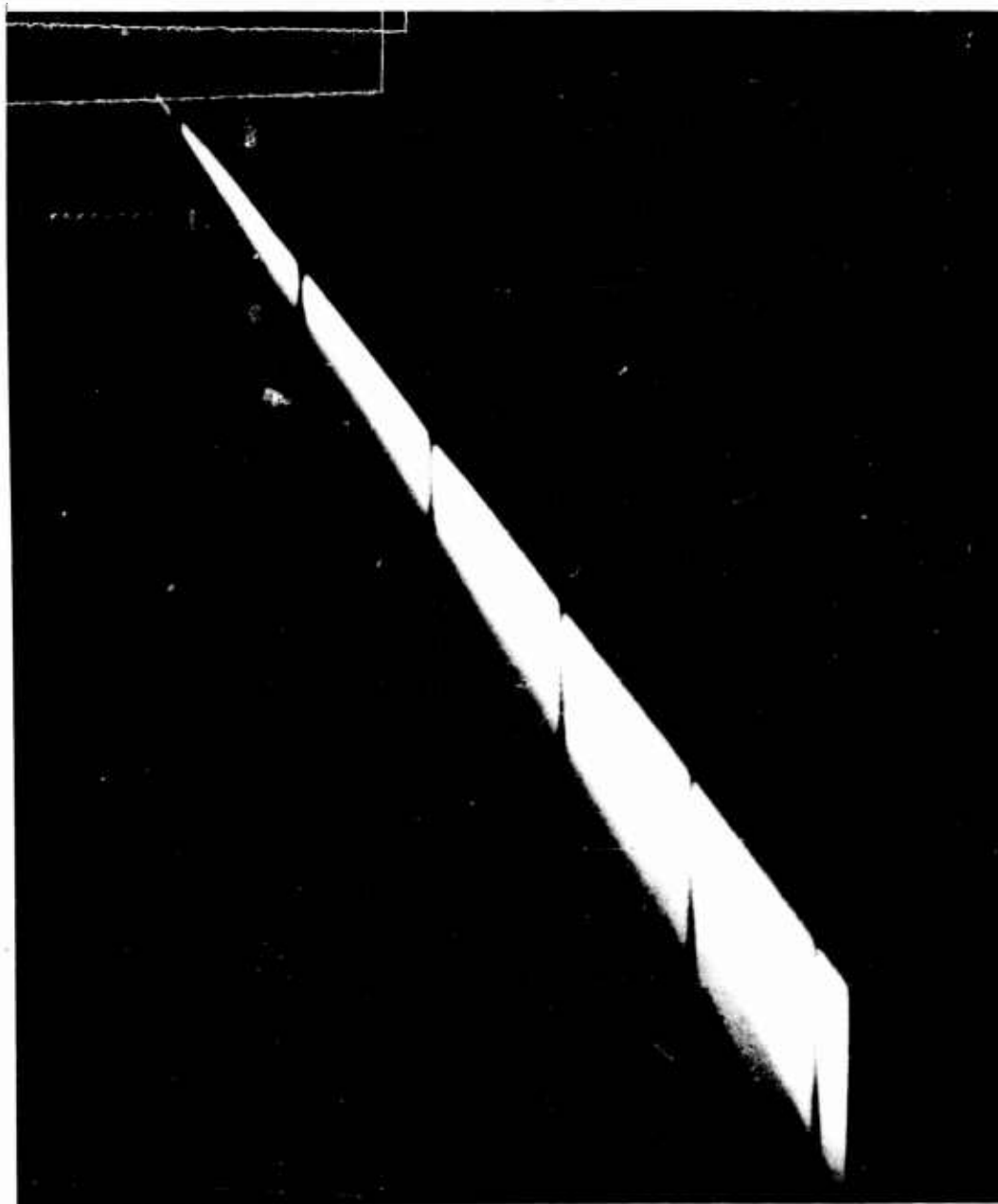


Fig. 3 - Typical good quality smear-camera record. Time increases downward; the air shock is moving from left to right. The gaps in the trace are from the fiducial tapes on the slit.

Table I - Results of Twelve Experiments

## A - Pressed TNT

Pure TNT

$$\rho_0 = 1.636 \pm .002 \text{ gm/cc}$$

$$D = .6932 \text{ cm/}\mu\text{sec.}$$

<u>Shot No.</u>	<u>T<sub>0</sub> °K</u>	<u>P<sub>0</sub> bars</u>	<u>U<sub>s</sub> cm/μsec</u>	<u>U<sub>p</sub> cm/μsec</u>	<u>P bars</u>
2172	285.7	.7959	.7340	.6708	478.4
2173	293.7	.8091	.7567	.6924	503.3
2174	297.2	.8091	.7417	.6781	477.6

## B - Grade A Composition B

62.8 ± 0.8% RDX

$$\rho_0 = 1.717 \pm .002 \text{ gm/cc}$$

$$D = .7985 \text{ cm/}\mu\text{sec}$$

2167	293.2	.7972	.8673	.7966	654.9
2168	292.7	.7972	.8699	.7990	660.0
2182	301.2	.8100	.8679	.7972	648.7

## C - 77/23 Cyclotol

77.0 ± 0.7% RDX

$$\rho_0 = 1.752 \pm .002 \text{ gm/cc}$$

$$D = .8274 \text{ cm/}\mu\text{sec}$$

2186	298.7	.8021	.8640	.7935	641.9
2190	293.7	.8014	.8763	.8050	671.0
2191	294.2	.8013	.8867	.8147	685.9

## D - Octol

77.6 ± 1.5% HMX

$$\rho_0 = 1.821 \pm .002 \text{ gm/cc}$$

$$D = .8494 \text{ cm/}\mu\text{sec}$$

2181	299.2	.8101	.8862	.8142	681.1
2184	295.2	.8099	.8777	.8063	676.9
2185	301.2	.8020	.9074	.8339	702.4

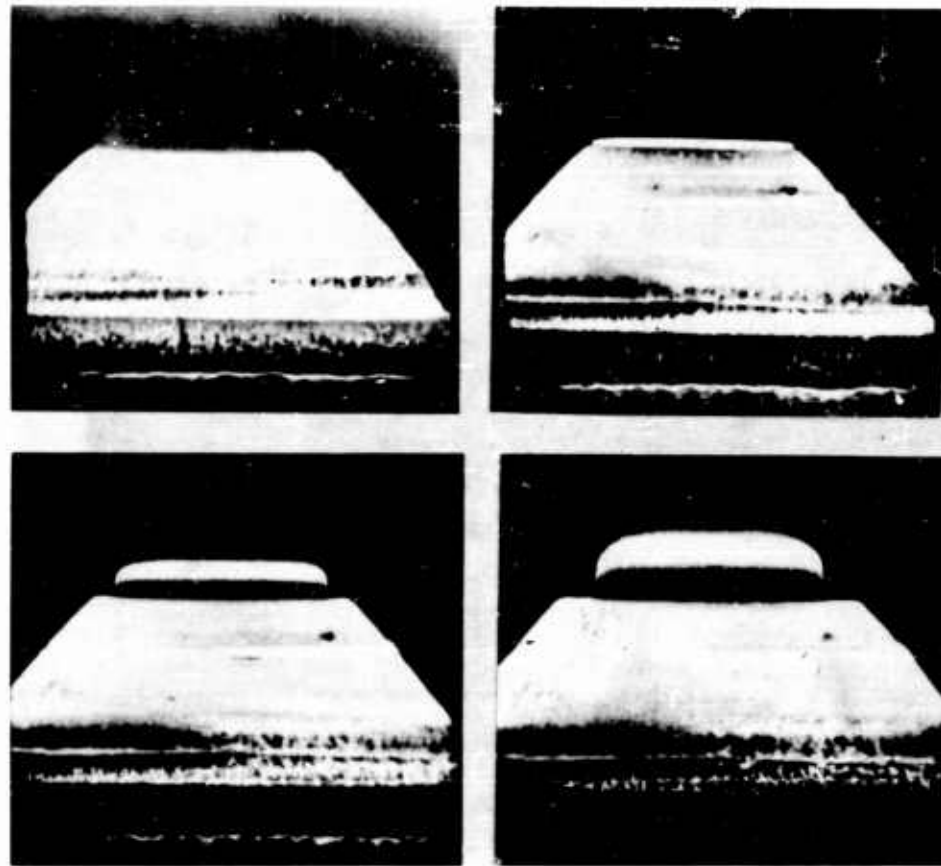


Fig. 4 - Four pictures selected from a framing-camera sequence of twenty-five. The time interval between the pictures shown is five microseconds. The detonation and shock waves are moving upward. The first picture shows the explosive before emergence of the detonation wave, the second shows the air shock within one microsecond after formation, and the third and fourth pictures show the air shock after 1.7 in. and 3.4 in. of further travel respectively.

after first deleting data for about the first 1/4-in. of motion where some evidence of curvature was seen and for distances greater than the charge radius where edge effects might affect the velocity. The resulting shock velocities ( $U_s$ ) are listed in Table I for the twelve shots (three shots for each of four explosives) along with initial conditions ( $T_o$ ,  $P_o$ ) and calculated particle velocities ( $U_p$ ) and shock pressures ( $P$ ). The detonation velocities given were calculated from experimental  $D-\rho_o$  relations obtained by previously described methods (5). The difference between the air shock velocities of Composition B given in Table I and that quoted in Reference 1 is due to the failure to apply a 5% parallax correction to the Reference 1 gas data. Insertion of values of  $P$ ,  $U_p$ ,  $\rho_o$ , and  $D$  from Table I into Equations 1, 2, and 3 yield  $\gamma$  and  $P_{cj}$  by successive iteration. The values so obtained are given in Table II and compared with values, corrected to the same density, obtained from measurements of the shock attenuation in dural (2).

The rather distinct difference in the TNT  $\gamma$  and  $P_{cj}$  obtained by the two methods indicates that assumption of constant  $\gamma$  equation of state to approximately 500 bars is not justified for TNT. The  $\gamma$  and  $P_{cj}$  from the two methods for the other three explosives agree rather well, however. It is indeed remarkable that the assumption of constant  $\gamma$  holds so well at these widely separated pressures, at least so far as hydrodynamic variables are concerned. While this agreement does not assure constancy of  $\gamma$  in the intervening region, the data of Reference 1 at eleven pressure points for Composition B prejudices one to expect constancy of  $\gamma$  in the intervening region for Cyclotol and Octol also.

Table II - Calculated  $\gamma$  and  $P_{cj}$  Compared with Dural Data

## A - Pressed TNT

	Shot No.			Average	Ref. 2	% Differ- ence
	<u>2172</u>	<u>2173</u>	<u>2174</u>			
$\gamma$	2.794	2.704	2.765	$2.754 \pm 1.4\%$	3.172	-13.2
$P_{cj}$ (kb)	207.2	212.2	208.8	$209.4 \pm 1.0\%$	188.4	+11.1

## B - Composition B

	Shot No.			Average	Ref. 2	% Differ- ence
	<u>2167</u>	<u>2168</u>	<u>2182</u>			
$\gamma$	2.714	2.707	2.714	$2.712 \pm 0.1\%$	2.769	-2.1
$P_{cj}$ (kb)	294.7	295.3	294.7	$294.9 \pm 0.1\%$	290.4	+1.5

## C - Cyclotol

	Shot No.			Average	Ref. 2	% Differ- ence
	<u>2186</u>	<u>2190</u>	<u>2191</u>			
$\gamma$	2.831	2.789	2.753	$2.791 \pm 1.1\%$	2.798	-0.3
$P_{cj}$ (kb)	313.1	316.6	319.6	$316.4 \pm 0.9\%$	315.8	+0.2

## D - Octol

	Shot No.			Average	Ref. 2*	% Differ- ence
	<u>2181</u>	<u>2184</u>	<u>2185</u>			
$\gamma$	2.836	2.864	2.769	$2.823 \pm 1.4\%$	2.844	-0.7
$P_{cj}$ (kb)	342.5	340.0	348.6	$343.7 \pm 1.0\%$	341.8	+0.6

\* This explosive was not reported in Reference 2 but data were obtained in the identical manner described there.

References

1. W. E. Deal, Phys. Fluids 1, 523 (1958).
2. W. E. Deal, J. Chem. Phys. 27, 796 (1957).
3. IBM 704 Code HUG.
4. F. R. Gilmore, Rand Corp. Report No. RM 1543 (1955).
5. Campbell, Malin, Boyd, and Hull, Rev. Sci. Instr. 27, 567 (1956).

## STRONG SHOCKS IN POROUS MEDIA \*

James L. Austing

H. S. Napadensky

R. H. Stresau \*\*

J. Savitt

Armour Research Foundation

Chicago 16, Illinois

### INTRODUCTION

Various theories have been advanced to explain qualitatively the complex phenomena encountered in the detonation process. The most widely quoted of these theories is that proposed by von Neumann (1). This theory makes the argument that the initial shock at the detonation front is a non-reactive one in which the explosive is compressed to a high pressure-density point on the Hugoniot curve for the unreacted explosive. Then there follows a period of chemical reaction in which each of the intermediate unreacted explosive-reaction product mixtures follows the Rankine-Hugoniot assumptions. Such a theory gives rise to a pressure spike in the detonation head, and this pressure in the non-reactive shock is higher than the Chapman-Jouguet pressure at the end of the reaction zone. While this theory is broadly accepted, some investigators have failed to observe the predicted spike. Cook (2), for example, has proposed an alternate mechanism, particularly for gaseous explosives. This mechanism suggests that the initial shock compresses the explosive to a pressure equal to that of the Chapman-Jouguet point. Then the pressure across the reaction zone is equal to the Chapman-Jouguet pressure, due to a high thermal conductivity in the reaction zone itself. Similar reasoning is then extended to solid explosives, and data are presented which seem to support the contention that there is no spike in the detonation head.

Some of the investigators who have detected the von Neumann spike have found variations in its shape. For example, Mallory and Jacobs (3) detected a plateau in the spike for TNT which they interpreted as an indication that the reaction proceeded at an appreciable rate only after an inception period. This was evidence that the reaction in TNT proceeds according to a thermal mechanism. On the other hand, Duff and Houston (4) observed a sharply peaked pressure profile for Composition B with no evidence of a plateau. This was

\*Supported by U.S.A.E.C. under Contract No. AT(11-1)-528

\*\*Consultant, 7 Summit Road, Lake Zurich, Illinois



an indication that the reaction is essentially a surface burning reaction. Other investigators may find different profiles in the reaction zone, depending on the types of explosives studied and the experimental techniques used.

It is readily seen that there are differing views as to which model correctly predicts the behavior of the detonation process. All of these models are based on purely speculative reasoning which in some cases appears to be supported by adequate experimental evidence. But in the past the conclusions which were made on the basis of evidence from these various experiments have been contradictory, and this in turn leads to the different detonation models. At this point we should ask ourselves why has it not been possible to predict an adequate model which is based on fundamental considerations and which ties together all facets of experimental data. One reason for this is the complete lack of quantitative equations of state for unreacted explosives, particularly solid explosives. But in attempting to arrive at a reasonable equation of state, the porosity of the medium must not be ignored. Therefore, an experimental technique which enables us to obtain data for the derivation of an equation of state for a porous material, we believe, should be extended to the application of determining equations of state of unreacted solid explosives.

For the past several years, Armour Research Foundation has been engaged in a fundamental research program in the field of nuclear reactor safety. This program has resulted in the development of an experimental technique to observe the dynamic response of porous media used in the design of blast shields for nuclear reactors. Various porous materials such as Flintkote Insulboard, pine, maple, and redwood have been studied at high rates of loading by means of this technique. However, this paper is concerned entirely with data on the Flintkote. A Hugoniot curve has been constructed based on the data obtained from the propagation of the shock wave in the medium. This curve, together with basic thermodynamic identities, has led directly to the calculation of the temperature rise across the shock front. The combination of the Hugoniot curve and the temperature data provides the necessary information from which an equation of state of the Insulboard material may be derived. We recognize that these data in themselves have no direct bearing on the behavior of explosives. However, the results we have obtained are of interest at a meeting of this type because in some ways Flintkote is similar to a solid explosive, especially with respect to its porosity.

#### EXPERIMENTAL TECHNIQUE

Shocks in porous media such as Flintkote and wood have been observed by means of an experimental technique which also allows us to obtain the dynamic stress-strain data of these materials at very high rates of loading. A schematic diagram of the experimental arrangement is shown in Fig. 1. Essentially, the experimental set-up consists of a cylindrical porous specimen on which a reference grid is painted. The specimen rests between a very heavy steel anvil and a cylindrical aluminum or steel plate, weighing anywhere from one to twelve pounds, as shown in Portion A of Fig. 1. We have referred to this plate as the "driving plate". The top of the driving plate contains a cup into which a low density charge of loose tetryl is loaded. The initiation system is supported six to eight inches above the tetryl charge, and consists of an electric blasting cap and a tetryl pellet which rests on an aluminum sheet. The aluminum sheet serves as a source of fragments to insure a more or less uniform plane wave initiation of the tetryl charge.

We will return to Fig. 1 shortly, but it is of interest to observe photographs of the set-up first. Figure 2 shows a typical specimen and its reference grid. The specimen in this instance is 1/2 inch thick pine. Figures 3 and 4 are photographs which depict the set-up in its various stages of assembly. Figure 3 shows a 1-inch thick specimen mounted between the anvil and the driving plate, with the tetryl charge on top of the driving plate. Figure 4 shows the specimen and driving plate assembly mounted in a shield which prevents fragments and smoke from obscuring the reference grid on the specimen.

We will now return to Fig. 1. Here we see a schematic representation of the method which we have used to observe the dynamic response of these porous media. This consists of a smear camera, which contains a narrow slit which is cut in the direction of displacement and which is immediately in front of the film. The image of the reference grid is focused on this slit, and the film travels in a direction perpendicular to the direction of displacement of the driving plate. A suitable time interval reference mark is photographed onto the moving film, with the result that we are able to obtain a displacement-time record of the dynamic event. Figure 5 is a photograph of the entire experimental set-up. The smear camera and the associated gear for the timing mark and firing pulse are shown in this photograph. The driving plate is also clearly visible.

In each experiment then, the sequence of events is as follows: A 100-foot roll of film begins its travel through the camera, and after it has reached proper speed the blasting cap receives the firing pulse automatically from the gear used with the camera. The detonation of the tetryl pellet hurls a spray of fragments from the aluminum sheet toward the loose tetryl charge, as shown in Portion B of Fig. 1. The detonation of the loose charge

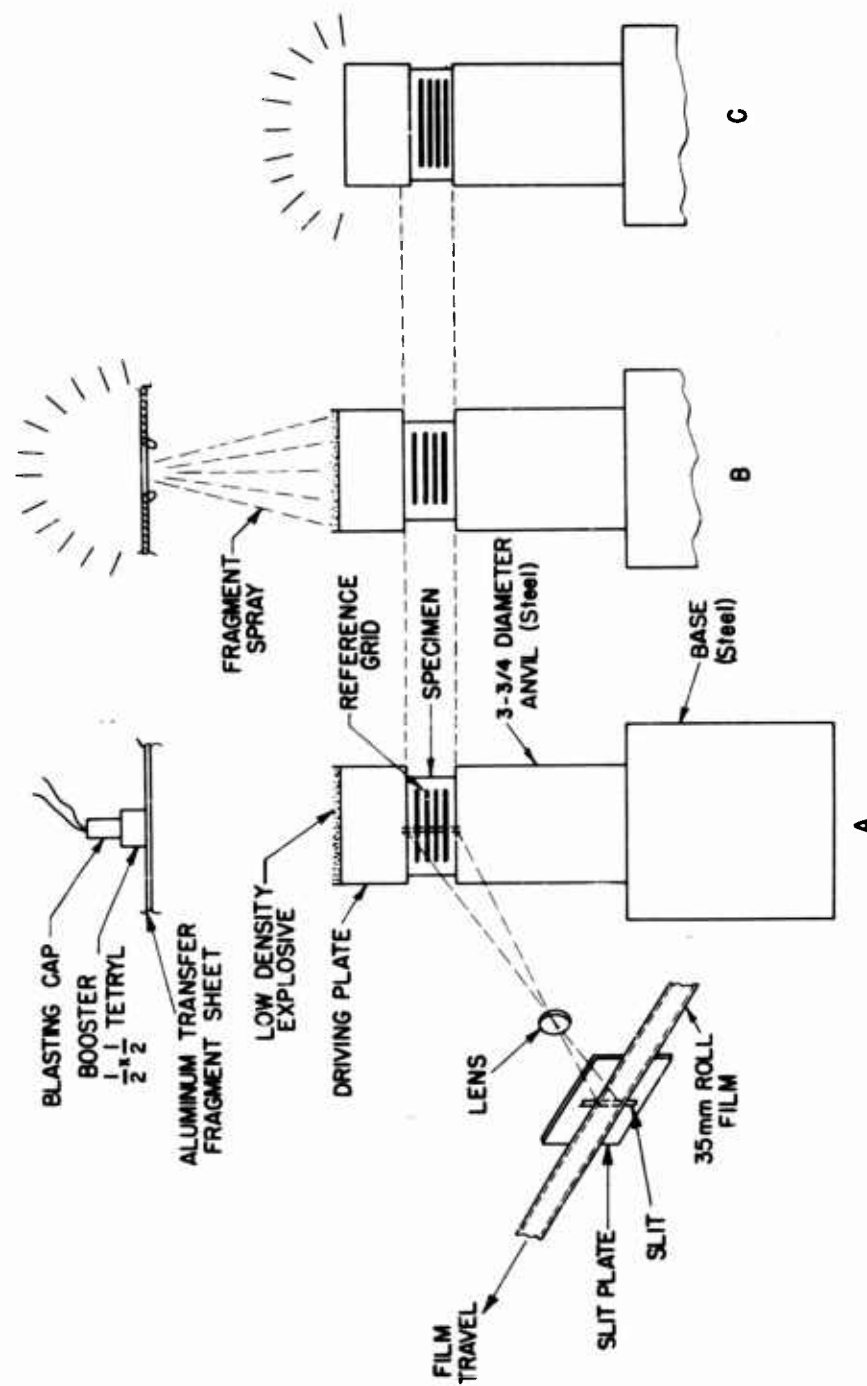


Fig. 1 - Test arrangement



Fig. 2 - One-half inch thick pine specimen showing reference grid

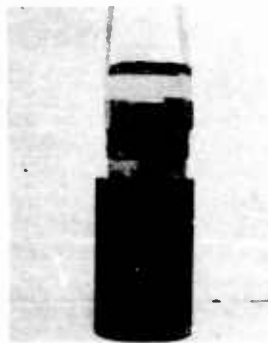


Fig. 3 - Specimen mounted between anvil and driving plate



Fig. 4 - Assembly of Fig. 3 mounted in fragment and smoke shield



Fig. 5 - The complete experimental set-up showing associated electronic gear

causes a nearly instantaneous acceleration of the driving plate, and the driving plate moves downward so as to compress the specimen, as shown in Portion C of Fig. 1. The specimen in turn resists this compression, so that eventually the driving plate comes to rest, at which time the specimen imparts an upward velocity to the driving plate. Figure 6 shows a 1/2-inch pine specimen, before and after compression.

#### TYPICAL RECORDS OBTAINABLE

At this point it is of interest to view some of the typical records which are obtained on the film of the smear camera. Such a record, for Flintkote-Insulboard, is shown in Fig. 7. In this figure, the bounds of the specimen, the lower bound of the driving plate, and the upper bound of the anvil have been clearly identified. The reference grid on the specimen enables us to observe the propagation of the shock wave, as well as multiple reflections of the shock wave. The driving plate reference lines are also apparent, and these are used to obtain a dynamic stress-strain curve for the material.

Figure 8 shows a typical smear record obtained for a pine specimen in which the grain was oriented for application of force radial to growth rings. Here, the shock wave travels at a much higher velocity than that through the Flintkote, and the multiple reflections are not apparent.

#### HUGONIOT CURVE AND EQUATION OF STATE

The data which can be obtained from these smear camera records which we have just considered enables us to construct a Hugoniot curve for the material, and from this it is possible to calculate the temperature rise across the shock front. This has been done for Flintkote-Insulboard, and the procedure which we have used will now be discussed.

The construction of the Hugoniot curve, first of all, is accomplished through the use of the well-known equations for conservation of mass and momentum across a shock front. These equations are, respectively:

$$\rho_0 D = \rho(D-u) \quad (1)$$

$$P = \rho_0 D u + P_0 \quad (2)$$

where:  $\rho_0$  is the density of the medium ahead of the shock front  
 $\rho$  is the density of the medium behind the shock front  
 $D$  is the velocity of the shock  
 $u$  is the particle velocity behind the shock front  
 $P_0$  is the pressure ahead of the shock front  
 $P$  is the pressure behind the shock front



Fig. 6 - One-half inch thick pine specimen  
before and after compression

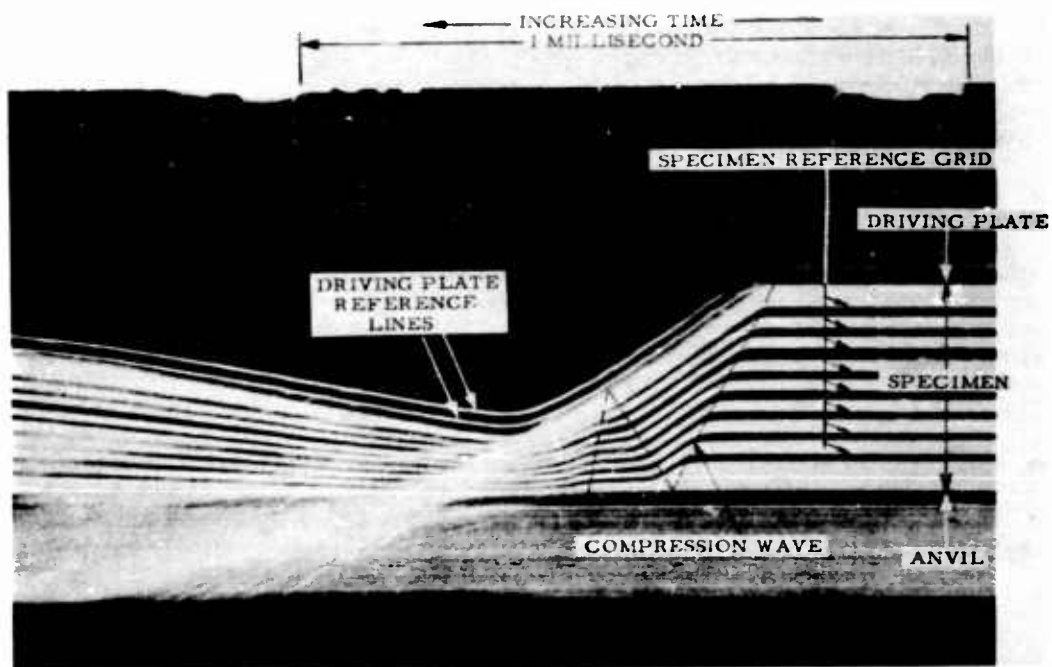


Fig. 7 - Smear camera record of the dynamic  
response of Flintkote insulboard

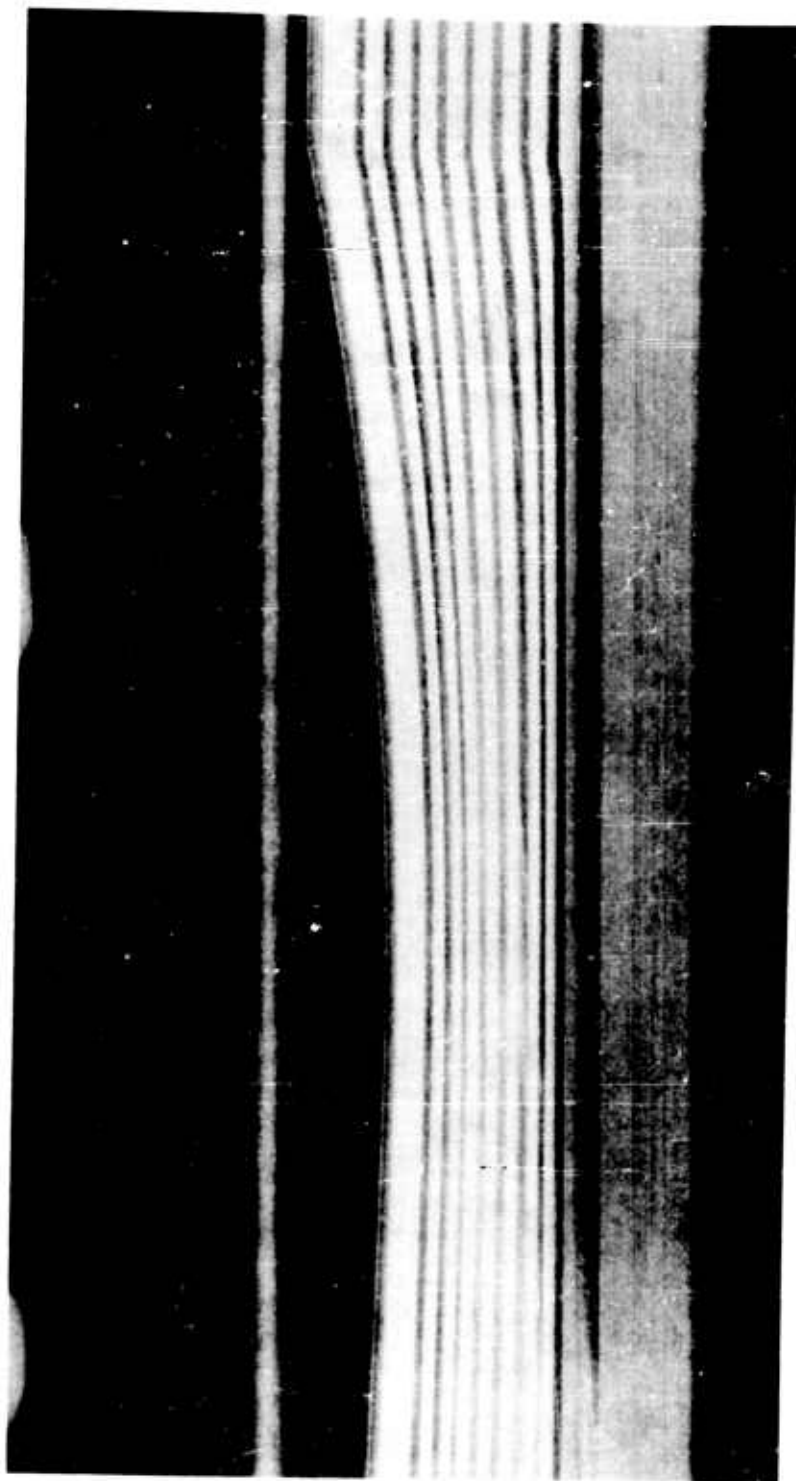


Fig. 8 - Smear camera record of dynamic response of pine, grain oriented for application of force radial to growth rings

These equations are in a form which assumes that the particle velocity ahead of the shock front is zero. In terms of specific volumes, Equation (1) becomes

$$\frac{V}{V_0} = \frac{D-u}{D} \quad (3)$$

where:

$V_0 (= \frac{1}{\rho_0})$  is the specific volume of the media ahead of the shock front

$V$  is the specific volume of the media behind the shock front

From each record, the shock velocity of the compression wave and the particle velocity behind the shock front can be calculated directly from the time-displacement slopes of the reference grid. These velocities then lead directly to the calculation of the relative volume  $V/V_0$  from Equation (3). If it is assumed that the initial pressure is atmospheric, the pressure  $P$  can be calculated from Equation (2) with the knowledge that  $\rho_0$ , the density of the medium ahead of the shock front, is also the density of the sample before being subjected to compression. This procedure has been employed for a whole series of records of experiments on Flintkote-Insulboard, and the resulting data points which determine the Hugoniot curves for the first shock are summarized in Tables I and II. On most records, the velocity of the shock wave appeared to be constant, but there seemed to be a rather random variation in the particle velocities as the shock wave propagated through the medium. We were unable to explain this. Consequently, the particle velocities as calculated are reported in the tables. This causes a corresponding variation in the pressure and relative volume.

The pressure-relative volume points in Tables I and II form the basis for the Hugoniot curve which is shown in Fig. 9. Each dotted line corresponds to one set of experimental points from one of these tables. As stated above, the unexplained variation in the particle velocity, together with the assumption of constant shock velocity, causes a corresponding variation in the calculated pressure and relative volume across the shock front, and this is reflected in the figure. For purposes of comparison, the curve for static compression of the medium is shown in Fig. 9 along with the Hugoniots. The static curve was calculated from load-deformation data which were obtained on a standard compression test machine.



TABLE I  
Hugoniot Data for First Shock in Flintkote Insulboard,  
1" Thick Specimens

Shot Number	Original Density, lb/in <sup>3</sup>	Shock Velocity, ft/sec	Particle Velocity, ft/sec	Pressure, psi	Relative Volume, $\frac{V}{V_0}$
52	0.0103	590	253	586	0.571
			249	577	0.578
			240	556	0.593
			240	556	0.593
			241	559	0.592
			241	559	0.592
			240	556	0.593
			240	556	0.593
			241	559	0.592
			232	539	0.606
			230	534	0.610
			228	529	0.613
			228	529	0.613
			234	543	0.602
			234	543	0.602
			226	525	0.617
			230	534	0.610
53	0.0105	565	184	421	0.674
			182	416	0.678
			184	421	0.674
			187	427	0.669
			186	425	0.671
			183	419	0.676
			180	412	0.681
			164	377	0.710
			167	383	0.704
			164	383	0.710
			167	377	0.704
			167	377	0.704
			168	385	0.703
			162	372	0.713
			170	390	0.699
			161	370	0.715
			174	399	0.692

TABLE I (Cont'd)

Shot Number	Original Density, lb/in <sup>3</sup>	Shock Velocity, ft/sec	Particle Velocity, ft/sec	Pressure, psi	Relative Volume, $\frac{V}{V_0}$
57	0.0102	467	53	107	0.885
			48	99	0.897
			45	94	0.903
			44	92	0.905
			45	94	0.903
			43	91	0.907
			46	96	0.900
			46	96	0.900
			47	97	0.898
			44	92	0.905
			44	92	0.905
			42	88	0.909
			43	90	0.907
			49	101	0.894
			44	92	0.905
132	0.0115	534	181	428	0.662
			169	401	0.684
			166	394	0.690
			162	384	0.698
			170	402	0.684
			172	406	0.679
			168	398	0.686
135	0.0113	542	126	301	0.786
			121	291	0.777
			116	278	0.787
			115	277	0.788
			117	282	0.784
			117	282	0.784
			117	282	0.784
			114	274	0.791
			137	328	0.747

TABLE I (Cont'd)

Shot Number	Original Density, lb/in <sup>3</sup>	Shock Velocity, ft/sec	Particle Velocity, ft/sec	Pressure, psi	Relative Volume $\frac{V}{V_0}$
136	0.0113	506	156	347	0.692
			157	349	0.690
			160	355	0.684
			162	360	0.679
			160	355	0.684
			158	351	0.688
			157	349	0.690
			156	346	0.692
			156	346	0.692
			160	355	0.684
			159	353	0.686
			157	349	0.690
			157	349	0.690
			157	349	0.690
			157	349	0.690
			157	349	0.690
			157	349	0.690
137	0.0113	519	75	177	0.856
			68	162	0.869
			68	162	0.869
			69	164	0.867
			69	164	0.867
			70	165	0.866
			67	161	0.870
			64	152	0.878
139	0.0116	528	52	126	0.901
			137	326	0.738
			136	325	0.738
			135	323	0.744
			133	317	0.749
			132	315	0.750
			131	314	0.754
			132	315	0.750
			132	315	0.750
			133	317	0.749

TABLE I (Cont'd)

Shot Number	Original Density, lb/in <sup>3</sup>	Shock Velocity, ft/sec	Particle Velocity, ft/sec	Pressure, psi	Relative Volume, $\frac{V}{V_0}$
140	0.0113	541	136	323	0.750
			130	310	0.760
			127	303	0.766
			124	297	0.771
			124	297	0.771
			124	297	0.771
			124	297	0.771
			124	297	0.771
			124	297	0.771
143	0.0114	443	65	136	0.855
			62	130	0.858
			65	136	0.855
			66	138	0.849
			65	136	0.855
			66	138	0.849
			65	136	0.855
			61	127	0.861
			65	136	0.855
			55	117	0.875
			57	122	0.868
			53	113	0.879
			55	117	0.875
			67	140	0.847
			67	140	0.847
			65	136	0.855
			65	136	0.855

TABLE II

Hugoniot Data for First Shock in Flintkote Insulboard  
1/2" Thick Specimens

Shot Number	Original Density, lb/in <sup>3</sup>	Shock Velocity, ft/sec	Particle Velocity, ft/sec	Pressure, psi	Relative Volume, $\frac{V}{V_0}$
54	0.0100	540	167	351	0.690
			175	367	0.676
			169	355	0.685
			177	372	0.671
			161	339	0.704
			162	341	0.699
			155	327	0.714
			160	337	0.704
			160	337	0.704
58	0.0103	692	220	600	0.681
			214	584	0.690
			199	544	0.712
			187	512	0.729
			181	496	0.738
59	0.0106	620	53	143	0.915
			52	142	0.916
			49	135	0.920
			48	133	0.921
			60	162	0.902
62	0.0104	845	25	94	0.970
			24	91	0.983
			27	102	0.968
			27	102	0.968
133	0.0112	564	162	395	0.713
			154	376	0.726
			152	372	0.730
			153	373	0.728
			148	360	0.737

TABLE II (Cont'd)

Shot Number	Original Density, lb/in <sup>3</sup>	Shock Velocity, ft/sec	Particle Velocity, ft/sec	Pressure, psi	Relative Volume, $\frac{V}{V_0}$
142	0.0112	528	122	284	0.769
			118	275	0.775
			118	275	0.775
			122	284	0.769
			135	312	0.746
			132	305	0.751
			135	312	0.746
			132	305	0.751
			131	303	0.752

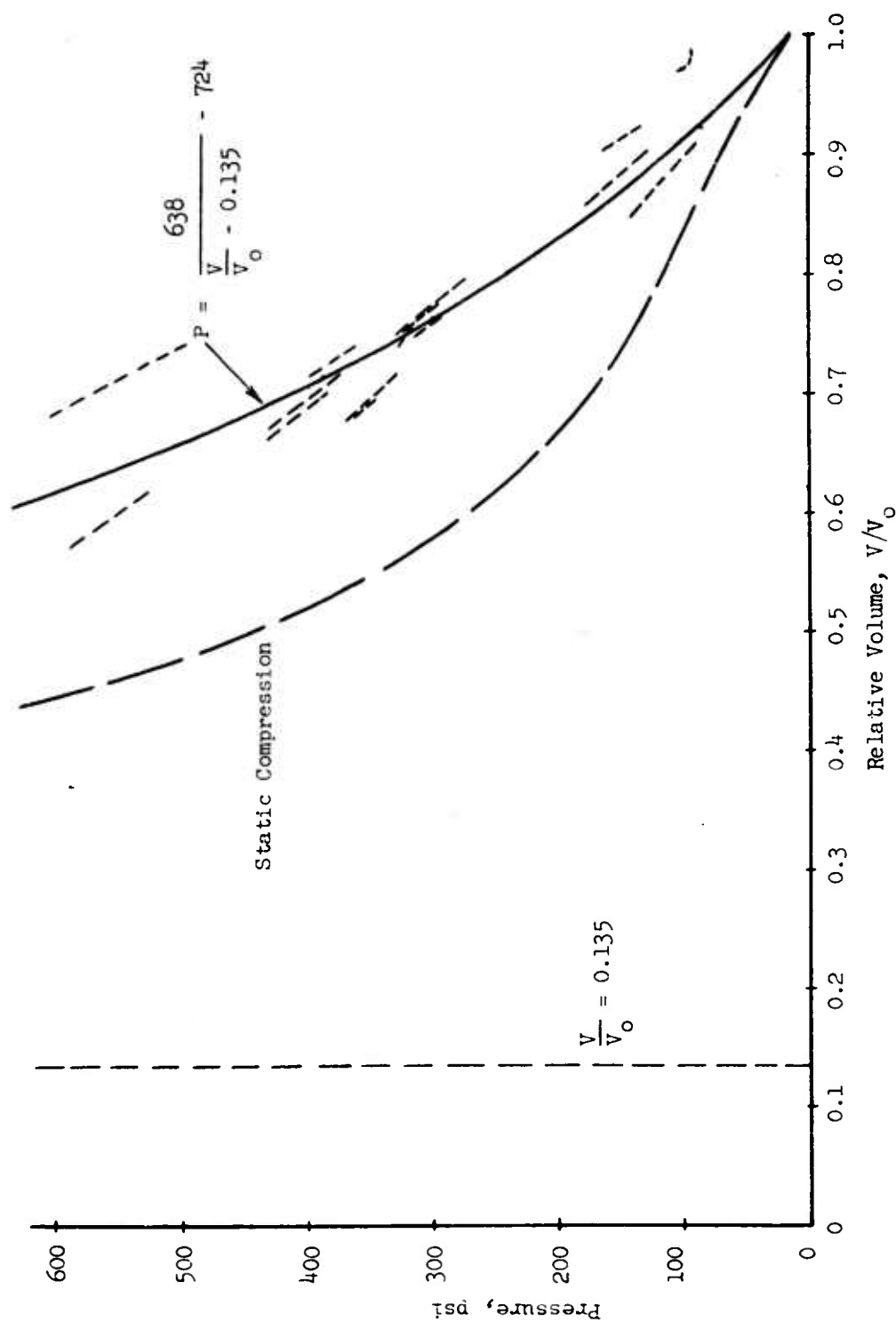


Fig. 9 - Curves of Hugoniot compression and static compression in Flintkote insulboard

Several considerations were involved in attempting to fit an equation through the experimental Hugoniot points: (1) Since a Hugoniot curve is a locus of end points on a shock compression, the curve must pass through the initial point ( $V/V_0 = 1$ ,  $P = 14$  psi) and a point which represents a reasonable average of the Hugoniot points; (2) the equation should have an asymptote at some finite relative volume between zero and one, since a porous material will approach a limiting density as the compressive stress increases to very high values; and (3) the equation should be as simple as possible. The static stress-strain data for Flintkote-Insulboard (the same data which are represented in Fig. 9) at very high stresses were used to calculate the relative volume asymptote, with the result that

$$\lim_{P \rightarrow \infty} \frac{V}{V_0} = 0.135$$

This is shown as a vertical dotted line in Fig. 9. To determine what mathematical function would best describe the experimental points, we attempted to rectify the data. In so doing we discovered that two types of plots yielded essentially straight lines. These included the plots of pressure  $P$  versus  $1/(V/V_0 - 0.135)$  and  $\log P$  versus  $\log(V/V_0 - 0.135)$ . Since the former of these plots was simpler and would yield a function with a relative volume asymptote, the equation of the Hugoniot was assumed to fit a hyperbola of the form

$$(P + a) \left( \frac{V}{V_0} - 0.135 \right) = k$$

Determination of the constants  $a$  and  $k$  showed that this equation is as follows:

$$P = \frac{638}{\frac{V}{V_0} - 0.135} - 724 \quad (4)$$

Equation (4) has been plotted in Fig. 9.

The method for the calculation of the temperature rise across the shock front was suggested to us in a published article by Walsh and Christian (5). We have used this method, but have derived the working equations in a slightly different manner\*. Our derivation begins by assuming that energy is a function of temperature and volume, that is

$$E = E(T, V)$$

---

\* The thermodynamic identities used in this derivation can be verified in any good thermodynamics text. For example, reference (6) is suggested.



from which

$$dE = \left( \frac{\partial E}{\partial T} \right)_V dT + \left( \frac{\partial E}{\partial V} \right)_T dV$$

$$dE = C_V dT + \left( \frac{\partial E}{\partial V} \right)_T dV \quad (5)$$

where  $C_V$  is the heat capacity at constant volume. From the first law of thermodynamics,

$$dE = TdS - PdV \quad (6)$$

Differentiating equation (6) with respect to volume at constant temperature, we have

$$\left( \frac{\partial E}{\partial V} \right)_T = T \left( \frac{\partial S}{\partial V} \right)_T - P \quad (7)$$

However, the thermodynamic identity

$$\left( \frac{\partial S}{\partial V} \right)_T = \left( \frac{\partial P}{\partial T} \right)_V$$

may be substituted into equation (7) with the result that

$$\left( \frac{\partial E}{\partial V} \right)_T = T \left( \frac{\partial P}{\partial T} \right)_V - P \quad (8)$$

Substitution of equation (8) into equation (5) results in

$$dE = C_V dT + \left[ T \left( \frac{\partial P}{\partial T} \right)_V - P \right] dV$$

from which

$$\frac{dE}{dV} = C_V \left( \frac{dT}{dV} \right) + T \left( \frac{\partial P}{\partial T} \right)_V - P \quad (9)$$

The Hugoniot equation for conservation of energy across a shock front is

$$E - E_0 = \frac{1}{2} (P + P_0)(V_0 - V)$$

Differentiating this equation, we obtain

$$\frac{dE}{dV} = -\frac{1}{2}(P + P_0) + \frac{1}{2}(V_0 - V)\left(\frac{dP}{dV}\right)_{\text{Hugoniot}} \quad (10)$$

Substitution of equation (10) into equation (9) results in the following differential equation:

$$\frac{dT}{dV} + \frac{\left(\frac{\partial P}{\partial T}\right)_V}{C_V} T = \left[ \left(\frac{V_0 - V}{2}\right)\left(\frac{dP}{dV}\right)_{\text{Hugoniot}} + \frac{P - P_0}{2} \right] \frac{1}{C_V} \quad (11)$$

Equation (4), the empirical Hugoniot equation, may be differentiated with respect to volume as follows:

$$\left(\frac{dP}{dV}\right)_{\text{Hugoniot}} = -\frac{638}{V_0 \left(\frac{V}{V_0} - 0.135\right)^2} \quad (12)$$

Equations (4) and (12) may be substituted into equation (11). If  $P_0$  is assumed to be equal to 14 psi, equation (11) reduces to the following:

$$\frac{dT}{dV} + \frac{\left(\frac{\partial P}{\partial T}\right)_V}{C_V} T = \left[ 319 \frac{\left(\frac{V}{V_0} - 1\right)}{\left(\frac{V}{V_0} - 0.135\right)^2} + \frac{319}{\left(\frac{V}{V_0} - 0.135\right)} - 369 \right] \frac{1}{C_V} \quad (13)$$

Equation (13) is a linear differential equation in which  $C_V$  is assumed to be constant, and in which  $\left(\frac{\partial P}{\partial T}\right)_V$  and

$$319 \frac{\left(\frac{V}{V_0} - 1\right)}{\left(\frac{V}{V_0} - 0.135\right)^2} + \frac{319}{\left(\frac{V}{V_0} - 0.135\right)} - 369$$

are functions of volume alone. For purposes of simplification, let

$$b = \frac{\left(\frac{3P}{T}\right) V}{C_V} \quad (14)$$

$$f\left(\frac{V}{V_0}\right) = 319 \frac{\left(\frac{V}{V_0} - 1\right)}{\left(\frac{V}{V_0} - 0.135\right)^2} + \frac{319}{\left(\frac{V}{V_0} - 0.135\right)^2} - 369 \quad (15)$$

so that equation (13) simplifies to

$$\frac{dT}{d\left(\frac{V}{V_0}\right)} + V_0 b T = \frac{V_0}{C_V} f\left(\frac{V}{V_0}\right) \quad (16)$$

where the differential  $d(V/V_0)$  has been introduced to put equation (16) into a form which is consistent with equation (15). To solve equation (16), it is necessary to introduce the integrating factor

$$e^{\int V_0 b d\left(\frac{V}{V_0}\right)} = e^{V_0 b \left(\frac{V}{V_0}\right)}$$

such that

$$\begin{aligned} \left[ e^{V_0 b \left(\frac{V}{V_0}\right)} \right] \frac{dT}{d\left(\frac{V}{V_0}\right)} + V_0 b T \left[ e^{V_0 b \left(\frac{V}{V_0}\right)} \right] \\ = \frac{V_0}{C_V} f\left(\frac{V}{V_0}\right) \left[ e^{V_0 b \left(\frac{V}{V_0}\right)} \right] \quad (17) \end{aligned}$$

Integration of equation (17) results in

$$T e^{V_0 b \left(\frac{V}{V_0}\right)} = c + \frac{V_0}{C_V} \int f\left(\frac{V}{V_0}\right) e^{V_0 b \left(\frac{V}{V_0}\right)} d\left(\frac{V}{V_0}\right) \quad (18)$$

The integration constant  $c$  can be evaluated from the following boundary conditions,

$$T = T_0, \quad \frac{V}{V_0} = 1$$

Equation (18) then reduces to the following expression for temperature as a function of relative volume:

$$T = T_0 e^{V_0 b (1 - \frac{V}{V_0})} + \frac{V_0}{C_V} \int_1^{V/V_0} f(\frac{V}{V_0}) e^{V_0 b (\frac{V}{V_0})} d(\frac{V}{V_0}) \quad (19)$$

Equation (19) is the working equation which enables the calculation of the temperature rise across the shock front.

The integration of the function

$$f(\frac{V}{V_0}) e^{V_0 b (\frac{V}{V_0})} d(\frac{V}{V_0})$$

in equation (19) was performed graphically. The value of the specific volume  $V_0$  was obtained from the average of the experimentally determined values from each experiment. The value of the heat capacity  $C_V$  was estimated to be 0.25 cal/gm °C. The exponent  $b$  contains the partial derivative  $(\partial P / \partial T)_V$  which can be evaluated from the thermodynamic identity

$$\left(\frac{\partial P}{\partial T}\right)_V = - \left(\frac{\partial (\frac{V}{V_0})}{\partial T}\right)_P \left(\frac{\partial P}{\partial (\frac{V}{V_0})}\right)_T$$

Here,  $(\partial (V/V_0) / \partial T)_P$  is the thermal coefficient of volume expansion (estimated to be 0.00001/°C), and  $(\partial P / \partial (V/V_0))_T$  can be obtained from the static curve in Fig. 9. The exponents in equation (19) were of such small magnitude that

$$e^{V_0 b(1 - \frac{V}{V_0})} \approx 1$$

$$e^{V_0 b(\frac{V}{V_0})} \approx 1$$

so that to a very good approximation

$$\Delta T = \frac{V_0}{C_V} \int_1^{\frac{V}{V_0}} f\left(\frac{V}{V_0}\right) d\left(\frac{V}{V_0}\right) \quad (20)$$

Thus, the graphical evaluation of equation (20) leads directly to the determination of the temperature increase. The results of this calculation as a function of relative volume are as follows, assuming that the specific heat of the medium remains constant:

Relative Volume , $V/V_0$	Temperature Rise, °C
1.0	0
0.9	0.01
0.8	0.05
0.7	0.19
0.6	0.58
0.5	1.58

These data are plotted in Fig. 10, and show an almost insignificant temperature rise even in the region of our strongest shock at about  $V/V_0 = 0.65$ .

#### DISCUSSION

The experimental technique which was described earlier in this paper has made it possible to calculate data which may be used to derive an equation of state for a porous material. The Hugoniot can be calculated directly from one record. This has been done for Flintkote-Insulboard, with the result that the strongest Hugoniot compressions have been to pressures of about 550 psi and relative volumes of about 0.65. The temperature rise associated with a shock wave of this strength is in the neighborhood of 0.3°C. This data appears to be consistent in general with that reported by Walsh and Christian (5), who report a rise of 15°C, for example, at a shock pressure of 15 kilobars in aluminum.

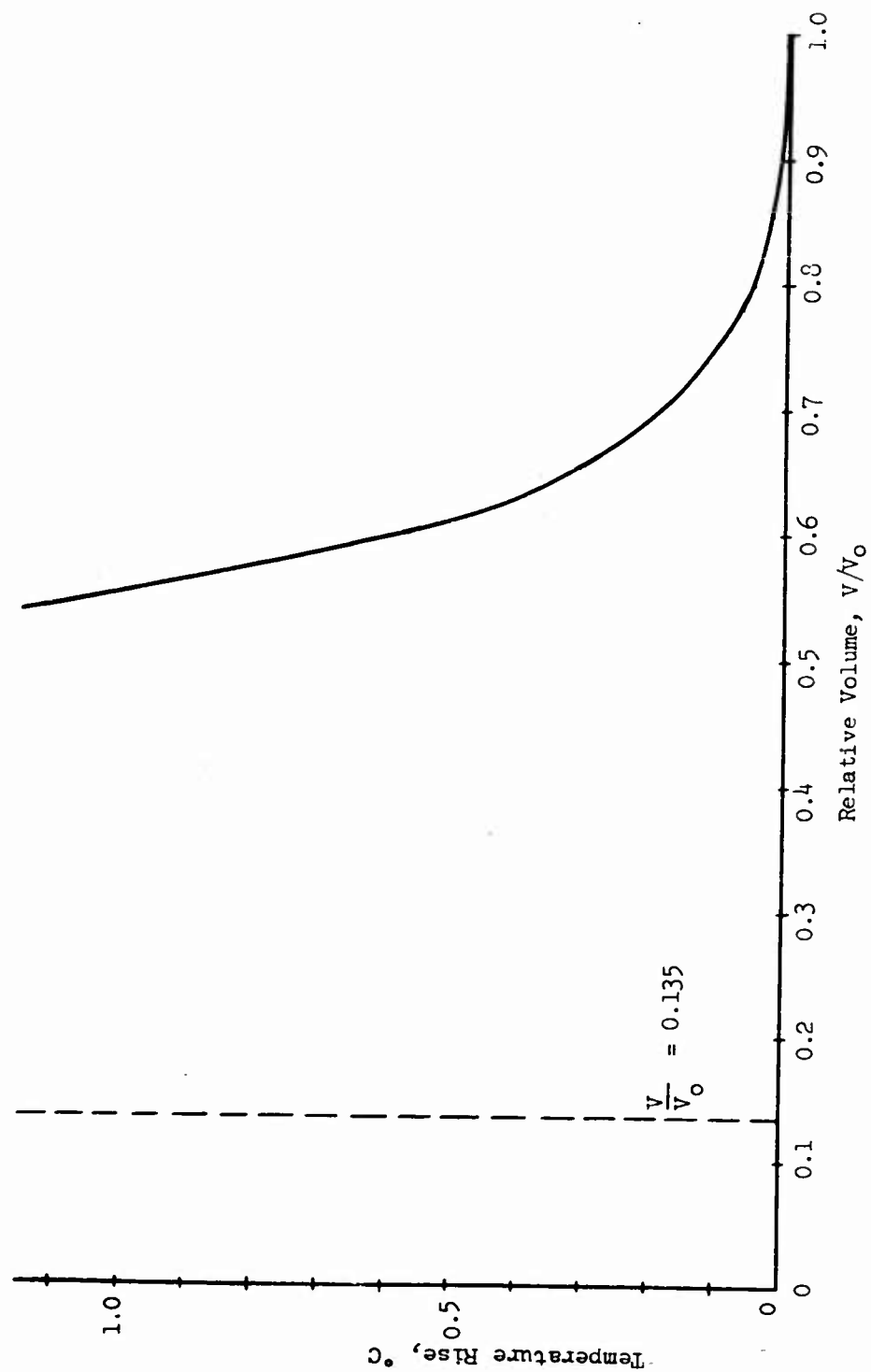


Fig. 10 - Graph of the temperature rise due to Hugoniot compression in Flintkote insulboard

We feel that this experimental technique can be used to obtain similar data for the construction of an equation of state for non-reacting explosives. Napadensky, Stresau, and Savitt (7) have obtained smear camera records of the propagation of non-reactive shocks in explosives. These records are similar to those shown in Fig. 7 and 8, but the velocity of the shock wave is too great for accurate analysis. This problem will be solved by the use of smear cameras which write at higher speeds.

#### ACKNOWLEDGEMENTS

The authors wish to express their appreciation to all persons who assisted in the various phases of the work reported in this paper. These persons include W. Mandelco who constructed the various pieces of equipment used in the experimental portions of the program; W. Hartman and J. Wagner who assisted in the firing of the experiments; and R. Blomquist and C. Love who performed a significant portion of the numerical calculations.

#### REFERENCES

1. von Neumann, J., "Theory of Detonation Waves", OSRD Report No. 549 (1942)
2. Cook, M. A., Filler, A. S., Keyes, R. T., "Mechanism of Detonation", Technical Report No. XII, University of Utah, November 15, 1954
3. Mallory, H. D. and Jacobs, S. J., "The Detonation Zone in Condensed Explosives", Paper No. 17, 2nd ONR Symposium on Detonation, Washington, D. C., February 9-11, 1955.
4. Duff, Russell E. and Houston, Edwin, "Measurement of the Chapman-Jouguet Pressure and Reaction Zone Length in Detonating High Explosive", Paper No. 16, 2nd ONR Symposium on Detonation, Washington, D. C., February 9-11, 1955.
5. Walsh, John M. and Christian, Russel H., "Equation of State of Metals from Shock Wave Measurements", Phys. Rev., 97, 6 (March 15, 1955)
6. Zemansky, Mark W., "Heat and Thermodynamics", McGraw-Hill Book Company, New York (1957)
7. Napadensky, H. S., Stresau, R. H., and Savitt, J., "The Behavior of Explosives at Impulsively Induced High Rates of Strain", presented at this meeting.

## THE BEHAVIOR OF EXPLOSIVES AT IMPULSIVELY INDUCED HIGH RATES OF STRAIN\*

H. S. Napadensky, R. H. Stresau\*\*, and J. Savitt  
Armour Research Foundation  
Chicago 16, Illinois

### Experimental Technique

A sensitivity test has been devised wherein cylindrical specimens of explosives of the order of a pound in weight are squeezed between an explosive driven plate and a massive anvil. The experimental technique is illustrated in Fig. 1. Essentially, the metal plate is accelerated by means of the plane wave initiation of a low density charge of high explosive in such a manner as to compress the explosive test specimen. The motions of the plate and the lines of a reference grid which is stencilled on the specimen are observed either by means of a Fastax Streak Camera which records time-displacement histories, or by means of the Beckman and Whitley Model 189 Framing Camera which records the behavior of the whole surface of the sample under impact.

A typical streak camera record is shown in Fig. 2. The acceleration of the plate is so nearly instantaneous that the acceleration time is barely resolved by the streak camera. The subsequent **negative** acceleration by the action of the specimen, which shows as a quite measurable curvature of the streak camera record, is a measure of the pressure exerted upon the driving plate by the specimen and, hence, of the stress within the specimen. For each point on the curve it is then possible to measure the displacement which is proportional to the strain of the specimen; the first time derivative (or slope) which is proportional to the rate of strain; and the second time derivative (or curvature) which is proportional to the stress in the material. Dynamic stress-strain data are thus obtainable. The propagation of compression waves through the sample is visible as the progressive displacement of the reference lines stencilled on the specimen. Thus, both the non-reactive shock wave propagation velocity and the particle velocities can be measured almost point-to-point

---

\* Supported by AFSWC under Contract No. AF29-(601)-2133

\*\* Consultant, 7 Summit Road, Lake Zurich, Illinois



over the area of a record such as Fig. 2. Continuity and momentum conservation conditions may be applied to reduce these data to shock pressure-density relationships for the explosive.

An example of a Beckman & Whitley Framing Camera record of the dynamic compression of an unconfined cast Comp B specimen is seen in Fig. 3. (The event is front lighted by means of an Argon Flash Bomb). The deformation of the specimen is clearly seen. The over-all geometrical change in the specimen is noticeable as a gradual "mushrooming" of the cylinder with time. Stripes were drawn on the explosive every  $1/4$  of an inch. The changes in distance between stripes, as one proceeds from frame to frame, can be used as a measure of local changes in density with time. One can observe the non-reactive shock wave as it travels through the specimen. This is noticeable on the prints as a progressive brightening of the surface of the sample. From Fig. 3, the non-reactive shock velocity and pressure within the specimen are readily calculated.

#### Typical Records and Interpretation

With an experimental technique as the one described above, it is possible to observe the behavior of the explosive over a wide range of impulsive loading conditions, by varying the mass of the driving plate, the quantity of driving charge used, and the size of the explosive test specimen. At one extreme the shock transmitted through the driving plate is of sufficient intensity to initiate detonation before or at the instant it reaches the face of the anvil. Examples of this are seen in Figs. 4, 5, and 6. Figure 4 shows selected frames, taken 4 microseconds apart, of the compression and initiation of an unconfined cylinder of Comp B, 3 inches in diameter by 3 inches high, weighing 570 grams. The force was applied by means of a steel plate weighing 1418 grams which impacted the explosive specimen at approximately 600 ft/sec. The time between impact and initiation was about 26 microseconds. A high-order detonation of the explosive appears to have started at the bottom of the specimen as evidenced by the bright spot at the bottom of frame 6, indicating the inception of the reaction at the explosive-anvil interface. The shape of the detonation profile as seen in frames 7 and 8 also shows that the detonation starts at the bottom of the explosive and moves upward into the previously shocked specimen. Figure 5, showing selected frames 1.05 microseconds apart, is another example of detonation occurring at the instant the shock wave reaches the anvil. In this case the center of reaction appears to begin in the lower left-hand corner of frame 4, 12.5 microseconds after impact, and progresses back upward into the specimen. The explosive sample was 9404 PBX, 2.5 inches in diameter by 2.34 inches high. Figure 6 shows the impact and the initiation of a cylinder of 9404 PBX, 2.5 inches in diameter by 2.34 inches high. The time between the frames is 1.05 microseconds. In this case the shock intensity was of sufficient strength to initiate detonation before it reached the face of the anvil. The detonation is first observed in frame 7 and appears to have started at about

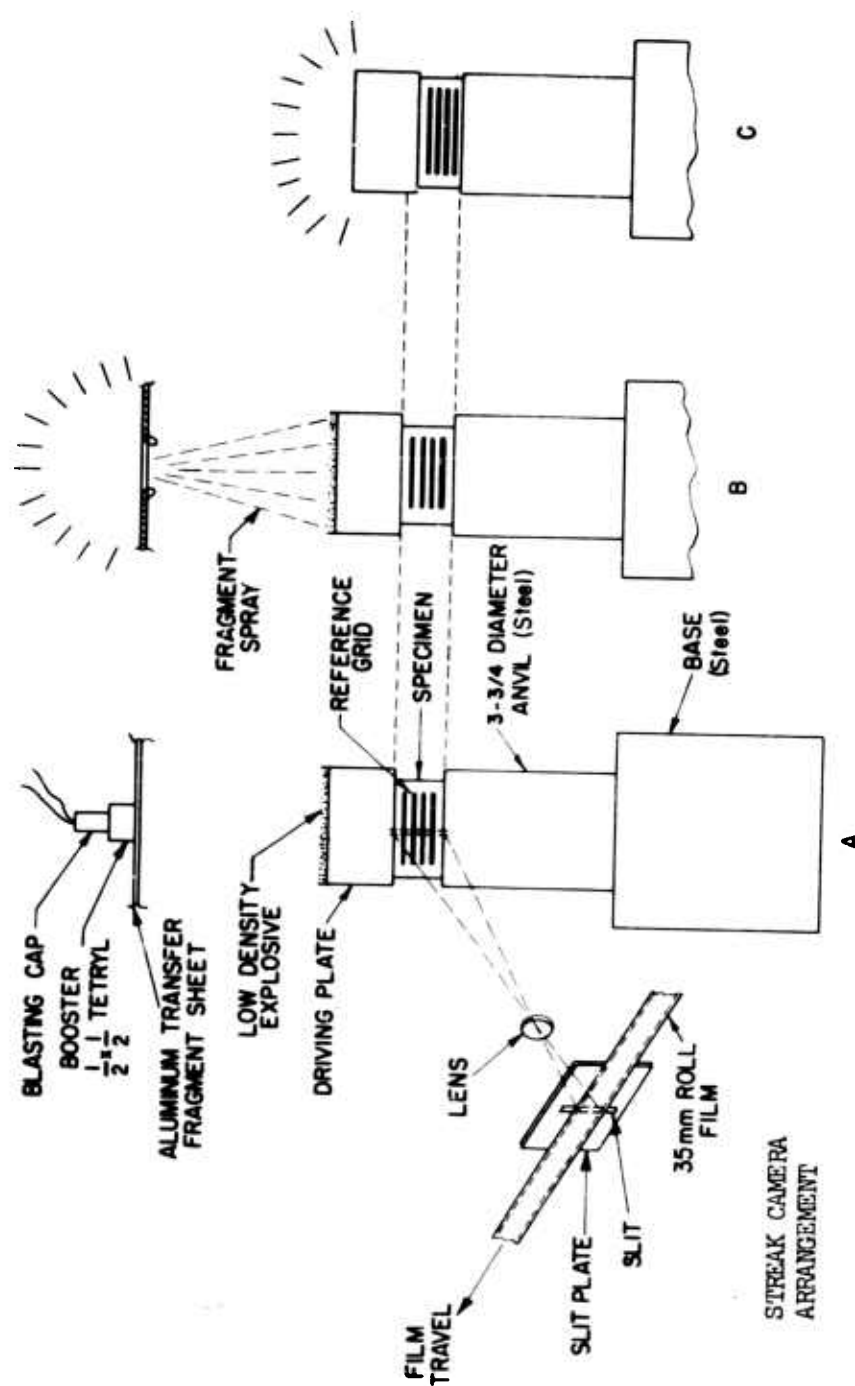


Fig. 1 - Test arrangement

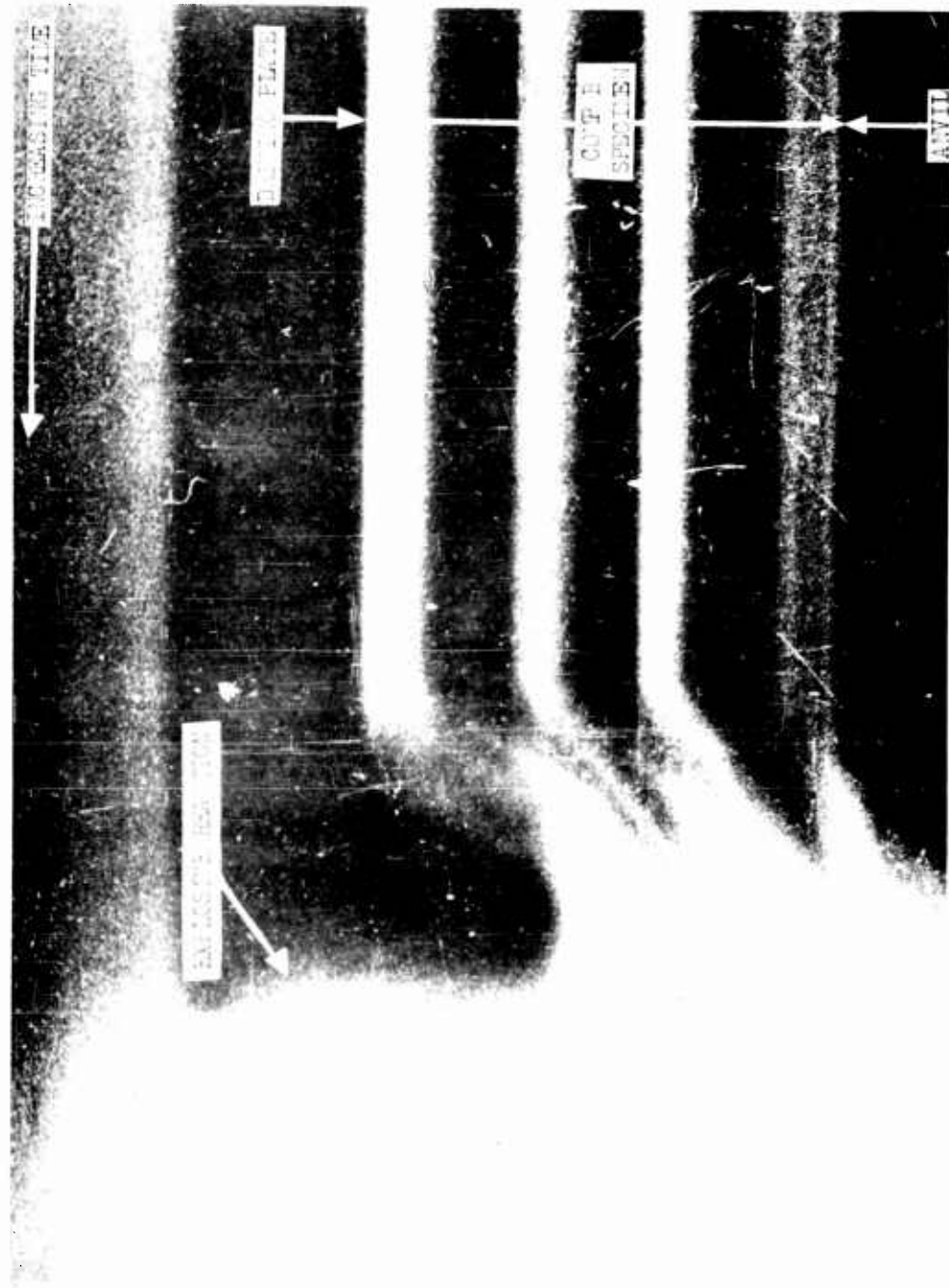


Fig. 2 - Streak camera record of dynamic response to impact of Comp B,  
time from impact to initiation - 200 microseconds

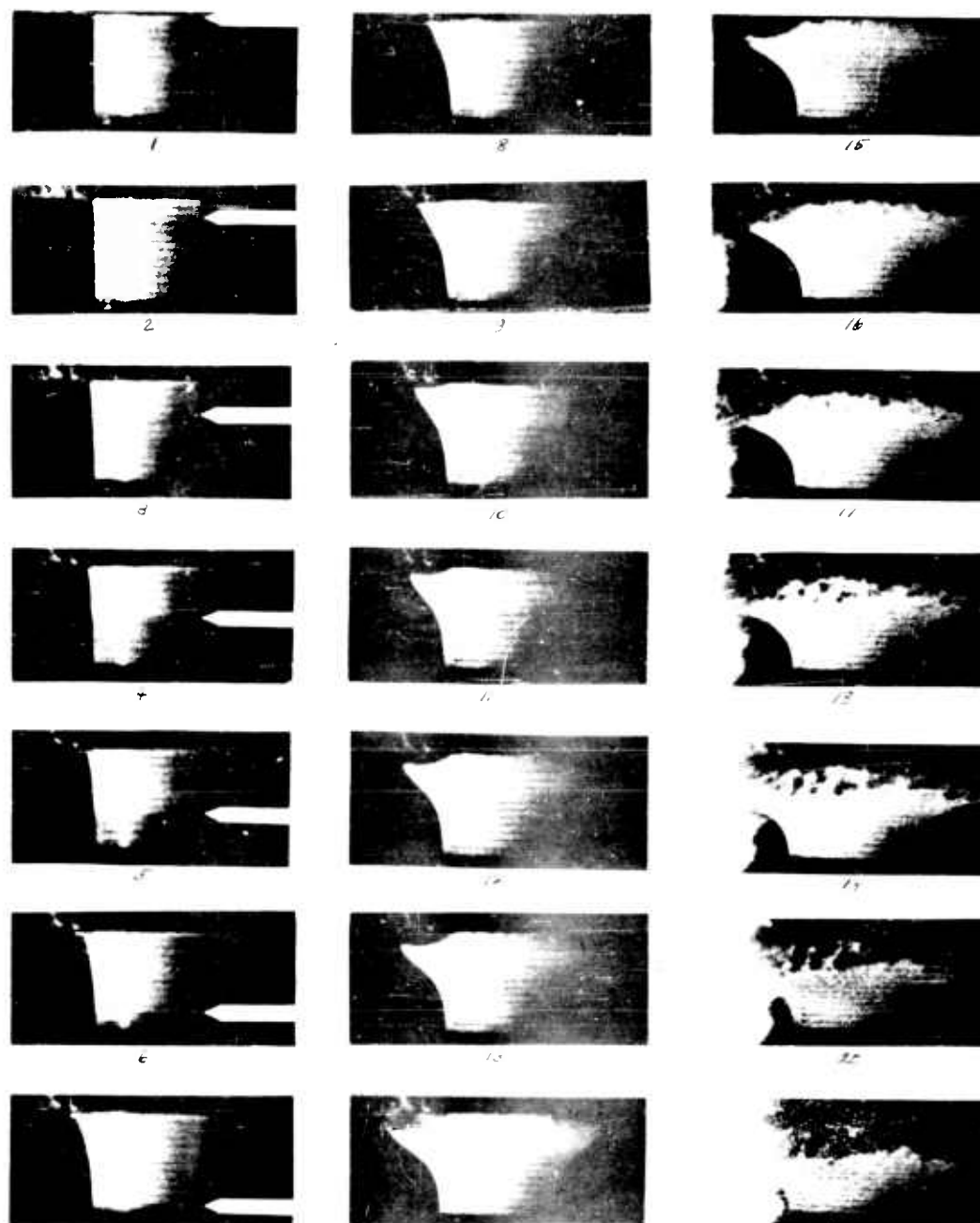


Fig. 3 - Framing camera sequence showing deformation under impact of a cast Comp B cylinder, arrows indicate shock front, 4 microseconds between frames. (Bright light to the left of frames 16-21 is that of explosive light source appearing in the field of view.)

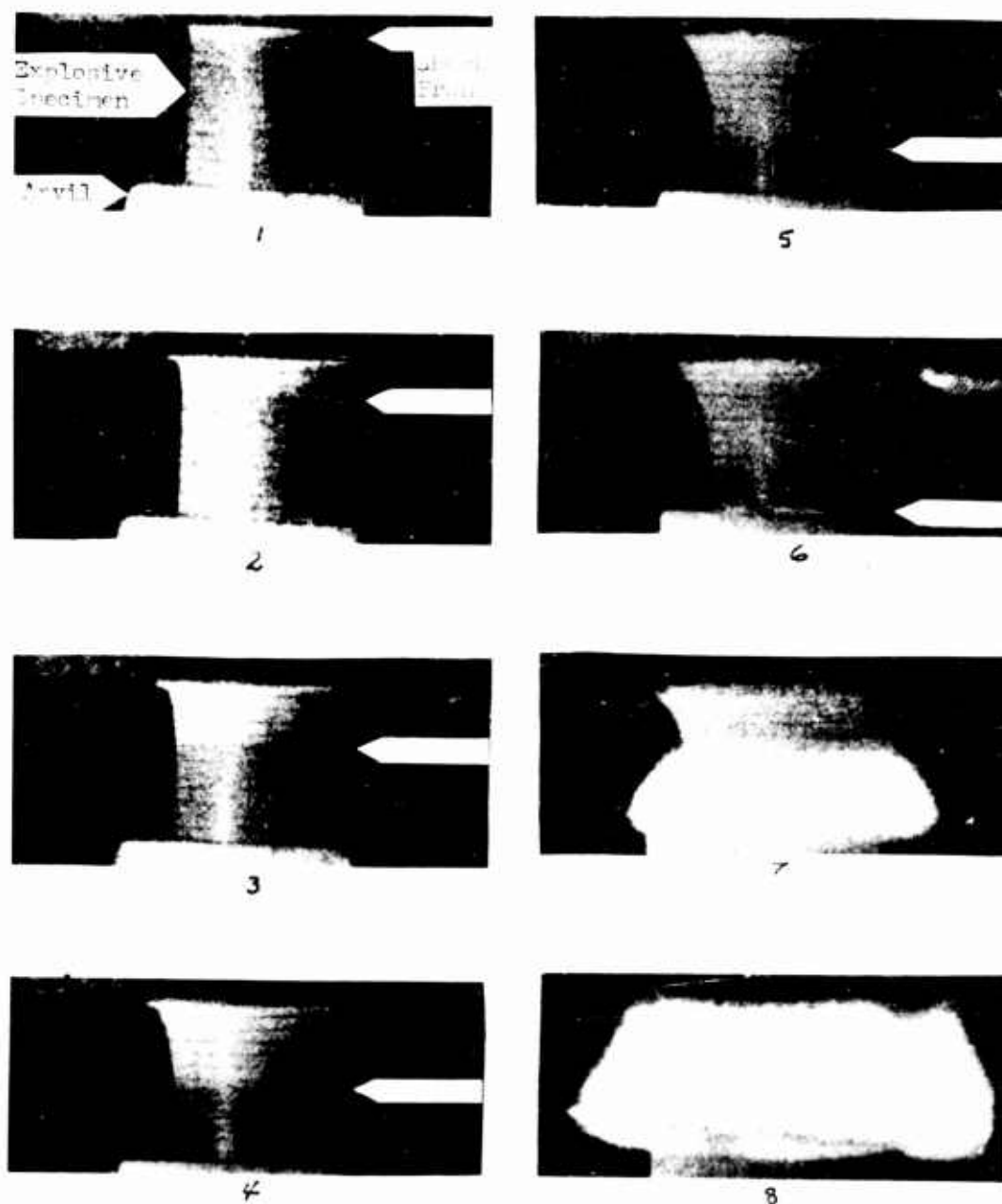


Fig. 4 - Framing camera sequence showing impact initiation of an unconfined Comp B cylinder 3 inches diameter by 3 inches high. 4 microseconds between frames.

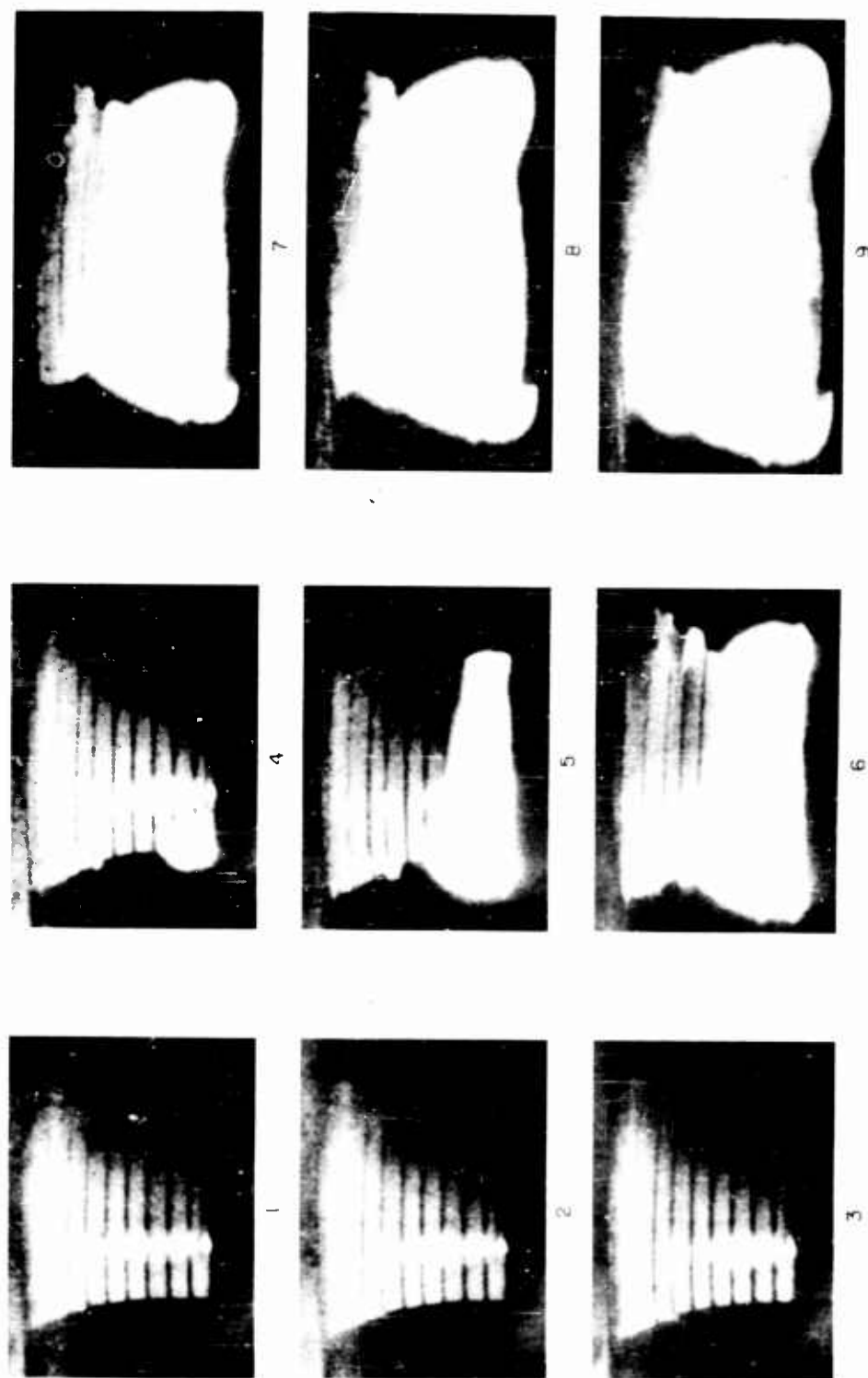


Fig. 5 - Framing camera sequence showing the inception and growth of a detonation in 9404 PBX, 1 microsecond between frames

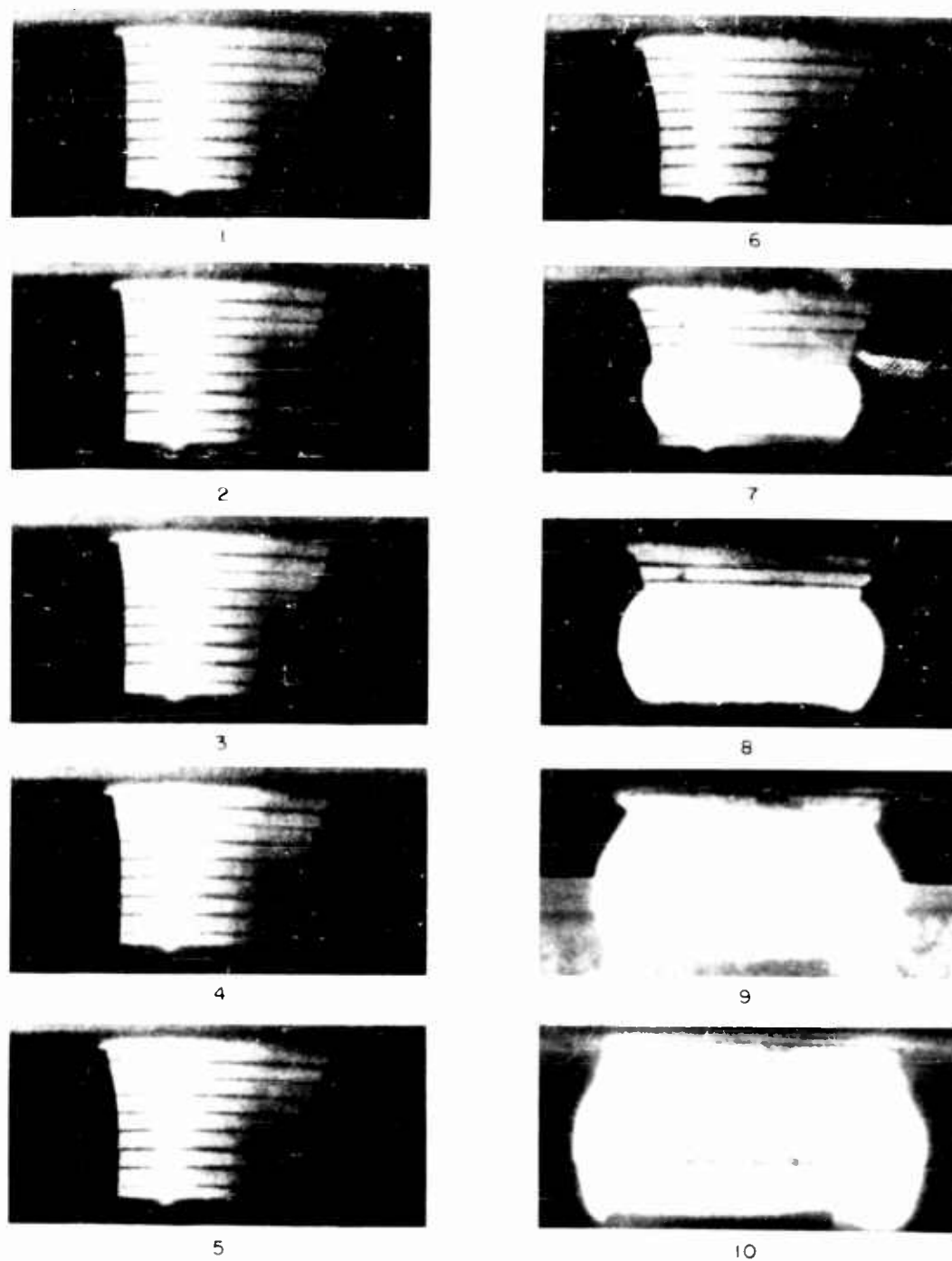


Fig. 6 - Framing camera sequence showing forward and reverse propagation of a detonation in 9404 PBX, 1 micro-second between frames.

1.6 inches from the top of the sample. The reaction occurs 10.5 microseconds after impact, and propagates both in the forward and reverse direction. In these cases the initiation mechanism is probably similar to that of earlier experiments of Cachia and Whitbread (1), Eichelberger and Sultanoff (2); Cook, Pack and Gey (3); Marlow and Skidmore (4); and Savitt (5). They have observed that the depth in the explosive at which initiation occurs depends upon the pressure of the incident shock, the lower the pressure the deeper the point of initiation. This has been explained by Cosner and Sewell (6) by the fact that if the shock wave entering the charge is above a minimum intensity it will be supplemented by a chemical reaction; the pressure build-up from the reaction is dependent on the shock intensity. Therefore, when the initial shock intensity is high, the pressure build-up from chemical reaction is fast, and so initiation takes place near the explosive-metal interface. When the initial shock intensity is lower, the pressure build-up from the chemical reaction is slower, and initiation takes place farther from the explosive-metal interface. An alternate explanation may be based on the generality that reaction rates in explosives are so highly dependent upon temperature, that for a rate of any given order of magnitude, it is described with fair accuracy in terms of a threshold or ignition temperature, combined with applications of the general principles of the behavior of non-reactive compressive waves. A shock traversing a barrier or gap, is generally modified, particularly in its pressure-time profile, by impedance discontinuities and the reverberations of the gap or medium. The important contrast of the emergent wave to the incident wave is the lack of the nearly discontinuous increase in peak pressure which is characteristic of a stable shock. As the emergent wave propagates through the acceptor explosive, the higher pressure components of the wave tend to overtake the front so that the discontinuous pressure rise at the front increases in magnitude. Since the temperature increase associated with a single Hugoniot compression to a given pressure is appreciably greater than that associated with either adiabatic compression or a series of Hugoniot compressions to the same maximum pressure, the threshold temperature for a reaction rate of the order of magnitude of that associated with detonation is attained when the discontinuous rise at the front acquires sufficient magnitude. It is probable that, in some cases, this mechanism is combined with that suggested by Jacobs (7) in which the overtaking wavelets are evolved as a result of incipient reaction of the explosive, due to the passage of the essentially nonreactive shock.

At the threshold of initiation, however, the time between initial movement of the plate and the evidence of explosion is long enough for many reverberations of the shock between the driving plate and the anvil. The streak camera record shown in Fig. 2 is an example of an observation of this type. It shows the impact and subsequent initiation of a Comp B specimen, 3 inches in diameter by 1 1/2 inches in height, weighing 90 grams. It was impacted by a steel plate weighing 1475 grams, at a velocity of 206 ft/sec. The time from initial impact to initiation was about 200 microseconds. Here the



mechanism of initiation is probably similar to that proposed by Wenograd (8), whose comparison of impact experiments with reaction kinetic data suggests that an impact explosion of high explosives is a phenomenon intermediate between a low temperature thermal decomposition and a detonation. It might be noted that the time to reaction observed here is of the order of that assumed by Wenograd for the duration of impact.

A third mechanism is implied by observations, in some instances, where the explosion originates in explosive dust external to the original charge dimensions. The streak camera record of Fig. 7 is one of many observations of this behavior. It illustrates the response to impact of a Comp B specimen, 3 inches in diameter by 1 inch high, weighing 181 grams. It was impacted by an aluminum plate weighing 504 grams, at a velocity of about 600 ft/sec. In this example wide stripes were painted on the specimen. The broad bright vertical bands seen on the left of Fig. 7 is light from the reacting explosive. In this case the time from impact to reaction is about 280 microseconds.

Where no explosion results, data are obtained regarding the shock pressure-density relationships for the unreacted explosive as well as the inter-relationship of stress, strain, and strain-rate in the impulsively loaded explosive specimen. Some of the data obtained thus far are plotted in Fig. 8, stress vs strain, and Fig. 9, strain vs strain-rate for Comp B.

### Conclusion

The importance of nonuniformity of energy distribution in initiation is clearly illustrated in these experiments. The change in internal energy density as calculated from shock hydrodynamics or from changes in kinetic energy of the driving plate is never sufficient to raise the average temperature to a point where rapid reaction should be expected. An example of this can be shown by referring to the experiment whose framing camera record is illustrated in Fig. 4. One can observe the non reactive shock wave as it travels through the specimen. This is noticeable as the progressive brightening of the surface of the explosive. From this observation, a shock velocity of about 10,000 ft/sec is calculated. A particle velocity of 600 ft/sec is obtained from streak camera observations. From the conservation equations for a shock wave one readily calculates; a pressure of 9 kilobars, and a density of 1.7 grams/cm<sup>3</sup>, which results in an energy increase of 4.07 cal/gram for the shocked explosive. The maximum possible temperature rise due to the internal energy increase calculated (assuming a specific heat of 0.24 cal/gm for Comp B) is only 17°C. However, if one calculates the temperature rise due to the adiabatic compression of a trapped gas bubble, by

UNCLASSIFIED

Napadensky, Stresau, Savitt

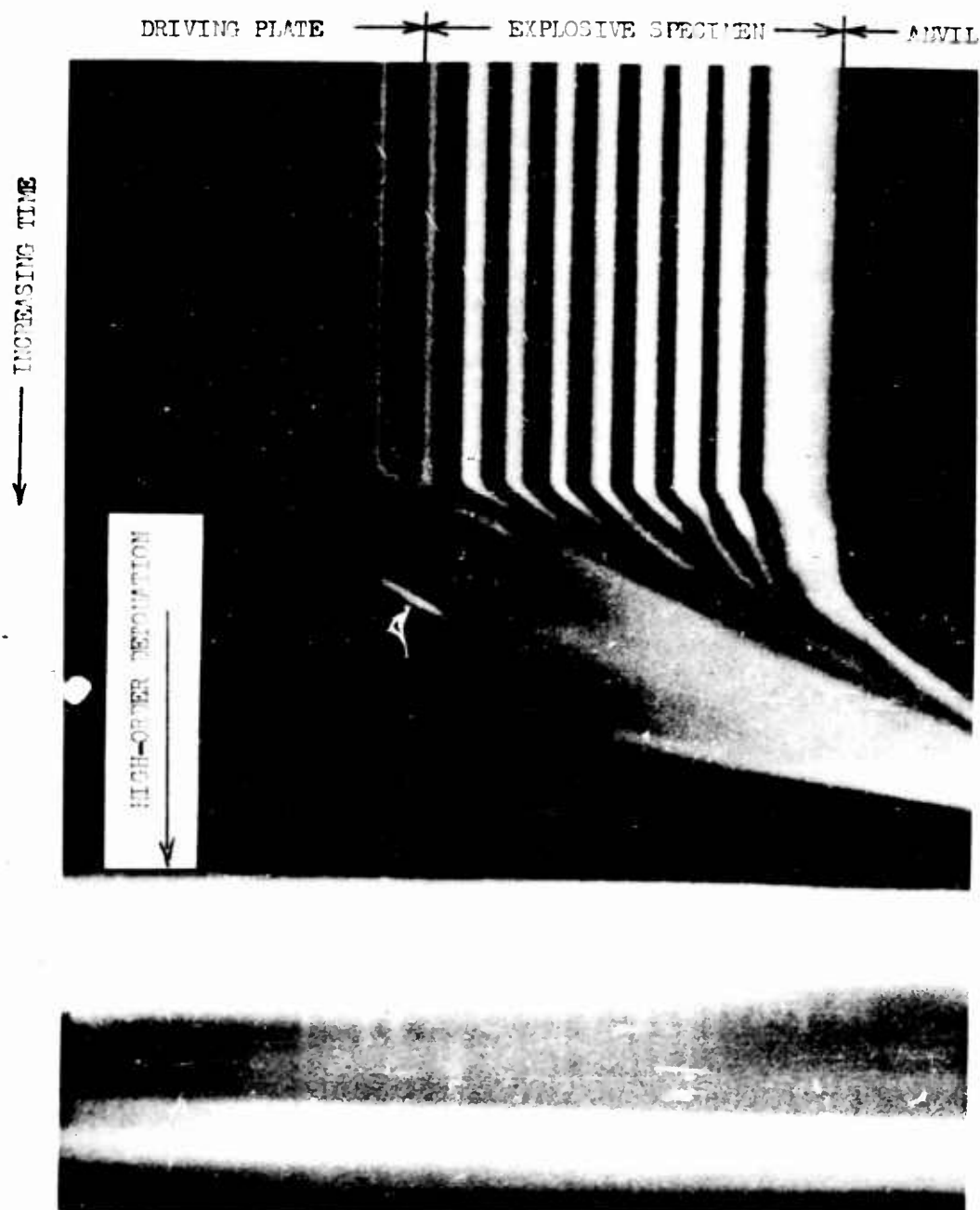


Fig. 7 - Streak camera record of dynamic response to impact of Comp B, time from impact to initiation - 280 microseconds.

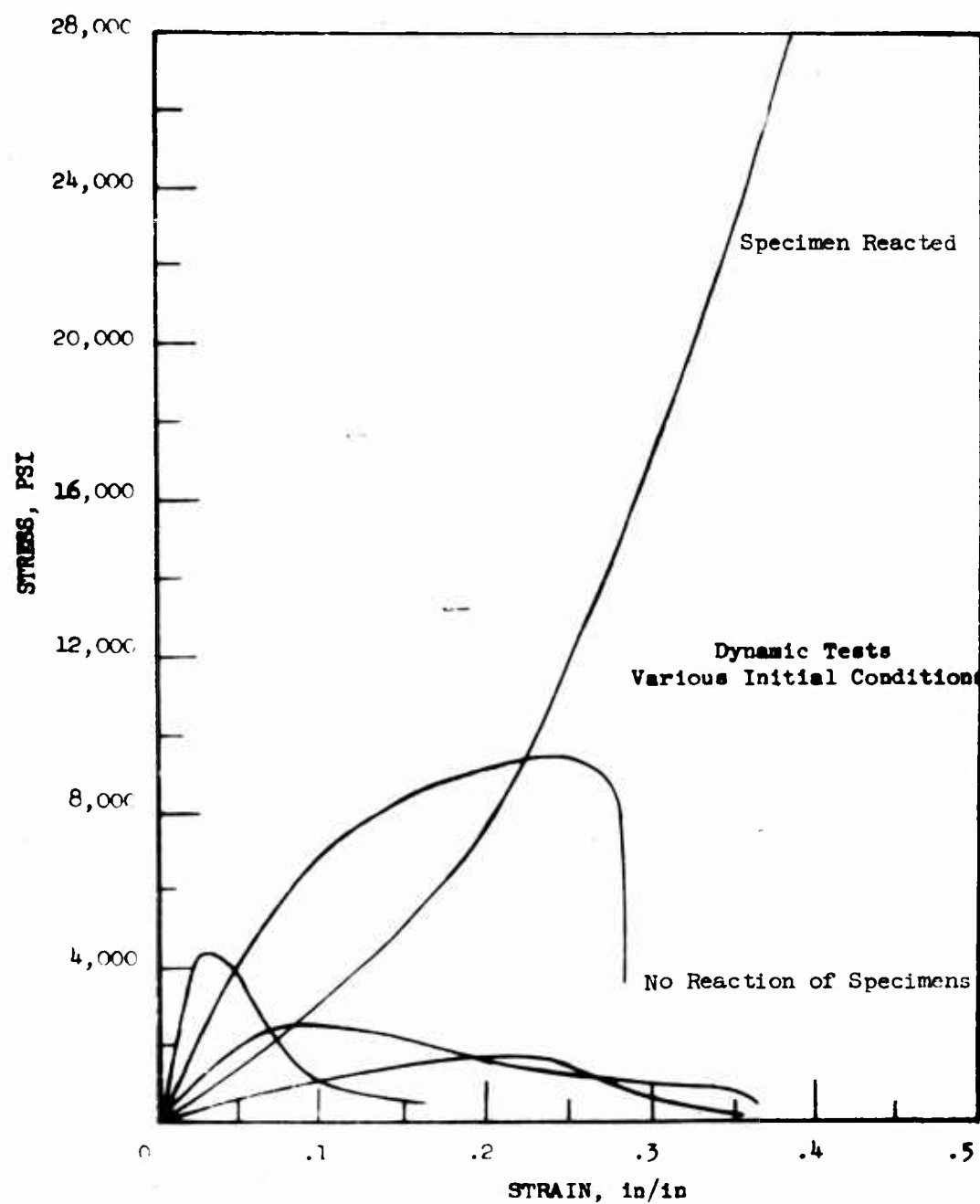


Fig. 8 - Stress vs strain curves for Comp B

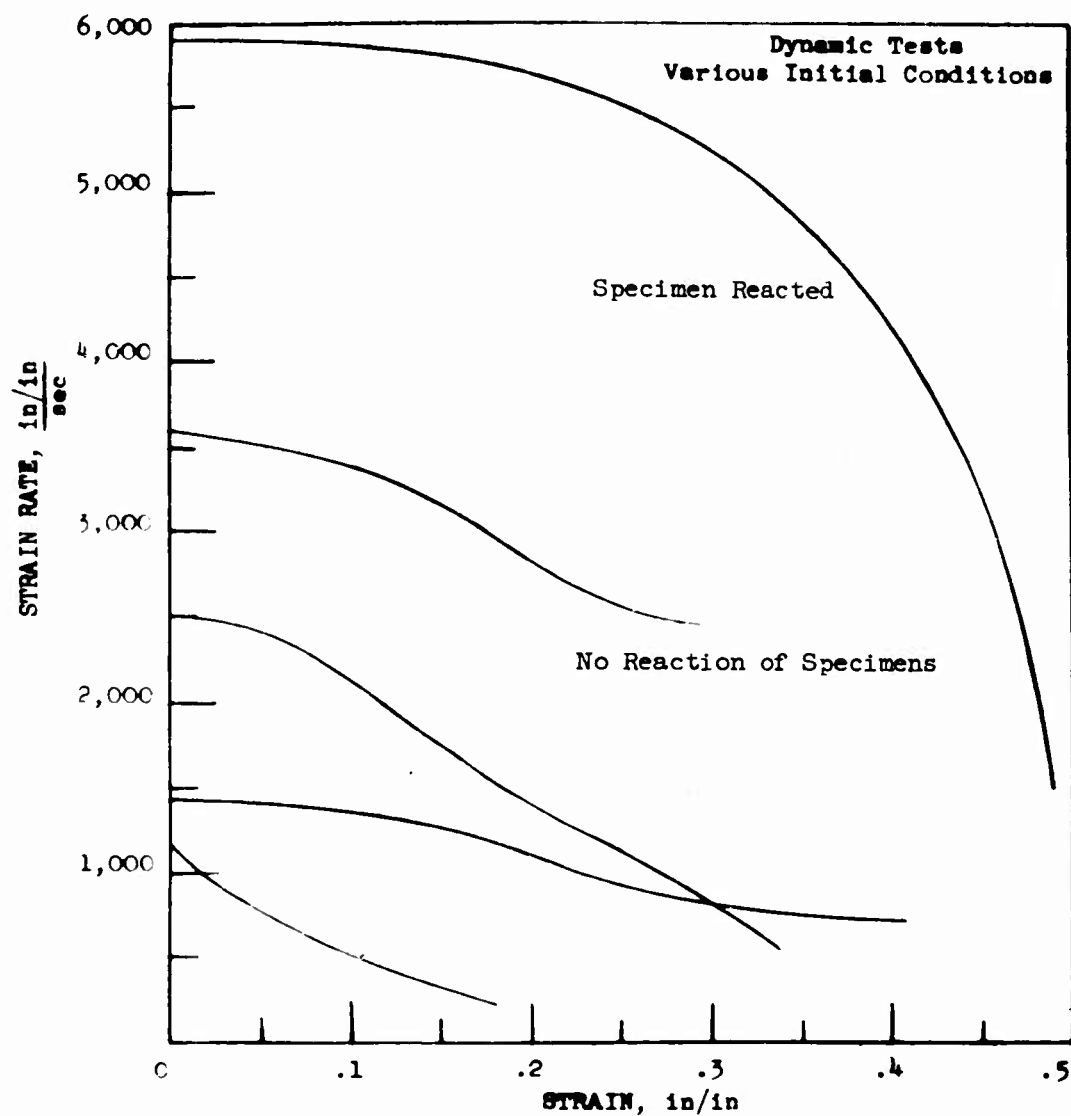


Fig. 9 - Strain rate vs strain curves for Comp B

the relationship  $T/T_0 = (P/P_0)^{1/\gamma}$ , a temperature rise of about 3500°C is obtained. But even this temperature rise, which is about 10 times the critical hot spot temperature needed for initiation, does not insure a reaction growing to completion. The heat and gaseous products generated as a result of the compression must evolve in the explosive charge more rapidly than they are dissipated in order for the reaction to accelerate.

One can easily realize that the value of the data obtained in impact sensitivity experiments may be increased considerably by theoretical considerations of the impact initiation process. The initiation process is clearly quite complex. However the analysis of simplified models which are still representative of the condition within the explosive, after impact, might be tractable. One such model has been suggested by the authors in an earlier paper (9). This model assumes that in a porous explosive material:

- (1) A sudden impact load has resulted in the compression of interstitial gases.
- (2) This compression is not uniformly distributed.
- (3) At some point in the explosive the pressure is appreciably higher than elsewhere.
- (4) The compression has heated the gas to above the "ignition temperature" for the explosive.
- (5) The principal mechanism of reaction propagation is that of "deflagration".
- (6) The principal mechanisms of heat dissipation is the flow of the product gases through the interstices.

In this model of a porous explosive medium, we assume that the interstitial spaces, a volume which is small compared to the explosive charge and large compared with an individual particle or pore, are filled with hot compressed gas. The gas flows through the porous medium at a rate that is related to the pressure gradient by the partial differential equation

$$\frac{k}{\mu(1+m)f} \nabla^2 P^{1+m} = \frac{\partial P^m}{\partial t},$$

where  $m$  = ratio of specific heat at constant volume to that at constant pressure,  $\mu$  = viscosity of the gas,  $f$  = porosity of the explosive,  $k$  = permeability of the explosive,  $t$  = time and  $P$  = pressure of the gas.

At the same time the explosive deflagrates at the grain surface at a rate related to the pressure by an empirical formula of the form  $U = a + bP^v$ . Since  $PV = nRT$ , and  $dn/dt = (V/RT)(dP/dt)$ , and  $UA = (a + bP^v) A = dn/dt$  the substitution  $dP/dt = 1/m P^{1-m} dP^m/dt$  results in the equation  $(a + bP^v) A RT/m / VP^{1-m} = dP^m/dt$ , where  $A$  is the surface area of particles per unit volume.

The complete relation between the evolution and the dissipation of gas in our system is now given by

$$\frac{k}{\mu(1+m)f} \nabla^2 P^{1+m} + (a+bP)P^{m-1} \frac{ARTm}{V} = \frac{dP^m}{dt}$$

In the three-dimensional case, because of spherical symmetry we can write the above equation as

$$\frac{k}{\mu(1+m)f} \left( \frac{\partial^2 P^{1+m}}{\partial r^2} + \frac{2}{r} \frac{\partial P^{1+m}}{\partial r} \right) + (a+bP^{\frac{1}{2}}) P^{m-1} \frac{ARTm}{V} = \frac{dP^m}{dt},$$

with the boundary conditions,  $P(r,0) = p_1 + p_2 e^{-r^2 p_3^2} \quad (0 < r < r_1),$

$$P(r_1, t) = P_1 \quad (t > 0)$$

$$\frac{dP(0,t)}{dr} = 0$$

The solution of the above equation will enable us to determine under what conditions an expanding reaction will occur which will carry on to detonation, and when the reaction is dying. This dying reaction can occur when the rate at which the gas is flowing out of the system is greater than the rate at which it is being evolved, due to burning of the explosive material. Data of the type reported herein will aid in the interpretation of solutions to the equation.

#### Acknowledgement

The authors are especially indebted to J. Gershon and W. Hartman for their assistance in the photographic work and in performing the experiments.

:mc

#### Bibliography

- (1) G. P. Cachia and E. G. Whitbread, "The Initiation of Explosives by Shock", *Proceedings of the Royal Society, Series A*, Vol. 246, No. 1245, 29 July 1958, p. 268
- (2) R. J. Eichelberger and M. Sultanoff, "Sympathetic Detonation and Initiation by Impact", *Ibid*, p. 274
- (3) M. A. Cook, D. H. Pack and W. A. Gey "Deflagration to Detonation Transition in Solid and Liquid Explosives", *Ibid*, p. 281
- (4) W. R. Marlow and I. C. Skidmore "The Initiation of Condensed Explosive by Shock Waves from Metals", *Ibid*, p. 284.
- (5) J. Savitt, "Some Observations on the Growth of Detonations" Navord Report No. 3753, 25 August 1954

- (6) L. N. Cosner and R. G. S. Sewell, "Initiation of Explosives Through Metal Barriers", Proceedings of Detonation Wave Shaping Conference, 5-7 June 1956 p. 235
- (7) S. J. Jacobs, "A Theory Concerning the Initiation of Detonations by Shocks", Ibid, p. 248
- (8) J. Wenograd, "The Correlation of the Impact Sensitivity of Organic High Explosives With Their Thermal Decomposition Rates" Proceedings of the Gilbert B. L. Smith Memorial Conference on Explosive Sensitivity, 2 June 1958, p. 130
- (9) R. H. Stresau and H. S. Napadensky "Thermal Unbalance and Initiation", Ibid, p. 191.

## INITIATION AND GROWTH OF DETONATION IN LIQUID EXPLOSIVES

F. C. Gibson, C. R. Summers,  
C. M. Mason, and R. W. Van Dolah  
Bureau of Mines  
Pittsburgh, Pennsylvania

### Introduction

The mechanism whereby detonation is initiated in condensed phase explosive systems, though the subject of many experimental and theoretical investigations, continues to elude definition. Of continuing interest in the high-explosives field, sensitivity to initiation of detonation has assumed increased importance in the liquid monopropellant and high-energy solid propellant fields. This sensitivity is typically evaluated, among other methods, by a gap-sensitivity test where the sample, suitably contained, is subjected to shock from a standard explosive donor after attenuation by passage through an inert barrier. The development of this test is described by Jacobs (1). One form has been recommended as a "standard test" for evaluating the sensitivity of liquid monopropellants (2).

Although the gap test is capable of yielding quite reproducible results when applied to many systems, many anomalous results occur. As an example, neat nitromethane will yield nearly identical "gap values" whether the containing cup is of aluminum or steel. Other systems, such as 50-50 nitroglycerine-ethylene glycol dinitrate, (NC/EGDN), show a much lower apparent sensitivity (smaller gap value) in steel cups than in aluminum cups, with glass cups giving even smaller gap values. Clearly, the test does not measure a sensitivity that is characteristic only of the liquid explosive alone; rather, the sensitivity measured depends, in part, upon the nature of the containers. Further, Cook and associates (3) have pointed out that the mechanism whereby initiation occurs under card-gap test conditions may be extremely pertinent to the problem of deflagration-to-detonation transition in solid propellants. With these problems in mind, the Bureau of Mines began studying the card-gap test.

Many theories of initiation have been proposed (3-7). Bowden's hot-spot theory, originally developed for the drop-weight case -- which relies on the adiabatic compressional heating of



bubbles -- has been criticized by Bolkhovitinov (8) and by Johannson and Selberg (9), who point out that the relaxation times for the minute bubbles postulated to be present are too short for the compression to be adiabatic. Bolkhovitinov hypothesizes an alternative mechanism where the crystallization of the liquid under pressure is the causative heat source. Johannson (10) proposes that vapor or droplet burning in the bubbles must be responsible for the initiation at low-impact energies. Indeed, Bowden and Jafee recognized the importance of the vapor-phase decomposition in the initiation of liquid explosives. Andreev (7) suggests that the burning of a droplet suspension is important in the transformation of deflagration to detonation. Interestingly enough, this same idea of a burning suspension of particles of explosive is postulated by Cachia and Whitbread (11) as being important in their experiments on the shock initiation of single crystals of Cyclonite (RDX). In considering the initiation of air-free nitroglycerin, Selberg (12) attempts to calculate the particle velocity of the shock wave required. In contrast, Cook and contemporaries (3) suggest that initiation occurs only with the development of both a pressure-generated "metallic state" and a "plasma" which can provide the postulated requirement of high heat conductivity. A further consequence of this theory is the projection of a "plasma" from the end of the charge under some conditions (13). Jacobs (1), however, has suggested that the experiments described by Cook may be explained by alternate hypotheses.

We believe the results reported herein suggest a mechanism for initiation under card-gap test conditions and provide, as well, a possible explanation for the off-the-charge-end "plasma" phenomenon.

#### Experimental Details

Liquid systems were chosen by the Bureau of Mines because they are more amenable to photographic study. Shock and detonation phenomena were examined by direct- and schlieren-photographic methods and by a resistance element technique recently developed to measure continuously detonation velocities (14). The photographs were made both with an instantaneous (0.5  $\mu$  sec. exposure) Rapa-tronic camera<sup>1/</sup> and the Cordin high-speed framing camera<sup>2/</sup> of the U. S. Naval Propellant Plant at Indian Head, Maryland.

---

<sup>1/</sup> A product of Edgerton, Germeshausen and Grier, Inc., 160 Brookline Ave., Boston, Mass.

<sup>2/</sup> A product of the Cordin Company, 1637 Pioneer Rd., Salt Lake City 4, Utah.

Several charge configurations were used in these experiments. Initiation was accomplished by an attenuated shock wave, from an explosive donor, into the transparent vessel containing the liquid explosive. A drawing of a typical charge configuration is shown in Figure 1.

Preliminary work indicated that a rubber barrier would be a satisfactory shock attenuator to yield delayed ignitions and considerable predetonation activity of interest. Typically, it was found that a rubber barrier 2.6 cm. thick would provide initiation delay times of 5 to 15  $\mu$  sec. for granular explosives and about 50  $\mu$  sec. for the 50-50 nitroglycerin-ethylene glycol-dinitrate (NG/EGDN) mixtures used for most of this investigation. In some experiments, the usual stack of cellulose acetate cards (2) was employed with comparable results.

To permit a study of the effects of geometry and wall materials, the confining vessels used were either round Plexiglas tubes or tubes having square cross sections where the front and rear (viewing sides) were Plexiglas; the side walls were steel, aluminum, or Plexiglas. In most cases a mirror was positioned at 45° above the tube to provide a simultaneous end-on view of the event. In other cases, a steel witness plate, 1/4 inch thick, was positioned on top of the charge.

Because the early stage of the shock excitation is nonluminous, it was necessary to provide background light to silhouette the event. This was provided by an exploding wire fabricated of a 10-cm. length of 5 mil. aluminum wire. A simple white paper corner reflector was positioned behind the wire. A capacitive discharge energy of 216 joules was applied to the wire through a synchronizing hydrogen thyratron with suitable delay provided to allow optimum buildup of luminosity. The exploding wire was placed 7-1/2 cm. behind a translucent paper screen which was, in most cases, ruled with lines one centimeter apart to provide convenient reference.

The donors were 14 gram tetryl pellets initiated either by a No. 8 electric blasting cap or a short length of Primacord which was, in turn, initiated by a No. 8 blasting cap. All tests were conducted with the liquid at a temperature of 25°C.

#### Experimental Results

A complete framing-camera sequence of one explosive test, Figure 2, illustrates the complexity of the initiation process. This charge configuration was identical to that shown in Figure 1, except that the charge contained a resistance element. The vessel was a 23 mm. i.d. Plexiglas tube, 11 cm. long, filled with NG/EGDN and shocked by a 14-gram tetryl donor through a 2.6 cm.-thick rubber

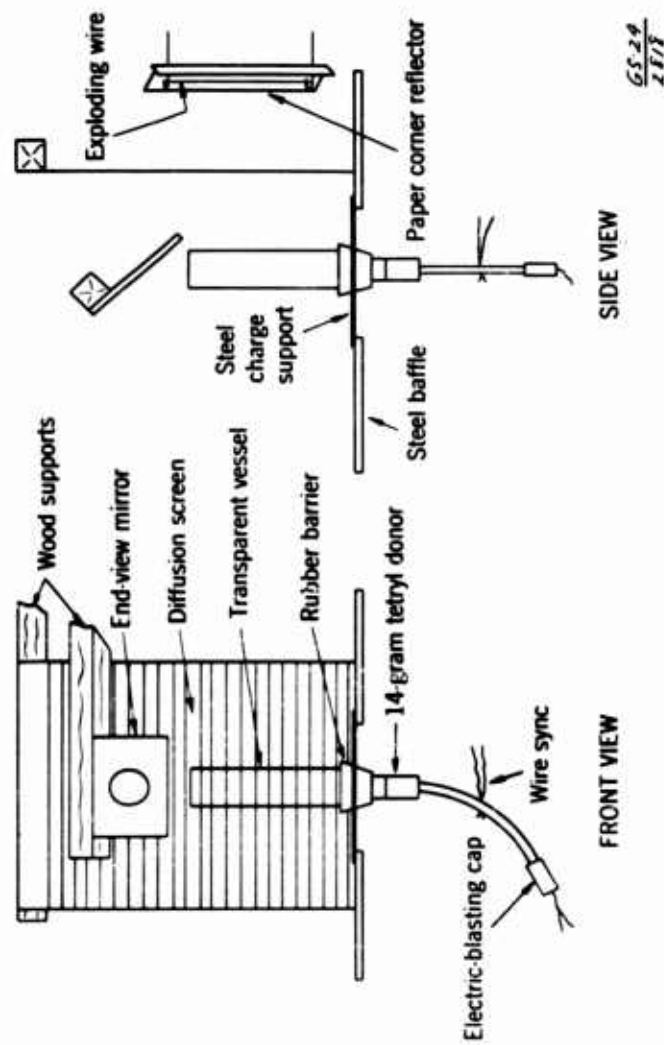


Fig. 1 - Drawing of a typical test vessel configuration used for initiation and growth studies in liquid explosives

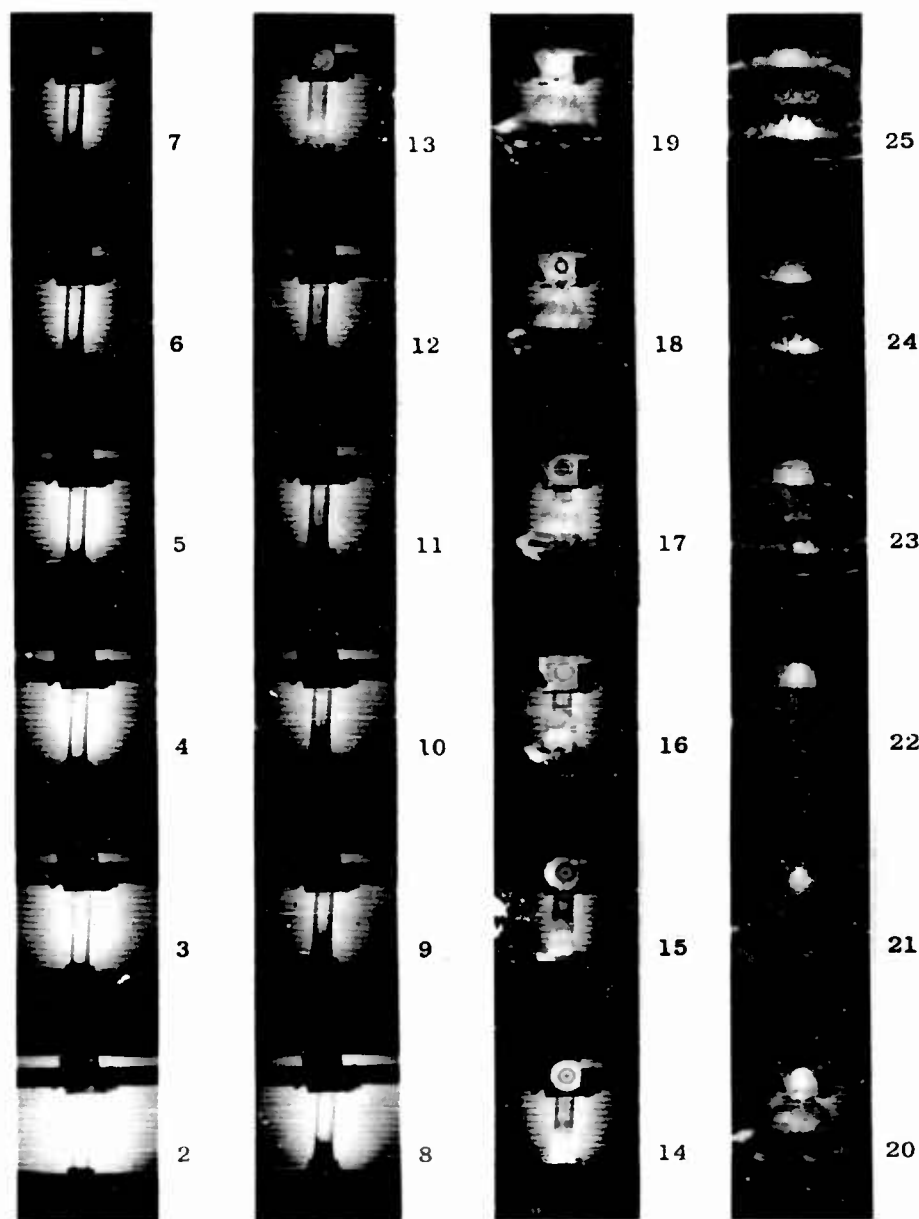


Fig. 2 - A framing camera sequence of the initiation and growth of detonation in a NG/EGDN mixture, contained in a 23 mm. i.d. tube. Both axial and peripheral initiation is shown. The interframe time is 4.2 sec. and the frame exposure time is 1.4  $\mu$ sec. A resistance element was prepositioned in the charge.

barrier. Interframe time was  $4.2 \mu \text{ sec.}$  and the exposure time per frame was  $1.4 \mu \text{ sec.}$  The end-on view of the event appears in the mirror inclined at about  $45^\circ$  to the charge axis and positioned off the charge end.

In frame 3, the shock wave is seen emerging from the barrier. A nonluminous disturbance moves up the tube at a rate of about  $1.6 \text{ mm}/\mu \text{ sec.}$ ; this is slightly higher than sonic velocity for the liquid. In frame 9, about  $25 \mu \text{ sec.}$  later, an axial disturbance, nonluminous in its early stages, begins to appear. Later, this disturbance develops into a spearhead, showing a lateral, luminous growth at its base and moving downstream through the column at  $2.5 \text{ mm}/\mu \text{ sec.}$  This is approximately sonic velocity for the cylindrical plastic container. This axial disturbance would thus appear to result from the interaction of the transverse waves generated in the liquid by the compression waves in the vessel wall.

In frame No. 12, the reaction occurs not only on the axis, but early peripheral initiation also is seen in the mirror view. In frame 13, the luminous reactive region is seen to develop at the interface between the liquid and the vessel wall, but little lateral pressure is created. By frames 15 and 16, two initiation regions are indicated and the vessel has begun to yield. The axial disturbance has reached the charge end and has spread along the meniscus in frame 15 and a suspension of droplets is driven off the end in a fountain-like ejection. These particles decompose during passage through the atmosphere above the charge, as indicated in the end-on view of frame 18 and later frames.

The peripheral initiation of the NG/EGDN mixture is more clearly shown in the selected frames (18, 20, 22, and 24) taken from another shot, Figure 3. This sequence was photographed with an interframe time of  $1.4 \mu \text{ sec.}$  and an exposure time of  $0.90 \mu \text{ sec.}$  The diameter of the confining vessel was 35 mm. i.d., about 50 percent larger than that used in the tests described in Figure 2; the length was the same. Because of the greater diameter, the axial disturbance was less severe and initial luminous reaction occurred only at the liquid explosive-vessel wall interface, as shown clearly in the end-on view (Figure 3). The hairy structure of the products cloud is perhaps caused by the ejection and subsequent reaction of explosive after passage through the longitudinal tension cracks in the plastic vessel wall. The broad luminous zone is propagating at a rate of about  $7 \text{ mm}/\mu \text{ sec.}$  This is approximately the normal hydrodynamic velocity for detonating NG/EGDN.

The intense spearheaded axial disturbance, evidenced in Figure 2, is further illustrated in Figure 4. In Figure 4, the vessel was not instrumented with a resistance element. This single frame  $0.5 \mu \text{ sec.}$  Rapatronic camera photograph shows the opacity caused by the wall-liquid interaction at the vessel top and the cracks at the base from which liquid explosive is later ejected.

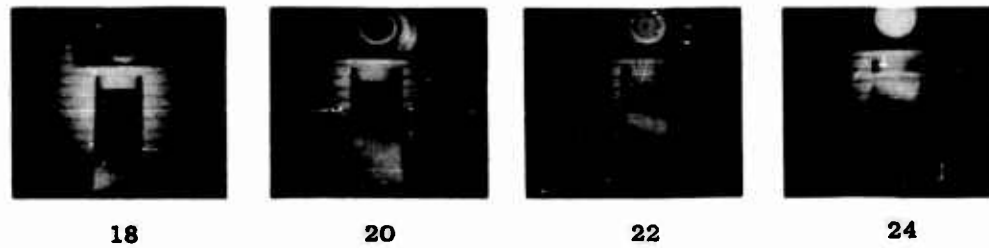


Fig. 3 - Selected frames of a sequence in a 35 mm. i.d. vessel showing only peripheral initiation in a NG/EGDN mixture. The interframe time between adjacent frames was 1.4  $\mu$ sec. and the frame exposure time was 0.90  $\mu$ sec.



Fig. 4 - A Rapatronic camera photograph, single frame exposure, showing the predetonation activity in a column of NG/EGDN. No resistance element was employed. Exposure time was approximately 0.5 sec.

The early suspicion that the formation of an axial spearhead depended upon the presence of the resistance wire element was thus eliminated. In other similar pictures, taken without back lighting, the luminosity of the base of the spearhead is clearly evident.

By employing a square plastic tube, the complex wave interaction can be further examined. Figure 5 illustrates the beautifully symmetrical pattern of luminous and nonluminous phenomena occurring at an intermediate point in the initiation process. This frame, selected from a full sequence, had an exposure time of  $1.4 \mu$  sec. The tube was 22 mm. x 22 mm. x 75 mm. and had been shocked through a rubber barrier in the usual manner. The top of the grey zone, seen in the front view, represents the position of the compression wave in the plastic container and also seen where the luminous zones merge in the center, is the point where the transverse sonic waves intersect in the liquid.

In Figure 6, four selected frames are shown from a framing camera sequence where a standard card-gap (2) configuration was used. The time between adjacent frames is  $4.2 \mu$  sec.; the exposure time is  $1.4 \mu$  sec. Again, a square plastic tube was used with a 2.6-inch card-gap (plastic) and two 1-5/8-inch-diameter by 1/2-inch-long tetryl boosters. This result was a high-order detonation, as evidenced by the photographic sequence and also by the clean-cut hole that resulted in the witness plate. The failure of the plate is evident in the fourth frame shown. Again, the wall is the locus for initiation, but the reaction is seen to spread quickly and uniformly across the vessel. The bright spot under the witness plate in frame 9 is an air bubble, but it did not serve as a nucleus for initiation.

A rather similar card-gap test configuration is shown in Figure 7. Here, two sides of the tube were steel and the plastic barrier was only 3.75 cm. thick. The same type donor was used in this test as for that shown in Figure 6, the framing rate was also the same. In this sequence the reaction is predominately along the side walls of the vessel and although reaction developed throughout the entire container by frame 16, the detonation reaction was incomplete and the witness plate was recovered essentially undamaged. These two shots indicate an anomaly which may result from using a witness plate as a criterion for detonation.

In another experiment (Figure 8), a square cross-section tube with two sides of aluminum was employed, together with a rubber barrier. The early stage of the initiation is not unlike that obtained with a plastic card barrier as shown in Figure 6. Instead of a witness plate, an end viewing mirror was used. The incipient ignition, seen in frame 7, has,  $4.2 \mu$  sec. later, developed into a reaction which has engulfed the base of the charge. In frame 10, a luminous cloud, giving the appearance of the plasma reported by Cook (3), is seen at the end of the charge resting on the liquid explosive meniscus.



Fig. 5 - A single frame, from a sequence, of detonating NG/EGDN in a plastic vessel having a square cross section. The end-on mirror shows the symmetry of shock interaction and peripheral initiation. The exposure time was  $1.4 \mu\text{sec}$ .

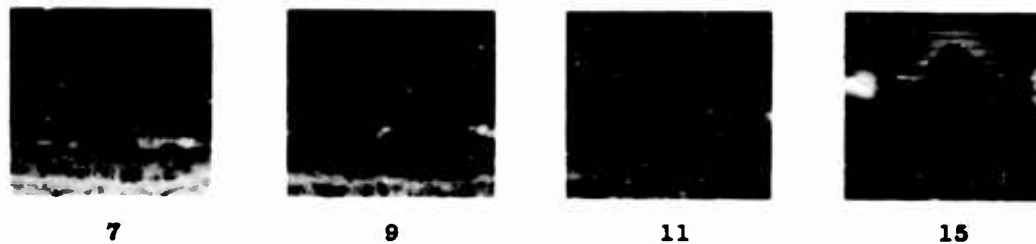


Fig. 6 - Selected frames from a sequence of a detonation in NG/EGDN for a typical card-gap configuration. A plastic tube having a square cross section, a plastic barrier thickness of 2.6 inches, and a 4 inch x 4 inch x  $1/4$  inch witness plate were used. A high order detonation resulted which punched a clean hole in the witness plate. The adjacent interframe time was  $4.2 \mu\text{sec}$ , and the frame exposure time was  $1.4 \mu\text{sec}$ .



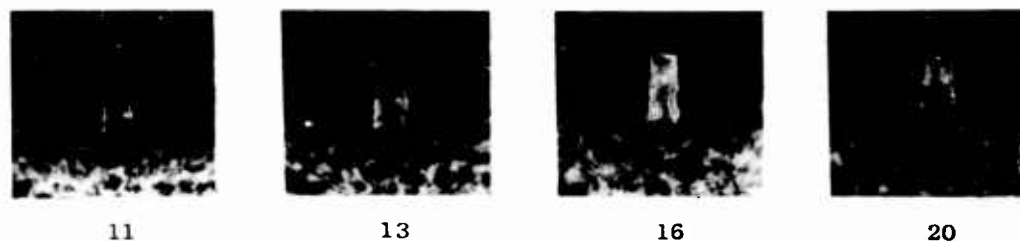


Fig. 7 - Photograph of a card-gap configuration in which the side walls were steel; gap thickness was 1.5 inches (vs. 2.6 inches for Fig. 6). Initiation is at the metal wall surfaces. Reaction was predominately low-order, little witness plate damage resulted. The interframe is  $4.2 \mu\text{sec.}$  and frame exposure time is  $1.4 \mu\text{sec.}$

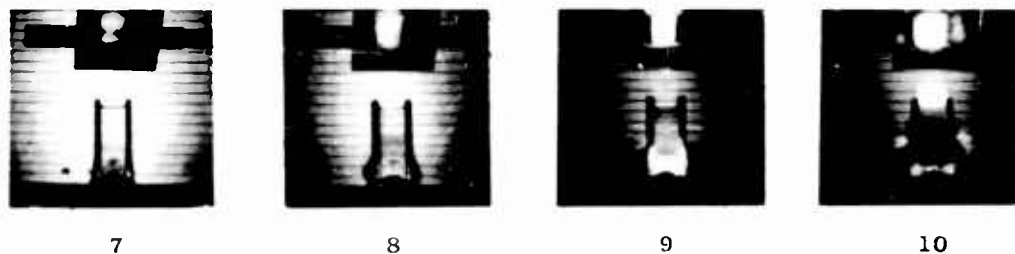


Fig. 8 - Frames selected from a sequence of detonating NG/EGDN in a vessel of square cross section and with two aluminum side walls. A rubber shock attenuation-barrier was used. Early initiation stages are similar to the card-gap tests, except that the locus for initiation appears to be in a central region. In frame 10 a luminous cloud is seen at the end of the charge resting on the meniscus although the reaction has not as yet reached the end of the charge.

The nature of the off-end luminous zone, seen in the preceding photograph, may be explained by the results in Figure 9. The vessel is a 35 mm. i.d. cylinder. Frame 6 shows the shock wave entering the column; in frame 8, two zones are discernible, the uppermost caused by the shock wave in the wall and the opaque region at the base of the charge due to shock activity in the unreacted liquid. Merging in frames 10 and 12, these zones have enveloped the entire charge by frame 14. A reaction at the wall, occurring at the base of the column in frame 16, has, by frame 18, reached the end of the charge; however, at this instant an opaque fountain (dark cloud) of unreacted droplets or mist of explosive is ejected from the surface of the liquid. In frame 19 this cloud has grown and is reacting as a droplet suspension in the off-end atmosphere. Also visible in frame 19 is an annular droplet formation caused by ejection of material near the wall subsequent to the central fountain shown in frame 18. The appearance of this off-end phenomenon could readily be misconstrued as a "plasma", since it would probably have electrical characteristics of a "plasma" when evaluated by probe techniques and certainly appears to have the photographic attributes of the "plasma" described in the literature by Cook, et al. (3, 13).

The results obtained using a hybrid confining vessel are shown in Figure 10. In this experiment, one side wall is aluminum and the other is steel; a rubber barrier is employed. Selected frames from the sequence indicate effects caused by the nature of wall material. The interframe time is  $2.1 \mu$  sec. and the exposure is  $1.4 \mu$  sec/frame. The event is symmetrical in the early stages; by frame 5 the effect of the difference in wall composition becomes noticeable in that the side view shows the precursor wave along the steel to be advancing ahead of the wave along the aluminum. In contrast to this, the end view indicates that the locus of an early reaction, which appears to die out, is at the aluminum wall. In frame 6 a symmetrical axial disturbance forms which, by frame 9, appears to bend toward the aluminum wall. In frame 12 the ejection of a droplet formation is evident with the greater jet action in the vicinity of the steel. By frames 14 and 15, pockets of reaction appear along the steel interface and in frame 16 the off-end droplet cloud has reacted in passage into the air at the charge end.

The schlieren photograph in Figure 11 clearly shows the multiplicity of lateral waves induced in the explosive by shock waves in the steel side walls. This is a single-frame Rapatronic camera photograph taken  $25 \mu$  sec. after entry of the shock wave into the NG-EGDN filled vessel. The charge contained a resistance element. The opaque region at the base of the charge represents the disturbance in the liquid explosive.

The effect of the presence of metal surfaces in repressing detonation failures in nitromethane was reported by Campbell and associates (15). The experiments involved streak camera studies of detonation in tubes of glass, dural, and glass tubes lined with

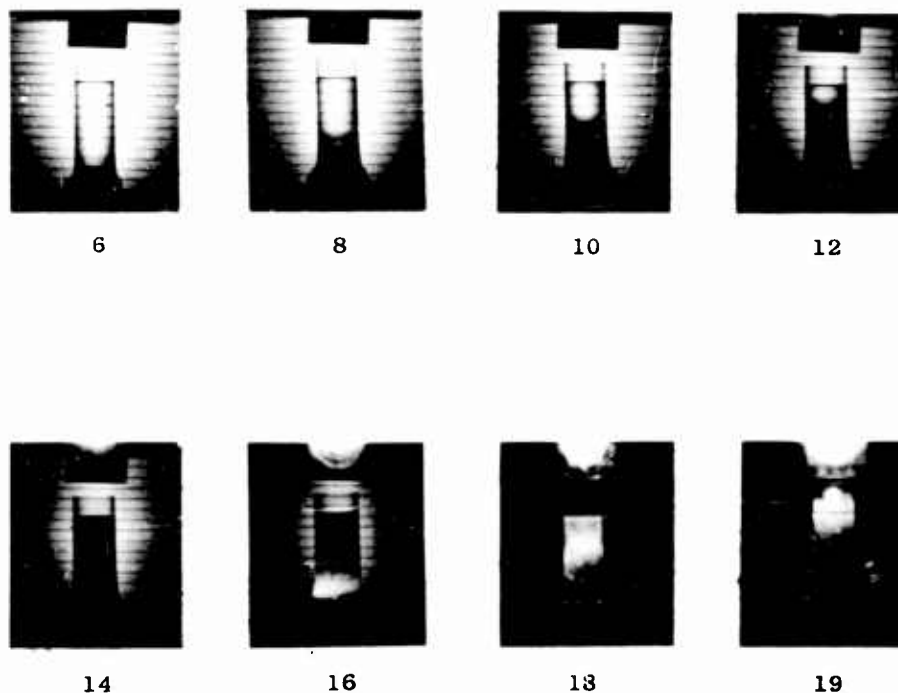


Fig. 9 - The development of the off-end luminous cloud is shown in the selected frames from a sequence of detonating NG/EGDN in a 35 mm. i.d. Plexiglas tube. Predetonation activity is shown in the early stages of the event and in frame 18 an opaque axial droplet ejection is clearly evident, in frame 19 (4.2  $\mu$ sec. later) this material has reacted on its passage into the atmosphere. In addition, an annular formation has developed during the interframe time of 4.2  $\mu$ sec. and exposure time of 1.4  $\mu$ sec. This may be an example of the phenomena referred to in the literature as a "plasma."

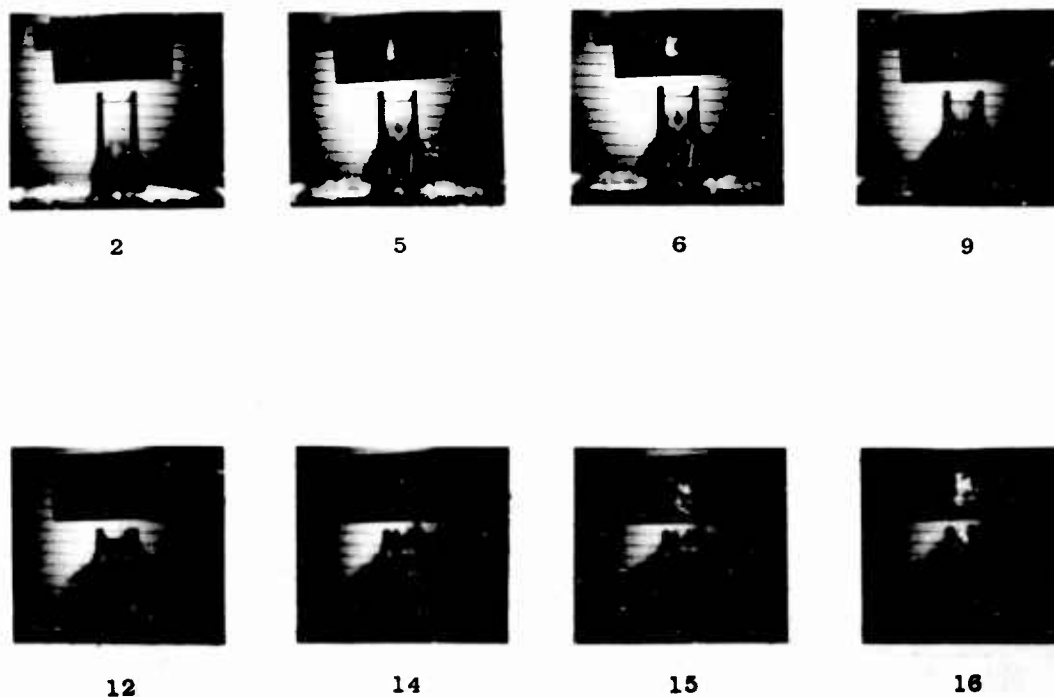


Fig. 10 - Selected frames from a sequence of detonating NG/EGDN showing the effect of wall material. The left side wall is aluminum and the right wall steel. Luminosity is first discernible in the region of the aluminum but is later followed by reaction at the steel wall. Adjacent frames were  $2.1 \mu\text{sec}$ . apart and frame exposure was  $0.14 \mu\text{sec}$ . The jet of unreacted explosive is visible and the locus of reaction is shown in the end-on mirror view.



Fig. 11 - A Rapatronic camera schlieren photograph of the lateral waves in the body of a detonating NG/EGDN mixture.

various metal foils. Campbell and his fellows concluded that the action of metal foils in repressing failures was due to the confinement provided by the foil where the density, compressibility, and thickness of the material are the important parameters. No discernible effect was observed due to the specific nature of the surface. In our experiments, using relatively thick (3.1 mm.) side walls, the wall material seemed to play an important role in establishing the locus of initiation.

Resistance-element records for two types of initiation of detonation in NG/EGDN are shown in Figure 12. In one case (Figure 12(a)) in which the barrier was a 2.6 cm. long rubber cylinder snugly fitting into the plastic acceptor tube, the shock waves were sufficiently intense to cause the detonation to occur after a delay of 25  $\mu$  sec. and at a point about 1.6 cm. into the charge. In the other case (Figure 12(b)), where shock attenuation was provided by the conventional-type rubber barrier (shown in Figure 1), a delay of about 45  $\mu$  sec. resulted and initiation to detonation originated at a distance of 5.2 cm. from the barrier. During the delay, the wire-element record shows a period of erratic behavior where no orderly propagation is indicated; however, ultimately, at least on the axis, the hydrodynamic velocity was attained. Our conclusion is that had these tests been instrumented only by witness plates, the first result would have been "positive," the second a "failure". Under these conditions, the detonation velocities measured over discrete intervals would have been recorded as high and low, respectively.

#### Discussion and Conclusions

These photographic studies indicate that the stimulus given to a sample in the card-gap test is anything but simple. Evidently, the usual concept of a sample being subjected to a "pure shock" is rather naive and quite inadequate. Rather, the sample is subjected to a wide range of interacting forces. Consideration of these interactions leads us to suggest a new mechanism for the initiation of detonation in liquid explosives. The mechanism is essentially one of cavitation established by shock excitation (16), possibly with additional heating of the liquid provided by shear forces resulting from differential particle velocities in the liquid and between the liquid and the container walls. A minor contribution to heating may result from compression of the liquid.

If a liquid body is exposed to intense acoustic vibrations -- and the intensity of the stimulus in the tests described is unquestionably high -- gas bubbles will be formed from the dissolved gases. Such gas pockets may first exist as small invisible bubbles of microscopic dimensions. These bubbles, finely dispersed throughout the liquid, constitute weak points in a liquid whose tensile strength is determined by the largest bubble present. In addition,

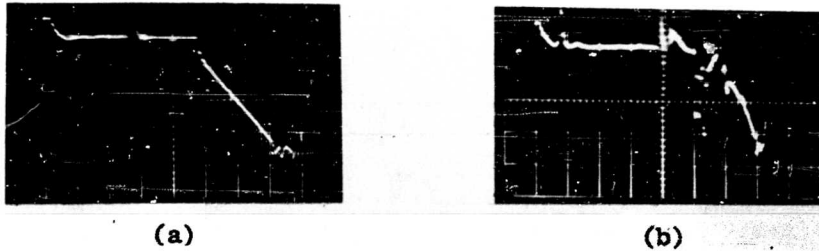


Fig. 12 - Oscillographic record of a wire element employed for the continuous determination of detonation velocities. (a) Waveform resulting from a high order propagation in NG/EGDN in which the steady state velocity is  $8.6 \text{ mm}/\mu\text{sec}$ . A piston type rubber barrier was used giving an abnormally high apparent velocity which may have been due to precompression during the  $25 \mu\text{sec}$ . delay before reaction began. (b) Waveform resulting from a test using the conventional charge configuration (Fig. 1). A period of erratic behavior is indicated prior to establishment of a  $7.5 \text{ mm}/\mu\text{sec}$ . propagation. Time base is  $5 \mu\text{sec}/\text{div}$  on the abscissa and distance is  $3.6 \text{ cm}/\text{div}$  on the ordinate.

impurities, such as dust particles, provide nuclei for the formation of additional cavities. Other weak points would be found in the gas nuclei contained in small imperfections in the container wall. In a reactive system, such as NG/EGDN, the vapors in the voids would be capable of exothermic decomposition. Bowden and associates (4), have postulated that the adiabatic heating of such cavities would be a source of local reaction; however, Bolkhovitinov (8) and Selberg (12) disagree with this theory, based on consideration of thermal relaxation times for the very small bubbles ( $10^{-3}$  to  $10^{-9}$  mm.).

During cavitation, the small bubbles may coalesce into larger bubbles of a size sufficient for compression to result in adiabatic heating. Importantly, any decomposition of the vapor or droplets in the bubbles which results in the production of gas, also results in an increase in bubble size. The time required for the foci to grow through coalescence and reaction may well account for the long delays observed in the initiation process.

An analogy of the cavitation process has been observed in solid plastic rods. Figure 13 shows a section of 1-1/4 inch Plexiglas rod after it has been subjected to the shock waves from a 1-1/4 inch diameter explosive donor. That part of the rod immediately adjacent to the explosive was completely destroyed but a portion of the rod recovered shows a well defined spearhead of multiple tensional fractures. This is to be compared with Figures 2 and 4 showing the spearhead observed in 50-50 NG/EGDN. Each fracture gives the appearance of a small cone pointed toward the explosive donor. This solid analog lends support to the suggestion that initiation processes comparable to those observed here in liquids may play an important role in the sensitivity of solid propellants.

The nature of "low-order detonations" continues to elude definition. These phenomena are characterized by low apparent velocities of a luminous, pressurized, or ionized front. Because the luminosity, pressure, and ionization are all less than that associated with a normal detonation, less than complete reaction is the usual assumption. Tacitly, the process is otherwise assumed to resemble a detonation (17). The broad luminous zone, the complex pressure interactions between wall and contents, and the erratic ionization observed with the resistance element raises questions as to the validity of this assumption. Further investigation of "low-order detonations" are planned by the Bureau of Mines because of their potential importance in the safe handling of explosives and propellants.

#### Acknowledgment

This research was supported by the Advanced Research Projects Agency, Department of Defense, Order No. 44-59.

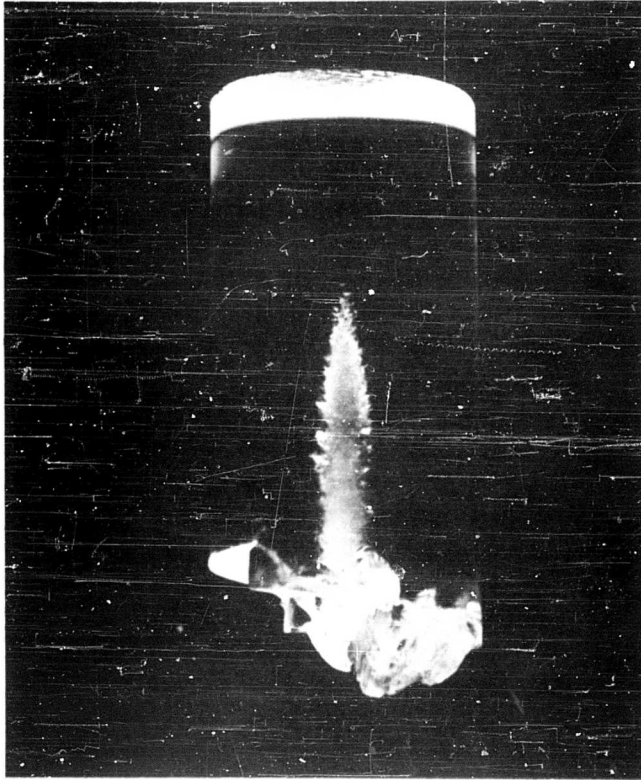


Fig. 13 - Photograph showing the effect of shock wave interaction in a solid Plexiglas rod which had been used as a barrier in a card-gap test. The effect of tension and the attenuation of the shock wave with distance into the rod is clearly shown. Similar effects in liquids would produce cavitation.



List of References

1. S. J. Jacobs, Recent Advances in Condensed Media Detonations, J. Am. Roc. Soc. 30, 151-8 (1960).
2. Liquid Propellant Test Methods, Test No. 1, Card-Gap Test for Shock Sensitivity of Liquid Monopropellants, The Liquid Propellant Information Agency, Applied Physics Laboratory, The Johns Hopkins University, March 1960.
3. M. A. Cook, D. H. Pack, L. N. Cosner, and W. A. Gey, Instrumented Card-Gap or SPHF-Plate Test, J. Appl. Phys. 30, 1579-84, (1959).
4. F. P. Bowden and A. D. Yoffe, Initiation and Growth of Explosion in Liquids and Solids, Cambridge University Press, Cambridge, England, (1952).
5. G. B. Kistiakowsky, Initiation of Detonation of Explosives, Third Symposium on Combustion and Flame and Explosion Phenomena, The Williams and Wilkins Company, Baltimore, Maryland, (1949), 560-5.
6. A. J. B. Robertson, The Thermal Initiation of Explosion in Liquid-Explosives, *ibid.* 545-51.
7. K. K. Andreev, Some Considerations on the Mechanism of Initiation of Detonation in Explosives, Proc. Roy. Soc., 246, 257-67, (1958).
8. (a.) L. G. Bolkhovitinov, On the Theory of the Initiation of an Explosion by the Falling Weight Tests, Dokl. Akad. Nauk, USSR, 125 (3), 570-2 (1959). (b.) L. G. Bolkhovitinov, A Possible Mechanism for the Initiation of Liquid Explosives, *ibid.* 126 (2), 322-4 (1959). Translated and issued by Technical Information and Library Services, Ministry of Aviation, December 1959.
9. C. H. Johannson and H. L. Selberg, The Ignition Mechanism of High Explosives, App. Sci. Res. A 5, 439-49 (1955).
10. C. H. Johannson and others, The Initiation of Liquid Explosives by Shock and the Importance of Liquid Break Up, Proc. Roy. Soc., 246, 160-7 (1958).
11. G. P. Cachia and E. G. Whitbread, The Initiation of Explosives by Shock, Proc. Roy. Soc., 246, 268-73 (1958).
12. H. L. Selberg, Initiation of Nitroglycerin by Shock Waves, Appl. Sci. Res. A 5, 450-2 (1955).

13. M. A. Cook, R. T. Keyes, and L. L. Udy, Propagation Characteristics of Detonation-Generated Plasmas, J. Appl. Phys., 30, 1881-92 (1959).
14. F. C. Gibson, M. L. Bowser and C. M. Mason, Method for the Study of Deflagration to Detonation Transition, Rev. Sci. Inst., 30, 916-9 (1959).
15. A. W. Campbell, M. E. Malin, and T. E. Holland, Detonation in Homogeneous Explosives, Proceedings of Second ONR Symposium on Detonation, Office of Naval Research, Department of the Navy, Washington, D. C. (1955), 336-59.
16. I. R. Jones and D. H. Edwards, An Experimental Study of the Forces Generated by the Collapse of Transient Cavities in Water, J. Fluid Mechanics, 7, 596-609 (1960).
17. Rudi Schall, The Stability of Slow Detonation, Z. fur angew. Phys., 6, 470-5 (1954).

INITIATION CHARACTERISTICS OF MILDLY  
CONFINED, BUBBLE-FREE NITROGLYCERIN

C. H. Winning  
E.I. du Pont de Nemours and Company  
Gibbstown, New Jersey

Background Information

The many initiation studies that have been conducted indicate that initiation, especially by near-minimum influences, is controlled by many physical conditions. Nitroglycerin was first prepared in 1846 and much information has been obtained about the initiation process and associated conditions since the initial work on nitroglycerin by Sobrero and Nobel.

Prior to 1892, Berthelot concluded that the impact energy in the drop-weight initiation test was sufficient to heat only a small portion of a nitroglycerin sample to the detonation temperature (Ref. 1). Direct evidence concerning energy requirements and the details of the localized process was obtained many years later by Bowden and co-workers (Ref. 2). These investigators found that the applied energy required for impact-initiation was only  $5-25 \times 10^{-4}$  cal. in the presence of an air bubble. The heat developed within a small bubble by adiabatic compression accounts for  $10^{-10}$  to  $10^{-7}$  cal. In the absence of bubbles the applied energy required for impact initiation was higher by many orders of magnitude, namely, 2.5-25 cal.

The importance of air bubbles in dense, gelatinized nitroglycerin explosives is well known in the explosives industry. For instance, blasting gelatin (approximately 91% nitroglycerin, 8% nitrocotton, 1% chalk) may become so insensitive from loss of occluded air during storage that initiation by a commercial blasting cap is well-nigh impossible.

Bowden often found the build-up time from deflagration to detonation of nitroglycerin to be 20-150  $\mu$ s starting from a hot spot in a confined film. In some unpublished work by the writer the build-up times for the underwater shock-wave initiation of nitroglycerin in polyethylene bags often were much longer, namely 1-15 ms, if the near limiting conditions for initiation existed. This work involved sympathetic detonation tests between primer and receptor charges spaced to obtain various shock wave energies, or pressures. At a distance for consistent propagation from a 73 g. cast pentolite primer, namely 8 ft., the shock-wave energy was only about 0.025 cal./cm<sup>2</sup>,

and the pressure 75 atmospheres (Ref. 3). Undoubtedly air bubbles were present in the nitroglycerin. Bowden found that the building-up process of initiation of nitroglycerin from an adiabatically compressed air bubble in a film could be accomplished if the bubble volume was compressed by a ratio of 20/1, which corresponds to a pressure increase from 1 atmosphere to about 50, or to an initial adiabatic bubble temperature of about 500°C. In both Bowden's work and ours the build-up to detonation was slowest if a minimum intensity initiating influence was exerted.

Earlier work at this Laboratory gave reason to consider that more than microscopic or very localized effects might be involved in the initiation of bubble-free, unconfined nitroglycerin. Whereas nitroglycerin may readily be caused to detonate from a small hot spot in a thin, confined film, it fails to propagate far from even a large primer if confined only in a paper tube (soda straw) having a diameter of about 4 mm. This diameter is approximately the critical size for propagation of slightly confined nitroglycerin.

#### Method of Investigation

A framing camera was used to take a sequence of 25 pictures of the initiation process in 20 to 60  $\mu$ s. The subjects were back-lighted with an argon flash lamp in order to reveal shocks, rarefaction clouds, and gas clouds.

A commercial blend of 70/30-nitroglycerin/ethylene glycol dinitrate (EGD) which had the characteristic yellow tint of the clear liquid was used. The material was passed through double dry filter papers prior to use. For brevity, and in accord with common industrial usage, the blend of nitrate esters will be referred to as NG throughout this paper.

The cells containing NG were either rectangular or cylindrical. The rectangular cells had windows of either glass or 1 mil "Mylar"\* (10<sup>-3</sup> in. thick). The latter material was used for most of the investigation. The cylindrical cells were made of "Mylar" that was cemented to a disk-shaped base of "Lucite"\*\*. The smallest dimension of the cell in different experiments ranged between 3/4 in. and 3 in.

In order to minimize shock reflections and rarefaction clouds in the undetonated NG near a slow-acting initiating influence, some of the cells were immersed in tanks containing either water or a denser aqueous salt solution.

Initiating influences were applied by several methods. Arc discharges and exploding bridge wires were set off within NG-filled cells, using a source of 5000 v. from a 3  $\mu$ fd condenser that was triggered through a 5C22 hydrogen thyratron tube. No. 8 and other blasting caps of the arc-firing type also were used as initiators. The No. 8 caps started to expand about 2-1/2  $\mu$ s after the spark discharge.

Other experimental details will be mentioned where they apply.

\*Registered trademark for polyester film of E.I. du Pont Nemours & Co., Inc.

\*\*Registered trademark for acrylic resin of E.I. du Pont de Nemours & Co., Inc.

## Initiation Studies

### Arc Discharge in NG

The photographs revealed that the initial highly luminous reaction about a spark discharge (0.01 cm. gap) in NG soon diminished in luminosity. The photographic record is indicative of an initial temperature greatly exceeding 3000°K. The initial radial expansion rate of the hot gas globe in the NG was 150-200 m./sec., but this rate diminished to about 50 or 60 m./sec. 25  $\mu$ s after the discharge. The rate decreased to about 35 m./sec. in another 25  $\mu$ s.

The approximate energy of the spark discharge in NG was 4.5 cal. if we assume that half of the condenser energy was transmitted to the discharge points.

An attempt was made to produce an accelerated reaction in the vicinity of sparks by firing two successive ones 0.2 cm. apart, in a time interval of 10  $\mu$ s. The objectives were as follows: (1) to project compressed liquid, preferably as spray, into the first hot gas globe, (2) to create additional pressure between arcing regions, and (3) to start a larger hot reaction zone. Johansson, Selberg (Ref. 4) and co-workers (Ref. 5) considered some of these effects when investigating the shock initiation of NG and of another liquid, nitric acid-dinitrotoluene. Fig. 1 shows the events 13-47  $\mu$ s after firing the first of two sparks in NG. The second spark, fired 10  $\mu$ s after the first, produced no significant acceleration of the reaction in the NG. The radial rate of gas expansion around the initial discharge diminished to about 70 m./sec. between 20 and 40  $\mu$ s after the first discharge. The two cylindrical objects (0.6 cm. x 1.3 cm.) evident on either side of the arcs were solid rubber supports for the terminal wires that were set to provide a gap distance of 0.01 cm.

### Exploding Bridge Wire in NG

A high voltage pulse was applied to a resistance bridge wire that was immersed in NG. The wire was about 0.25 cm. long and 0.005 cm. in diameter. The very luminous, high-temperature reaction around this exploding bridge wire also proceeded with diminishing luminosity and rate of radial expansion. The radial expansion rate was about 60 m./sec. after 35  $\mu$ s, and about 22 m./sec. after 200  $\mu$ s.

### No. 8 Blasting Cap in NG

An initiator having the strength of a No. 8 blasting cap is considered an adequate, dependable initiator for practically all explosives that are capable of propagating a stable detonation at diameters up to about one inch. The heat of reaction of the explosive charge in the cap is about 600 cal. However, in the absence of adhering bubbles on a cap immersed in NG, usually only a very slow or a partial reaction of the NG occurred.

Fig. 2 shows two NG cells (2 in. x 2 in. x 3 in., inside dimensions; glass windows), each of which contained a No. 8 cap having a transparent plastic shell instead of the usual metal shell. Thus the luminosity of the cap reaction was evident from its beginning. The left cell contained water, the right one NG. A delayed-action, destroying pellet for the NG is evident outside the cell at the right. The third picture in the sequence shows similar luminosity and gas expansion, and similar shock waves in the two liquids. Thus

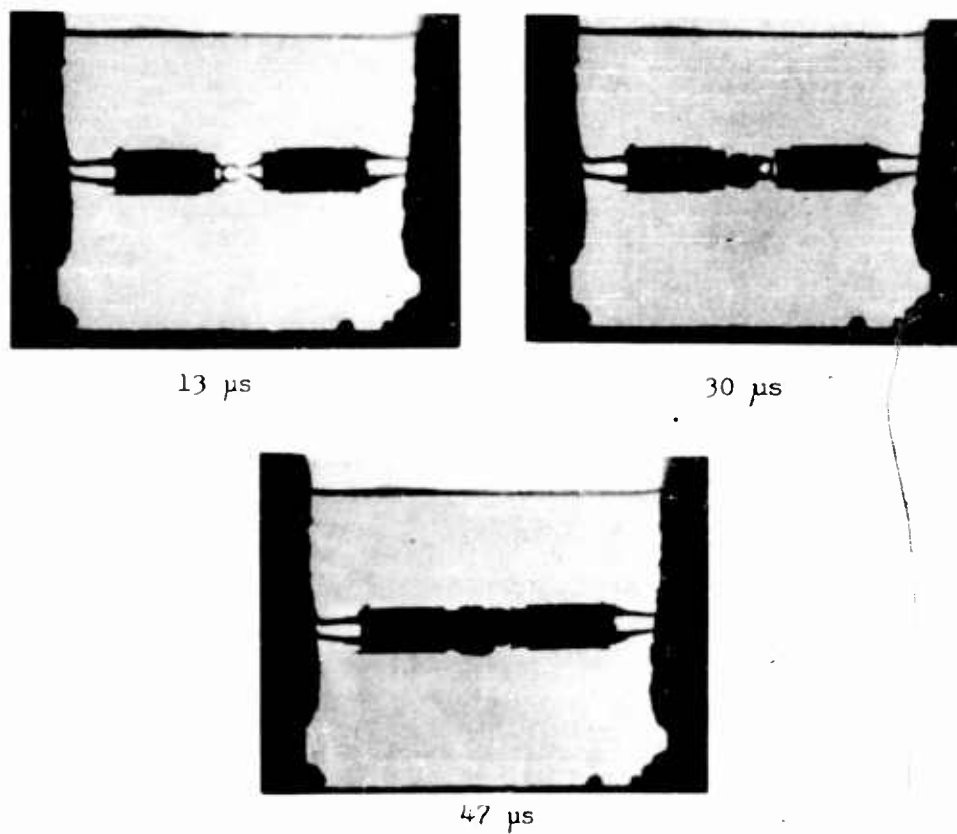


Fig. 1 - Consecutive sparks in NG. Stated times are relative to the firing of the first spark

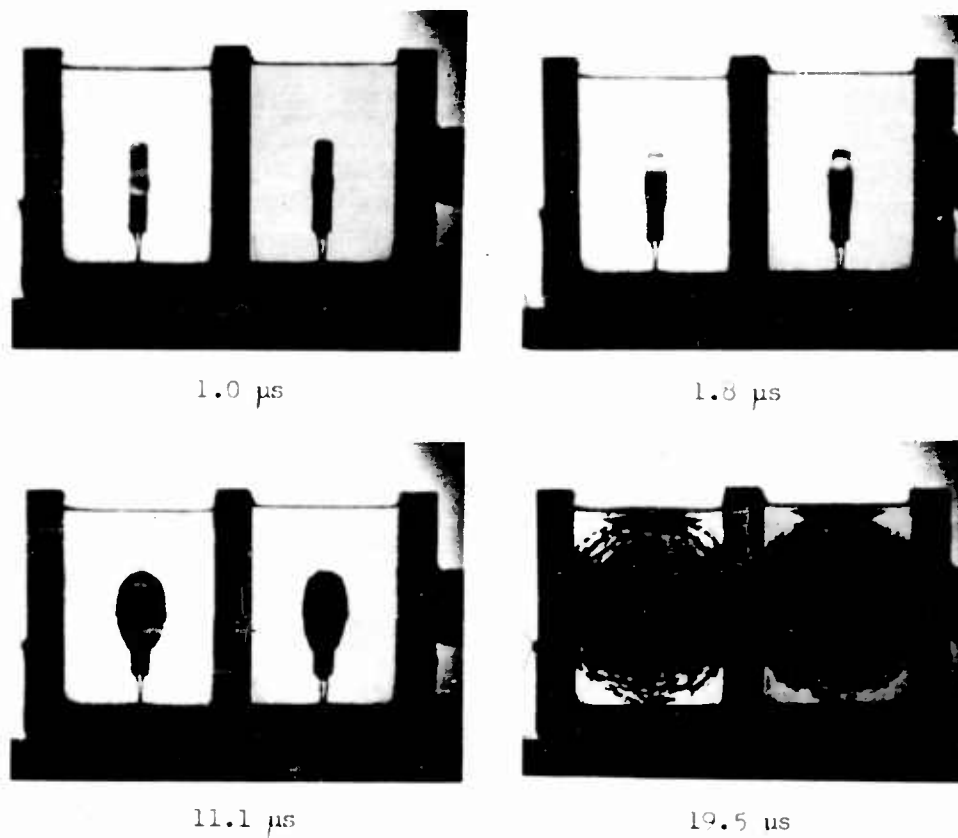


Fig. 2 - No. 8 plastic shell caps fired in water (left) and in NG (right). Stated times are relative to the start of cap expansion.

neither a high velocity detonation nor appreciable deflagration started in the NG. The fourth photograph shows comparable glass breakage and also the start of a dark rarefaction cloud below the surface of both liquids. The over-all result is typical of that obtained with caps having the standard cap shell of metal.

The effect of occluded air on initiation is shown in Fig. 3. Fine, aerated powders, (cork dust and "Microballoons"\*) were secured in narrow lines on opposite sides of a No. 8 cap by use of a thin film of rubber cement. Luminous detonation at about 7500 m./sec. started very suddenly from each aerated region.

Although not illustrated in Figs. 2 and 3 a high velocity detonation occasionally started suddenly at the shock front about 0.3 cm. from the end of a cap having a conical indented end, which is standard construction. This end-initiation by converging shock influence did not depend on the presence of an air bubble in the indentation. The tests were conducted with the indented end of the cap up, and, as usual, the adhering bubbles were dislodged with a wire probe.

The indented end of a No. 8 cap (shell of commercial bronze) is the source of a high-velocity metal jet if a cap is detonated in air, but not if it is detonated in NG without a bubble in the cavity. A cap jet in air having a characteristic velocity of 2800-3500 m./sec. may be shot into NG from a distance of 2.5 cm. above the NG surface without starting a high-velocity detonation during a penetration exceeding 4 cm. During this penetration, the jet hole in the NG typically attained a diameter of 0.7 cm., and a surface layer of NG burned to a depth of 0.8 cm. In the absence of a delayed-action destroying pellet, it is possible that in some tests the NG would burn partially or completely without detonating. On the other hand, a cap jet caused a pulverulent, aerated dynamite containing 50% NG to detonate at nearly its characteristic velocity (for cartridges of 1-1/4 in. diameter) within 5 us after jet impact.

The third picture in Fig. 4 shows the delayed, luminous initiation of NG at high velocity by a No. 8 cap that was centrally situated within the cell. In this experiment the cell width was only 7/8 in. (front to back). In the third picture the faintly visible shock from the cap (in the clear NG) has a velocity of 1700 m./sec. The initial shock velocity at the cap boundary was about 3500 m./sec. The shock front in this NG cell was followed within about 0.6 cm. by a dark appearing rarefaction cloud, in which the luminous detonation started 5.4 us after the initial cap expansion. The gas cloud from the cap is obscured by the rarefaction cloud around it. The start of delayed, high-velocity, luminous detonation within a rarefaction cloud prompted further investigation of this phenomenon. Additional interest arose because the hot gas cloud was sufficiently transparent for a brief interval to reveal the presence of the non-luminous gas cloud from the cap. Photographs 3 and 4 in Fig. 4 also show the surface effect of hot gas projected from above by a blasting cap having no metal end.

Fig. 5 shows a single picture from a sequence which was  
\*Registered trademark for hollow, unicellular, urea-formaldehyde plastic spheres of Standard Oil Co. of Ohio



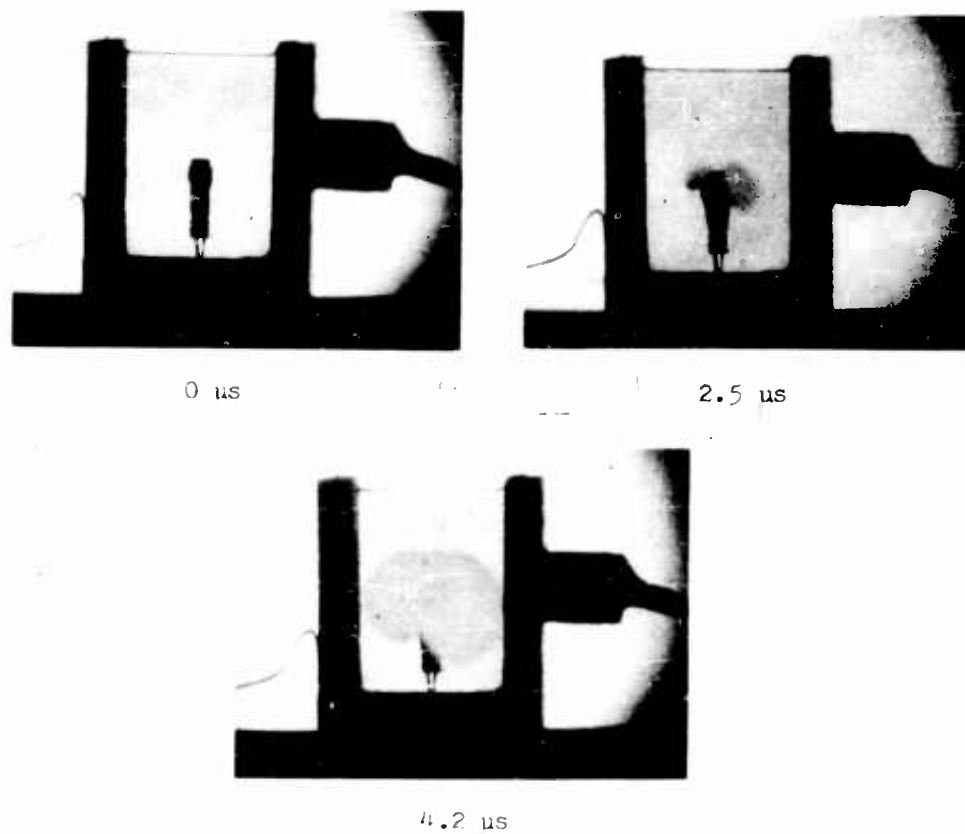


Fig. 3 - No. 8 cap fired in NG - "Microballoons" and cork dust, respectively, on opposite sides of cap.

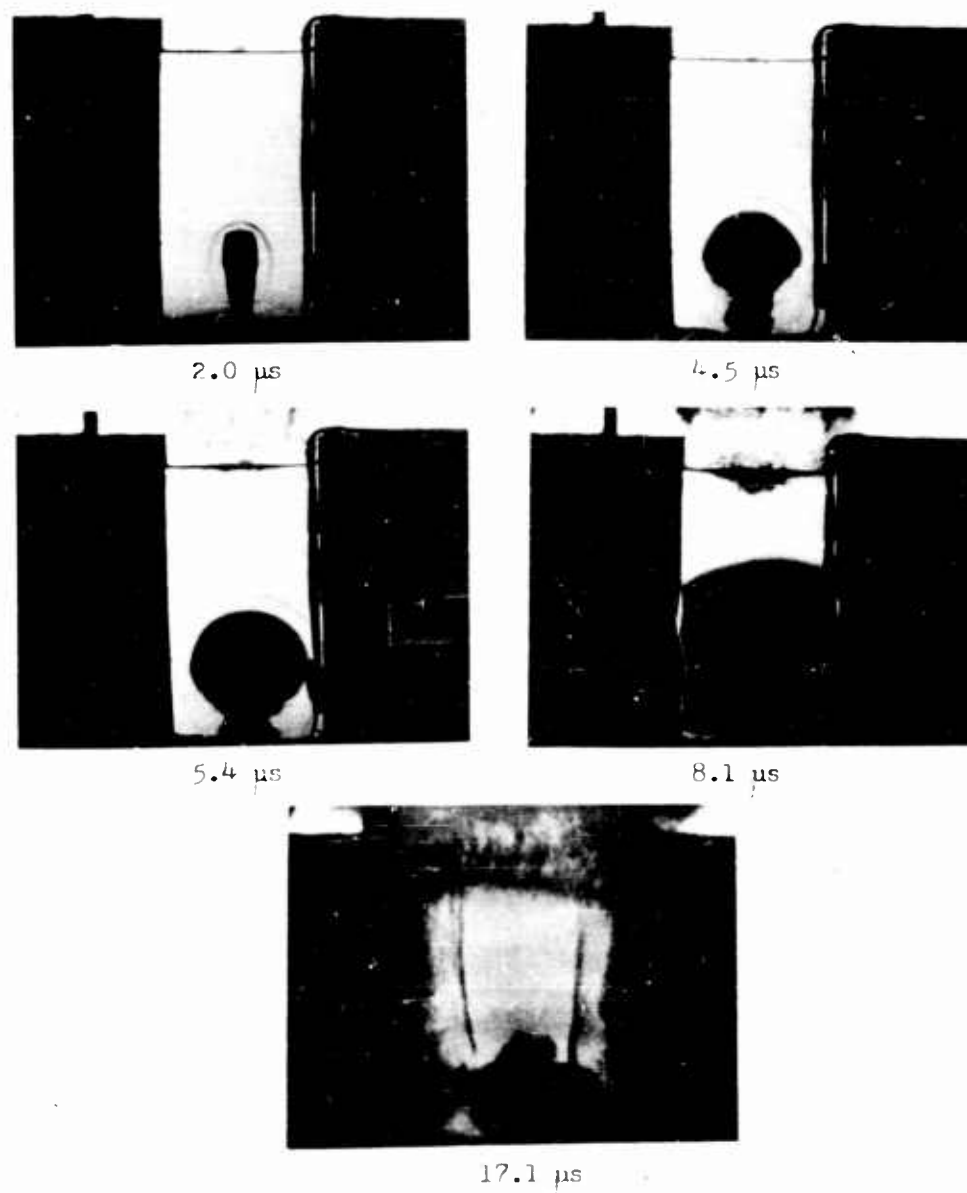


Fig. 4 - No. 8 cap fired in NG cell 7/8 in. thick. Open-end cap fired 1-1/2 in. above the NG surface.

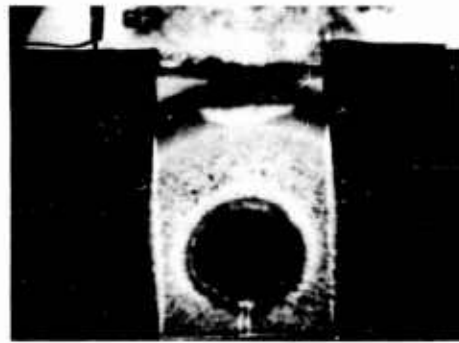
similar to that in Fig. 4. The width of the cell in Fig. 5 was  $1/4$  inch more than that in Fig. 4, namely  $1-1/8$  in. The dark rarefaction cloud and the delayed initiation therein again occurred. The highly transparent gas cloud from the detonation of NG is of additional interest, for in it the dark gas cloud from the cap and also the cap wires are clearly evident. An equally transparent gas cloud was not consistently reproducible. Its formation appeared to depend on the high-velocity detonation (at about 8000 m./sec.) of preshocked NG in a rectangular cell, containing a rarefaction cloud.

Initiation of NG by caps under other physical conditions was then investigated, as shown in Fig. 6. Cylindrical cells of NG were immersed in water to modify the shock reflections. At the right a single cap was located in a cylinder of NG having a diameter of  $3/4$  in. To the left of a plywood barrier was a larger cell containing two caps  $3/8$  in. apart. This large cell had a diameter of 3 in. The third picture shows the absence of luminous, high-velocity detonation 58  $\mu$ s after simultaneous firing of the three caps. However, it is of interest to note in the second picture that a faintly luminous region existed temporarily in the small cylinder; that is, in the rarefaction region above the oval gas cloud from the cap. The intersecting shocks between the adjacent caps in the large cell did not initiate any noticeable reaction. A flat rarefaction cloud is evident above the two caps in the third picture. This cloud appeared and disappeared intermittently during the picture sequence.

Shock reflections in NG were essentially eliminated by immersing an NG cell in a dense salt solution. (The solution density was 1.34 at 25°C. The composition was as follows:  $\text{NH}_4\text{NO}_3$  - 33.0%,  $\text{NaNO}_3$  - 23.0%,  $\text{H}_2\text{O}$  - 44.0%). The solution was contained in a cubic tank, 10 in. in each dimension. Thus the effect with regard to shock reflections was essentially that of shooting a cap at the center of a 10 in. cube of NG, except that the "Lucite" base of the cylinder produced a near-by rarefaction cloud. The diameter of the cylinder containing the NG was 3 in. The two pictures of Fig. 7 reveal a slow, nonluminous expansion around the cap. Cracks in the glass window of the tank started to obscure the view after about 148  $\mu$ s. The radial expansion rate was accelerating slowly toward the end of the observation period, and had attained 440 m./sec. after 148  $\mu$ s.

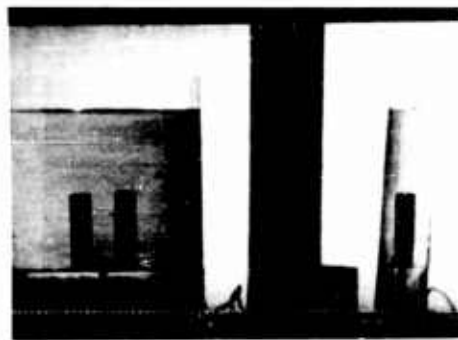
Because NG reacted so slowly to the influence of a blasting cap, it was of interest to know the effect of a cap in a nonexplosive liquid having comparable density. Fig. 8 shows the effect of No. 8 caps in a chlorinated hydrocarbon, "Aroclor"\* No. 1254 (a liquid having a density 1.54 at 25°C.). The two cylinders of "Aroclor",  $1-1/4$  in. and 3 in. diameter, were immersed in water. A transient rarefaction cloud was formed in the upper portion of the small cylinder, but not in the large one. In the large cell the reflected rarefaction from the more distant wall was weak and thus no rarefaction cloud was formed. The gas globe around the cap in the small cylinder was only slightly smaller after 25  $\mu$ s than the globe around the cap in NG shown in Fig. 5 (after 29  $\mu$ s). The radial rate of gas expansion in the large cylinder of "Aroclor" was 300 m./sec. 25  $\mu$ s after the

\*Registered trademark for chlorinated hydrocarbons of Monsanto Chemical Co.



24  $\mu$ s

Fig. 5 - No. 8 cap fired in NG cell 1-1/8 in. thick. Open-end cap fired 1-1/2 in. above the NG surface.



0  $\mu$ s



29  $\mu$ s



58  $\mu$ s

Fig. 6 - No. 8 caps fired simultaneously in cylindrical NG cells that were immersed in water.

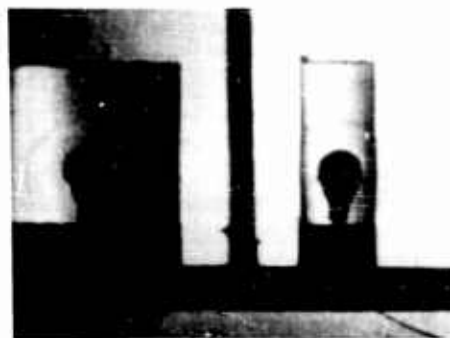


90  $\mu$ s



148  $\mu$ s

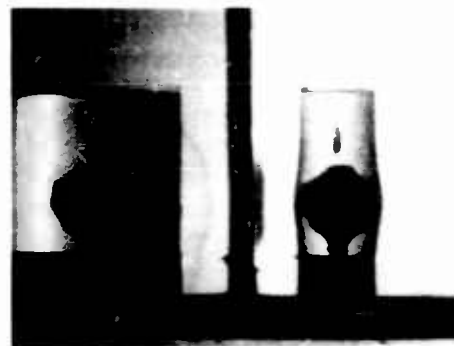
Fig. 7 - No. 8 cap fired in cylindrical NG cell that was immersed in dense aqueous solution.



8.4  $\mu$ s



22.4  $\mu$ s



25.2  $\mu$ s



39.2  $\mu$ s

Fig. 8 - No. 8 caps fired in cylindrical cells containing "Aroclor". The cells were immersed in water.

start of cap expansion, but the rate was diminishing.

Pictures not shown here indicate that the radial rate of gas expansion in water-immersed "Aroclor" diminished to almost zero after 100  $\mu$ s, when the gas globe radius was 2.6 cm. After the same time interval a cap in water-immersed NG caused radial gas globe expansion at 350 m./sec., when the gas globe radius was 4.3 cm. The hot gas volume in NG was about twice that in "Aroclor" after 50  $\mu$ s, but after 10  $\mu$ s the volume in NG was five times that in "Aroclor", indicating that a small amount of reacting NG added its effect to that of the cap.

#### Intersecting Shocks from Special Large Caps

Intersecting shock conditions tending to promote delayed initiation of NG are shown in Fig. 9. A mirror above the cell permitted photographing a downward view in addition to the direct view. The inside length, width, and depth of the cell were 4 in., 3 in., and 2-1/2 in., respectively. The two special caps contained 14 gr. of PETN in the base charge, and were 1/2 in. in diameter to provide an approximately symmetrical charge. The second cap was electrically fired 18  $\mu$ s after the first, at which time a rarefaction shock from the first cap was reflected from the upper surface, and after reflected rarefaction shocks had collided in the bisecting plane of the lower left corner. Delayed initiation of the NG, 29  $\mu$ s after firing the first cap, was evident in the lower left corner of the cell, rather than at the cap location, indicating that this rarefaction zone was more favorable for the development of the deflagration to detonation process. The mirror view of a luminous crescent between the caps indicates the possible existence of a second initiation center between the two caps, where the shock from the second cap acted on the rarefaction cloud proceeding downward from the surface above the first cap.

#### Discussion

The application of different types of intense initiating influences to the interior of essentially unconfined, bubble-free NG gives evidence of low sensitivity and reluctant build-up of deflagration to detonation in a liquid explosive that has been used successfully as a sensitizer for many dynamites, but generally in dispersed, aerated form.

The reaction started in NG by a No. 8 blasting cap proceeds slowly and may not lead to detonation of the sample, as indicated on occasion by recovery of residual material. The relatively small amount of reaction of NG caused by a cap in 50-100  $\mu$ s is indicated approximately by the difference in gas volume in comparison with the gas volume produced by a similar cap in "Aroclor".

A rough estimate may be made of the pressure and temperature in the NG adjacent to the strong shock sources, such as the No. 8 blasting cap. Extrapolation of time-distance curves for shock travel give initial velocities of 3000-3500 m./sec. The correspond-

Note: The possibility of initiation at dust spots on the surface of the NG was eliminated by providing a thin layer of Nujol on the surface. Undesirable absorption of NG by the wood of the cell was prevented by coating the inner surface with shellac.)

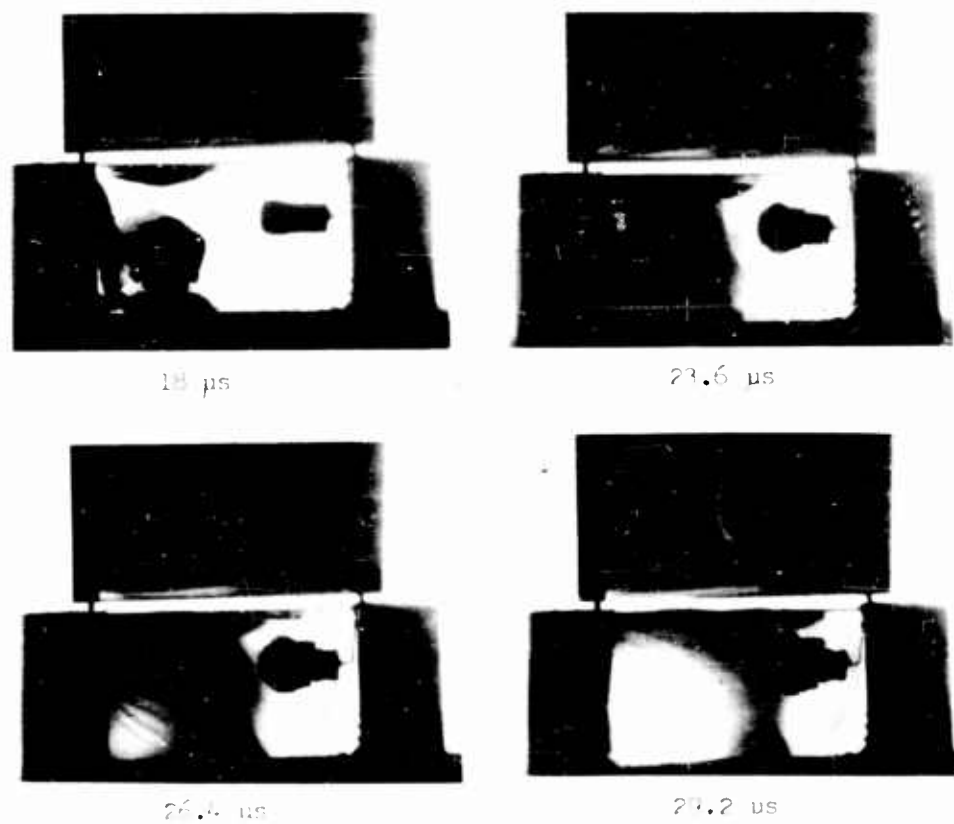


Fig. 9 - Delayed initiation of NG. Special caps contained 14 gr. PETN. Stated times are relative to the firing of the first cap.

ing initial movement of the expanded copper cap shells is not always clearly evident, and the measurements of boundary positions are not accurate because these boundaries were viewed through shock fronts that initially were highly curved. A material velocity of 600-800 m./sec. corresponds approximately to the aforementioned shock velocities. Applying the relationship,  $P = \rho U \mu$ , gives an initial shock pressure of about 40,000 atmospheres. ( $P$  = pressure,  $\rho$  = density,  $U$  = shock velocity,  $\mu$  = particle velocity). The associated transient temperature elevation at the shock front may be estimated by the simplified assumption that also was applied by Selberg (Ref. 6). Accordingly,  $T = \frac{\mu^2}{2C}$ , where  $C$ , the heat capacity, is  $1.7 \times 10^7$

ergs/g. If  $\mu = 8 \times 10^4$  cm./s., then  $\Delta T = 192^\circ\text{C}$ . Since the ambient temperature was about  $25^\circ\text{C}$ , the peak transient temperature was  $217^\circ\text{C}$ .

The failure of NG to develop a rapidly accelerating detonation when exposed to a highly luminous arc discharge or to a high-velocity cap jet (from outside the NG) is evidence of rapid energy dispersion within the nitroglycerin. The energy is dispersed mainly by shock waves of insufficient duration and/or temperature to produce initiation. The cap jet velocity of 3500 m./sec. is much higher than the bullet velocity of 1100 m./sec. which Zippermayr found inadequate for the initiation of NG contained in a synthetic rubber bag. He employed a steel bullet having a diameter of 4.4 mm. (Ref. 7).

The occurrence of delayed initiation in an opaque rarefaction zone raises questions about the mechanism of the event. The creation of the opaque obscuring region can be delayed in increasing the cell dimension in the direction of the field of observation and work along this line is in progress.

#### References

1. Berthelot, M., Explosives and Their Power. English translation by C. Napier and William Macnab, John Murray, London, 1892.
2. Bowden, F.P. and Yoffe, A.D., Initiation and Growth of Explosions in Liquids and Solids. Cambridge at the University Press, 1952.
3. Cole, R.H., Underwater Explosions. Princeton University Press, 1948.
4. Johansson, C.H. and Selberg, H.L., Appl. Sci. Res., V, A, 439 (1955).
5. Johansson, C.H. and others, Proc. Roy. Soc. (London) Discussion, A246, 160 (1957).
6. Selberg, H.L., Appl. Sci. Res., V, A, 450 (1955).
7. Zippermayr, M., Explosivstoffe, 3, 25 (1955).



## SHOCK INITIATION OF DETONATION IN LIQUID EXPLOSIVES\*

A. W. Campbell, W. C. Davis, and J. R. Travis  
University of California, Los Alamos Scientific Laboratory  
Los Alamos, New Mexico

### INTRODUCTION

The processes involved in the initiation of explosives have been the subject of much experimentation and theoretical speculation, and many investigators have contributed to an understanding of the problem. An excellent review of recent work has been made by S. J. Jacobs.<sup>(1)</sup> Of particular relevance to the work to be described here is the paper of Hubbard and Johnson,<sup>(2)</sup> who, in calculational experiments, have studied shock induced thermal explosion. Their calculations agree very well with the conclusions from the work described here.

In this paper experiments are described which show that nitromethane and other explosives in the homogeneous state are initiated as a result of shock heating. The initiation process is essentially a thermal explosion. Before describing the experiments, some of which are indirect, the general sequence of events which take place in the explosive will be described to aid in understanding the purpose of each experiment.

The general plan was to study the behavior of explosive when subjected to a smooth, plane shock wave of constant amplitude. Plane wave lenses<sup>(3)</sup> were combined with additional high explosive and inert shock-attenuator plates to produce a shock wave of the desired amplitude in the test explosive (see Fig. 1). The behavior of the test explosive was then observed before the intrusion of edge effects or of reverberations in the attenuator. When a shock wave, strong enough to produce detonation within a few microseconds, is generated in nitromethane, the explosive behind the shock front is compressed to about  $5/8$  of its original volume and simultaneously is heated to a high temperature estimated to be 1140°K. It has been possible to calculate the compression by impedance-matching calculations, and also measure the compression directly with fair accuracy. On the other hand, it has not been possible to measure the shock temperature; instead,

\* Work done under auspices of the U. S. Atomic Energy Commission.

the temperature has been calculated by approximate methods.

The shock-heated explosive reacts very slowly at first, but the reaction rate accelerates due to self-heating, and detonation results. This acceleration of the reaction rate first becomes important at the attenuator-explosive interface, where the high temperature has prevailed longest. In the laboratory frame of reference the resulting detonation wave sweeps forward at a velocity which is the sum of the particle velocity behind the initial shock front and the detonation velocity of compressed, unreacted explosive. This detonation wave overtakes the initial shock wave and temporarily overdrives detonation in the unshocked explosive ahead of it.

The conclusions drawn in this paper are based on more than 300 separate experiments. Because not all of them can be presented in detail, they have been grouped into types of experiments. Many of each type have been done, and a few selected ones are described in enough detail for the reader to see what data can be obtained and how it has been used. We have tried to furnish enough of the experimental results to provide evidence to support every conclusion. In no case does a conclusion rest upon a single experiment, although in several cases only one experiment is described.

#### Recording Equipment

The equipment used in the experimental work described in this paper included a smear camera, a framing camera, and raster chronographs. The smear camera had a maximum writing speed of 9.2 mm/ $\mu$ sec at F/6 and had correction for the elastic distortion of the rotating mirror.<sup>(4)</sup> In the space direction the maximum resolution amounted to 400 line pairs. The time resolution was  $5 \times 10^{-9}$  sec.

The framing camera was capable of 15-frame sequence with a minimum exposure time of  $2 \times 10^{-7}$  sec and a time interval between frames of  $2.5 \times 10^{-7}$  sec. Resolution was 300 line pairs vertically and 200 line pairs horizontally. Maximum aperture was F/20.

The electronic chronographs and techniques for using them are described elsewhere.<sup>(5)</sup> Maximum time coverage per chronograph was about 150  $\mu$ sec with a standard error per transit-time reading of about  $3 \times 10^{-9}$  sec.

#### Type I Experiment: External Velocity Profile

In the experiments designated as Type I a smear camera was used to record the progress of the initial shock wave in the explosive under study and to observe the transition to high-order detonation. The charge arrangement is diagrammed in Fig. 1.

A shock wave of appropriate amplitude was sent into a nitromethane charge from the booster-attenuator system. The nitromethane was illuminated from behind by an argon flash for a shadowgraph picture. The smear camera recorded the vertical progress of this shock wave and of the ensuing detonation wave over a distance as shown by the scale in Fig. 2. After the detonation wave left the field of view of the camera it passed into a 5.08-cm diam tube in which the steady-state

"stick" velocity was measured by the pin technique<sup>(5)</sup> with the electronic chronographs.

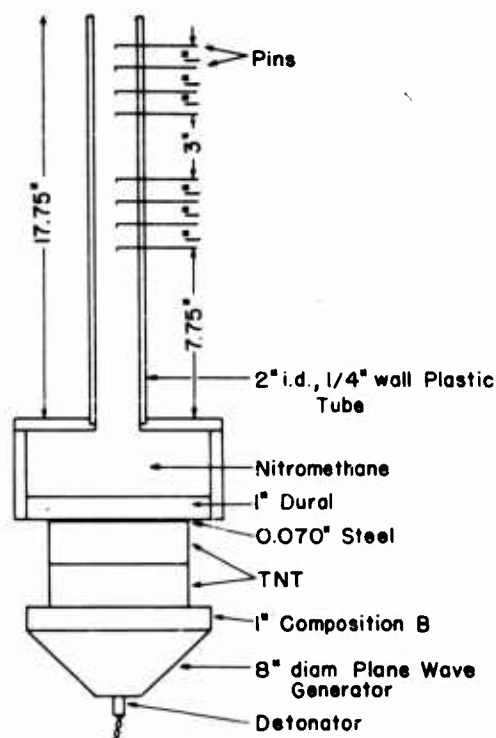


Fig. 1. Charge setup for nitromethane velocity profile experiment. Shot D-5772. The camera optic axis was parallel to and about 2 cm about the dural attenuator plate. The nitromethane was backlit by an argon flash charge.

In Fig. 2 are displayed both the field of view of the smear camera and a space-time record of the initiation process. It should be pointed out that the optic axis of the camera obviously could not be arranged to be tangent to the shock wave throughout its travel. The optic axis was aligned parallel to the bottom of the nitromethane box and at a distance above it coinciding with the anticipated shock transition point. This geometrical compromise contributed a maximum error of 2% to the observed velocities.

The results of two shots are listed in Table I. These shots were chosen because only in these two were steady-state stick velocities obtained in addition to the plane-wave velocities of the initial shock and of the detonation wave immediately after the transition. Unfortunately, the shock waves from these booster-attenuator systems were

not sufficiently uniform for accurate measurements and the plane-wave velocities in Table I are low. Best estimates of these velocities from additional experiments are entered at the bottom of the table.

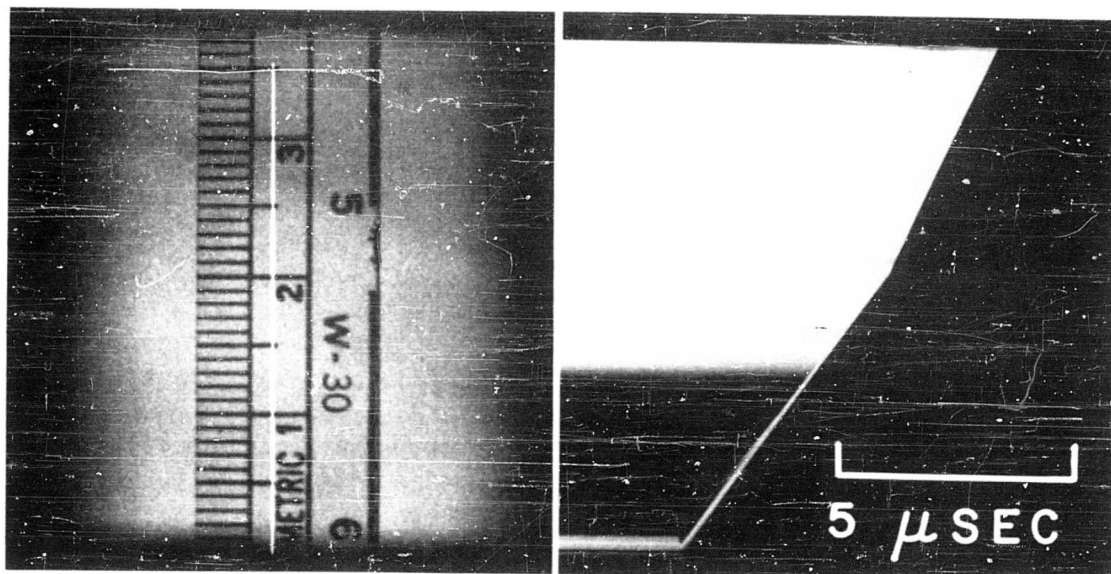


Fig. 2. Left half of picture shows camera view of scale mounted in nitromethane box shown in Fig. 1 with slit image superimposed as a white line. Right half of picture is the smear camera record from the charge of Fig. 1. Time increases to the right. The lighting is such that the lower record is a shadowgraph, and shows the shock front as a bright line. The shock moves up at constant or slightly decreasing velocity from the bottom. At about 21 mm from the bottom, the detonation wave overtakes the shock, as evidenced by the sudden change in velocity. The detonation in the compressed nitromethane can not be seen in this picture. This picture can be compared directly with Fig. 3, Lines III and VI.

A booster-attenuator system of the type used for these experiments was fired to determine the velocity of the free surface of the attenuator plate. A knowledge of the equation of state of the plate and the shock velocity in the nitromethane allows a determination of the pressure and the particle velocity in the nitromethane, using standard impedance matching methods.<sup>(17)</sup> The pressure was determined to be 81 kbar, and the particle velocity 1.6 mm/ $\mu$ sec, with an accuracy of about 5%. As will be shown later, the induction time is a very sensitive function of the shock pressure, and since the range of induction times over which it is possible to work is limited, the pressure in all experiments is about the same.

TABLE I

## External Velocity Data For Nitromethane

<u>Shot Number</u>	<u>Initial Shock Velocity (mm/<math>\mu</math>sec)</u>	<u>Detonation Velocity (mm/<math>\mu</math>sec)</u>	<u>Stick Velocities</u>	
			<u>Pin Numbers</u>	<u>(mm/<math>\mu</math>sec)</u>
D-5772	4.33	6.57	1-5	6.24
			2-6	6.36
			3-7	6.24
			4-8	6.22
D-5773	4.24	6.85	1-5	6.24
			2-6	6.25
			3-7	6.26
			4-8	--
	(4.50)*	(6.90)*	AVE. <u>6.26</u>	

\* Best estimates from camera records of other shots.

The camera records of the initiation process show three interesting features. The initial shock wave proceeds at a constant or slightly decaying velocity, indicating that it is essentially a non-reactive wave; the transition is very abrupt, which we have found to be characteristic of homogeneous explosives; and the detonation velocity immediately after the transition shows an overshoot of about 10%, decreasing in a few microseconds to the normal detonation velocity.

The presence of overshoot can be demonstrated with the use of the average stick velocity as follows. From the work of Campbell, Malin, and Holland<sup>(6)</sup> we find the stick velocity of nitromethane to be given by the following equations,

$$\text{at } 91.3^{\circ}\text{F} \quad D = 6.2125 - 0.00517 (1/d) \quad (1)$$

$$\text{at } 22.5^{\circ}\text{F} \quad D = 6.3745 - 0.01705 (1/d) \quad (2)$$

where  $D$  is the detonation velocity in mm/usec and  $d$  is the explosive diameter in centimeters (confined in glass tubes). A linear interpolation is made to obtain an expression for the velocity at  $70^{\circ}\text{F}$ , the temperature of the nitromethane in the experiments discussed here.

$$\text{at } 70^{\circ}\text{F} \quad D = 6.2627 - 0.00885 (1/d) \quad (3)$$

From (3) the velocity for a stick of 5.08-cm diam is found to be 6.25 mm/usec. This value is compared with the average stick velocity in Table I, and the difference is added to the constant term of (3) to obtain a corrected estimate of the plane-wave detonation velocity for the lot of nitromethane used in the experiments discussed here. Comparison of this estimate (6.27 mm/usec) with the best estimate for the overdriven velocity entered in Table I (6.90 mm/usec) reveals the overshoot to be 0.63 mm/usec, or approximately 10%.

## Type II Experiment: Internal Velocity Measurements

Given the results of the Type I experiments, the next problem was to locate the origin of the high-order detonation wave. This was done in Type II experiments.

It was assumed that the chemical reaction accompanying detonation could best be identified by observing the change in electrical resistivity accompanying it. To this end nitromethane could be prepared with a resistivity up to 5 megohm-cm. In contrast, the reaction zone of the high-order detonation in this explosive was known to be quite conducting.

After several preliminary experiments had been carried out using a pin technique, it became apparent that high-order detonation originated at the attenuator-explosive interface. The general sequence of events is as shown in Fig. 3. Curve I represents the shock wave in the attenuator moving toward the attenuator-explosive interface. Along II, the interface moves to the right with local particle velocity while a rather non-reactive shock wave precedes it along III. High-order detonation originates at the interface and follows Curve IV to the transition point, V, where it overtakes the initial shock wave and passes into the unshocked explosive, proceeding along VI.

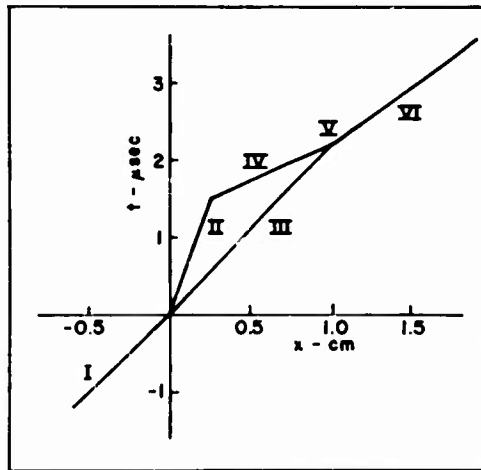


Fig. 3. Sequence of events in the initiation of a homogeneous explosive.

Because it was very difficult to obtain sufficiently uniform initiation over a sufficiently large area, a detailed pin record of the events in a single shot, as diagrammed in Fig. 3, was not attempted. (A camera record of these events is given in the section on Type IV Experiments below.) Instead, the pin technique was employed to measure the particle velocity  $U_p$  and the detonation velocity  $D^*$  in the

compressed nitromethane behind the initial shock wave .

In Fig. 4 is shown the experimental arrangement. The plastic at

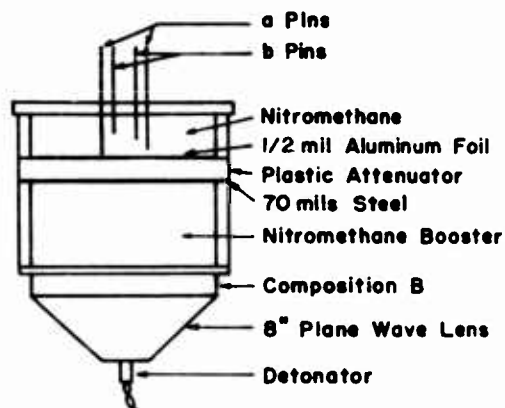


Fig. 4. Charge arrangement for Type II experiments. Sixteen a pins were arranged in a 1-in. diam circle at distances alternately 10 mils and 160 mils from the aluminum foil. Sixteen b pins were arranged in a 5/8-in. diam circle, half of them at 315 mils and the other half at 750 mils standoff.

the plastic-explosive interface was coated with a  $\frac{1}{2}$ -mil ( $5 \times 10^{-4}$  in.) aluminum foil as a ground electrode. Eight pairs of pins were arranged above the interface in a 1-in. circle to yield eight measures of the interface velocity, Curve II of Fig. 3. Eight additional pairs of pins were arranged in a 5/8-in. diam circle to yield eight measures of the detonation velocity, Curve IV of Fig. 3.

The pins were designed so as to minimize pin drift in the surrounding mass flow. The first 16 pins were made of 3-mil diam tungsten wire, and the second 16 were made of 15-mil wire with the ends tapered 1 in 4. The tapered section was terminated with a flat surface 5 mils in diameter to facilitate measurement of the pin location relative to the plastic-explosive interface.

The apparent values obtained in an experiment of this type are listed in Table II. These values are in error by an unknown amount because of drift of the pins in the mass flow of the surrounding explosive. This drift causes the observed values of the particle velocity to be lower than the true one and causes the detonation velocity values to be too high.

A first-order correction to the apparent values of  $U_p$  and  $D^*$  can be made as follows. Referring to the schematic drawing, Fig. 5, Pins 1, 2 sense the motion of the plastic-explosive interface; high-order detonation occurs in Interval c; Pins 17, 18 sense the motion of the detonation wave; and the detonation wave overtakes the initial shock



TABLE II

## Internal Velocity Data for Nitromethane

Shot Number E-0374

Pin Numbers	Apparent Particle Velocity $U_p$ (mm/ $\mu$ sec)	Pin Numbers	Apparent Detonation Velocity $D^*$ (mm/ $\mu$ sec)
1-2	1.356	17-18	12.644
3-4	1.438	19-20	12.835
5-6	1.256	21-22	10.894
7-8	1.177	23-24	10.257
9-10	1.286	25-26	10.455
11-12	1.286	27-28	10.330
13-14	---	29-30	---
15-16	1.351	31-32	9.779
AVE.	1.307	AVE.	11.027

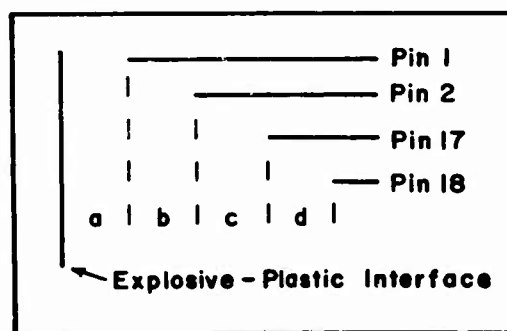


Fig. 5. Diagram for use in velocity calculations in Type II experiments.

wave beyond Interval  $d$ . The following symbols are defined:

$W$	Pin drift velocity.
$U_p$	Interface velocity.
$D^*$	Detonation velocity in compressed nitromethane.
$b$	Distance between Pins 1, 2, measured normal to interface.
$d$	Distance between Pins 17, 18, normal to interface.
$t_1$	Time between signals from Pins 1, 2.
$t_2$	Time between signals from Pins 17, 18.

The assumption is made that the pins drift at constant velocity,  $W$ , after contact by the initial shock wave. The further assumption is made that the velocity of the initial shock wave is  $4.5 \text{ mm}/\mu\text{sec}$  (see Table I). The following relation then holds,

$$U_p t_1 = b - \frac{b}{4.5} W + W t_1 \quad (4)$$

where  $\frac{b}{4.5} W$  is the distance Pin 1 drifts during the time required for the initial shock wave to traverse the Interval  $b$ .  $W t_1$  is the distance Pin 2 drifts during the time required for the interface to move from the tip of Pin 1 to the tip of Pin 2. A similar relation holds for the motion of the high-order detonation wave.

$$D^* t_2 = d - \frac{d}{4.5} W + W t_2 \quad (5)$$

It is assumed that the detonation velocity,  $D^*$ , is equal to the detonation velocity of uncompressed nitromethane (rounded to  $6.30 \text{ mm}/\mu\text{sec}$ ) plus an increment due to the density increase behind the initial shock wave plus the local particle velocity:

$$D^* = 6.30 + 3.20 (\rho - \rho_0) + U_0 \quad (6)$$

where the velocity dependence on density is taken to be  $3.20 \text{ mm}/\mu\text{sec g/cc}$ ,<sup>(6)</sup> and  $\rho_0$  and  $\rho$  are the initial ( $1.125 \text{ g/cc}$ ) and final densities, respectively, of the nitromethane. Since

$$\rho - \rho_0 = \frac{U_p}{U_s - U_p} \rho_0 \quad (7)$$

$$D^* = 6.30 + 3.20 \frac{U_p}{4.5 - U_p} \rho_0 + U_p \quad (8)$$

In solving Equations 4, 5, 8 simultaneously, the value of  $b/t_1$  is taken to be 1.30 (Table II) and  $d/t_2$  is taken to be  $11.0 \text{ mm}/\mu\text{sec}$ . The following results are then obtained:

$$\begin{aligned} W &= 0.56 \text{ mm}/\mu\text{sec} \\ U_p &= 1.70 \text{ mm}/\mu\text{sec} \\ D^* &= 10.19 \text{ mm}/\mu\text{sec} \end{aligned}$$

From the expression,

$$P = \rho_0 U_p U_s, \quad (9)$$

the pressure behind the initial shock wave can be calculated. Taking the value of 1.70 mm/μsec for  $U_p$  and 4.5 mm/μsec for  $U_s$  the pressure is found to be 86 kb.

The approximation made in Equation (6) is not justified by any simple theory. There must be additional velocity changes from the change in pressure and the change in initial internal energy. These will be of opposite sign and may cancel, but they cannot be shown to be small by any method yet found. The calculation is included because it seems to agree so well with the results of the pressure measurements described for the Type I experiments. It would also be possible to estimate the pin drift velocity and arrive at about the same result, because the corrections to the pin data are small. The fact that the detonation velocity in the compressed explosive can be found by making only the density correction and using the coefficient found from experiments performed by varying the initial temperature at ambient pressure is interesting, but has not yet been related to the theory. The detonation velocity in compressed liquid TNT can also be closely approximated by making a similar density correction.

## Type III Experiment: Observation of Detonation Light

For nitromethane and other transparent explosives, clarification of initiation behavior can be obtained by viewing a test charge normal to the shock wave and photographing the light generated by the charge itself. The charge setup is shown in Fig. 6.

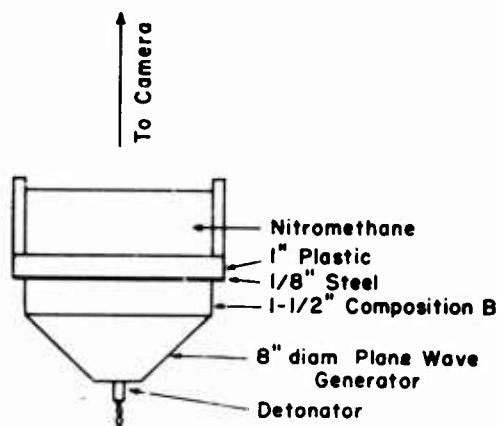


Fig. 6. Charge setup for Type III Experiments. Shot E-0609

The smear camera record obtained for nitromethane initiated by the attenuator-booster system of Fig. 6, is shown in Fig. 7. At time F, the initial shock wave entered the nitromethane as indicated by the flash of light from a bubble mounted on the attenuator surface. A detonation spread from this bubble (see Experiment VIII for discussion of effects of bubbles). At time A, detonation appeared across 4 in. of the attenuator surface, simultaneous within 0.08 usec. This weak light comes from detonation in the nitromethane which has been compressed by the initial shock. This detonation overtakes the shock, giving a sharp increase in intensity on the film at time B which soon decays to the intensity of steady-state detonation.

Better measurement of  $U_p$  and  $D^*$  can be made from records of this type than from Type II experiments in which it is necessary to assume constant pin drift velocity.

The distance  $d$  at which the detonation  $D^*$  overtakes the shock can be computed along two paths as can be seen in Fig. 8. Equating the expressions so obtained gives a relation between the velocities,  $U_p$ ,  $U_s$ , and  $D^*$ . Thus

$$d = U_s t_1 = U_p (t_1 - t_2) + D^* t_2$$

this equation can be solved for  $D^*$  by substituting into it the meas-

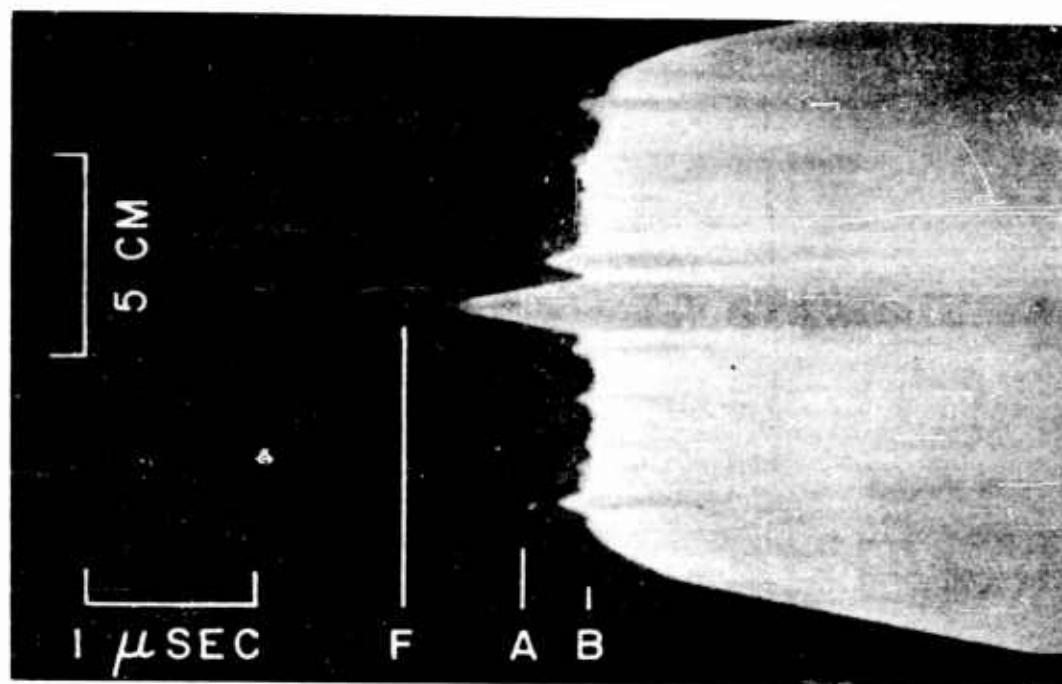


Fig. 7. Smear camera record of detonation light from nitromethane charge of Fig. 6. Shot E-0609. Time increases to the right.

F: The flash of a bubble marks the time of entry of the shock wave into the nitromethane.

A: Detonation initiates at the attenuator-nitromethane interface.

B: Time at which the detonation in the compressed nitromethane overtakes the shock wave.

The times used in the text are defined as follows:

$$t_1 = B - F$$

$$t_2 = B - A$$

$$t^* = A - F = \text{induction time}$$

ured values of  $U_s$ ,  $U_p$ ,  $t_1$  and  $t_2$ . The free-surface velocity of one booster-attenuator system was measured, and the impedance match technique gave  $U_s = 4.5 \text{ mm}/\mu\text{sec}$  and  $U_p = 1.6 \text{ mm}/\mu\text{sec}$  as described in the section on Type I Experiments. These values correspond to a pressure of 81 kbar. These values will be assumed to be identical in all the experiments, because the pressure changes from one experiment to another are only about 5%. The values of  $t_1$  and  $t_2$  from several experiments, and the calculated values of  $t^*$  are given in Table III, Column 4. The four shots for which data are given in the table are those which illustrate this paper, and averages are presented for

another series of shots.

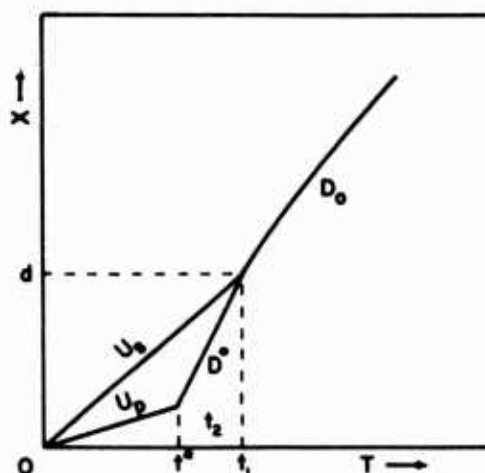


Fig. 8. Space-time representation of initiation behavior of nitromethane. The initial shock enters the nitromethane at time 0.

$U_s$  = Shock velocity

$U_p$  = Particle velocity

$D_0$  = Detonation velocity, steady-state

$D^*$  = Detonation velocity in compressed nitromethane

$t^*$  = Induction time

It is instructive to compare the results obtained for  $D^*$  with the solutions to Equation (9) obtained by substituting from Equation (8) to eliminate  $D^*$ . Equation (9) may then be solved for  $U_p$ , giving

$$U_p = U_s - \frac{1}{2}(D_0 - \alpha \rho_0)t - \left( [U_s - \frac{1}{2}(D_0 - \alpha \rho_0)t]^2 + U_s D_0 t - U_s^2 \right)^{\frac{1}{2}} \quad (10)$$

where  $t = t_2/t_1$ ,  $D_0$  is the normal detonation velocity, and  $\alpha$  is the velocity dependence on density used in Equation (6). For the same values used in Experiment II,

$$U_p = 4.5 - 1.35t - (16.2t + 1.82t^2)^{\frac{1}{2}} \quad (11)$$

The assumptions made in this analysis are that initiation occurs at the nitromethane-attenuator interface, that  $D^*$  is adequately represented by Equation (8), and that both  $D^*$  and  $U_s$  are constant. The results are given in Columns 6, 7, and 8 of Table III.

The light from the detonation in the compressed nitromethane is

weaker than that from the normal steady-state detonation. The difference in brightness corresponds to a temperature difference of about 180°K between two black bodies of brightnesses equal to those of the two detonations. We interpret this brightness difference to mean that the detonation in compressed nitromethane has a lower temperature than detonation in normal explosive. Little of the light from the former explosive is absorbed by the nitromethane behind the shock front, since its intensity remains constant as the detonation approaches the shock wave.

It is important in these shots that the initial shock wave be plane and smooth. Although the time of arrival of the shock which entered the nitromethane of Fig. 7 was the same at every point within 0.01  $\mu$ sec, some fuzziness in the initiation is apparent. This is due to small pressure variations across the wave front. Several points detonated 0.1  $\mu$ sec before the rest and a strong interaction is visible where the shock was overtaken by the by the detonation. Further discussion of this point is included in Type VII experiments.

TABLE III

Results of Detonation Light Observations

Shot Number	$t_1$ ( $\mu$ sec)	$t_2$ ( $\mu$ sec)	$D^*$ (a) (mm/ $\mu$ sec)	$t$	$U_p$ (mm/ $\mu$ sec)	$D^*$ (b) (mm/ $\mu$ sec)	P (kb)
E-0609	1.07	0.37	9.99	0.346	1.62	9.95	82
D-6207	1.22	0.41	10.25	0.336	1.67	10.10	85
	2.94	1.00	10.14	0.340	1.65	10.03	84
E-0577	4.53	1.39	11.08	0.306	1.82	10.57	92
E-0634	1.07	0.36	10.16	0.339	1.65	10.05	84
	1.61	0.53	10.50	0.326	1.72	10.25	87
Averages of 13 shots:			10.44	0.328	1.71	10.22	86.6
Mean Deviations:			$\pm 0.50$	$\pm 0.020$	$\pm 0.10$	$\pm 0.30$	$\pm 5.0$

(a) Calculated assuming  $U_s = 4.5$  mm/ $\mu$ sec,  $U_p = 1.6$  mm/ $\mu$ sec, and  $P = 81$  kbar.

(b) Calculated assuming Equation (8).

Type IV Experiments:  
Smear Camera Record of Complete Initiation Process

Each of the three preceding types of experiments was aimed at obtaining information about some part of the initiation process. The combined experimental results gave a picture of events as diagrammed in Fig. 8. When this stage of the investigation had been reached it was felt to be desirable to obtain a single record showing all of the events in their proper relationship. For this purpose the charge arrangement shown in Fig. 9 was designed.

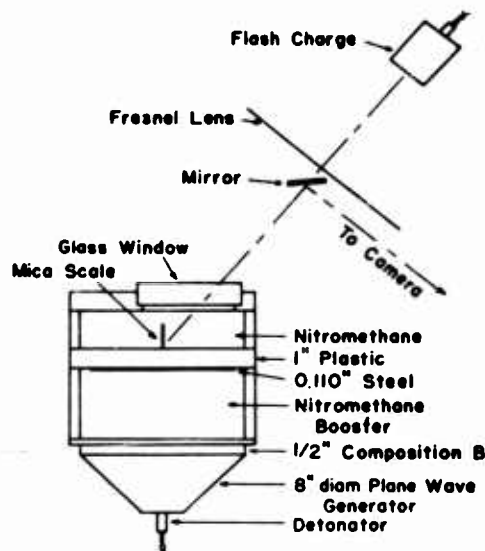


Fig. 9. Charge arrangement for Type IV Experiments.

A scale was inserted in the nitromethane to be studied to aid in recording the progress of the various waves. This scale was designed to have as little mass as possible so as to minimize its effect on the initiation process. It was made of two sheets of mica, each less than 1-mil thick. One face of one sheet was finely ground so as to make it a good scatterer of light. Then a scale was formed on the surface by depositing evaporated aluminum through a grid, leaving narrow uncoated lines as graduations. Finally, the coated surface was cemented to the second sheet of mica with Canada balsam. This filled the scratches, leaving the graduations transparent. The distance from the bottom of the scale to the first line was  $1/8$  in.; the distance between lines was  $1/4$  in.

The scale was illuminated with light from an argon shock light-

Unclassified



source using a plastic Fresnel lens to image the source on the subject. After the light left the Fresnel lens, it passed by successive reflection from the front surface of the plastic attenuator, to the scale, to a small mirror before the Fresnel lens and, finally, to the objective lens of the smear camera.

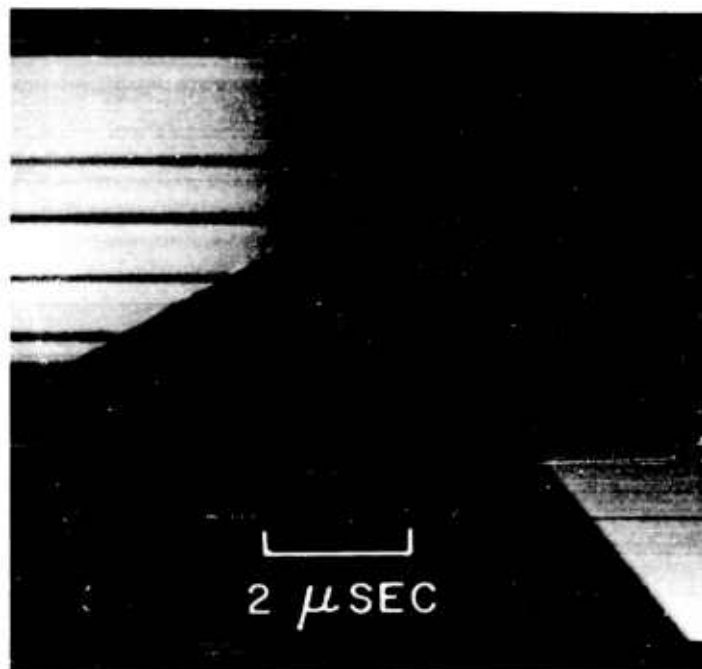


Fig. 10. Smear camera record of Type IV Experiment.

Figure 10 shows the smear camera record from such a shot, and Fig. 11 is a diagrammatic interpretation of the record. The explanation is as follows. At Time 1 the argon light source began to illuminate the scale, the graduations producing the Lines a, b, c, d. At Time 2, the attenuated shock wave entered the nitromethane and proceeded up the scale as shown by Line A. Line B shows the motion of the attenuator-explosive interface, and just above it is a line formed by the motion of Graduation a and a second line due to a flaw in the scale.

At Time 3, initiation occurred at the plastic-nitromethane interface, and argon shock light was no longer reflected from the plastic to the scale. Consequently, the scale appeared less bright and detonation light was recorded through the transparent Graduation d. High-order detonation in the compressed nitromethane followed the Line C. The intersection of Lines C and B shows that initiation occurred at the plastic-nitromethane interface.

The intersection of Lines C and D is the point on the scale at

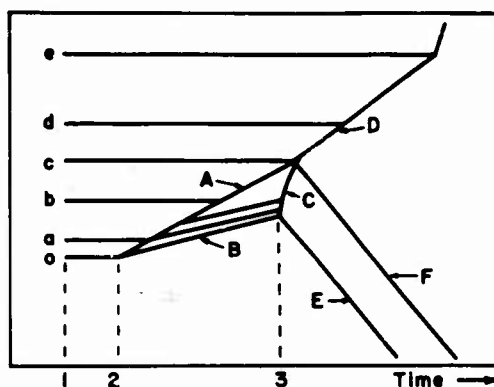


Fig. 11. Explanatory diagram of Fig. 10. Time 2-3 is induction time.

which the detonation wave in the shocked nitromethane overtook the initial shock wave. Detonation in unshocked nitromethane then proceeded along Line D. Along Line E the initiation of detonation at the attenuator-explosive interface spread to points progressively farther from the charge axis, and along Line F the detonation wave overtook the initial shock wave, the departure from verticality (simultaneity) showing that the latter wave was not flat.

## Type V Experiment. Dependence of Induction Time on Initial Temperature

The time between the entrance of the initial shock and initiation, the induction time, should be strongly dependent on the initial temperature of the nitromethane. A series of Type III experiments was performed in which the initial temperature of the nitromethane was varied from 1.5°C to 45°C. The same booster-attenuator system, shown in Fig. 6, was used for all shots. Since the pressure of the initial shock wave was dependent on the density, a small correction should be made for the change of density with temperature. The booster-attenuator system was kept at 25°C for all shots. The nitromethane in a plastic box was controlled at the desired shot temperature to within 1°C, then mounted on the attenuator a few minutes before firing. The temperature at several points in the nitromethane was monitored with thermocouples throughout the experiment. Results of several shots with different lots of nitromethane are given below.

TABLE IV

Results of Induction Time vs Initial Temperature Experiments

	Shot Number	Temperature (°C)	Induction Time (μsec)
Lot 1	E-0590	1.7	5.0
	E-0588	26.8	1.8
Lot 2	E-0602	6.3	1.5
	E-0603	36.7	0.57
	E-0598	45.5	0.45

These results illustrate the strong dependence on the ambient temperature. About 10% decrease (30°K) in the ambient temperature produces an increase of 300% in the induction time. The two lots of nitromethane came from different bottles from the same supplier. The effects of sensitizing and desensitizing agents are large. For any quantitative measurement of induction time it is necessary that all the nitromethane come from the same bottle and be used within a few days.

Type VI Experiment. Dependence of the Induction  
Time on the Initial Shock Pressure

In performing the experiments already described, it soon was discovered that the induction time depended strongly on the initial shock pressure, and close control of the booster-attenuator system was nec-

essary to get reproducible results.

To measure this dependence a shot was made following the pattern of Type III experiments. A step was machined into the upper surface of the attenuator so that one half was  $\frac{1}{4}$  in. thicker than the other. This resulted in pressures into the nitromethane on either side of the step which differed by 3.3%. This pressure difference was determined on a replicate booster-attenuator system by optical measurements of the shock and free-surface velocities of the plastic and by subsequent impedance-matching calculations. As can be seen from the data in Table V, the inductions times differed by 26%. This result was supported by additional experiments. These data may be interpolated to show that a 10-mil change in the thickness of the plastic attenuator produces a 1% change in the induction time.

TABLE V

Results of Induction Time vs Shock Pressure Experiments

Shot Numbers B-4485, B-4488

Attenuator Thickness (inches of plastic)	P (kb)	t* ( $\mu$ sec)
1.20	86	2.26
0.95	89	1.74

#### Type VII Experiment. Effect of Rough Initiating Shock Wave

The variations in induction time observed across the attenuator plate of every shot fired indicated that very small pressure variations caused large effects. The plastics used in most shots were of optical quality, because the standard quality showed more pronounced variations. These facts suggested that variations in the attenuator caused tiny shock wave interactions in the liquid nitromethane, with consequent formation of small local hot spots. The experiments to be described were designed to discover how much the induction time would be shortened by interactions of controlled size purposely introduced.

These shots were identical with those of Type III experiments, except that grooves were ruled in one half of each Plexiglas attenuator plate. In the shot illustrated in Fig. 12, the grooves, of triangular cross section, were 20 mils deep and spaced 25 mils apart so that the tops were sharp. The Plexiglas was coated with a thin layer of paint to prevent attack by the nitromethane. The two induction times, 1.9 and 0.8  $\mu$ sec, are strikingly different. The smallest grooves tried, 6 mils deep and 8 mils apart, still caused a decrease in the induction time, but only by 15%. The shock impedance of the Plexiglas and the nitromethane are so close together that the amplitude of the ripples in the emergent shock is only 5% as large as the grooves themselves. It is easy to see that if the wave emerging from

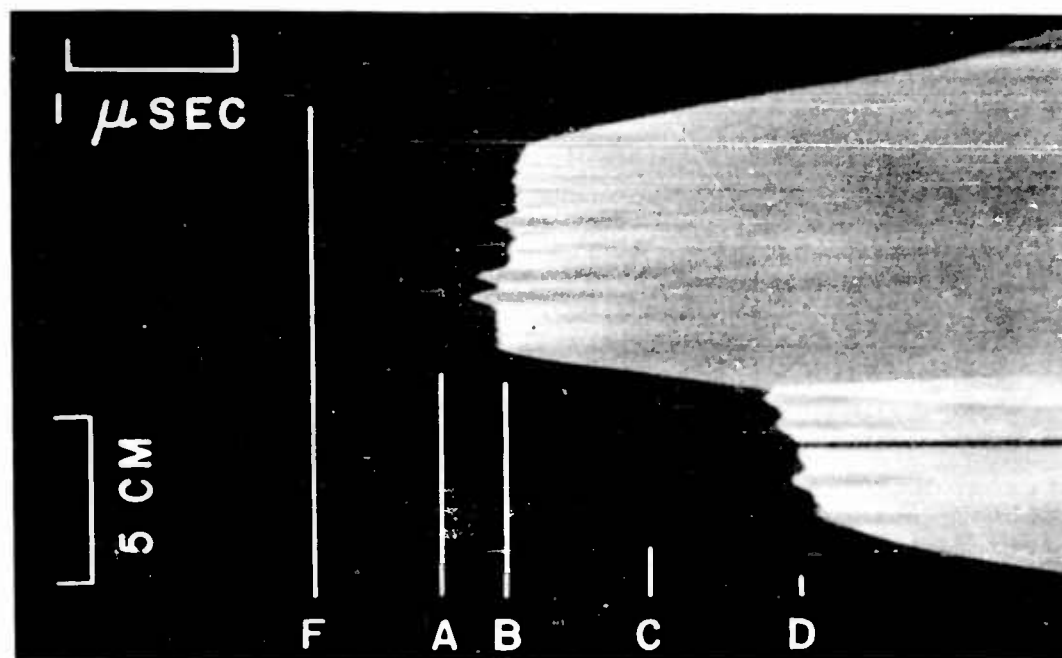


Fig. 12. Smear camera record of effect of rough shock wave on induction time.

F: Shock enters nitromethane.

A: Detonation is initiated in compressed nitromethane at interface between nitromethane and grooved attenuator plate.

B: D\* overtakes shock.

C: Detonation is initiated at interface of nitromethane and smooth attenuator plate.

D: D\* overtakes shock.

Induction time,  $t^*$ : Over grooved plate A - F.  
Over grooved plate C - A.

Shot D-6207.

the attenuator is not almost perfect, the induction time will be artificially shortened. It is apparently impossible to be sure that any of these experiments gives the induction time corresponding to a perfectly plane shock wave.

#### Type VIII Experiment. Effect of Bubbles

In the description of Type III experiments it has been pointed out that a gas bubble can cause initiation as soon as the shock hits it. The experiments to be described here were performed to investigate initiation by bubbles of various gases. In the course of the

investigation, knowledge of the effects of shock wave interactions suggested that the major effect of the bubble was to produce a shock interaction. Therefore, "bubbles" of solids were also introduced.

The experiments were done exactly as those of Type III, with the gas bubbles on the surface of the attenuator plate. It was found that a very small amount of silicone vacuum grease on the plastic plate would hold the bubbles in place under the surface of the nitromethane.

Bubbles, formed by forcing gas through a capillary into nitromethane, were caught under clean glass. Because the contact angle between the nitromethane and glass was zero, the trapped bubbles were spherical. The diameter of each bubble was measured and each bubble was transferred under nitromethane to the shot box. In position on the attenuator plate, the shape of the bubble was no longer spherical. Hereafter, the diameter measure is used to mean a bubble having the volume of a sphere of that diameter.

Several kinds of initiation behavior, for a shock of given strength, result from the presence of a bubble in nitromethane. If the bubble is sufficiently large, in the order of 0.7 mm in diameter, detonation will spread almost immediately from it after it is shocked. Smaller bubbles, in the order of 0.4 mm, cause some reaction to take place in the nitromethane, but detonation occurs at or near the shock front after it has run a distance dependent on bubble size and the initiating conditions. From still smaller bubbles, initiation will not occur on our time scale, although the bubble may glow for several microseconds. Figure 13 shows these three cases for argon bubbles mounted in nitromethane.

To determine whether shock heating of the gas, or heating of the explosive in a local region due to the pressure interaction at the bubble is the more important cause of this initiation behavior, bubbles of gases with different  $\gamma$ 's were introduced. Argon ( $\gamma = 1.67$ ) and butane ( $\gamma = 1.1$ ) should be heated to quite different temperatures when shocked. The argon bubbles caused initiation in a slightly smaller time than butane bubbles of the same diameter, but the effect was much less than would be expected from the anticipated large temperature difference. To show conclusively that the pressure interaction is the effective cause, small pieces of plastic and tungsten, as well as bubbles, were introduced into nitromethane. Both of these, although raised to a relatively low temperature by the shock wave, caused initiation with close to the same induction time as the bubbles, as can be seen in Fig. 14. Most of the apparent delay occurs because the plastic and tungsten extended farther into the nitromethane than the bubbles.

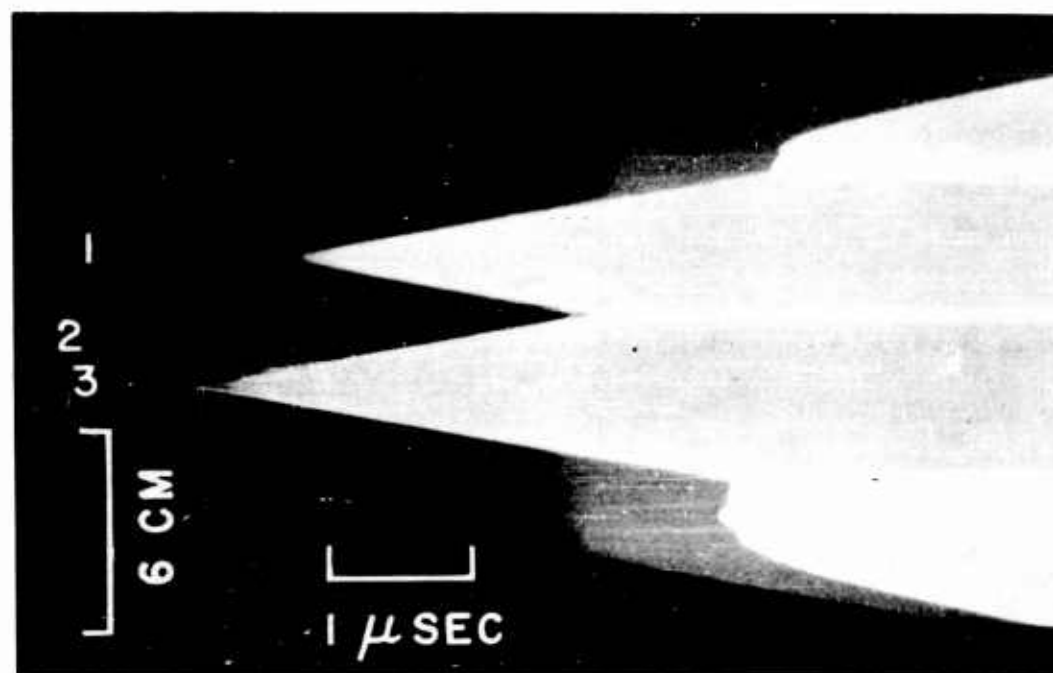


Fig. 13. Smear camera record of bubbles in nitromethane.  
Time increases to right.  
Argon bubbles: 1. 3/4 mm diam.  
2. 1/2 mm diam.  
3. 1 mm diam.  
Shot E-0577.

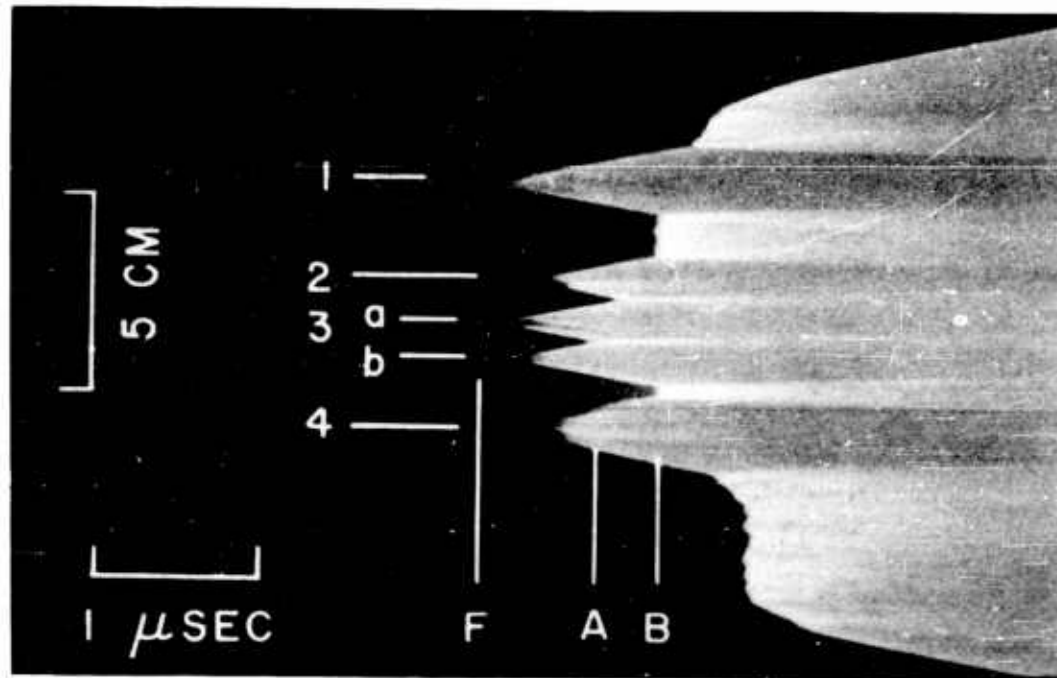


Fig. 14. Smear camera record of initiation of nitromethane by pressure interactions. Time increases to the right.

F: Shock enters nitromethane.

A: Detonation is initiated at attenuator-nitromethane interface.

B: Detonation overtakes shock.

1: Air-filled hole in attenuator, 1-mm diam, 1/2-mm deep covered with 1/2-mil Mylar.

2. Tungsten rod, 1-mm diam, 2-1/2-mm long (1-3/4-mm extension into nitromethane).

3a. Air bubble.

3b. Argon bubble, 0.8-mm diam.

4. Plastic, approximately 1-mm diam.

The lower part of the picture shows delayed initiation, probably due to a defect in the plastic attenuator.

Shot E-0634.



## Type IX Experiment. Other Explosives

The results described thus far were obtained with nitromethane. To be sure they were not unique to nitromethane, twenty-five experiments, chiefly of Types I and III, were done with other liquids, namely, molten DINA, molten TNT, and Dithelite 13 (63/24/13  $\text{HNO}_3$ , nitrobenzene,  $\text{H}_2\text{O}$ ). One striking difference appeared. The weak light from the detonation in the shocked liquid was not observed for any of these. All three are yellow but transparent enough to transmit enough light from a source as bright as the detonation in compressed nitromethane to be photographed. Otherwise, the behavior was the same as for nitromethane. The overshoot brightness which quickly decreased to steady-state intensity was observed. Bubbles produced the same effects as in nitromethane. We believe that the same mechanisms are active in these explosives as in nitromethane but the detonation behind the initial shock has an even lower temperature than was found for nitromethane.

Finally, the initiation of single crystals of PETN has been found to occur exactly as does initiation of nitromethane. The experiments are described in Reference 7. The smear camera record reproduced there, similar to Fig. 2, can be interpreted in the same way as are Type I experiments here.

Preliminary information about three of these explosives is listed in Table VI. The values are approximate.

TABLE VI

## Initiation Data for Other Explosives

Explosive	P (kb)	T (°C)	t* (μsec)	D* (mm/μsec)
TNT	125	85	0.7	11.0
Dithelite 13	85	25	1.8	12.2
PETN	112	25	0.3	10.9

## DISCUSSION OF RESULTS

Many authors have considered thermal explosion theory to be important in explaining the process of initiation.<sup>(1)</sup> Among these the recent treatment by Hubbard and Johnson<sup>(2)</sup> is perhaps the most pertinent here. They developed a theory for a semi-infinite homogeneous explosive, and from calculations observed the general behavior which we have observed independently in experiments. They found that when an element of explosive had been subjected to a shock wave of the proper strength, a time interval, referred to as a "time delay" or an "induction time", ensued in which almost no chemical reaction took place. Then complete reaction occurred in a relatively very short

time, and this reaction then moved forward as a detonation wave.

Unfortunately, Hubbard and Johnson attempted to apply their theory to the experimental results of Majowicz and Jacobs<sup>(8)</sup> for physically inhomogeneous explosives, where the initiation mechanism was quite different.<sup>(9)</sup> The theory is more suitably applied to the process of initiation in nitromethane. In what follows, the attempt will be made to follow the notation and treatment of Hubbard and Johnson.

The assumption is made that the reaction in nitromethane follows an Arrhenius rate law containing the term  $\exp E_A/RT$ , where  $E_A$  is the activation energy,  $R$  is the gas constant, and  $T$  is the local temperature. The substitution is made for  $T$ ,

$$T = (E_0/C_V) + (Qf/C_V) \quad (1)$$

where  $E_0$  is the specific internal energy behind the initial shock wave,  $Q$  is the heat of explosion per gram,  $f$  is the fraction of unit mass reacted, and  $C_V$  is the average specific heat at constant volume. The following expression is ultimately obtained for the reaction time:

$$t = \nu^{-1} \int_0^f (1 - f')^{-N} \exp[\epsilon/E_0 + Qf'] df' \quad (2)$$

where  $t$  is the induction time,  $\nu$  is the "collision frequency",  $N$  is the order of the reaction, and  $\epsilon = C_V E_A/R$ . Since most of the reaction time is due to values  $f \approx 0$ , the integral becomes

$$t = \nu^{-1} (E_0/C_V)^2 (Q/C_V)^{-1} (E_A/R)^{-1} \exp \left[ (E_A/R) (E_0/C_V)^{-1} \right] \quad (3)$$

The values in parentheses correspond to temperatures.

$$E_0/C_V = T_0 \quad (4a)$$

$$Q/C_V = T_f \quad (4b)$$

$$E_A/R = T_A \quad (4c)$$

Here,  $T_0$  is the temperature behind the initiating shock,  $T_f$  is the temperature of the reaction products, and  $T_A$  is the activation temperature. In Equation (4b)  $C_V$  is the average specific heat of the reaction products, and the value is taken to be the same as that for the unreacted explosive. Equation (3) may then be rewritten in the form

$$t = \nu^{-1} T_0^2 (T_f T_A)^{-1} \exp T_A/T_0 \quad (5)$$

We now wish to calculate a value of  $t$  using the following experimental data for nitromethane.

$\nu$	: $10^{14.6}/\text{sec}$	Ref. 10
$E_A$	: 53,600 cal/g	Ref. 10
$U_s$	: 4.5 mm/ $\mu\text{sec}$	
$U_p$	: 1.70 mm/ $\mu\text{sec}$	
$P$	: 86 kbar	
$\rho_0$	: 1.125 g/cc	Ref. 11
$Q$	: 1.28 kcal/g	Ref. 12
$C_v$	: 0.41 cal/g/ $^{\circ}\text{C}$	Ref. 13

The value of  $T_0$  is computed from the following two relations,

$$\Delta E = \frac{1}{2} p \Delta v \quad (6)$$

and

$$T_0 = 300 + \Delta E/C_v \quad (7)$$

where  $\Delta E$  is the increase in internal energy across the initiating shock.  $\Delta E$  was found to be 345 cal/g giving the result

$$T_0 = 1140^{\circ}\text{K} \quad (8)$$

$T_f$  corresponds to the temperature of the reaction products in the detonation wave in the compressed nitromethane. Estimated from  $Q/C_v$  the value of  $T_f$  is found to be  $4260^{\circ}\text{K}$ . (This value may be compared with the value of  $3200^{\circ}\text{K}$  obtained by W. C. Davis<sup>(14)</sup> from photographic brightness measurements.) Inserting appropriate values in Equation (4c)

$$T_A = 27,000^{\circ}\text{K} \quad (9)$$

Substitution of these temperature values in Equation (5) gives

$$t = 0.6 \mu\text{sec} \quad (10)$$

This value of  $t$  is in good agreement with our experimental observations when due regard is given to the uncertainties in the numerical values used in the calculation. These very crude calculations can be used only as order-of-magnitude confirmation. The agreement is no doubt in large part fortuitous, because the thermochemical numbers may change as the pressure is increased.

A similar calculation for the PETN data, using the measured thermochemical data of Robertson<sup>(15)</sup> or of Cook and Abegg<sup>(16)</sup> shows rea-

sonable agreement. The two sets of data give values which bracket our experimental values.

An estimate of the sensitivity of the induction time to variation of the temperature behind the initial shock wave is obtained from Equation (5) by taking logarithms and differentiating

$$\frac{dt}{t} = 2 \frac{dT_0}{T_0} - \frac{T_A}{T_0} \frac{dT_0}{T_0} \quad (11)$$

Substituting the values calculated above for  $T_A$  and  $T_0$  and collecting terms gives

$$\frac{dt}{t} = - 21.7 \frac{dT_0}{T_0} \quad (12)$$

Equation (12) shows that for a change in the initial shock temperature of 1%, or 11.4°K, in the calculation leading to Equation (10), the reaction time is changed by 21.7% or 0.13  $\mu$ sec. This agrees with the experimentally observed sensitivity of the induction time to initial shock strength found in Type VI experiments, although the sensitivity is expressed in terms of temperature rather than pressure.

The extreme sensitivity of the induction time to changes in the initial shock temperature is characteristic of homogeneous explosives and is responsible for the extreme difficulty found in obtaining experimentally reproducible induction times. Intrusion of strong rarefactions, as Hubbard and Johnson's calculations showed, lowered the local temperature and stopped chemical reaction. It was this effect of rarefaction from the charge boundaries and in the Taylor wave from the booster system which forced the use of the large-diameter charges described in this paper, and which prevented even then the study of initiation involving induction times of more than a few microseconds.

Local increases in the shock temperature can also be effected by reflecting the mass flow from inclusions of higher shock impedance than nitromethane, or by causing local convergences in the mass flow, which result in increased compressional heating of the explosive. If these local increases in temperature are great enough, reaction will take place. The results of this reaction may be to hasten the onset of detonation throughout the shocked explosive, as in the Type VII experiments, or if a single defect is large enough, the result may be the onset of detonation over a very small area, as shown by the Type VIII experiments. It follows that the stronger the initial shock wave the more easily can chemical reaction be effected at hot spots.

These experiments have presented severe problems of technique, not all of which have been solved satisfactorily. The quantitative measurements for use in an accurate comparison with thermochemical calculations can not yet be made. The explosive varies enough from batch to batch, even with the most careful purification, that one cannot specify the explosive properly. Even though one may determine an activation energy and "frequency" factor, one does not know to what explosive they belong. The shock waves used were not flat-topped pressure pulses, having been generated from detonation waves with

drooping Taylor waves even when very large charges were used. The sensitivity of the initiation to small shock wave interactions has been demonstrated, but it has not yet been possible to demonstrate that the attenuator plates do not have small inhomogeneities which are present in all experiments. These, if they are present, do not affect the qualitative conclusions, but they might invalidate quantitative results. All of these difficulties must be overcome before quantitative measurements can be presented as dependable.

The qualitative results are, however, completely unambiguous. The experiments show clearly a thermal explosion resulting from shock heating. Excellent agreement with the simple theory is demonstrated. The details of the process have all been examined. The experiments also show that small shock-wave interactions have large effects on the initiation process. These interaction experiments give a very useful insight into the differences between the initiation of homogeneous explosives and the more complicated problem of the initiation of inhomogeneous explosives, because they provide some view of the common ground between the two.

#### ACKNOWLEDGEMENTS

It is a pleasure to remember and acknowledge the help, advice, and encouragement the authors have received from many people over the past few years while this work was being done. Most of them are members of the GMX Division of the Los Alamos Scientific Laboratory. Some of the early work with nitromethane was done by Dr. T. P. Cotter, Jr., and it served as a starting base. The Type IV experiments were carried through by W. H. Morton, and he furnished ideas for many of the details of their arrangement. The careful work of O. G. Winslow in supervising the execution of the experiments has been invaluable.

#### REFERENCES

1. S. J. Jacobs, Am. Roc. Soc. J. 30, 151 (1960).
2. H. W. Hubbard and M. H. Johnson, J. Appl. Phys., 30, 765 (1959).
3. J. H. Cook, Research, 1, 474 (1948).
4. T. E. Holland and W. C. Davis, J. Opt. Soc. Am., 48, 365 (1958).
5. A. W. Campbell, M. E. Malin, T. J. Boyd, Jr., J. A. Hull, Rev. Sci. Instr., 27, 567 (1956).
6. A. W. Campbell, M. E. Malin, and T. E. Holland, Second ONR Symposium on Detonation, Washington, D. C. (1955).
7. T. E. Holland, A. W. Campbell, M. E. Malin, J. Appl. Phys., 28, 1217 (1957).
8. J. M. Majowicz and S. J. Jacobs, "Initiation to Detonation of High Explosives by Shocks", presented at Lehigh Meeting of Fluid Dynamics Division, American Physical Society, Nov. 1957.
9. A. W. Campbell, W. C. Davis, J. B. Ramsay, J. R. Travis, "Shock Initiation of Solid Explosives". This Symposium.
10. T. L. Cottrell, T. E. Graham, T. Y. Reid, Trans-Faraday Soc., 47, 584 (1951).
11. A. Makovsky and L. Lenji, Chem. Revs., 58, 627 (1958).

12. Personal communication from C. L. Mader, Los Alamos Scientific Laboratory.
13. W. M. Jones and W. F. Giaque, J. Am. Chem. Soc., 69, 938 (1947).
14. Unpublished data, W. C. Davis, Los Alamos Scientific Laboratory.
15. A. J. B. Robertson, Trans-Faraday Soc., 44, 977 (1948).
16. M. A. Cook and M. T. Abegg, Ind. Eng. Chem., 48, 1090 (1956).
17. M. H. Rice, R. G. McQueen, and J. M. Walsh, "Compression of Solids by Strong Shock Waves", Solid State Physics, Advances in Research and Applications, Volume VI, Eds. F. Seitz and D. Turnbull (Academic Press, Inc., New York, 1958).

## SHOCK INITIATION OF SOLID EXPLOSIVES\*

A. W. Campbell, W. C. Davis, J. B. Ramsay, and J. R. Travis  
University of California, Los Alamos Scientific Laboratory  
Los Alamos, New Mexico

### INTRODUCTION

In this paper we shall describe an experimental investigation of the initiation of inhomogeneous solid explosives by strong, plane shock waves, with high-order detonation taking place in less than 10  $\mu$ sec. The initiation process is observed to be very complicated, and still is not understood in detail. A previous paper<sup>(1)</sup> has discussed the initiation of liquid and other homogeneous explosives, which show a behavior much different from that of solid inhomogeneous explosives.

There has been much experimentation on the initiation of solid explosives, and recent papers are well reviewed elsewhere.<sup>(2-5)</sup> No attempt will be made in this paper to review the published work on the subject. The work of Majowicz and Jacobs<sup>(6)</sup> is especially pertinent, because their experiments are similar to ours, and their observations agree with ours in many respects.

The conclusions of this paper are based on more than 200 separate experiments, and not all of them can be described or even discussed here. A selected few of the experiments are described to provide evidence in support of the conclusions drawn. No conclusion is based on an isolated result, although in some cases only one result is presented here.

Experiments<sup>(1)</sup> with liquids and other homogeneous explosives have shown that initiation results from shock heating of the liquid, and that the simple ideas of thermal explosion explain all of the phenomena adequately if the shock wave is plane and smooth. If the shock wave is uneven, regions of convergent flow exist, and the local increase in compression results in "hot spots" which, because of the strong dependence of the reaction rate on the temperature, strongly influence initiation.

In polycrystalline explosives, the shock wave is rough with local convergences caused by the inhomogeneous nature of the explosive.

-----  
\* Work done under the auspices of the U. S. Atomic Energy Commission.

Smear camera photographs show that the detonation wave front in pressed or cast explosive is rough, indicating that the flow is irregular in its fine detail. Reaction takes place in these very small regions of convergence distributed throughout the explosive, and makes a major contribution to initiation. Initiation thus depends strongly on the type, number, and distribution of the inhomogeneities which cause the shock interactions.

The techniques employed, which have evolved in the course of the work, are sometimes elaborate and difficult. The descriptions of the experiments have been grouped as types of experiments, and often the grouping is according to technique rather than scientific purpose. To help the reader to understand why some of the experiments were done, a brief description of the initiation behavior of solid explosives, as shown by these experiments, is presented here without any evidence or detail.

When the shock wave enters the explosive, it proceeds at a slowly-increasing velocity for a distance which is a function of the shock pressure. Then the velocity increases in a short but measurable time to the value associated with high-order detonation. The velocity transition is not abrupt as it is in the case of liquids, nor is there any strong overshoot in the detonation velocity after the transition, again in contrast to the behavior of liquids. Retonation (detonation backwards through the partially-reacted explosive) has not been observed, although retonation in small diameter sticks has been reported by Cook<sup>(7)</sup> and others.

The initial pressure of the shock wave in the explosive under study has been determined by the use of a method which is not completely satisfactory, but which is the only method available at present. In the experiments described in this paper, the shock wave enters the explosive from a booster-attenuator system, which has an inert (usually metal) plate in contact with the explosive. The assumption is made that the pressure and particle velocity are the same on both sides of the attenuator-explosive interface, the usual boundary conditions when dealing with shock waves in inert materials. Because we are studying initiation, which cannot be a steady state, these boundary conditions cannot be exactly correct. The free-surface velocity of the attenuator is measured and the approximation is made that the particle velocity,  $U_{PA}$ , is equal to one-half the free-surface velocity. Other experimental data include the initial density,  $\rho_{OE}$ , and the initial shock velocity,  $U_{SE}$ , in the explosive. Assuming that the shock Hugoniot of the attenuator material is known, the free-surface velocity measurement permits the evaluation of the shock pressure,  $P_A$ , and the particle velocity,  $U_{PA}$ , in the attenuator. The pressure,  $P_E$ , and the particle velocity,  $U_{PE}$ , in the explosive are then found by determining the intersection of the attenuator rarefaction locus, approximated by reflecting the attenuator Hugoniot about the line  $U_{PA} = \text{constant}$ , and the locus for the state of the explosive, given by the conservation of momentum relation

$$P_E/U_{SE} = \rho_{OE} U_{PE} .$$



This process is illustrated in Fig. 1. For a more detailed discussion of the method of calculation, see, for example, Reference 8.

When the shocked material is an explosive, the equation  $P_E = \rho_{OE} U_{SE} U_{PE}$  holds for a steady state detonation, but the process of initiation cannot be regarded as a steady state. In the experiments to be described, the explosive reacts to some small extent immediately behind the shock front, and the extent of reaction increases as the shock wave proceeds. In the region near the explosive-metal interface where only a small part of the explosive reacts, the above expression for the pressure will hold with sufficient accuracy to be useful. Throughout this paper values of the pressure in the explosive will be understood to include some error from this source.

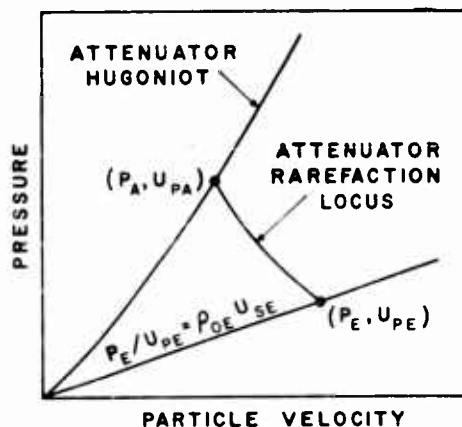


Fig. 1. Graphic method of obtaining shock pressure and particle velocity in under-initiated explosive.

#### EXPERIMENTAL

##### Type I Experiment: Wedge Technique with Smear-Camera Records

The solid explosives studied here are not transparent and must therefore be studied by observing a free surface, if camera techniques are to be used. An explosive booster-attenuator system used to send a shock wave into the explosive to be studied is shown in Fig. 2. The latter explosive is in the form of a wedge, so that progress of the shock or detonation wave can be seen as motion along the slant face. This motion can be observed best if the slant face has been covered with a thin (0.00025 in.) film of aluminized Mylar plastic<sup>(6)</sup> and illuminated with an intense light source. The alignment is such as to reflect the light from the plastic film to the camera.

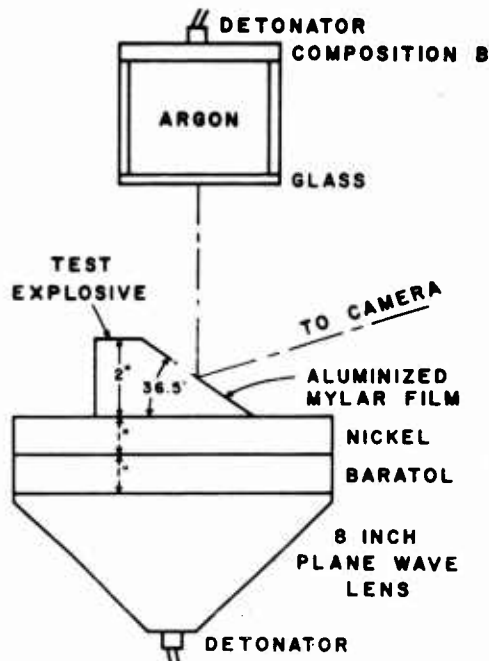


Fig. 2. Charge arrangement for Type I experiments.

As the shock wave proceeds along the slant face, the mass motion of the explosive causes a tilt of the reflecting surface so that the light is no longer reflected to the camera. This arrangement gives a sharp cut-off of light and a well-defined record. The smear camera is aligned along a line of steepest descent of the wedge and is focussed on the slant face.

Figure 3 shows a smear camera record, which is just a space-time plot, obtained with this technique, and Fig. 4 shows the interpretation. The velocity of the shock wave is obtained from the slope of the space-time plot. The free-surface velocity of the attenuator plate is measured with electrical contactors spaced above the plate, or with camera techniques applied to a duplicate booster-attenuator system. Using the method described in the Introduction the pressure and particle velocity behind the initial shock in the explosive can be estimated.

The results of the analysis of the record reproduced in Fig. 3 are given here as an example of the information obtainable from experiments of this type. The explosive wedge was made of cyclotol (65/35 RDX/TNT) with an initial density,  $\rho_{OE}$ , of 1.71 g/cc and a base angle of the wedge of  $36^\circ 25'$ .

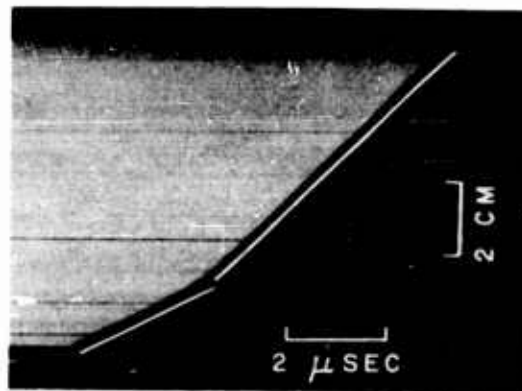


Fig. 3. Smear camera record of the cyclotol (65/35 RDX/TNT) wedge shown in Fig. 2. Light reflected from the slant face of the wedge is cut off as the shock wave moves up the wedge. Two straight lines have been added for ease in visualizing the curvature of the space-time plot. Time increases to the right; the toe of the wedge is at the bottom. Space scale applies to the slant face. Shot D-6082.

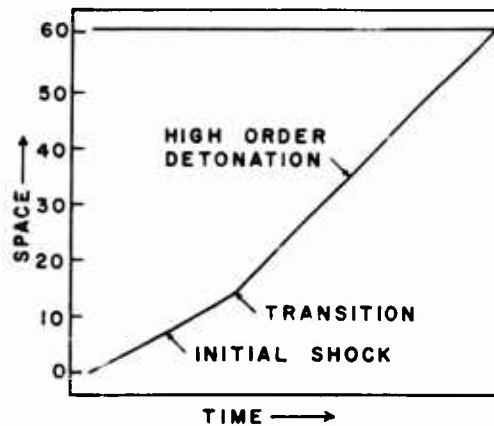


Fig. 4. Interpretation of smear camera record of Fig. 3. This figure is a tracing of the camera record.

A space-time plot was made of the smear-camera record by dividing the space dimension into 61 equal parts, as shown in Fig. 4, and reading the corresponding time values. After converting the space values to distance of shock travel in the wedge, polynomials of first, second and third degree were fitted to the first 14 points and to the last 45 points, thus omitting the region of the greatest curvature. It was

found for the initial shock that the second-degree polynomial gave a better fit than either the first- or third-degree polynomials. For the portion of the curve above the transition to high-order detonation a second-degree equation also gave the best fit. In the latter fit, although the quadratic coefficient was statistically significant, its magnitude indicated that it could have resulted from imperfections in the booster wave. The equations obtained for the smear camera record shown in Fig. 3 were the following:

$$\begin{array}{ll} \text{Initial Shock} & X = 0.1198 + 3.5334t + 0.2452t^2 \\ & (0.0263) (0.0406) (0.0134) \end{array}$$

$$\begin{array}{ll} \text{High-order Detonation} & X = -9.152 + 7.521t + 0.0457t^2 \\ & (0.169) (0.0665) (0.0062) \end{array}$$

where the standard deviation of each parameter is shown in parentheses. The units of  $X$ , the space coordinate taken perpendicular to the wave front, are mm, and the units of  $t$ , the time coordinate, are  $\mu\text{sec}$ . The constant terms have no significance, but both equations have the same origin. For the initial shock equation, the coefficient of the linear term is the initial velocity, and the coefficient of the quadratic term is the acceleration. The high-order detonation begins at about 2.8  $\mu\text{sec}$ , and the velocity at that time is, from the equation, 7780 m/sec. The high-order, steady-state, plane detonation wave velocity for this explosive is  $8000 \pm 20$  m/sec. The difference is not significant, as it may be due to small imperfections in the wave.

The significant value of the quadratic term in the polynomials for the initial shock indicates a steady acceleration of the shock wave. No significant indication of overshoot was obtained by fitting higher-order polynomials to the high-order detonation region. Analytical fits to the data in the region of maximum curvature do not reveal any departures from a smooth acceleration of the shock prior to the onset of high-order detonation. It should be noted that all results obtained with this technique assume that the shock wave comes through the attenuator simultaneously over the region covered by the wedge to be studied, and that the pressure profile is identical at each point over the same area. Tests of the booster systems used justify these assumptions.

A very large number of experiments of this type have been done using the cyclotol mentioned, both pressed and cast, pressed TNT of various grain sizes and densities, plastic-bonded HMX, and plastic-bonded RDX. All of these experiments have shown the same qualitative behavior, and with good explosive the quantitative results are reproducible.

#### Type II Experiment: Wedge Technique with Framing Camera Records

Framing camera photographs often give qualitative information in a more rapidly assimilated form than do smear camera photographs.

The accuracy of measurements from framing camera pictures is usually not very good, but the photograph can be easily understood. Figure 5 shows a series of frames of a wedge of the same type as described in Experiment I. The wedge is immersed in a saturated aqueous solution of zinc chloride ( $\rho = 1.9 \text{ g/cc}$ ), which is a fairly good impedance match to the explosive (65/35 RDX/TNT) of the wedge. The shock pressure in the solution supports the wedge at the sides and along the slant face so that the wedge holds together throughout the entire interval covered by the framing sequence.

In the first 5 frames the shock can be seen moving up the slant face of the wedge and reducing the reflectivity of the explosive surface, which is brilliantly illuminated by an argon-flash light source. Then in Frame 6 the detonation wave begins as revealed by a change in reflectivity of the wedge surface. The detonation wave runs to the top of the wedge and the strong shock in the zinc-chloride solution emerges into the atmosphere producing a bright air shock which moves downward, obscuring the subject. The demarcation between the region traversed by the initial, weak shock wave and the region of complete detonation remains stationary and sharply defined to the end of the framing sequence; no detonation is observed.

-----

Fig. 5. (On following page.) Framing camera sequence showing the transition between the initial shock wave and the high-order detonation wave in a cyclotol wedge immersed in a saturated aqueous solution of zinc chloride. Time between frames: 0.5  $\mu\text{sec}$ . Time increases from left to right and from top to bottom. In the setup photograph, A is the light source, B is the subject wedge, C is the opening through which the camera views the subject reflected in the mirror D. Shot C-1437.

-----

#### Type III Experiment: Resistivity Technique

The purpose of this type of experiment was to study the resistivity of shocked, inhomogeneous solid explosive during the initiation process. It seemed reasonable to assume that chemical reaction in the explosive would be accompanied by a decrease in the resistivity. For electrical field strengths up to a few thousand volts per centimeter cyclotol exhibits a resistivity like that of a good plastic, i. e., of the order of  $10^{15} \text{ ohm-cm}$ . On the other hand the resistivity of a detonation wave is quite low, of the order of  $10^{-1} \text{ ohm-cm}$ . (See, for example, Refs. 9, 10.)

Figure 6 shows an experimental arrangement used to study the changes in resistivity of shocked solid explosive. The electrodes used were made of silver foil 0.0005 in. thick and 1/16 in. wide. These electrodes were inserted between 4-in. cubes of explosive which had been lapped flat; the blocks were then clamped together under a

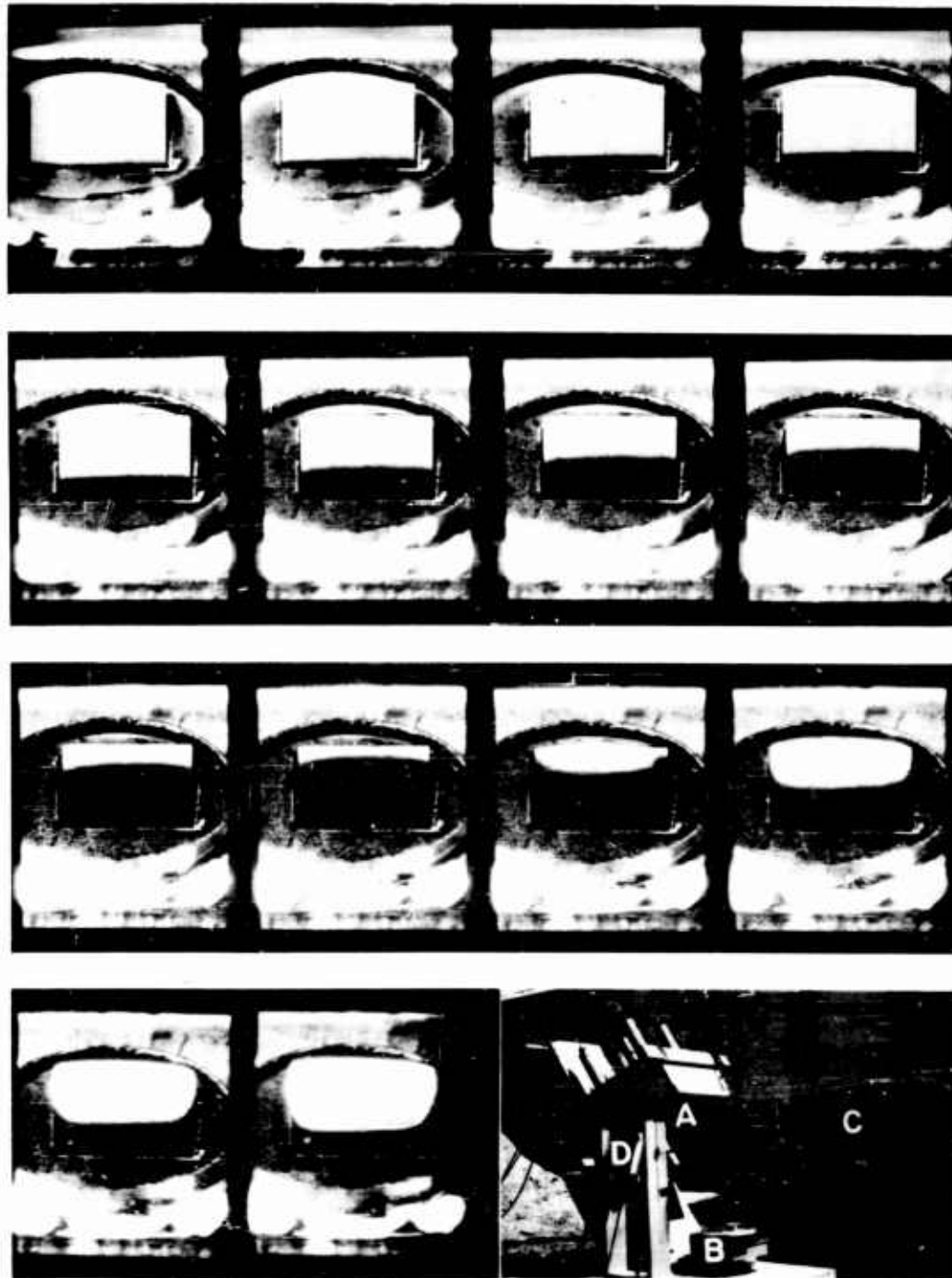


Figure 5

pressure of approximately 60 psi in an effort to eliminate any air gap from the joint. The experiment was arranged with the long axis of the foils perpendicular to the shock wave.

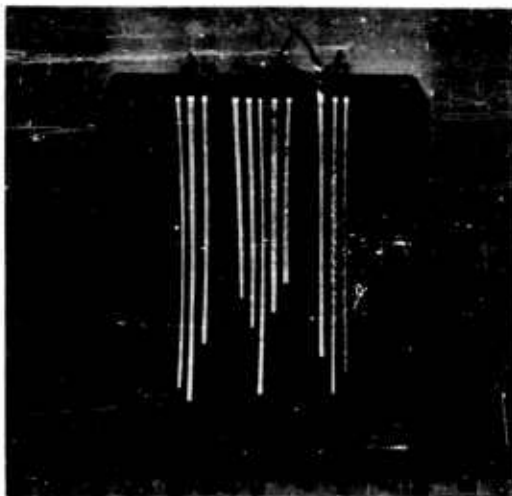


Fig. 6. Electrode placement for resistivity experiments. The center electrode in each of the three groups is connected to ground. The two fiducial signal electrodes are not shown. Shot B-4696.

Usually ten signals were taken from a single shot. The first signal was produced by the first motion of the brass driving plate and denoted the entry of the shock into the explosive under study. This signal was sent to all recording channels as an initial fiducial. The next four signals were taken from the region traversed by the initial shock wave, and a second four were taken in the region traversed by the detonation wave. One signal from each of these groups was sent to each of the four recording channels. The tenth signal, taken from the top of one of the blocks of explosive, which were 4 in. thick, was again distributed to all four channels as a final fiducial.

The signal circuits used with the electrodes are shown in Fig. 7. Selected batteries were used as low-impedance sources of current in the circuits intended to sense the resistivity behind the initial shock wave. Figure 8c shows the signal in a battery circuit when the electrodes were connected by a shock-driven brass plate. Comparison of this signal with the other two of Fig. 8 shows that the rise times of these two signals are not limited by circuit parameters but were controlled by conditions behind the shock wave.

The records from these resistivity experiments (see Ref. 11 for a description of the recording equipment) showed first of all that the explosive immediately behind the initial shock wave was quite conducting, but not so conducting as that behind a detonation wave. They also showed that the onset of conductivity occurred immediately behind

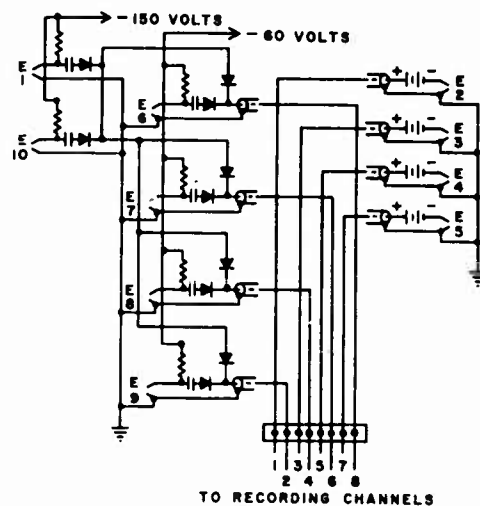


Fig. 7. Circuit used in resistivity experiments. Circuit components: resistors, 1 megohm; capacitors, 500  $\mu\text{F}$ ; diodes, IN140; batteries 45 V, Eveready Type W365F; coaxial cables, 33 ohm. Electrodes are numbered as listed in Table I.

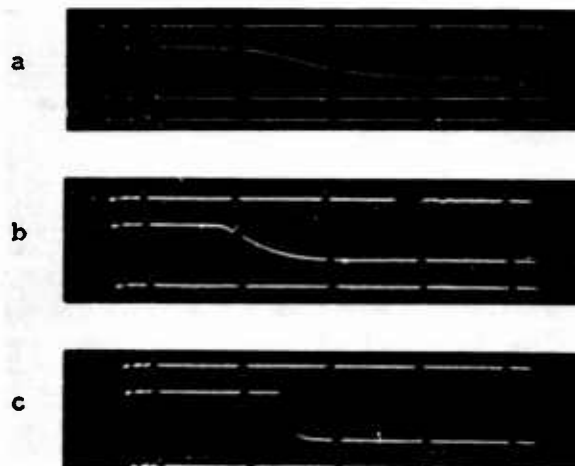


Fig. 8. Chronograph records from resistivity experiments. Time between marks, 0.50  $\mu\text{sec}$ . Time proceeds from left to right and from top to bottom. (a) Signal E2 of Table I. (b) Signal E5 of Table I. (c) Signal from battery circuit of Fig. 7 when signal electrode is grounded by shock-driven brass plate. Shots D-4695, B-4703.



the shock front. The space-time data of a single shot are displayed in Table I. A straight line was fitted to the first five points by the method of least squares, and a second straight line was fitted to the second five points. By referring to the results of Type I experiments it can be seen that the velocities obtained as the slopes of the least-squares curves, listed in Table I, are not inconsistent with velocities for the initial shock wave and for the detonation wave from previous work. The agreement is as good as can be expected, since with the few points available the quadratic terms cannot be resolved.

TABLE I

Shot No. B-4695. Explosive: 65/35 RDX/TNT,  $\rho_0 = 1.71$  g/cc.

Electrode Number	x(a) (mm)	t(a) ( $\mu$ sec)	$\Delta t$ (b) ( $\mu$ sec)	Velocity(c) (mm/ $\mu$ sec)	Distance to Transition(c) (mm)
E1	0	0	- .038		
E2	1.95	(0.73-)	(+ .253) <sup>(d)</sup>		
E3	2.95	0.781	+ .077		
E4	5.56	1.266	- .027		
E5	6.57	1.510	- .011	4.43	7.96
E6	12.76	2.437	- .006		
E7	24.91	3.998	+ .018		
E8	32.88	4.999	+ .010		
E9	50.37	7.173	- .029		
E10	101.60	13.693	+ .008	7.90	

- (a)  $x$  is the distance from the attenuator-explosive interface to the end of the electrode.  $t$  is the time interval from entry of the wave into the explosive to contact of the wave with the electrode.
- (b)  $\Delta t = t_{\text{obs}} - t_{\text{calc}}$ .  $t_{\text{calc}}$  is obtained from the least-squares fits to the data.
- (c) Calculated from least-squares fits to data. Transition point is taken as the intersection of the two curves.
- (d) This error seems to be due to the very slow rise of the signal and the resultant difficulty in locating the beginning of the signal. See Fig. 8a.

In Fig. 8a is shown the signal from electrode E2 of Table I, while Fig. 8b is the record from electrode E5. Although it would be difficult, if not impossible, to measure from such records the resistivity of any volume element behind the initial shock wave, the records do show that the resistivity behind the wave decreases as the point of transition to high-order detonation is approached. It is instructive to plot the rise-time of the signals against the distances of the corresponding electrodes from the transition point, the rise-time being defined as the time to 50% of maximum deflection. A curve drawn through these points tends to zero rise-time in the neighborhood of the velocity transition. At 50% deflection point the battery voltage was equally divided between the impedance of the coaxial cable (33 ohms) and the sum of the impedances of the battery and the gap between the electrodes. The battery impedance was about 4.5 ohms, and the impedance of the gap between the electrodes was therefore 28.5 ohms. If the region of low resistivity extends for a considerable distance behind the shock, the resistance between a pair of electrodes will decrease as the shock moves along them. The plot shows that the resistance decreases more rapidly as the shock progresses, which means that the resistivity of the explosive immediately behind the shock front becomes smaller as the shock approaches transition to detonation. Six experiments of this type using the same lot of explosive show excellent agreement of velocities, transition distance, and even conductivity at each level.

#### Type IV Experiment: Doubly-Shocked Explosive

The results reported thus far raised the question as to whether the explosive traversed by the initial shock wave ever reacted completely. For example, the framing-camera sequence presented in the discussion of the Type II experiments showed the boundary, corresponding to the transition to high-order detonation, to remain sharply defined throughout the period of observation; this implies that the explosive traversed by the initial shock wave had not detonated and that the initial shock wave was converted into a detonation wave without the contribution of a large fraction of the chemical energy available in the initial layer.

The state of this initially-shocked layer, the imminence of complete reaction, and the susceptibility of this layer to initiation by a second shock was investigated by the experimental arrangement shown in Fig. 9. A layer of Styrofoam of density 10.5 lbs/cu ft was used as the shock attenuator immediately adjacent to the explosive under study (HMX/plastic-94/6). The first reverberation in the foam supplied a second shock to the explosive. The wedge was immersed in an impedance matching solution of  $\text{ZnCl}_2$ , so that no rarefaction was reflected into the wedge.

Figure 10 shows the smear-camera record of such a shot. The values of the initial shock velocity,  $U_s$ , and the high-order detonation velocity,  $D$ , were found to be 3.93 mm/ $\mu\text{sec}$  and 9.20 mm/ $\mu\text{sec}$ , respectively. From Type I experiments on the plastic-bonded HMX the particle velocity,  $U_p$ , was interpolated to be 0.55 mm/ $\mu\text{sec}$ . Using

these data, the base angle,  $\theta$ , of the explosive wedge after passage of the initial shock wave was calculated from the relationship

$$\tan \theta = \tan 20^\circ (U_S - U_P) / U_S$$

where the initial wedge angle was  $20^\circ$ . Using this value of  $\theta$  and the camera record of the second shock, the velocity of the latter was calculated to be 5.62 mm/ $\mu$ sec.

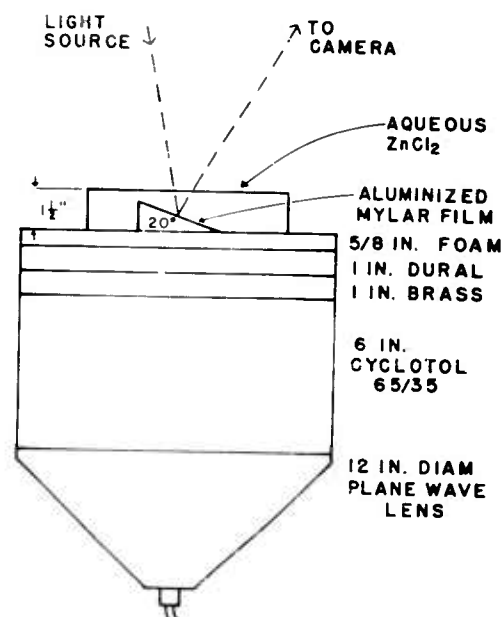


Fig. 9. Charge arrangement for doubly-shocking plastic bonded HMX. Shot D-6851.

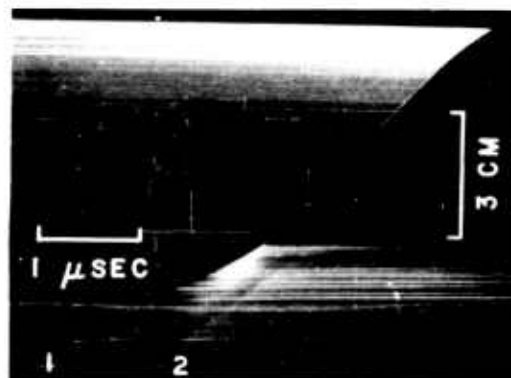


Fig. 10. Smear camera record of doubly-shocked wedge of

plastic-bonded HMX. First and second shocks are labeled 1, 2, respectively. The first shock starts at the bottom and moves up and to the right at almost constant slope, until detonation begins and the slope becomes greater. The curvature at the upper right in the detonation line is an edge effect. The second shock starts at the bottom about 1.4  $\mu$ sec later and moves at higher velocity. The space scale applies to the slant face. Shot D-5861.

The second shock wave corresponds to an important increase in pressure over the 39 kbar of the first shock, although sufficient data are lacking for an accurate calculation of this increase. The Rayleigh line intersects the initial Hugoniot at 100 kbar, however, so the pressure is near 100 kbar. That it is not a detonation wave is evident from the wave's low velocity relative to that of the detonation wave observed in the upper part of the wedge. This result suggests both that complete reaction was not imminent in the initially-shocked layer of explosive and that the initial shock has in fact desensitized this layer.

#### Type V Experiment: Nitromethane-Carborundum Mixtures

Following the hypothesis that the difference in the initiation behavior of physically homogeneous and inhomogeneous explosives is in fact due to the inhomogeneities, an experiment was designed to convert nitromethane, which had been extensively studied in the homogeneous state<sup>(1)</sup>, into an inhomogeneous explosive by the addition of Carborundum grit. The charge was arranged as shown in Fig. 2, except that the booster-attenuator system was 12 in. in diameter. It consisted of a plane-wave lens, 2 in. of baratol, 3/4 in. of brass, 3/4 in. of Lucite, and 3/4 in. of brass.

The charge of nitromethane and Carborundum is shown in Fig. 11. A wedge-shaped container made of Homolite plastic was used to hold the explosive mixture in contact with the brass attenuator plate. The Carborundum was #150 grit settled to a density of 1.90 g/cc with a reproducibility better than 0.003 g/cc. Nitromethane was introduced at the bottom of the wedge by means of a hypodermic needle as shown in Fig. 11. The addition of the nitromethane was carried out slowly to displace the air in the interstices and brought the final charge density to 2.32 g/cc. Finally, a narrow strip of aluminized Mylar was stretched along the slant face of the wedge to act as a mirror as required in the Type I experiments.

The firing record obtained from the Carborundum-nitromethane mixture is shown in Fig. 12. It can be seen that the velocity transition is characteristic of inhomogeneous explosives, i. e., it is a smooth, gradual process. The velocity of the initial shock wave was 2.47 mm/ $\mu$ sec and the pressure was 23 kbar. These values are to be compared with 4.5 mm/ $\mu$ sec and 85 kbar for the initiating shock in pure nitromethane. The detonation velocity in the mixture was 4.44

mm/ $\mu$ sec as compared to 6.30 mm/ $\mu$ sec for pure nitromethane. Thus, addition of Carborundum to nitromethane sensitizes it and the resulting mixture initiates in the same way as do inhomogeneous solids. Five experiments of this type have shown excellent agreement.

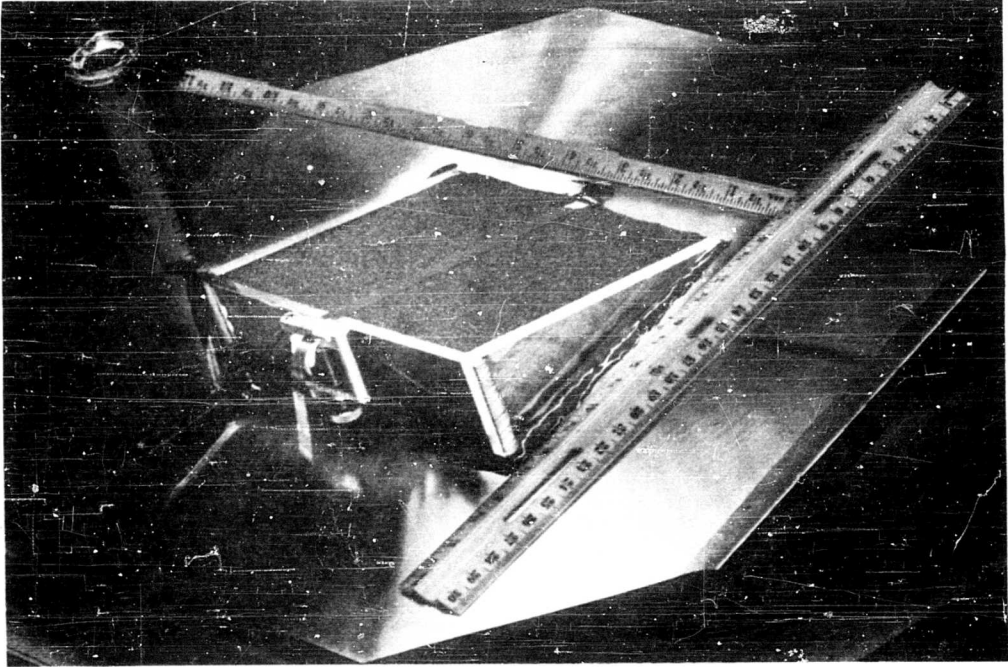


Fig. 11. Nitromethane-Carborundum charge mounted on brass shock-attenuator. Base angle of wedge:  $20^\circ$   
Shot D-6853.

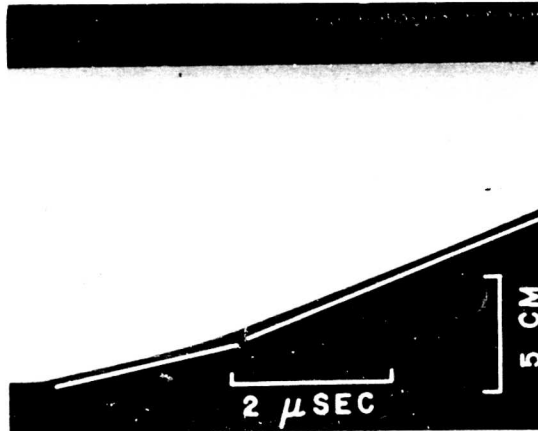


Fig. 12. Smear camera record from nitromethane-Carborundum charge in Fig. 11. The space scale applies to the slant face. Shot D-6853

## Additional Experimental Results

In the course of the work on initiation, many data have been collected in addition to those already mentioned. In order to design an experiment to study initiation, it is necessary first to know what pressure is needed to initiate the explosive in a time convenient for the equipment available. Also, it is possible to get meaningful data only if the results can be reproduced. Reproducibility requires reproducible behavior of both the experimental piece and the booster system. Since the initiation behavior of a charge depends upon the nature and extent of the inhomogeneities present in it, it is these which must be evaluated in order to characterize and obtain the quality necessary in a charge to allow one to obtain valid results in initiation experiments. Type I experiments were used to explore these problems. Some of the results illustrate general behavior, and will be presented for that reason.

Wedges of the cyclotol described in the section Type I experiments were initiated with different boosters to determine where high-order detonation begins for different initial shock pressures. The pressures were obtained from the free-surface velocity of the attenuator plate used in the usual impedance match calculation with the initial shock velocity in the explosive. The data are plotted in Fig. 13.

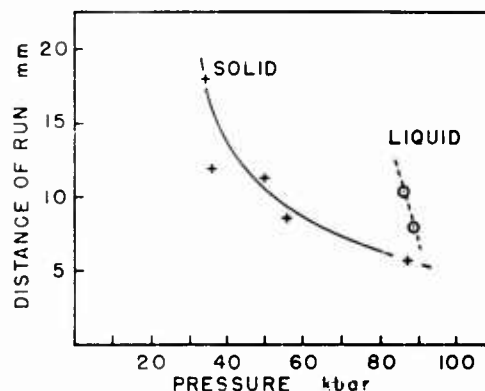


Fig. 13. Plot of distance of run of the shock wave before high-order detonation begins versus initial shock pressure. The solid explosive is cyclotol, and the liquid is nitromethane.

The errors result in large part from uncertainty about which point on the accelerating curve one should pick. The contrast between the behavior of liquid<sup>(1)</sup> and solid explosives is illustrated in Fig. 13 by including the similar curve for nitromethane. The distance in this case is the position of the shock wave when detonation begins at the

back surface. The great difference in the slope of the two curves is evidence that while in liquids the shock must heat all the explosive to a high uniform temperature, resulting in a very strong dependence of the induction time on the temperature or shock pressure, in solid inhomogeneous explosive the important heating is at the defects in the structure where the temperature depends more strongly upon the nature of the defect than upon the shock pressure. It is easy to show that the average temperature in the shocked solid is too low at any of the pressures used to make the reaction proceed at a sufficient rate for detonation to occur in a few microseconds.

In Fig. 14 are plotted the results of some initiation experiments on TNT charges pressed from coarse- and fine-grained material. The coarse-grained TNT had a median particle size in the range 200-250  $\mu$ , while the fine-grained material, which was prepared by grinding the coarse, fell largely in the range 20-50  $\mu$ . One booster design was used for all of the shots, and the measured values of the pressure were 60 kbar  $\pm$  5%.

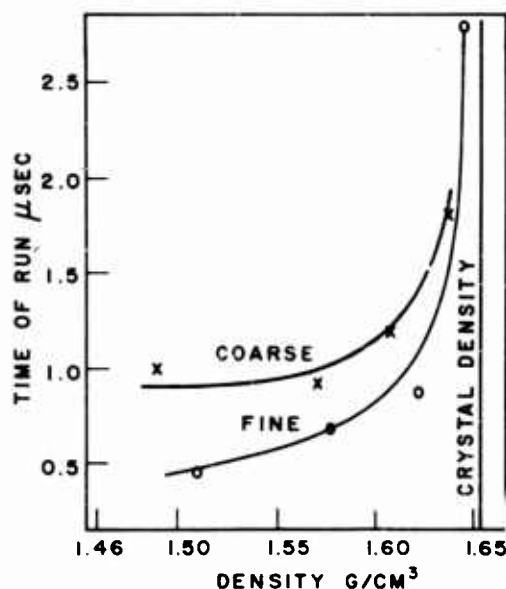


Fig. 14. Effects of initial density and particle size on the sensitivity of pressed TNT charges. Ordinates are times of run of initial shock waves as shown in Fig. 4.

From the plots of the data it can be seen that the charges made from fine-grained TNT were more sensitive than those made from coarse material. This agrees with general experience. Another important feature is the rapid decrease in sensitivity of both types of charges

as the density approaches crystal density (1.654 g/cc).

Figure 15 shows the results of initiation experiments on charges pressed from two lots of plastic-bonded HMX. The lots differed slightly in particle-size distribution. Again it can be seen that, as the limiting density is approached, the sensitivity decreases rapidly.

From these two sets of experiments it appears that at intermediate densities the particle size is more important than is the density in affecting the sensitivity, whereas at densities approaching the limiting value, the density becomes the more important factor. Furthermore, it seems reasonable to suppose that the initiation behavior gradually changes from that of an inhomogeneous explosive to that of a homogeneous one.

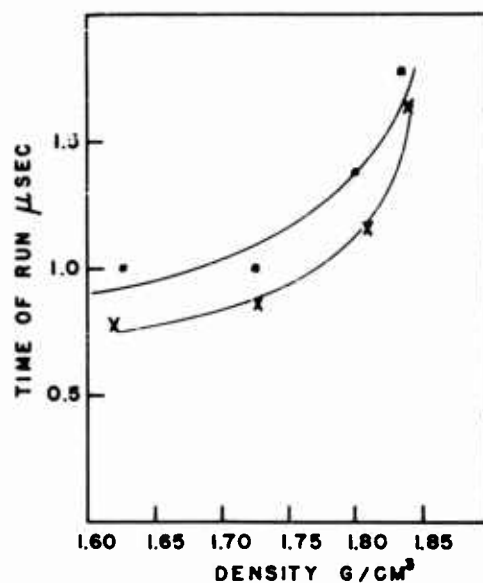


Fig. 15. Effect of density on the sensitivities of two lots of plastic-bonded HMX. Ordinates are times of run of initial shock waves as shown in Fig. 4.



## DISCUSSION OF RESULTS

In most of the experiments described in this paper our goal has been to put a smooth, plane shock wave with a sharply rising front and constant amplitude into the explosive charge to be studied and to observe the initiation behavior before the intrusion of edge effects or of reverberations in the shock attenuator. While edge effects were eliminated, the pressure profile was not flat-topped. To achieve the latter condition to good approximation would have required either very large charges, or that a good technique for throwing big metal plates be developed. Nevertheless, the shock waves were of sufficient quality to permit the drawing of a number of conclusions from the experimental results.

It is of interest first to contrast the initiation behavior of homogeneous and inhomogeneous explosives using Reference 1 as the source of information for the former. The contrasts are as follows:

(a) The initial shock wave in a homogeneous explosive shows a constant or slightly decaying velocity as a function of time; the corresponding wave in inhomogeneous explosive accelerates throughout its travel.

(b) The transition to high-order detonation is very abrupt in homogeneous explosive; the transition in inhomogeneous explosive is less so.

(c) The onset of high-order detonation in homogeneous explosive is accompanied by an overshoot in the velocity, amounting to about 10% in the case of nitromethane; no demonstrable overshoot has been recorded for inhomogeneous explosive in our experiments.

(d) Detonation is observed to originate at the shock attenuator-explosive interface in homogeneous explosive; at present it is believed probable that detonation occurs at or near the shock front in inhomogeneous explosives. It may be possible to clarify this point in the future by conductivity measurements.

(e) The experiments with nitromethane-Carborundum mixtures have shown that the mixtures are much more sensitive than the homogeneous liquid nitromethane. The inhomogeneities in the mixture cause shock interactions with resultant local heating. For initiation, the detailed structure of the shock properties of the explosive is more important than are the values of the thermochemical constants.

(f) The material behind the initial shock wave in homogeneous explosive is relatively non-conducting for electricity until the onset of detonation; in inhomogeneous explosive the material behind the initial shock front is quite conducting and becomes even more so as the transition to high-order detonation is approached.

(g) The initiation process in homogeneous explosive is much more sensitive to variation of the initial temperature or to variation of the shock pressure than it is in inhomogeneous explosive.

It is logical to attribute the differences between the initiation behavior of inhomogeneous and homogeneous explosives to the voids and other defects in the former. Work with nitromethane in Reference 1 and the results with nitromethane-Carborundum mixtures reported here show that convergences in the mass flow and impedance mismatches can

cause local reaction which influences importantly the initiation process. It is easy to show with a smear camera record that the detonation front in a pressed or cast explosive is quite rough, from which one can deduce that the mass flow is quite irregular in fine detail.

On the other hand gas bubbles and voids are perhaps the most commonly occurring defects in cast and pressed explosives. If we may assume that the number of voids between grains of explosive is proportional to the number of grains, then the coarse-grained TNT discussed above should have fewer, but larger, voids than the fine-grained TNT at the same density. Experimental results show that the latter explosive is more sensitive, and therefore, it may be concluded that a volume of fine voids is more efficient in producing chemical reaction than the same volume of coarse voids. This suggests the importance of a surface reaction.

The effect of increasing the number of voids and other sources of hot spots is to render a given explosive more sensitive. It is well known that an explosive becomes easier to initiate as the density is decreased. This effect of hot spots is supported here by the results obtained for nitromethane-Carborundum mixtures and by the data plotted in Figs. 14 and 15. When an explosive exists in an inhomogeneous state, the shock strength necessary to cause initiation need not be great enough to raise the entire mass to a sufficient temperature for a rapid reaction (thermal explosion) to occur, but need only activate a sufficient number of hot spots. This effect of hot spots also accounts for the small dependence of the sensitivity of inhomogeneous explosives on the initial temperature.

The amount of energy obtainable from a single hot spot must depend, among other things, upon the shock strength. Following the model of Rideal and Robertson<sup>(12)</sup> the higher the temperature around a hot spot, the longer the hot spot will continue to react and the more energy it will produce before being deactivated by loss of heat to the surroundings. An increase in shock strength will increase the temperature of the homogeneous explosive about a hot spot as well as, perhaps, increasing the dimensions and temperature of the hot spot itself.

The behavior of the undetonated layer of explosive in the Type IV experiments becomes understandable on the basis of hot-spot action. The primary sources of hot spots in the plastic-bonded HMX pressings are the impedance mismatch between the HMX and the plastic, and the small bubbles present. Passage of the first shock wave creates hot spots and causes some chemical reaction to take place. After the hot spots have been deactivated by loss of heat to their surroundings, the explosive is left in a more homogeneous state than before. The bubbles will have been collapsed and the impedance mismatches reduced by the greater compression of the less dense component. The explosive will then be much less sensitive to a second shock.

In view of the above considerations, the following picture of the initiation process has evolved. A shock entirely too weak to initiate a homogeneous explosive can activate hot spots and cause detonation when the explosive is sufficiently inhomogeneous. In an explosive pressed to near crystal density the hot spots due to bubbles are quite small and are deactivated quickly after passage of the shock.

The energy contribution to the shock wave by a particular hot spot is completed soon after the passage of the wave front. Detonation occurs at or near the front of the wave; explosive located before the transition does not detonate and is relatively insensitive to subsequent shocks. Because the detonation takes place near or at the front of the wave, there is little or no overshoot in the detonation velocity.

#### ACKNOWLEDGEMENTS

The authors are indebted to many people for help and advice over an extended period of time. Most of these are members of the GMX Division of the Los Alamos Scientific Laboratory. We are especially grateful to Group GMX-3 of this Laboratory for supplying the explosive for the experiments, which was of exceptional quality and without which the work could not have been done. Especial thanks are due to B. Hayes for much of the electronic technique used in this work.

#### REFERENCES

1. A. W. Campbell, W. C. Davis, J. R. Travis, "Shock Initiation of Detonation in Liquid Explosives". This Symposium.
2. Henry Eyring, R. E. Powell, G. H. Duffey, R. B. Parlin, Chem. Revs. 45, 69 (1949).
3. F. P. Bowden, et al., "A Discussion on the Initiation and Growth of Explosion in Solids", Proc. Roy. Soc. (London) 246, 146(1958).
4. F. P. Bowden and A. D. Yoffee, Initiation and Growth of Explosion in Liquids and Solids (Cambridge University Press, 1952).
5. S. J. Jacobs, "Recent Advances in Condensed Media Detonations", 30, 151 (1960), Am. Roc. Soc.
6. J. M. Majowicz and S. J. Jacobs, "Initiation to Detonation of High Explosives by Shocks", presented at Lehigh Meeting of Fluid Dynamics Division, American Physical Society, Nov. 1957.
7. M. A. Cook, The Science of Explosives (Reinhold Publishing Corporation, New York, 1958), p. 187.
8. M. H. Rice, R. G. McQueen, and J. M. Walsh, "Compression of Solids by Strong Shock Waves", Solid State Physics, Advances in Research and Applications, Volume VI, Eds: F. Seitz and D. Turnbull (Academic Press, Inc., New York, 1958).
9. B. Hayes, "On the Electrical Conductivity of Detonating High Explosives". This Symposium.
10. A. A. Brish, M. S. Tarasov, V. A. Tsukerman, Zhur. Eksp. i Teoret. Fiz. 37, 1543 (1960).
11. A. W. Campbell, M. E. Malin, T. J. Boyd, Jr., J. A. Hull, Rev. Sci. Instr. 27, 567 (1956).
12. E. K. Rideal and A. J. B. Robertson, Proc. Roy. Soc. A (London) 195, 135 (1948a).

## SHOCK INDUCED SYMPATHETIC DETONATION IN SOLID EXPLOSIVE CHARGES

Morton Sultanoff

Vincent M. Boyle

John Paszek

Ballistic Research Laboratories  
Aberdeen Proving Ground, Maryland

### Abstract

A study of the basic physical parameters for sympathetic initiation of high explosive receptor charges by the pressure pulse from a donor charge transmitted through barriers of air, steel, aluminum, lead, and copper has been conducted. A surface phenomenon, which has been shown to be a front of mechanical discontinuity supported by a chemically reacting core, has been observed to propagate at a constant, supersonic velocity. The core reaction is initiated provided the intensity of the incident pressure pulse is less than the detonation pressure of the explosive but above a threshold value which depends on the chemical composition and physical condition. The initial core reaction is a "low-order" chemical decomposition which produces a pressure considerably less than that associated with high-order detonation, and propagates at a supersonic rate, but much slower than a higher-order detonation. This reaction is confined to the central core of the explosive and its rate of propagation is determined by the intensity of the incident wave. The distances and times required for the reaction to change abruptly to high order detonation are uniquely determined, for a given explosive, by the intensity of the incident pressure wave. High order detonation is first observed at the surface of the charge coincident to the front of the mechanical discontinuity. However, the shape of that front, on emergence, indicates that initiation originated in the reacting core.

Invariably, for a considerable time after the beginning of the high-order reaction in the receptor charge, it propagates at a rate slightly greater than normal detonation rate.

While details of behavior vary with composition and geometry of the explosive, the qualitative features appear to be generally valid.

## Introduction

Studies have been made of the fundamental physical processes involved in the detonation reaction of solid explosives. These studies have led to an analysis of the parameters that control the sympathetic detonation of a receptor charge subjected to strong shocks transmitted through barriers of various materials. It is felt that these studies might lead to a fuller understanding of the detonation process and could also indicate a criterion of sensitivity based on physical quantities directly related to the explosive charges. Continuation of the research project reported formally first in a Ballistic Research Laboratories Report<sup>(1)</sup> in 1953 and subsequently in later reports<sup>(2,3)</sup> indicate the direction of this continued research with finer time and space resolution, employing new techniques for the investigation of the regime of transition from initiation to high-order detonation. Much of the earlier data were inferred from the observation of the surface conditions of receptor charges. The work covered by this report deals with the direct observations of the core reaction in the receptor. These new observations eliminate the errors and uncertainties introduced by the earlier inferences.

## Experimental Procedure

Except for some preliminary experiments with internally cast resistance wires<sup>(4)</sup> all of the data were obtained from photographic records<sup>(5)</sup>. Self-luminosity and auxiliary front lighting were used with streak-cameras, Kerr-cell single exposure shutters and multi-frame, high repetition rate, framing cameras.

The charges were arranged as shown in Figure 1 and, except where noted, were cast 50/50 pentolite sticks of 3/4 inch square cross-section, 3 inches long. Barriers of air, steel, dural, copper, lead and plastic have been tested. However, most of the data presented in this report represent a variety of barrier thicknesses of air, lead and dural.

Data for initiation by pellet impact were obtained with steel discs, driven intact, at velocities ranging from 500 to 1500 meters per second by metal-padded explosive sticks.

## Discussion-Specific Results

As a result of the methods for the determination of initial conditions in the receptor charges, the quantitative data obtained in these tests fall into three general categories, i.e. air-gap, metal barrier and pellet impact. However, the conditions leading to high order detonation can be described by a single physical model.

### 1. Initiation by Shock Through Air Gaps

The earliest investigations of shock initiation were concerned primarily with air barriers, and the time "t" and distance "d"

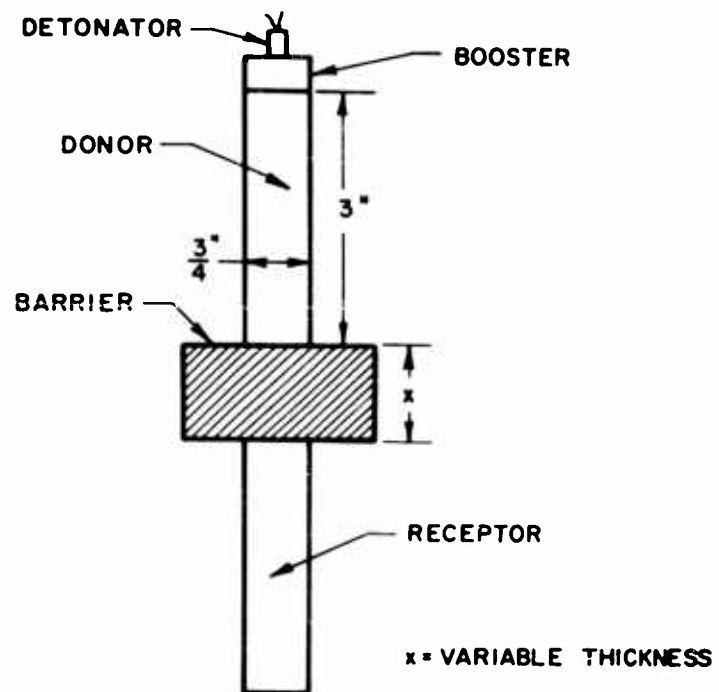


Fig.1 - Basic experimental arrangement

shown in Figure 2A, which is a typical streak-camera record, were the first observations made of the delay to detonation. More recent, front lighted records (Figure 2B) have shown that this time "t" consisted of at least two individual delays, i.e., the delay to ignition and the delay to high order detonation after ignition established a core reaction in the receptor stick. The direct measurements of the supersonic surface velocity<sup>(3)</sup> as a function of the width of the air gap in comparison with the velocities computed from the "t-d" data are shown in Figure 3.

For detonation induced by the air shock it is necessary to separate the contributions of peak pressure, impulse and possibly heat, to the reaction in the receptor. The pressure in the air shock at the face of the receptor is directly obtained from the Hugoniot relations for air, which are well known for the velocities involved. The pressure so obtained, cannot be used directly to obtain the pressure in the receptor, however. Theory and experiment both show that the peak pressure occurs when the high density detonation products, which are following closely behind and driving the air shock, impact the face of the receptor charge. A single rough measurement made at these Laboratories, (by Mr. Boyd Taylor) of the pressure developed in a Plexiglas receptor separated by a 1 inch air gap from a standard pentolite donor yielded an estimate of 300,000 PSI. At this gap distance, the pressure in the incident air shock is about 8,500 PSI and, allowing for a maximum theoretical eight-fold magnification in the reflected shock from a perfectly rigid wall, the pressure at the receptor face could be expected not to exceed 68,000 PSI as a result of the shock impact. The quantitative data presented relate the surface velocity and the delay to detonation in the receptor to the pressure in the incident wave. Recomputing to include the results of the single test with the Plexiglas receptor will increase the magnitude of this pressure, and will throw the air gap data into agreement with the metal barrier data.

## 2. Initiation by Shock Through Metal Barriers

The delay time and distance to detonation in receptor charges have been studied as functions of both the barrier thickness and barrier material with lead, dural, copper, and steel. However, sufficient data for quantitative as well as qualitative analysis have only been obtained with the lead and dural barriers.

Direct measurements of the pressure induced in the receptor charges could not be made with existing instrumentation and techniques. However, once the pressure in the barrier at the barrier-receptor interface is known, this information can be used with the extended high pressure Hugoniot curve published by Los Alamos<sup>(6)</sup>. By use of the pin technique, Dr. Floyd Allison at Carnegie Institute of Technology supplied the free surface velocities of barrier materials driven by contact donor charges. Using the relationship:

$$P = \rho_0 U_s U_p$$



(a)

(b)



Fig. 2 - (a) Streak camera record of sympathetic detonation by air shock showing the distance and delay time to detonation; (b) front lighted record of sympathetic detonation by air shock showing the surface shock propagating along the receptor.



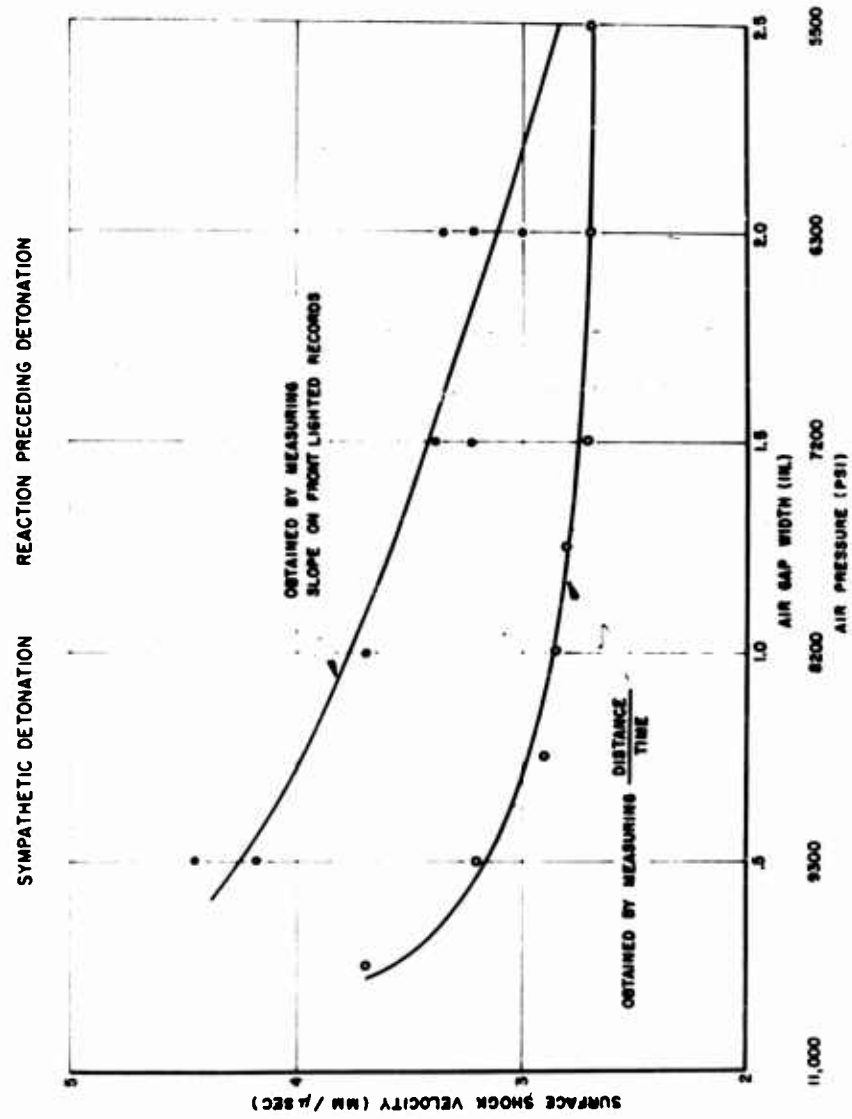


Fig. 3 - A comparison of front-lighted and distance/time measurements

where:  $P$  is pressure (dynes/cm<sup>2</sup>)  
 $\rho_0$  is barrier density (gms/cm<sup>3</sup>)  
 $U^0$  is shock velocity in the barrier (cm/sec)  
 $U^s$  is the barrier particle velocity (cm/sec),  
and is approximately  $1/2$  the free surface velocity,

the pressure transmitted to the receptor charge is computed. The relationship of the delay to detonation for lead and dural is shown as a function of these computed pressures in Figure 4.

To date, the pressure profile and consequently the impulse delivered to the receptor charge have not been measured. With new pressure transducer techniques, a program to determine values for this parameter is being initiated. However, the contribution of total impulse appears negligible in the comparison, shown in Figure 4, of data for two materials of widely different density and physical characteristics.

### 3. Initiation by Pellet Impact

Aluminum pads of various thickness were used on the ends of large explosive cylinders separating the charge and disc to be propelled. Tests were conducted with steel discs 1.5 inches in diameter and 0.125 inches thick weighing 28.32 grams with velocity of impact at the receptor ranging from 0.58 to 1.52 mm/ $\mu$ sec. Earlier evidence that peak pressure, not total energy delivered to the receptor, controlled the delays and velocities in the receptor led to the treatment of the plate as a free surface. Computations identical to those for metal barriers were made and the plot shown in Figure 5 indicates the close agreement of these data to those for metal barriers.

It appears most likely that the excessive scatter in the impact data resulted from oblique collision of the plate with the end of the receptor. Additional testing of the effects of oblique impact is being conducted to amplify this possibility.

### Discussion-General Results

An examination of the photographic exposures made in tests conducted with the air and metal barriers and impacting pellets made it immediately obvious that the initiation, the pre-detonation, and the "break-out" of high order detonation have the same physical characteristics for all these methods of transfer of energy to the receptor charge. Four conditions have been found to exist in the impacted receptors:

1. Detonation occurs with no measurable delay at the impacted face of the receptor.
2. A measurable supersonic surface shock of mechanical discontinuity proceeds at constant velocity in the receptor, and eventually high order detonation breaks out in this front.

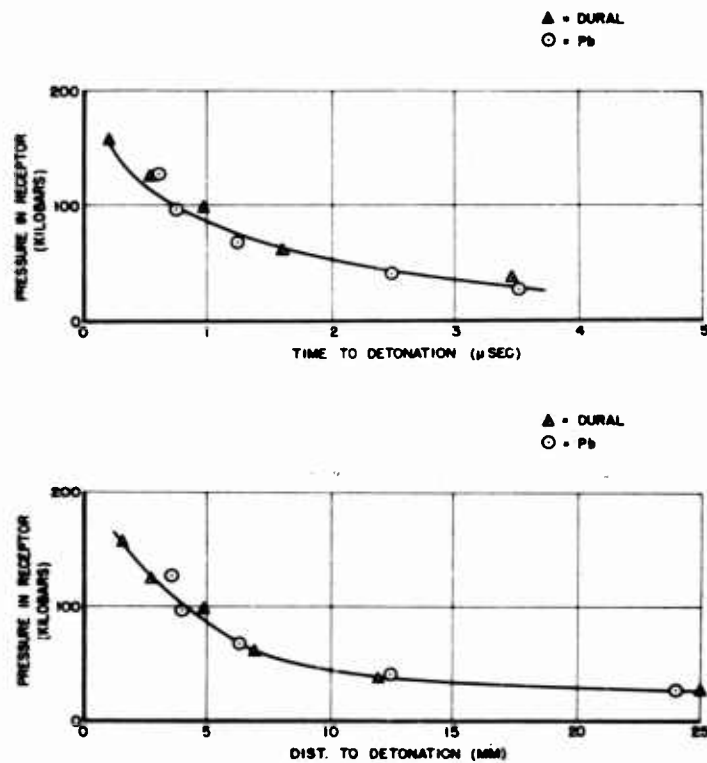


Fig. 4 - Pressure in receptor vs time to detonation, pressure in receptor vs distance to detonation

3. A measurable supersonic surface shock of mechanical discontinuity proceeds at constant velocity for the entire length of the stick and high order detonation is not observed.

4. A measurable supersonic surface shock of mechanical discontinuity is observed to gradually decay and be no longer observable as it approaches sonic velocity. High-order detonation does not occur.

The first of these conditions was not covered in this study, and the results which follow are only related to 2, 3 and 4 above.

The observation of a supersonic shock along the surface of the charge, proceeding at constant velocity, requires that energy be fed into that shock. This indicates that a chemical reaction has been initiated in the receptor. The lack of observation of this reaction at the surface does not preclude its existence. With receptors cut to lengths equal to, shorter than and longer than that distance at which high order detonation would be expected to occur for a given barrier condition, the results shown in Figure 6, which is a composite of a series of streak-camera records, were obtained for the core reaction. The profile of this reacting core can be observed to be changing shape in these records. Figure 7 is a plot of the velocity of the reaction (measured in the direction of the axis of the charge) at the center of the charge and at various radial distances from the center, as indicated. The shape of the reacting core at any given time is directly related to the difference in velocity, which is highest at the axis of the charge and decreases with radial distance. The non-reactive surface shock is joined by a continuous extension of the shock profile of the reactive core, and has the lowest velocity observed during the pre-high-order detonation regime.

The velocity of the surface shock has been found to be constant in each record. However, the magnitude of this velocity is a function of the barrier conditions. The core velocity along the axis has been measured and also shown to be constant from the photographic record of charges of different lengths, and measured as constant in a given charge by the resistance wire method mentioned earlier<sup>(4)</sup>. The magnitude of the axial velocity is also dependent on the barrier conditions.

The surface observation obtained for dural and lead barriers is plotted vs the transmitted pressure in the receptor charge (Figure 4), and it is indicated in this diagram that delay time and distance are directly dependent on pressure alone, and independent of impulse. A similar graph, Figure 3, is shown for air barriers but, as described under "Discussion" the pressure shown is that of the incident air shock. Figure 5 shows the similarity of data for pellet impact to those for metal barriers.

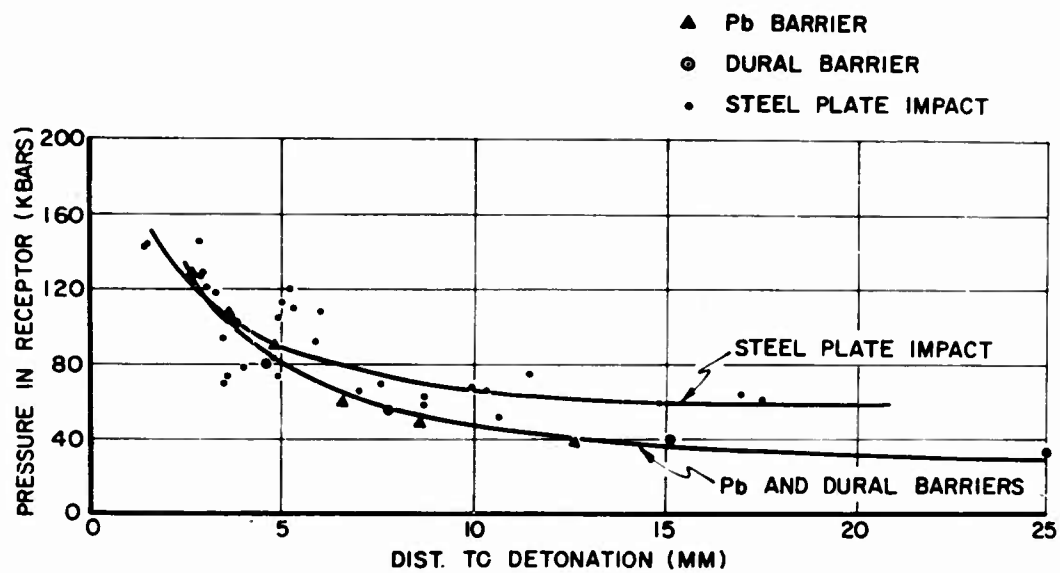


Fig. 5 - Impact initiation. Pressure in the receptor vs the distance to detonation



$x = 3.30 \text{ mm}$



$x = 9.58 \text{ mm}$



$x = 4.50 \text{ mm}$



$x = 11.07 \text{ mm}$



$x = 6.35 \text{ mm}$



$x = 12.70 \text{ mm}$



$x = 7.95 \text{ mm}$



$x = 14.30 \text{ mm}$

Fig. 6 - Series of streak camera records showing the core reaction emerging from the ends of short receptors ( $x$  = length of receptor)

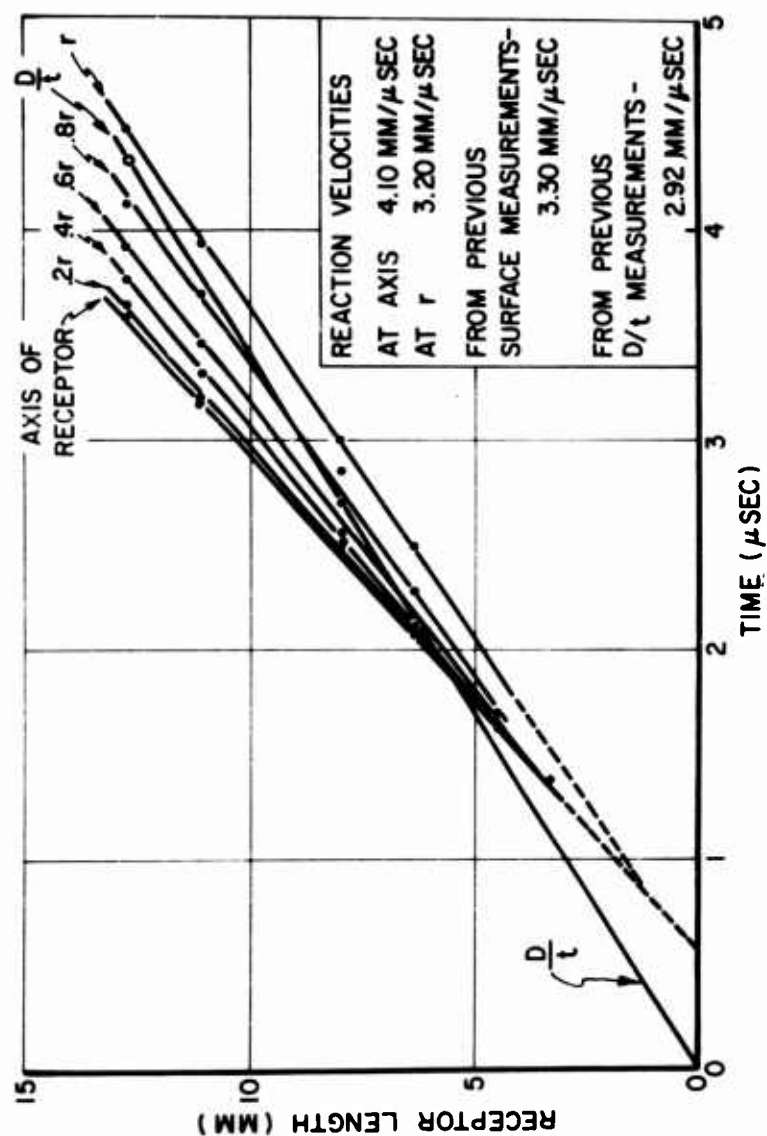


Fig. 7 - Sympathetic initiation - 1.5 in. air gap. Shock transit time in receptor vs receptor length plotted for different radii at rear surface of receptor.

In over three hundred tests conducted, the velocity of the high-order detonation that is induced in the receptor has been invariably about 1 1/2% higher than the velocity of detonation in the donor sticks. In two of these receptor sticks the detonation velocity has dropped abruptly to its normal value. A valid physical explanation for this observation cannot be made on the basis of information obtained in these firings.

### Conclusions

It follows from the results obtained with the air gaps, metal barriers and pellet impact studies of sympathetic initiation that a single physical model can be established for all of these conditions.

Although the nature of the initiation of the reaction is not known, there is no evidence to contradict the hot spot theory of Yoffe And Bowden<sup>(7)</sup>. Allowing that the reaction does start by adiabatic compression of trapped gases, mechanical heating, or a combination of both, the volume of this reaction and, as a consequence, its pressure and propagation velocity, are functions of the pressure of the initial shock transmitted to the receptor. As this reaction propagates internally, as seen in the results presented here, the rarefaction wave from the boundary is sufficiently strong to prevent surface detonation. However, the pressure of this internal shock is sufficiently great to manifest mechanical surface changes in the solid explosives, observable by front lighting techniques. If the rarefaction loss rate is less than the energy release rate, the internal pressure builds up to a point at which a discontinuous jump to a high order detonation occurs in a manner similar to that proposed by Von Neumann<sup>(8)</sup>. However, in this case the reaction moves from an  $n=k$  Hugoniot, in which  $1 > k > 0$ , to the  $n=1$  Hugoniot when the pressure reaches a value equal to that at the intersection of the  $n=k$  Hugoniot and the Chapman-Jouguet plane. If the rate of energy release is such that the pressure does not build up at a rate higher than the rate of dissipation in the rarefaction, then the reaction either continues at a constant rate or at a decreasing rate until it is no longer detectable.

It is also concluded that the contribution to this reaction by the shock from a donor charge passing through a barrier to the receptor charge is a function of the initial pressure in the receptor. Although the significance of the total energy in the pressure pulse is not evident in these experiments it is being investigated further to determine its role in the total reaction.



Bibliography

1. Sultanoff, M. and Bailey, R. A. "Induction Time to Sympathetic High Order Detonation in an Explosive Receptor Induced by Explosive Air Shock", Ballistic Research Laboratories Report No. 865, May 1953.
2. Sultanoff, M. "Explosive Wave Shaping by Delayed Detonation", Proceedings of First Symposium on Detonation Wave Shaping (sponsored by Picatinny Arsenal at the Jet Propulsion Laboratory, Pasadena, Calif.), 5-7 June 1956.
3. Eichelberger, R. J. and Sultanoff, M. "Sympathetic Detonation and Initiation by Impact", Proc. Roy. Soc. A, Vol. 246, pages 274-281.
4. Gibson, F. C., Bowser, M. L. and Mason, C. M. "Method for the Study of Deflagration to Detonation Transition", Review of Scientific Instruments, Vol. 30, No. 10, pages 916-919, October 1959.
5. Sultanoff, M. "Instrumentation for the Study of Explosive Reactions", Proceedings of the Third International Congress on High Speed Photography, Paris, France, October 1956.
6. Walsh, John M., Rice, Melvin H., McQueen, Robert G. and Yarger, Frederick L., "Shock Wave Compressions of Twenty-seven Metals. Equations of State of Metals", Physical Review, Vol. 108, No. 2 October 1957. Pressure in receptor gotten from Los Alamos curves for C-J pressure vs. particle velocity in Comp B.
7. Bowden, F. P. and Yoffe, A. D., "Initiation and Growth of Explosion in Liquids and Solids", University of Cambridge Press, London, 1952.
8. Von Neumann, John, "Theory of Detonation Waves" National Research Committee, OSRD Report, Institute for Advanced Study, Princeton, N. J. April 1, 1942.

## GROWTH OF DETONATION FROM AN INITIATING SHOCK

Julius W. Enig  
U. S. Naval Ordnance Laboratory  
Silver Spring, Maryland

**ABSTRACT:** Numerical computations have been carried out which depict the formation and structure of unsteady detonation waves in solid explosives. Two different methods were employed in the calculations. One takes into account the dissipative mechanisms of heat conduction and viscosity and the other is an application of Lax's method to a chemically reacting fluid. A simple chemical reaction is introduced which converts solid explosive to gaseous products through intermediate states, each of which has an appropriate equation of state.

A piston pushes with constant velocity against one surface of a chemically inert slab whose other surface is in intimate contact with a semi-infinite solid explosive and the growth of the resultant shock is followed. For sufficiently strong shocks, the chemical decomposition is initiated and the shock grows into a detonation wave. Other sample problems involving shock, detonation, or rarefaction waves are given.

### I. INTRODUCTION

In this paper we depict the formation and structure of unsteady one-dimensional detonation waves in solid explosives. In particular our attention is directed to the growth and structure of the reaction zone, the coupling of the latter with the shock region, and the critical time necessary for growth from initiation to detonation. Hirschfelder and Curtiss [1] have given the first discussion of steady-state detonations based on a complete set of hydrodynamic relations, including coefficients of diffusion, thermal conductivity, and viscosity, as well as chemical kinetics. They computed the composition, temper-

ature, and pressure as functions of distance in a steady state, plane gaseous detonation in which the irreversible unimolecular reaction  $[A] \rightarrow [B]$  takes place with the release of energy. Hubbard and Johnson [2] have utilized the von Neumann and Richtmyer "q" method [3], which was originally introduced in unsteady shock problems, for calculating unsteady detonation waves in solid explosives. This method involves the introduction of a psuedo-viscosity term into the hydrodynamic equations and has the effect of giving the correct entropy change across the shock front and arbitrarily limiting the width of the shock front to several mesh size thicknesses. In the cases that they treated it was found that the hydrodynamic motion and the release of chemical energy are practically independent as a consequence of the extreme temperature sensitivity of the reaction rate. The calculations showed that for a given pressure pulse applied to the boundary of an explosive, there exists a well defined delay time before a detonation is formed. Should the pressure pulse be of such finite duration that a rarefaction wave reaches the explosive particle before it has been maintained at high temperature for the appropriate delay time, then there will be no detonation. In their application to detonation problems all of the previously mentioned authors [1], [2] used the same equation of state for both the reactants and the detonation products. Ludford, Polachek, and Seeger [4] have obtained numerical solutions for unsteady flow containing shocks, in a perfect gas, in the absence of any chemical reaction or heat conduction.

In this paper we consider unsteady one-dimensional detonation waves in solid explosives where for the first time the dissipative mechanisms of heat conduction and viscosity are taken into account. While there is considerable doubt that the notions of viscosity and heat conduction can be used to describe the internal mechanism of the shock process because of the extremely small shock width ( $\approx 10^{-5}$  cm), they certainly do provide a process for changing the entropy across the shock. If, for example, a piston is driven with constant velocity into a fluid, a shock is set up which rapidly takes on steady state characteristics. The viscosity and thermal conductivity will determine the exact shape of the shock front, but the characteristics of the shock a sufficient distance behind the front are independent of the transport properties and do indeed satisfy the Rankine-Hugoniot relations. It has been known for a long time that in steady state solutions, the smaller the viscosity and thermal conductivity, the steeper the shock front. Indeed it is just these solutions which cast doubt on the applicability of these dissipative mechanisms to adequately describe the shock zone for at

least strong shocks. If however deflagration waves are considered then the transport properties must play an important role in determining the flow [5]. While we will in the future discuss deflagration and transition from initiation to deflagration to detonation we restrict ourselves now to detonation. In any case the use of transport phenomena should be at least as applicable as the "g" method to detonation problems.

Suppose a piston is driven with constant velocity against one surface of a slab of chemically inert material whose other surface is in intimate contact with a semi-infinite solid explosive. A shock will form and rapidly approach steady state values as it moves into the inert. This situation is depicted in Fig. 1.

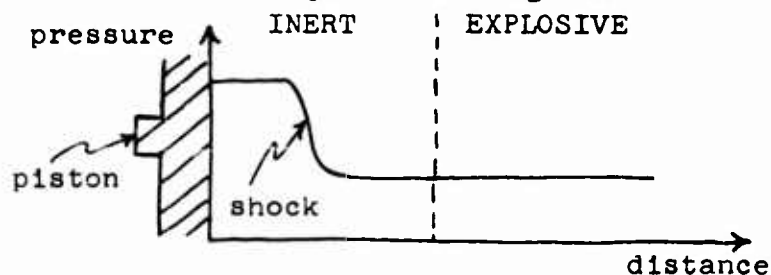


Fig. 1

What will happen when the shock reaches the inert-explosive interface? For simplicity assume that the equation of state and the physical properties of both materials are identical (only the chemical properties are different). As the shock passes over the inert and into the explosive it heats both to a temperature which can be easily calculated from the Rankine-Hugoniot relations and the caloric and thermal equations of state. Now the chemical decomposition of the explosive is governed by an Arrhenius term which is extremely sensitive to temperature; and if the latter is sufficiently low such that there exist only negligible reaction rates, then the steady shock merely propagates into the explosive. If on the other hand somewhere in the shock front the temperature is sufficiently high so that there do exist appreciable reaction rates, then the explosive material at the interface, which has been heated the longest, will eventually undergo a very rapid exothermic reaction. The pressure in that region will rapidly increase and drive a shock back into the inert and a high pressure zone of chemical reaction will move into the explosive. This is the process of initiation to detonation which will be discussed quantitatively in Section V.

To what extent do the transport properties, viscosity and thermal conductivity, affect the structure of the detonation wave? Von Neumann [6], Döring [7], and Zeldovitch [8], independently concluded that a detonation is a shock wave followed by a zone of chemical reaction provided transport properties are neglected. They assumed that the time for reaction to take place is long compared to the time for passage of the shock. If this assumption is true it should not make very much difference exactly how the shock is calculated, i.e. whether transport phenomena are included or the "q" method is used. In the examples that were considered Hirschfelder and Curtiss [1] found that there exists a strong coupling between the reaction zone and the shock zone when transport properties are included and therefore the solutions never come close to the von Neumann "spike". If the coupling is strong in the steady state detonation, must it have been strong during the initial stages of growth?

We now briefly describe another method that can be used for unsteady detonation calculations. This consists of applying the Lax [9] scheme to problems involving unsteady one-dimensional flow with chemical reaction. P. Lax has described a finite difference scheme for calculation of time dependent one-dimensional compressible fluid flows containing strong shocks. The novel feature of this method is the use of the conservation form of the hydrodynamic equations and, to a lesser extent, the particular way of differencing the equations. Putting the Lagrangean hydrodynamic equations in conservation form for the plane case is equivalent to writing each equation in the form

$$\frac{\partial A}{\partial t} + \frac{\partial F}{\partial x} = 0,$$

where A and F are dependent variables. The finite difference representation is taken as

$$A(x, t + \Delta t) - \frac{1}{2} [A(x + \Delta x, t) + A(x - \Delta x, t)] = \frac{\Delta t}{2\Delta x} [F(x + \Delta x, t) - F(x - \Delta x, t)].$$

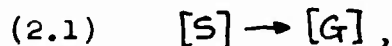
With this scheme there are no explicit dissipative mechanisms such as heat conduction or viscosity, or a "q" term, yet the entropy change across the shock is correctly given. We have introduced chemical reaction and find that the scheme also enables us to solve unsteady detonation problems. One advantage this method has over the Richtmyer and von Neumann and the viscosity, heat conduction methods is that the computational time is appreciably less than either. This will be explained in further detail in Section IV. Just as the "q" method, the Lax

scheme arbitrarily limits the width of the shock front to several mesh thicknesses.

## II. HYDRODYNAMIC EQUATIONS

### A. Viscosity and Heat-Conduction Scheme

If we consider the irreversible first order chemical reaction



then the equations of one-dimensional unsteady flow of a viscous heat-conducting compressible fluid consisting of species [S] and [G] may be written in the Eulerian form

$$(2.2) \quad \frac{1}{V} \frac{DV}{Dt} = \frac{\partial u}{\partial X}$$

$$(2.3) \quad \frac{1}{V} \frac{Du}{Dt} = -\frac{\partial}{\partial X} \left( p - \frac{4}{3} \mu \frac{\partial u}{\partial X} \right)$$

$$(2.4) \quad \frac{1}{V} \left( \frac{De}{Dt} + p \frac{DV}{Dt} \right) = \frac{\partial}{\partial X} \left( \lambda \frac{\partial T}{\partial X} \right) + \frac{4}{3} \mu \left( \frac{\partial u}{\partial X} \right)^2$$

$$(2.5) \quad e = e(T, \omega)$$

$$(2.6) \quad p = p(V, T, \omega)$$

$$(2.7) \quad \frac{1}{\omega} \frac{D\omega}{Dt} = -Z e^{-\frac{E^\ddagger}{RT}}$$

$$\frac{D}{Dt} = \frac{\partial}{\partial t} + u \frac{\partial}{\partial X}$$

where  $t, X, V, u, p, e, T, \omega, \mu, \lambda, E^\ddagger, Z$  and  $R$  are respectively the time, Eulerian position, specific volume, particle velocity, pressure, specific energy, temperature, mass fraction of species [S], coefficient of viscosity, thermal conductivity, activation energy, frequency factor, and specific gas constant. Equations (2.2), (2.3), (2.4), (2.5), (2.6) and (2.7) are respectively the equations for the conservation of mass, momentum, and energy, and the caloric and thermal equations of state, and the chemical kinetic equation which governs the conversion of unreacted solid explosive [S] to product gas [G]. It will be assumed that  $\mu, \lambda, E^\ddagger$ , and  $Z$  are constants.

For one-dimensional problems it is more convenient to use the Lagrangean form of the hydrodynamic equations since they reveal where each particle of fluid came from initially and hence supplies more information than the Eulerian form. In addition shocks and moving contact discontinuities can be more easily followed, and mass is automatically conserved.

To transform to Lagrangean coordinates we let  $x$  denote the  $X$ -coordinate of a small fluid element at time  $t = 0$  and  $X = X(x, t)$  denote that same fluid element at  $t > 0$ , so that  $x$  and  $t$  are regarded as independent variables. In this new coordinate system Eqs. (2.2)-(2.7) are respectively

$$(2.8) \quad \frac{\partial V}{\partial t} = V_0 \frac{\partial u}{\partial x}$$

$$(2.9) \quad \frac{\partial u}{\partial t} = V_0 \frac{\partial}{\partial x} \left( \frac{4}{3} \mu \frac{V_0}{V} \frac{\partial u}{\partial x} - p \right)$$

$$(2.10) \quad \frac{\partial e}{\partial t} = V_0 \left[ \frac{\partial}{\partial x} \left( \lambda \frac{V_0}{V} \frac{\partial T}{\partial x} \right) + \left( \frac{4}{3} \mu \frac{V_0}{V} \frac{\partial u}{\partial x} - p \right) \frac{\partial u}{\partial x} \right]$$

$$(2.11) \quad e = e(T, \omega)$$

$$(2.12) \quad p = p(V, T, \omega)$$

$$(2.13) \quad \frac{\partial \omega}{\partial t} = -Z \omega e^{-\frac{E^\dagger}{RT}}$$

where  $x$  is the Lagrangean space coordinate and the subscript 0 will always refer to initial values which in this paper will be assumed to be constant. The value of the Eulerian position  $X(x, t)$  is found from the relation

$$(2.14) \quad \frac{\partial X}{\partial t} = u$$

The equations may be made non-dimensional by the transformations

$$(2.15) \quad u = U(p_0 V_0)^{\frac{1}{2}}, \quad V = C V_0, \quad p = P p_0, \quad e = E p_0 V_0, \quad T = \theta T_0, \\ X = S L, \quad x = \xi L, \quad t = \frac{\tau L}{(p_0 V_0)^{\frac{1}{2}}}, \quad a = \frac{4\mu}{3L} \left( \frac{V_0}{p_0} \right)^{\frac{1}{2}}, \quad b = \frac{\lambda T_0}{p_0 L (p_0 V_0)^{\frac{1}{2}}}, \\ \nu = \frac{L Z}{(p_0 V_0)^{\frac{1}{2}}}, \quad \omega = \frac{E^\dagger}{RT_0},$$

where  $L$  is a characteristic length. In non-dimensional form the new equations are

$$(2.16) \quad \frac{\partial C}{\partial \tau} = \frac{\partial U}{\partial \xi}$$

$$(2.17) \quad \frac{\partial U}{\partial \tau} = \frac{\partial G}{\partial \xi} - \frac{\partial P}{\partial \xi}$$

$$(2.18) \quad \frac{\partial E}{\partial \tau} = \frac{\partial F}{\partial \xi} + (G-P) \frac{\partial U}{\partial \xi}$$

$$(2.19) \quad G = \frac{a}{C} \frac{\partial C}{\partial \tau}$$

$$(2.20) \quad F = \frac{b}{C} \frac{\partial \theta}{\partial \xi}$$

$$(2.21) \quad E = E(\theta, \omega)$$

$$(2.22) \quad P = P(C, \theta, \omega)$$

$$(2.23) \quad \frac{\partial \omega}{\partial \tau} = -\nu \omega e^{-\frac{\omega}{\theta}}$$

$$(2.24) \quad \frac{\partial S}{\partial \tau} = U.$$

#### B. Lax Scheme

If we utilize the Lax scheme then the non-dimensional Lagrangean equations for one-dimensional unsteady flow of a chemically reacting fluid are

$$(2.25) \quad \frac{\partial C}{\partial \tau} = \frac{\partial U}{\partial \xi}$$

$$(2.26) \quad \frac{\partial U}{\partial \tau} = -\frac{\partial P}{\partial \xi}$$

$$(2.27) \quad \frac{\partial}{\partial \tau} \left( E + \frac{U^2}{2} \right) = -\frac{\partial}{\partial \xi} (PU)$$

$$(2.28) \quad E = E(\theta, \omega)$$

$$(2.29) \quad P = P(C, \theta, \omega)$$



$$(2.30) \quad \frac{\partial \omega}{\partial \tau} = -\nu \omega e^{-\frac{\omega}{\theta}}$$

$$(2.31) \quad \frac{\partial S}{\partial \tau} = U$$

where Eq. (2.27) can be obtained from Eqs. (2.17) and (2.18) after setting  $F \equiv 0$  and  $G \equiv 0$ .

### C. Initial and Boundary Conditions

The initial conditions valid for  $0 \leq \xi \leq 1$  are

$$(2.32) \quad \begin{aligned} C(\xi, 0) = 1, P(\xi, 0) = 1, \theta(\xi, 0) = 1, \omega(\xi, 0) = 1, \\ U(\xi, 0) = 0, G(\xi, 0) = 0, F(\xi, 0) = 0, S(\xi, 0) = \xi, E(\xi, 0) = E_0 \end{aligned}$$

where  $E_0$  is a constant which depends on the caloric equation of state, and the initial particle velocity is assumed to be zero.

The boundary conditions valid for  $\tau > 0$  are

$$(2.33) \quad U(0, \tau) = U^{(0)}, \quad U(1, \tau) = U^{(1)}$$

$$(2.34) \quad F(0, \tau) = 0, \quad F(1, \tau) = 0$$

$$(2.35) \quad \begin{cases} \frac{\partial P}{\partial \xi} = 0, \frac{\partial \theta}{\partial \xi} = 0, \frac{\partial C}{\partial \xi} = 0, \frac{\partial G}{\partial \xi} = 0 \\ \frac{\partial \omega}{\partial \tau} = -\nu \omega e^{-\frac{\omega}{\theta}} \\ E = E(\theta, \omega) \\ \frac{\partial S}{\partial \tau} = U \end{cases} \quad \text{for } \xi = 0, 1$$

where  $U^{(0)}$  and  $U^{(1)}$  are taken to be constants. The boundary conditions, Eqs. (2.33) and (2.34), are prescribed while Eq. (2.35) are implied by Eqs. (2.33) and (2.34) and the differential equations (2.16)-(2.24). The boundary condition  $U(1, \tau) = U^{(1)}$  corresponds to a piston, initially at a distance  $L$  from the left hand piston, moving with constant velocity  $U^{(1)}$ .

## III. EQUATIONS OF STATE

When a detonation wave propagates in a solid explosive it converts the solid unreacted material [S] to gaseous detonation products [G]. It is therefore very necessary to describe these two states, and in fact all the intermediate states (which exist since the detonation is assumed not to take place instantaneously), by appropriate equations of state. This can be done in the following very simple manner if we assume that the specific energy and volume at any point vary linearly with the mass fractions of solid explosive and gaseous product, i.e.,

$$(3.1) \quad V = \omega \tilde{V}_s + (1-\omega) \tilde{V}_g$$

$$(3.2) \quad e = \omega \tilde{e}_s + (1-\omega) \tilde{e}_g$$

where  $\tilde{V}_s$ ,  $\tilde{e}_s$ ,  $\tilde{V}_g$ , and  $\tilde{e}_g$  are the specific volume and energy for the pure solid and gas respectively. We now choose for the caloric and thermal equations of state of the unreacted explosive [S] and gaseous detonation products [G] the following:

$$(3.3) \quad \tilde{e}_s = c_s T + \tilde{e}_s^*$$

$$(3.4) \quad \tilde{e}_s = \tilde{e}_{s_0} + \frac{1}{\gamma_s - 1} \left[ (p+B) \tilde{V}_s - (p_0+B) \tilde{V}_{s_0} \right]$$

$$(3.5) \quad \tilde{e}_g = c_g T + \tilde{e}_g^*$$

$$(3.6) \quad \tilde{e}_g = \frac{p \tilde{V}_g}{\gamma_g - 1} + \tilde{e}_g^*$$

where  $c_s$  and  $c_g$  are the specific heat capacities of the solid and gas respectively,  $\tilde{e}_s^*$  and  $\tilde{e}_g^*$  are the heats of formation, and  $\gamma_s$ ,  $\gamma_g$ , and  $B$  are constants. The subscript 0 as usual refers to initial values. Eliminating  $\tilde{e}_s$ ,  $\tilde{e}_g$ ,  $\tilde{V}_s$ , and  $\tilde{V}_g$  between the six equations Eqs. (3.1)-(3.6), and defining

$$(3.7) \quad E^* = \frac{\tilde{e}_s^* - \tilde{e}_g^*}{p_0 V_0}, \quad \beta = \frac{B}{p_0}, \quad K = (\gamma_s - 1) \frac{c_s T_0}{p_0 V_0}, \quad L = (\gamma_g - 1) \frac{c_g T_0}{p_0 V_0}$$

$$m = \frac{c_s - c_g}{p_0 V_0} T_0, \quad n = \frac{c_g T_0}{p_0 V_0},$$

leads to the non-dimensional caloric and thermal equations of state

$$(3.8) \quad E = (m\theta + E^*)\omega + n\theta$$

$$(3.9) \quad C = \omega \frac{K(\theta-1)+1+\beta}{P+\beta} + (1-\omega) \frac{L\theta}{P},$$

where  $V_0 \equiv \tilde{V}_{s_0}$  (since initially only explosive exists) and  $\tilde{e}_s^* - \tilde{e}_a^*$  is the specific heat of reaction. It is of importance to recognize that Eqs. (3.8) and (3.9) give different relationships between energy and temperature, and pressure, volume, and temperature for different mixtures of the two chemical species [S] and [G] (i.e. for different values of  $\omega$ ).

The temperature  $\theta$  can be eliminated between Eqs. (3.8) and (3.9) giving

$$(3.10) \quad \frac{E - \omega E^*}{m\omega + n} = \frac{P(P+\beta)C - \omega(1+\beta-K)P}{(P+\beta)(1-\omega)L + \omega KP}$$

The local sound speed  $c$  can be defined by the thermodynamic identity

$$(3.11) \quad \frac{c^2}{V^2} = P \frac{\partial P}{\partial e} - \frac{\partial P}{\partial V} = \frac{V_0}{P_0} \left( P \frac{\partial P}{\partial E} - \frac{\partial P}{\partial G} \right).$$

We then find

$$(3.12) \quad P \frac{\partial P}{\partial E} - \frac{\partial P}{\partial G} = \begin{cases} \frac{PK}{C(m+n)} + \frac{1}{C} \left( 1 + \frac{\beta}{P} \right) & \text{if } \omega = 1 \\ \frac{P}{C} \left( \frac{L}{n} + 1 \right) & \text{if } \omega = 0 \end{cases}$$

$$(3.13) \quad \frac{d\theta}{dE} = \begin{cases} \frac{1}{m+n} & \text{if } \omega = 1 \\ \frac{1}{n} & \text{if } \omega = 0, \end{cases}$$

which are quantities that will be needed in Section IV when we discuss the stability of the finite difference equations.

#### IV. FINITE DIFFERENCE EQUATIONS

##### A. Viscosity and Heat Conduction Scheme

In order to carry out the numerical solution of Eqs. (2.16)-(2.24), they must be replaced by an equivalent system of finite difference equations. The exact form of these equations is of course governed by stability considerations and a stability analysis as proposed by von Neumann must be carried out in order to verify that small errors will not grow during the computations. The following set of difference equations was used for the numerical calculations:

$$(4.1) \quad C_j^{n+1} - C_j^n = \frac{\Delta \tau}{2 \Delta \xi} (U_{j+1}^{n+1} - U_{j-1}^{n+1}) =$$

$$(4.2) \quad U_j^{n+1} - U_j^n = \frac{\Delta \tau}{2 \Delta \xi} [G_{j+1}^n - G_{j-1}^n - (P_{j+1}^n - P_{j-1}^n)]$$

$$(4.3) \quad E_j^{n+1} - E_j^n = \frac{\Delta \tau}{2 \Delta \xi} [F_{j+1}^n - F_{j-1}^n + (G_j^{n+1} - P_j^n)(U_{j+1}^{n+1} - U_{j-1}^{n+1})]$$

$$(4.4) \quad G_j^{n+1} = \frac{a}{2 \Delta \xi} \frac{1}{C_j^{n+1}} (U_{j+1}^{n+1} - U_{j-1}^{n+1})$$

$$(4.5) \quad F_j^{n+1} = \frac{b}{2 \Delta \xi} \frac{1}{C_j^{n+1}} (\theta_{j+1}^{n+1} - \theta_{j-1}^{n+1})$$

$$(4.6) \quad \theta_j^{n+1} = \theta(E_j^{n+1}, \omega_j^{n+1})$$

$$(4.7) \quad P_j^{n+1} = P(C_j^{n+1}, \theta_j^{n+1}, \omega_j^{n+1})$$

$$(4.8) \quad \omega_j^{n+1} - \omega_j^n = - \frac{\nu \Delta \tau}{2} (\omega_{j+1}^{n+1} + \omega_{j-1}^n) e^{-\frac{\omega}{\theta_j^n}}$$

$$(4.9) \quad S_j^{n+1} - S_j^n = \frac{\Delta \tau}{2} (U_j^{n+1} + U_j^n)$$

where we use the notation,

$$\xi = j \Delta \xi, \quad j = 0, 1, 2, \dots, J$$

$$\tau = n \Delta \tau, \quad n = 0, 1, 2, \dots,$$

$$U_{j-1}^{n+1} \equiv U(\xi - \Delta \xi, \tau + \Delta \tau), \text{ etc.}$$

For our particular problem,  $\theta_j^{n+1}$ , and  $P_j^{n+1}$ , in Eqs. (2.21) and (2.22) are evaluated from Eqs. (3.8) and (3.9). The system, Eqs. (4.1)-(4.9), is as a whole correct to

$O(\Delta\tau) + O(\Delta\xi^2)$ , and the system is explicit provided the quantities are solved for in the proper order. If all the variables are known at  $\tau = n\Delta\tau$  and there are boundary conditions at  $j=0$  and  $j=J$ , then the values at the new time  $\tau = (n+1)\Delta\tau$  can be computed in the following order:

$$U_j^{n+1}, S_j^{n+1}, C_j^{n+1}, G_j^{n+1}, E_j^{n+1}, w_j^{n+1}, \theta_j^{n+1}, F_j^{n+1}, P_j^{n+1}, j=2, 3, \dots, J-1.$$

An analysis of the stability of Eqs. (4.1)-(4.9) has been carried out and the results indicate that in the normal region, i.e. the region where the viscosity, heat conduction, and chemical reaction are negligible, the solution is stable provided the following criterion is satisfied:

$$(4.10) \quad \left[ P_j^n \left( \frac{\partial P}{\partial E} \right)_j^n - \left( \frac{\partial P}{\partial C} \right)_j^n \right]^{\frac{1}{2}} \frac{\Delta\tau}{\Delta\xi} \leq 2.$$

Here  $\Delta\tau$  is the time step from  $\tau^n$  to  $\tau^{n+1}$ . The term in brackets has already been evaluated in Eq. (3.12). In the shock region, i.e. the region where the viscosity and/or heat conduction dominate and the chemical reaction is negligible, the stability criterion is

$$(4.11) \quad \frac{\Delta\tau}{C_j^{n+1}(\Delta\xi)^2} \left[ \frac{a}{2} \left( 1 + \frac{C_j^n}{C_j^{n+1}} \right) + b \left( \frac{d\theta}{dE} \right)_j^{n+1} \right] \leq 2.$$

In the detonation region, i.e. the region where the chemical reaction is so rapid such that a relative change in mass fraction of, say, 0.1 occurs in a time step which is negligible compared to the hydrodynamic time step as determined by Eqs. (4.10) or (4.11), the stability criterion is determined by the condition

$$(4.12) \quad w_j^n - w_j^{n+1} \leq \epsilon_n w_j^n, \quad 0 < \epsilon_n < 1,$$

where  $\epsilon_n$  is a small number which may depend on the time step if desired. This leads to the condition

$$(4.13) \quad \Delta\tau \leq \frac{2\epsilon_n}{(2-\epsilon_n)\nu} e^{\frac{w}{\theta_j^n}}.$$

A condition which appears to be sufficient to insure stability is

$$(4.14) \quad \Delta \tau \leq \min_{0 \leq j \leq J} \left\{ 2 \Delta \xi \left( P_j^n \left( \frac{\partial P}{\partial E} \right)_j^n - \left( \frac{\partial P}{\partial C} \right)_j^n \right) + \frac{1}{C_j^{n+1} (\Delta \xi)^2} \left[ \frac{a}{2} \left( 1 + \frac{C_j^n}{C_j^{n+1}} \right) + b \left( \frac{d\theta}{dE} \right)_j^{n+1} \right]^2 \right\}^{-\frac{1}{2}}, \\ \left. , \frac{2 \epsilon_n}{(2 - \epsilon_n) \nu} e^{-\frac{\omega}{\theta_j^n}} \right\}$$

where the criteria for the normal and shock regions have been combined.

#### B. Lax Scheme

The appropriate set of difference equations is

$$(4.15) \quad C_j^{n+1} - \frac{1}{2} (C_{j+1}^n + C_{j-1}^n) = \frac{\Delta \tau}{2 \Delta \xi} (U_{j+1}^n - U_{j-1}^n)$$

$$(4.16) \quad U_j^{n+1} - \frac{1}{2} (U_{j+1}^n + U_{j-1}^n) = -\frac{\Delta \tau}{2 \Delta \xi} (P_{j+1}^n - P_{j-1}^n)$$

$$(4.17) \quad E_j^{n+1} - \frac{1}{2} (E_{j+1}^n + E_{j-1}^n) + \frac{1}{2} [U_j^{n+1,2} - \frac{1}{2} (U_{j+1}^{n,2} + U_{j-1}^{n,2})] = -\frac{\Delta \tau}{2 \Delta \xi} (P_{j+1}^n U_{j+1}^n - P_{j-1}^n U_{j-1}^n)$$

$$(4.18) \quad \theta_j^{n+1} = \theta(E_j^{n+1}, \omega_j^{n+1})$$

$$(4.19) \quad P_j^{n+1} = P(C_j^{n+1}, \theta_j^{n+1}, \omega_j^{n+1})$$

$$(4.20) \quad \omega_j^{n+1} - \frac{1}{2} (\omega_{j+1}^n + \omega_{j-1}^n) = -\nu \Delta \tau \omega_j^n e^{-\frac{\omega}{\theta_j^n}}$$

$$(4.21) \quad S_j^{n+1} - \frac{1}{2} (S_{j+1}^n + S_{j-1}^n) = \Delta \tau U_j^n.$$

The stability criterion valid everywhere is

$$(4.22) \quad \left[ P_j^n \left( \frac{\partial P}{\partial E} \right)_j^n - \left( \frac{\partial P}{\partial C} \right)_j^n \right]^{\frac{1}{2}} \frac{\Delta \tau}{\Delta \xi} \leq 1.$$

If  $\Delta \tau$  as chosen by Eq. (4.22) makes  $\omega_j^{n+1} < 0$ , set  $\omega_j^{n+1} = 0$ .

Comparing Eqs. (4.14) and (4.22), it is seen that the Lax scheme allows for the use of much larger time steps, since Eq. (4.11) is a much more restrictive criterion than Eq. (4.10) when shocks are present.

C. Initial and Boundary Conditions

The initial conditions valid for  $j = 0, 1, 2, \dots, J$  are

$$(4.23) \quad C_j^0 = P_j^0 = \theta_j^0 = \omega_j^0 = 1, \quad U_j^0 = G_j^0 = F_j^0 = 0, \quad S_j^0 = j \Delta t, \quad E_j^0 = m + n + E^*$$

The boundary conditions valid for  $n > 0$  are

$$U_0^n = U^{(0)}, \quad U_J^n = U^{(1)}$$

$$F_0^n = F_J^n = 0$$

$$P_0^n = \frac{1}{11}(18P_1^n - 9P_2^n + 2P_3^n), \quad P_J^n = \frac{1}{11}(18P_{J-1}^n - 9P_{J-2}^n + 2P_{J-3}^n)$$

$$\theta_0^n = \frac{1}{11}(18\theta_1^n - 9\theta_2^n + 2\theta_3^n), \quad \theta_J^n = \frac{1}{11}(18\theta_{J-1}^n - 9\theta_{J-2}^n + 2\theta_{J-3}^n)$$

$$(4.24) \quad C_0^n = \frac{1}{11}(18C_1^n - 9C_2^n + 2C_3^n), \quad C_J^n = \frac{1}{11}(18C_{J-1}^n - 9C_{J-2}^n + 2C_{J-3}^n)$$

$$G_0^n = \frac{1}{11}(18G_1^n - 9G_2^n + 2G_3^n), \quad G_J^n = \frac{1}{11}(18G_{J-1}^n - 9G_{J-2}^n + 2G_{J-3}^n)$$

$$\omega_0^n = \omega_0^{n-1} - \frac{1}{2} \nu \Delta t (\omega_0^n + \omega_0^{n-1}) e^{-\frac{\omega}{\theta_0^n}}, \quad \omega_J^n = \omega_J^{n-1} - \frac{1}{2} \nu \Delta t (\omega_J^n + \omega_J^{n-1}) e^{-\frac{\omega}{\theta_J^n}}$$

$$E_0^n = (m\theta_0^n + E^*)\omega_0^n + n\theta_0^n, \quad E_J^n = (m\theta_J^n + E^*)\omega_J^n + n\theta_J^n$$

$$S_0^n = S_0^{n-1} + \frac{1}{2} \Delta t (U_0^n + U_0^{n-1}), \quad S_J^n = S_J^{n-1} + \frac{1}{2} \Delta t (U_J^n + U_J^{n-1}).$$

$P_0^n$  is obtained by expanding  $P_1^n$ ,  $P_2^n$ , and  $P_3^n$  in a Taylor series about the point  $P_0^n$  and keeping terms up to  $O(\Delta t^3)$ . We then solve for  $\left(\frac{\partial P}{\partial t}\right)_0^n$  in terms of  $P_0^n$ ,  $P_1^n$ ,  $P_2^n$ ,  $P_3^n$  and then set  $\left(\frac{\partial P}{\partial t}\right)_0^n = 0$  to give the desired result. In similar manner we obtain  $P_J^n$ ,  $\theta_0^n$ ,  $\theta_J^n$ ,  $C_0^n$ ,  $C_J^n$ ,  $G_0^n$ , and  $G_J^n$ .

## V. SAMPLE CALCULATIONS

In order to demonstrate the feasibility of carrying out the solution of one-dimensional flow problems involving detonation waves by the proposed techniques, sample calculations were performed. In all the calculations the following data were used:

$$J = 100 ; U_j^n = 0 , n = 0, 1, \dots$$

$$\begin{aligned} \text{Inert and unreacted explosive: } \rho &= 10^5, K = 2.4584 \times 10^4, \\ L &= 2.00688 \times 10^4, m = -3.01032 \times 10^3, \\ \eta &= 1.00344 \times 10^4 \end{aligned}$$

$$\text{Explosive: } \omega = 50 , E^* = 3.92997 \times 10^4$$

The initial conditions are given by Eqs. (4.23). The boundary condition  $U_j^n = 0$  corresponds to a rigid wall at a distance  $L$  from the initial position of the left hand piston.

## Case 1

Type of problem: Shock in a chemically inert material.

$$\text{Boundary conditions: } U_0^n = 198.241 , n > 0$$

$$\text{Constants: } \alpha = 10 , b = 0 , \nu = 0$$

A chemically inert material is contained by a moving piston and a rigid wall.

## Case 2

Type of problem: Shock initiation to detonation at inert-explosive interface.

$$\text{Boundary conditions: } U_0^n = 119.101 , n > 0$$

$$\text{Constants: } \alpha = 10 , b = 0 , \nu = \begin{cases} 0 & \text{if } 0 \leq j \leq 29 \\ 10^{14} & \text{if } 30 \leq j \leq 100 \end{cases}$$

The situation depicted here corresponds to a composite material of identical equation of state and physical properties, where the chemically inert material lies in the region  $0 \leq \xi < 0.3$ , and the explosive is contained in  $0.3 \leq \xi \leq 1$ . A piston moves with constant velocity into the inert, and a rigid wall contains the explosive.



## Case 3

Type of problem: Shock initiation to detonation near inert-explosive interface.

Boundary conditions:  $U_0^n = 119.101$ ,  $n > 0$

Constants:  $a=4$ ,  $b=5 \times 10^4$ ,  $\nu = \begin{cases} 0 & \text{if } 0 \leq j \leq 29 \\ 5 \times 10^{12} & \text{if } 30 \leq j \leq 100 \end{cases}$

## Case 4

Type of problem: Shock initiation to detonation near inert-explosive interface.

Boundary conditions:  $U_0^n = 119.101$ ,  $n > 0$

Constants:  $a=4$ ,  $b=5 \times 10^4$ ,  $\nu = \begin{cases} 0 & \text{if } 0 \leq j \leq 29 \\ 10^{14} & \text{if } 30 \leq j \leq 100 \end{cases}$

## Case 5

Type of problem: Shock initiation to detonation at inert-explosive interface.

Boundary conditions:  $U_0^n = \begin{cases} 119.101 & \text{if } \tau \leq 0.000896 \\ 0 & \text{if } \tau > 0.000896 \end{cases}$

Constants:  $a=10$ ,  $b=0$ ,  $\nu = \begin{cases} 0 & \text{if } 0 \leq j \leq 38 \\ 5 \times 10^{12} & \text{if } 39 \leq j \leq 100 \end{cases}$

A piston moves with constant velocity into the inert and after a finite time is suddenly stopped.

## Case 6 (Lax Scheme)

Type of problem: Shock initiation to detonation in an explosive.

Boundary conditions:  $U_0^n = 198.241$

A piston moves with constant velocity into a solid explosive which is confined by the piston and a rigid wall.

In computations involving the use of viscosity or heat conduction, the use of realistic values for the transport phenomena demand that the characteristic mesh size used in the numerical solution be of the order of the shock thickness in gases [4] or a few angstroms in solids. Since this is impossible for practical problems, then  $\mu$  and  $\lambda$  must be made larger by at least several

orders of magnitude if the mesh width is to take on reasonable size. It has been found experimentally (numerical experimentation, that is!) that for the equations of state used here, the values of  $a$  and  $b$  that lead to stable shocks are approximately of  $O(10)$  and  $O(10^5)$  respectively.

For the piston velocity given in Case 1 we compute the steady state values behind the shock, shown in Fig. 2, to be  $P \approx 1.35 \times 10^5$ ,  $C \approx 0.712$ ,  $\theta \approx 3.68$ . These compare with the values  $P_H = 1.36804 \times 10^5$ ,  $C_H = 0.712727$ ,  $\theta_H = 3.79754$  which are obtained from the solution of the Rankine-Hugoniot equations. Actually the values very close to the piston are not those quoted above but we find that  $C$  and  $\theta$  are about 10% and 19% too large respectively. This type of behavior is also common to the "g" method and can be readily understood when it is noted that a linear or quadratic viscosity term gives rise to an abnormally high energy production in the region of a velocity discontinuity. Notice that in Case 1,  $\lambda = 0$ .

In Case 2, where the thermal conductivity is equal to zero, the first explosive particle that is heated by the steady shock crossing the interface must go to complete reaction first. This is clearly shown in Fig. 3. The value of  $\nu$  is sufficiently large so that reaction starts and goes to completion in the shock region. The detonation progresses to the right while a shock travels back into the inert.

In Case 3 the value of  $\nu$  is chosen so that appreciable chemical reaction starts only after the entire shock zone has heated the explosive particle. While the interface is first to react, heat conduction to the inert soon controls the temperature rise and complete reaction first occurs at some interior explosive particle. The pressure here goes up to about  $1.3 \times 10^5$  at  $\tau = 0.00130296$  as shown in Fig. 4. A rarefaction wave lowers the pressure at that point as shocks move toward the right and left. The latter shocks compress and bring about complete reaction of the neighboring partially reacted explosive particles which go to higher pressures. Hence the pressure curves contain a valley, a situation which did not occur in Case 2 where  $\lambda = 0$ .

Having  $\lambda \neq 0$  in Case 3 has an effect on the steady state values of the inert particles near the piston in a pure shock. The Rankine-Hugoniot equations lead to the values  $P_H = 6.19202 \times 10^4$ ,  $1/C_H = 1.29716$ ,  $\theta_H = 2.00978$ , for the dimensionless piston velocity  $U_H = 119.101$ . Comparing

## Case 1

On each curve the dots when read from left to right are the mass particles labeled  $j = 0, 2, 4, \dots$

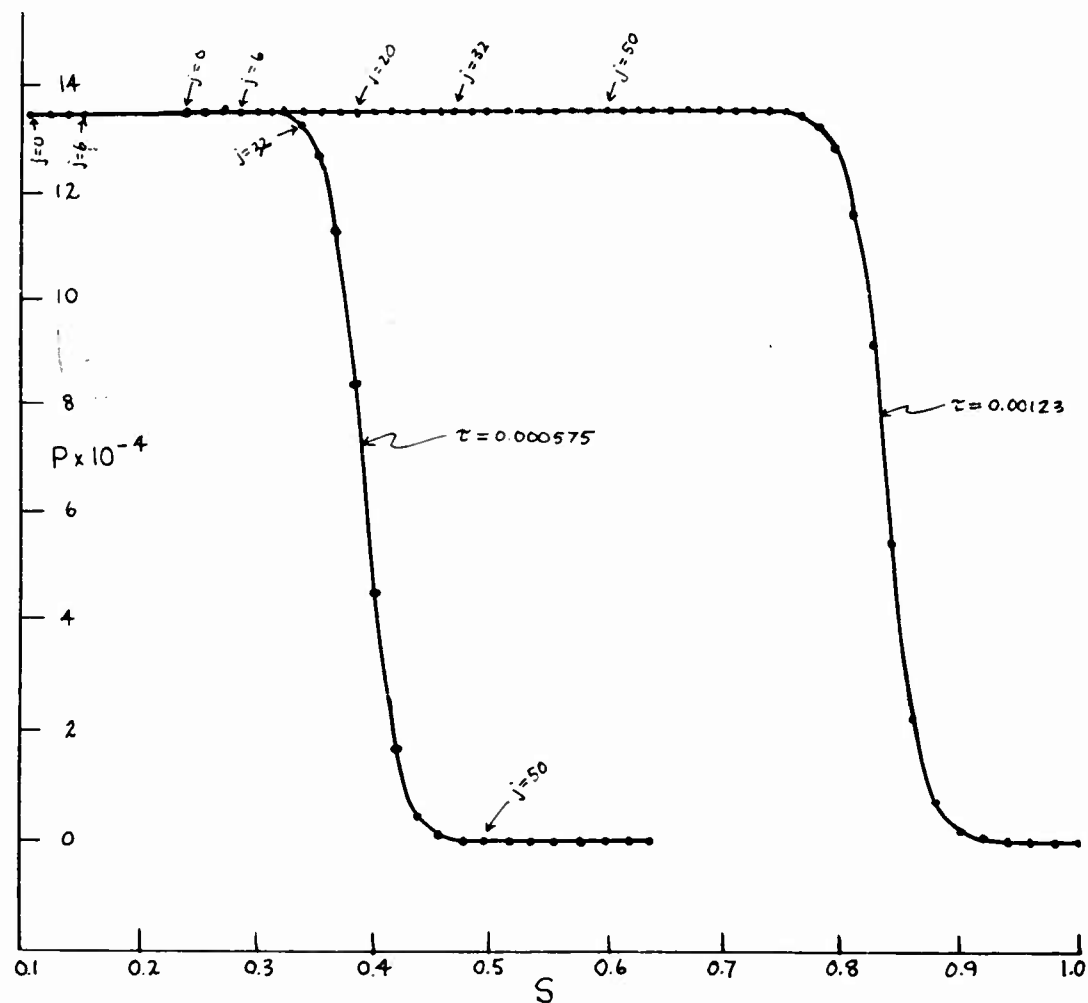


Figure 2. Pressure  $P$  vs. Eulerian position  $S$  for various values of the time  $\tau$ .

## Case 2

On each curve the dots when read from left to right are the mass particles labeled  $j = 0, 2, 4, \dots$

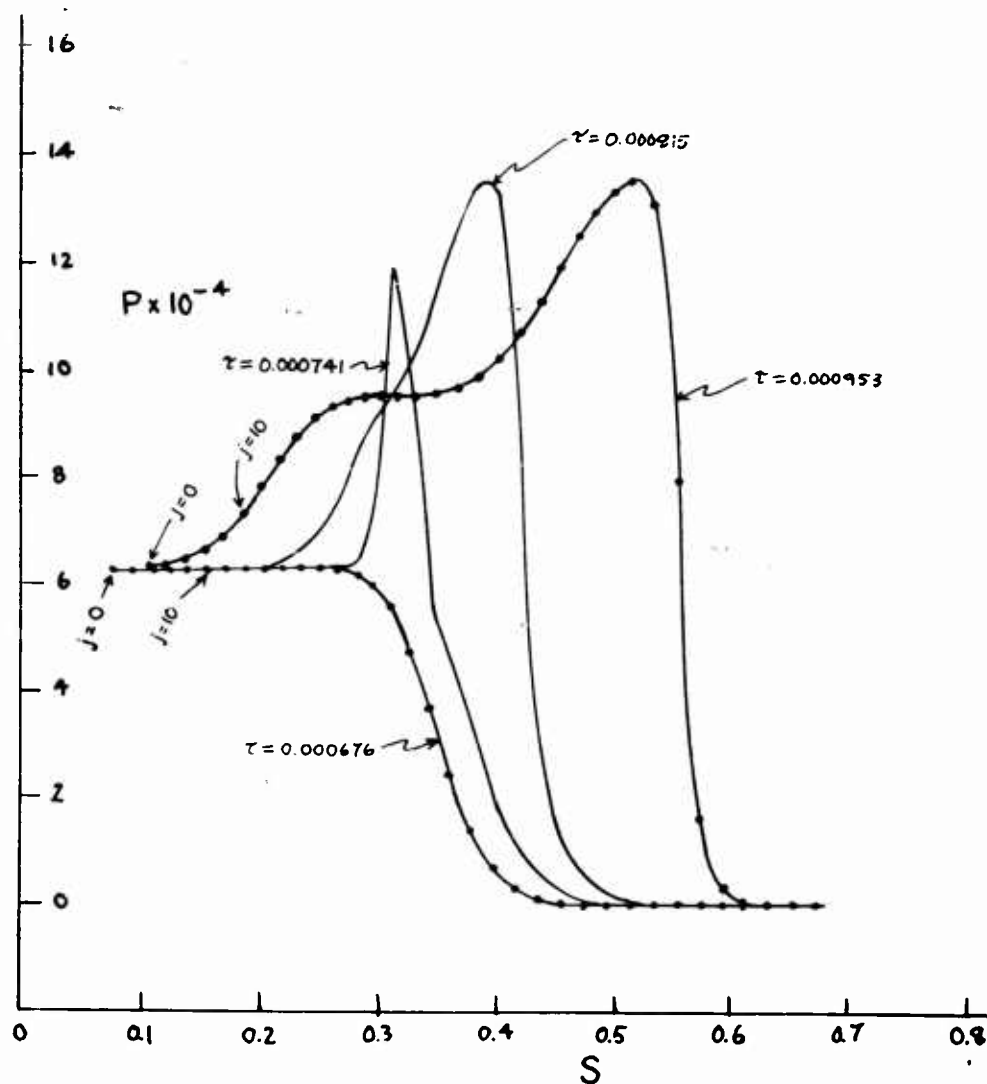


Figure 3. Pressure  $P$  vs. Eulerian position  $S$  for various values of the time  $\tau$ .

## Case 3

On each curve the dots when read from left to right are the mass particles labeled  $j = 0, 2, 4, \dots$ .

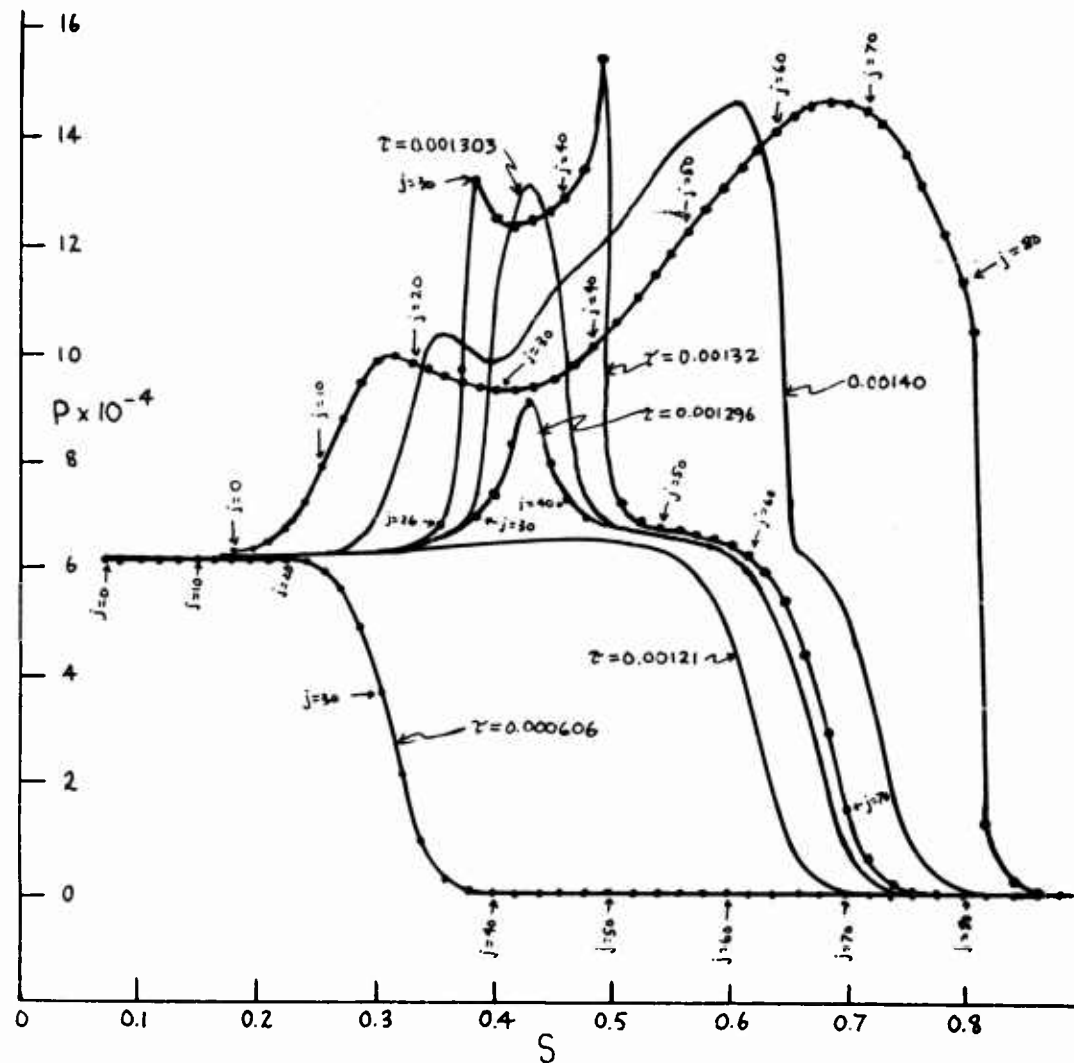


Figure 4. Pressure  $P$  vs. Eulerian position  $S$  for various values of the time  $\tau$ .

these values with computed values for the shock profile shown in Table I, we see that even in the region of piston, there is very good agreement in contrast with what is found when  $\lambda = 0$ . This can be explained as follows. We have already noted that the viscosity terms lead to abnormally high energies in the neighborhood of a velocity discontinuity. These high energy gradients can be considered, by use of the caloric equation of state, as abnormally high thermal gradients which in turn tend to remove the excess energy by heat conduction to the colder regions. Therefore while the temperature gradients are also falsified, they tend to compensate for the viscosity effect. By proper adjustment of the values of  $a$  and  $b$ , the correct values for the state variables can be found near the piston. Finding the correct value of the temperature near the piston is very important for problems where the piston strikes a highly temperature-sensitive explosive surface directly. For if the temperature is falsified in the direction of too high a value, as is done when we let  $\lambda = 0$ , or even more so when the "q" method is used, then detonation may occur when in reality the shock temperature is not sufficient to cause it.

Comparison of Figs. 4 and 5 representing Cases 3 and 4 respectively shows the effect of increasing the value of  $\nu$  so that complete reaction takes place in the shock zone. In Case 4 the reaction zone (i.e., the zone where

$0.001 \leq \omega \leq 0.999$ ) is never spread out over more than five or six particles. For Case 3, by the time the computation has reached  $\tau = 0.00144109$  (see Fig. 4), the reaction zone has been compressed to encompass two particles. Initially it was very much larger as can be seen from Table II where the mass fraction of unreacted explosive  $\omega$  at different particle numbers  $j$  is given for different values of  $\tau$ . Those points  $j$  such that  $0 < \omega_j < 1$  and that lie to the right of the zone of complete reaction, are in the shock zone.

In Case 5 the head of the centered rarefaction wave reached the interface at the time the latter had already undergone about 5% reaction ( $\omega(0.4, 0.0012) = 0.952$ ). The reaction was already extremely rapid so that it could not be quenched by the rarefaction wave. The interaction of the rarefaction wave and the detonation wave during the initial stages of growth of the latter is shown in Fig. 6.

In Case 6 we have extended the Lax scheme to detonation problems. The value of  $\nu = 10^8$  is sufficiently small so that as the shock travels through the explosive, the

TABLE I

Case 3 at $\gamma = 0.000006$ , time cycle $n=60$					
$j$	$S_j^{60}$	$1/c_j^{60}$	$10^2 U_j^{60}$	$\theta_j^{60}$	$10^4 p_j^{60}$
0	.0714	1.304	1.191	1.992	6.1634
2	.0869	1.298	1.192	1.995	6.1632
4	.1023	1.296	1.193	2.003	6.1632
6	.1178	1.294	1.194	2.011	6.1631
8	.1332	1.292	1.194	2.019	6.1635
10	.1487	1.291	1.193	2.023	6.1639
12	.1642	1.291	1.193	2.024	6.1648
14	.1796	1.291	1.193	2.023	6.1655
16	.1951	1.292	1.192	2.019	6.1643
18	.2106	1.293	1.192	2.014	6.1571
20	.2260	1.293	1.189	2.007	6.1335
22	.2415	1.291	1.181	1.995	6.0694
24	.2570	1.284	1.160	1.971	5.9124
26	.2727	1.268	1.111	1.921	5.5607
28	.2886	1.236	1.008	1.818	4.8552
30	.3051	1.182	.818	1.633	3.6656
32	.3225	1.113	.538	1.376	2.1632
34	.3409	1.054	.267	1.155	.9433
36	.3603	1.020	.102	1.047	.3217
38	.3800	1.006	.032	1.011	.0939
40	.4000	1.001	.009	1.002	.0249
42	.4200	1.000	.002	1.000	.0062
44	.4400	1.000	.000	1.000	.0015
46	.4600	1.000	.000	1.000	.0004
48	.4800	1.000	.000	1.000	.0001
50	.5000	1.000	.000	1.000	.0001
.	.	.	.	.	.
100	1.0000	1.000	.000	1.000	.0001

## Case 4

On each curve the dots when read from left to right are the mass particles labeled  $j = 0, 2, 4, \dots$

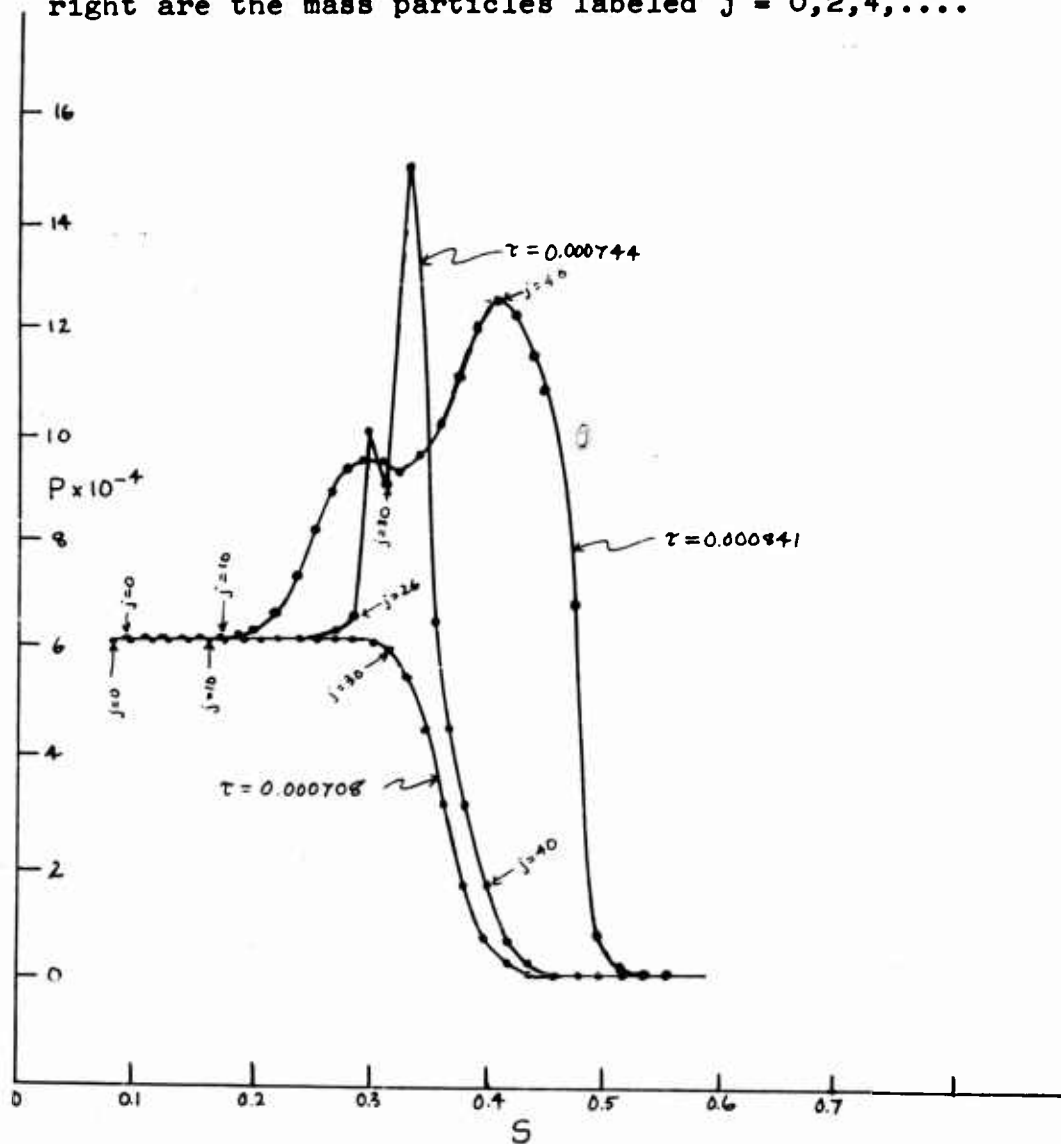


Figure 5. Pressure  $P$  vs. Eulerian position  $S$  for various values of the time  $\tau$ .



TABLE II  
Size of the Reaction Zone for Different Values of  $\tau$  for Case 3

j	$\omega_j^{90}$	$\omega_j^{110}$	$\omega_j^{120}$	$\omega_j^{130}$	$\omega_j^{140}$	$\omega_j^{160}$	$\omega_j^{230}$	$\omega_j^{330}$	$\omega_j^{360}$	$\omega_j^{430}$
28	1.000	1.000	1.000	1.000	1.000	1.000	1.000	1.000	1.000	1.000
30	.985	.961	.941	.898	.897	.886	0	0	0	0
32	.988	.962	.936	.842	.837	.664	0	0	0	0
34	.991	.966	.937	.728	.547	0	0	0	0	0
36	.994	.971	.943	.649	0	0	0	0	0	0
38	.996	.976	.951	.789	.743	0	0	0	0	0
40	.998	.981	.960	.874	.869	.734	0	0	0	0
42	.999	.985	.967	.915	.914	.897	0	0	0	0
44	.999	.989	.974	.939	.939	.932	0	0	0	0
46	1.000	.993	.980	.955	.955	.951	.933	0	0	0
48	.	.996	.985	.966	.966	.964	.954	0	0	0
50	.	.998	.990	.975	.975	.973	.967	0	0	0
52	.	.999	.994	.982	.982	.981	.976	0	0	0
54	.	.999	.996	.988	.988	.987	.983	0	0	0
56	.	1.000	.998	.992	.992	.991	.989	.490	0	0
58	.	.	.999	.996	.996	.995	.993	.984	0	0
60	.	.	.999	.998	.998	.998	.996	.990	0	0
62	.	.	1.000	.999	.999	.999	.998	.994	.735	0
64	.	.	.	.999	.999	.999	.999	.997	.995	0
66	.	.	.	1.000	1.000	1.000	.999	.999	.998	0
68	.	.	.	.	.	.	1.000	.999	.999	0
70	.	.	.	.	.	.	.	1.000	.999	.817
72	.	.	.	.	.	.	.	.	1.000	.999
74	.	.	.	.	.	.	.	.	.	1.000
:	.	.	.	.	.	.	.	.	.	.

where  $\tau^{90} = 0.000909$   $\tau^{110} = 0.001111$   $\tau^{120} = 0.001212$   $\tau^{130} = 0.0012965$   $\tau^{140} = 0.0012970$   
 $\tau^{160} = 0.001303$   $\tau^{230} = 0.001320$   $\tau^{330} = 0.001376$   $\tau^{360} = 0.001404$   $\tau^{430} = 0.001441$

## Case 5

On each curve the dots when read from left to right are the mass particles labeled  $j = 0, 2, 4, \dots$

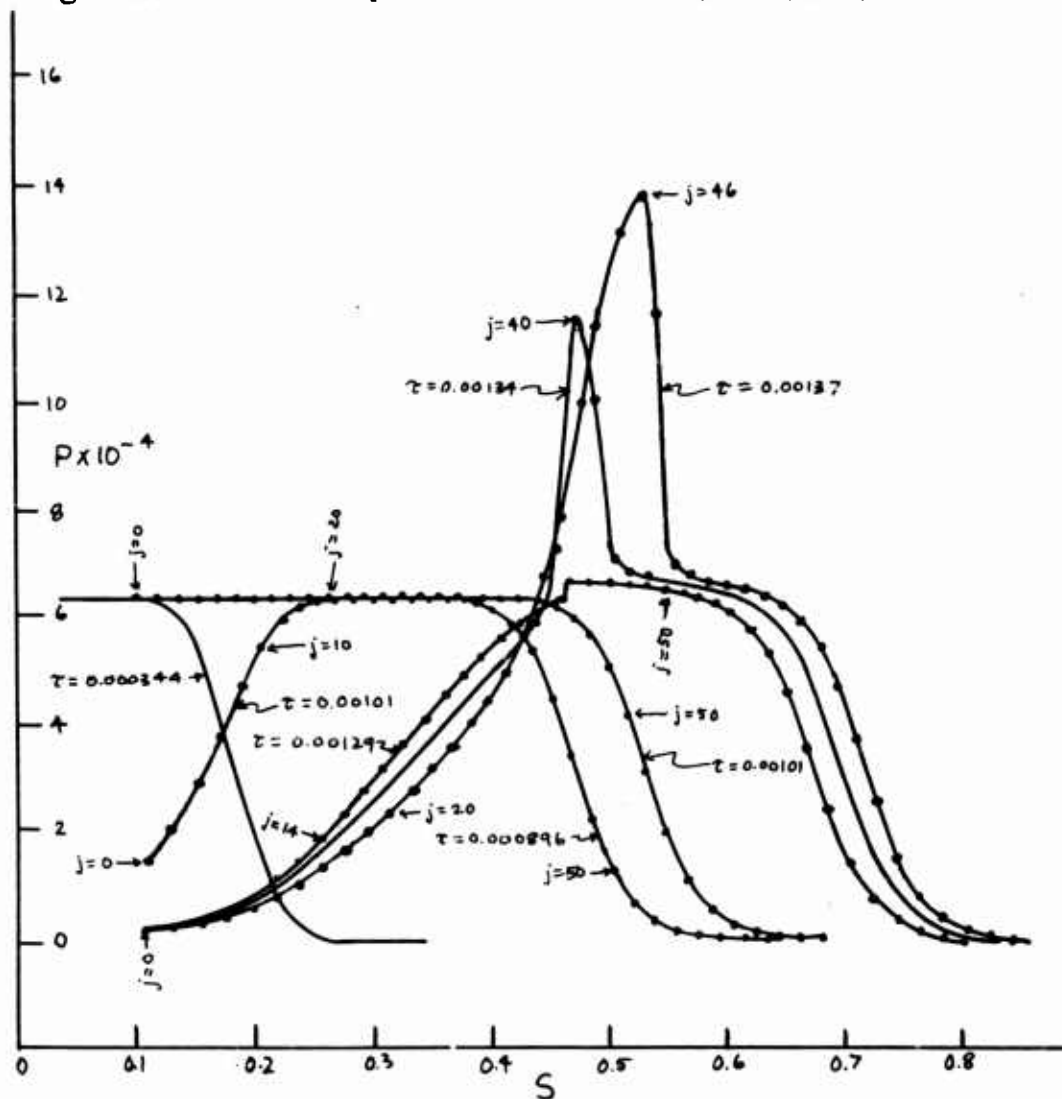


Figure 6. Pressure  $P$  vs. Eulerian position  $S$  for various values of the time  $\tau$ .

chemical reaction behind the shock zone is quite slow. Eventually a high pressure region of reaction forms ahead of the piston and well behind the shock front as is shown in Fig. 7. This high pressure region rapidly catches up to the shock front during the transition to steady state. The detonation wave is reflected off the rigid wall as a shock since all of the explosive has already been converted to detonation products. The steady state values for the dimensionless density, temperature, and pressure are 1.34, 6.15, and  $1.66 \times 10^5$  respectively. These compare with the Chapman-Jouguet values of 1.333, 5.87 and  $1.569 \times 10^5$ . It is felt that the correspondence between the two sets of values can be further improved by a more judicious choice of the finite difference representation of the boundary conditions for the Lax scheme.

Concerning the question of critical time necessary for growth from initiation to detonation, all our numerical calculations indicate that for one-dimensional problems if as little as one or two percent of the explosive has reacted, then a detonation wave will be established and will not be quenched by any reasonably strong rarefaction waves which may appear on the scene. Just as has been found by Hubbard and Johnson [2], we find that for very temperature sensitive reactions the time necessary to react the major portion of the explosive is small compared to the hydrodynamic time step necessary to influence motion.

#### ACKNOWLEDGMENT

The author would like to acknowledge interesting discussions on the topic with Dr. S. Jacobs.

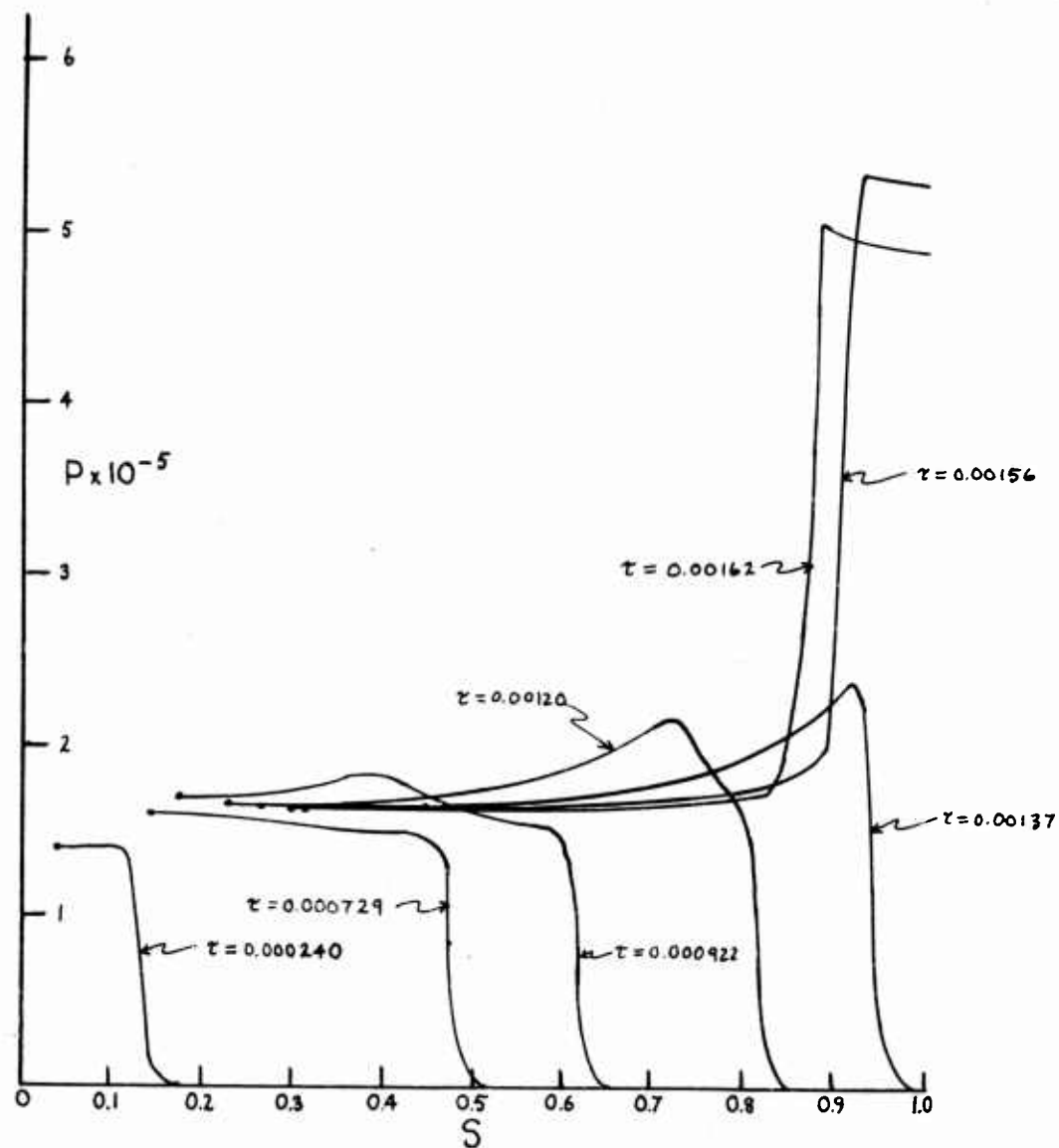


Figure 7. Pressure  $P$  vs. Eulerian position  $S$  for various values of the time  $\tau$ .

REFERENCES

1. J. O. Hirschfelder and C. F. Curtiss, J. Chem. Phys., 28, 1130 (1958).
2. H. W. Hubbard and M. H. Johnson, J. Appl. Phys., 30, 765 (1959).
3. J. von Neumann and R. D. Richtmyer, J. Appl. Phys., 21, 232 (1950).
4. G. Ludford, H. Polachek and R. J. Seeger, J. Appl. Phys., 24, 490 (1953).
5. R. Courant and K. O. Friedrichs, "Supersonic Flow and Shock Waves", (Interscience Publishers, New York, 1948).
6. J. von Neumann, O.S.R.D., Rept. No. 549 (1942).
7. W. Döring, Ann. Physik, 43, 421 (1943).
8. Y. B. Zeldovitch, J. Expt. Theoretical Phys. (USSR), 10, 542 (1940).
9. P. Lax, Comm. Pure and Appl. Math, 7, 159 (1954).

## INITIATION OF A LOW-DENSITY PETN PRESSING BY A PLANE SHOCK WAVE\*

G. E. Seay and L. B. Seely, Jr.  
Los Alamos Scientific Laboratory  
Los Alamos, New Mexico

The initiation of explosives by shocks has been studied most extensively by means of various gap sensitivity tests (1-3) where in general the geometry is somewhat complicated. Usually such tests employ non-planar shocks with large pressure gradients behind the front, and give results only in terms of the maximum thickness of the gap material which can cause detonation of the explosive. In principle, however, it should be possible to define the conditions of the initiating shock in the explosive itself (4,5). Tests in plane geometry, which can be designed for easier characterization of the shock, have been made on homogeneous explosives (6,7) and on high density solid explosives (8,9). For explosives pressed or cast to high densities, the importance of the discontinuities in the material is not in every case clear, there being some evidence that the type of initiation and even the mode of propagation change as the density approaches that of the crystal. Our interest lies in the sensitivity of granular explosives pressed to low densities, where the spaces between the particles constitute a large fraction of the total volume of the pressing. Here the interstitial gases or the discontinuities might be expected to play an important part in the initiation process. We have conducted tests on granular PETN pressed to a density of  $1.0 \text{ gm/cm}^3$ , corresponding to about 44% voids in the pressing. It is the purpose of this paper to present our first results and to discuss some of the difficulties involved in characterizing shocks in pressings of this density.

\* This work was performed under the auspices of the U. S. Atomic Energy Commission.

## EXPERIMENTAL

The experiments were carried out on wedge-shaped (6,9) PETN charges using a streak camera to record the initiation phenomena. A shock was produced by a special plane-detonation-wave generator and reduced to the proper pressure by means of impedance mismatching in an attenuator system. The surface of the attenuator, on which the wedge was placed, was illuminated by an explosive argon flash (10-12) so that the time of entry of the shock into the wedge could be determined from the start of motion of the attenuator surface. The appearance of first light from the PETN was taken to indicate the onset of detonation. Thus, we could determine the average velocity of the initiating disturbance and the distance it traveled into the charge before the detonation became apparent.

## The Shock System

It is possible to initiate explosives by means of a shock wave whose front has almost any shape in space and for which the pressure in the region behind the front drops in almost any way with time, but in general these characteristics of the wave are expected to affect the peak pressure necessary for initiation. For simplicity we desired a plane shock front followed by a constant-pressure region for the duration of the experiment, and in fact close approximations to both of these ideals were achieved. The shock system is sketched in Fig. 1.

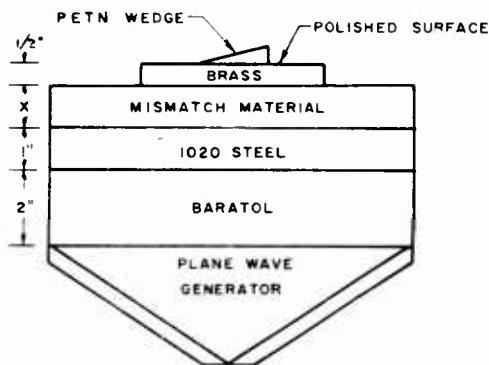


Fig. 1 Charge Arrangement for PETN Wedge Experiments.

An 8" diameter plane wave generator of the type described by J. H. Cook (13) was used to form a detonation wave which was plane to about  $\pm 0.12$  mm. Since a comparatively low pressure is sufficient to initiate PETN, 76/24 Ba(NO<sub>3</sub>)<sub>2</sub>/TNT (Baratol), which has a detonation pressure of about 140 kb, was used for the main charge. A one-inch thickness of SAE 1020 steel was placed on the Baratol. On this was placed a mismatch material, usually Lucite, in which the wave produced a pressure of about 30 kb. The next component in the attenuator was

brass (60.6% Cu, 39.3% Zn), in which a pressure of about 60 kb was produced. The PETN wedge sat on the surface of this brass, but, because of the mismatch at the brass-PETN interface, the pressure in the wedge was only a few kilobars.

Various attenuators, designed on this general plan, were evaluated in detail by use of an optical method for the measurement of free surface motion developed by Craig and Davis (14). As shown in Fig. 2, a wire (or other object with a well-defined edge) is placed above the surface to be measured and viewed at an angle with a streak camera. The surface is illuminated by an argon flash so that the wire and its image on the polished surface can be photographed. When the surface begins to move in the direction of the shock, the virtual image behind the surface will appear to move across the camera slit toward the wire. If we know the magnification  $M$ , the camera angle  $\theta$ , and the angle  $\alpha$  which the moving image makes with the wire on the film, then the free surface velocity is

$$U_{fs} = \frac{U_c \tan \alpha}{2M \sin \theta}$$

where  $U_c$  is the camera writing speed. Imperfections on the polished surface move at one-half the speed of the image of the wire, and can sometimes be used for measurements. Traces of such imperfections will show sudden bends at the onset of free surface motion, and, when there are many of them across the surface, they can be used to examine the planarity of the shocks.

By use of the quite accurate approximation (15) that the particle velocity  $U_p$  in the brass is one-half the measured free surface velocity  $U_{fs}$ , the shock pressure  $P$  in the brass plate was deduced from the published data on the Hugoniot for brass (16). It can be assumed that in most practical shock systems the pressure will drop to some extent behind the shock front. Such a falling pressure contour should produce a gradual lowering of the peak pressure as the wave progresses through a material. However, measurements of the free surface velocity for thicknesses of brass between 1/4" and 3/4" showed no detectable change. This indicated that the falloff in pressure produced a free surface velocity effect that lay within our experimental reproducibility, and from this we have estimated that the pressure decreased less than 4% as it travelled through this 1/2" thickness of brass.

The peak pressure was varied by changing the mismatch material or, when using Lucite, by changing its thickness. The thickness method of adjusting the pressure probably depends on the existence of the pressure drop postulated above.



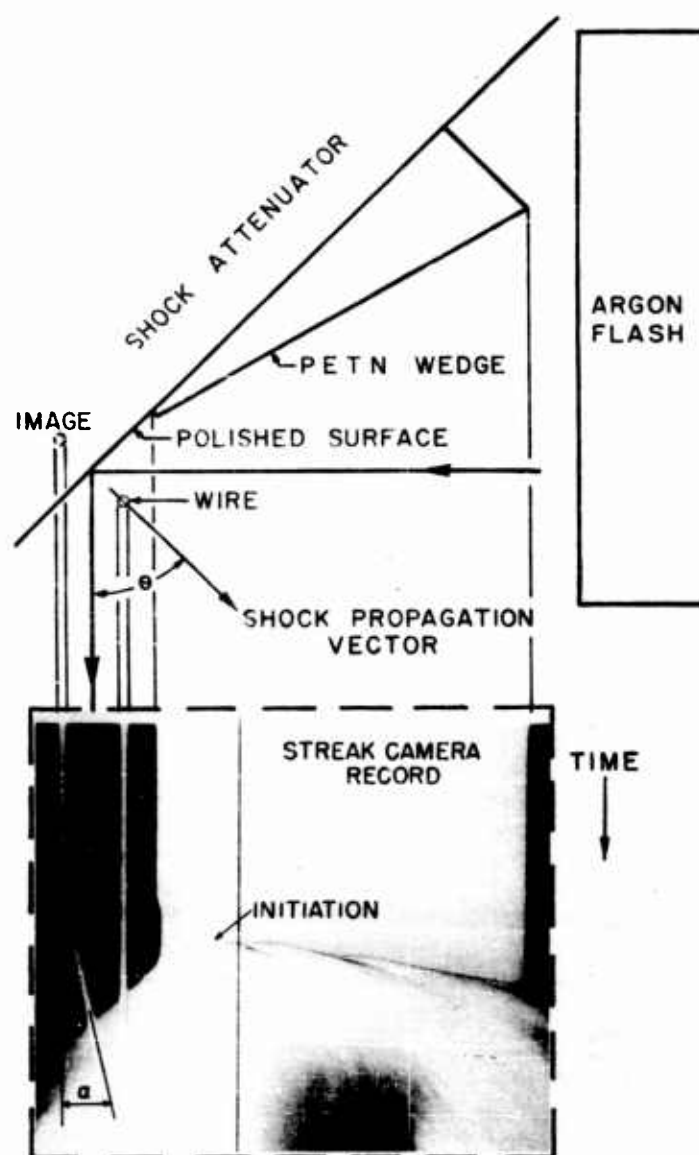


Fig. 2 Diagram of the Experimental Arrangement. A streak camera record, printed as a negative, has been positioned so as to show corresponding features. A wire and its image in the polished brass surface are used to determine the free surface velocity. The irregular line on the part of the film corresponding to wedge-face is the detonation. Irregularities are ascribed to uneven initiation across the surface of the shock within the PETN pressing.

## Explosives

In order to perform experiments at low density by the wedge technique it was necessary to obtain an explosive in a crystal form that would press easily to a reasonably uniform density and produce a pressing strong enough to permit shaping and handling. We also wished to pick a material that could be or had been studied (6) in the form of homogeneous large crystals. We believed there would be some advantage in using low shock strengths so that the contrast with the single crystal work would be striking. The sensitivity of low density PETN pressings recommended them on this score. There is a considerable amount of information on the crystallization of PETN (17). By fairly rapid crystallization long thin and irregular crystals can be produced which have a low bulk density and might be expected to press well. For all these reasons, PETN was chosen for study. Precipitation was accomplished by adding water to an acetone solution. This gave elongated prismatic crystals, somewhat twinned, a good fraction having re-entrant cavities along the main axis of the crystal. The specific surface, as measured with an air permeability apparatus, was about  $3000 \text{ cm}^2/\text{gm}$ . Wedges were fabricated by pressing such PETN to a density of  $1.0 \text{ gm/cm}^3$  in cylindrical pellets in a special die. This die could be partially disassembled so that the PETN contained in the remaining section could be shaved into a wedge at an angle of  $19.5$  degrees. The wedge was then removed from the second die section.

The first experiments were attempted with the PETN wedge surrounded peripherally by a part of the steel pressing die, but after a method had been developed for removing the wedge from the die it became clear that the die had perturbed the shock sufficiently to give erroneous results. In some early experiments a mirror was used on the angled wedge surface in the hope that it would permit observation of the initiating disturbance. This also was shown to give results that were misleading. Low density pressings of PETN are probably especially sensitive to these effects, since the velocity of the initiating shock is so low. The abandonment of mirrors and similar materials over the surface of the wedge meant that most of the experiments were performed in such a way that the initiating shock could not be observed in the PETN, since it was so weak as to be non-luminous. Therefore, we have measured the time and distance from the entry of the shock, as shown by the start of surface motion of the brass, to the start of detonation, as indicated by the first appearance of light intense enough to be recorded by our camera.

## RESULTS

A diagram of the experimental setup is shown in Fig. 2 together with a print of a typical camera record. Data from the experiments are presented in Table I. The values of Brass Free Surface Velocity could be determined to within about  $\pm 5\%$ . The greater variation among the three free surface velocities for 1 1/2" thick Lucite is believed due to wave tilt introduced by the use of two 3/4" pieces that had not been selected for flatness. Data in the Depth of Initiation and Time of Initiation columns were obtained by measuring the position and time where light was first recorded from the PETN. This was a difficult point to measure, and it could not be done with much accuracy. Nevertheless, the accuracy is sufficient to permit determination of the conditions under which the depth of initiation becomes very large.

The luminous trace from the wedge was identified as a detonation by comparison with strongly initiated wedges. In the first three shots listed in Table I the initiating shocks were strong, the delays were so short as to be almost obscured by the toe of the wedge, and the light from the waves travelled across the wedge with nearly constant velocity (corresponding to 5.8, 5.7, and 5.7 mm/sec through the pressing for shots 1, 2, and 3 respectively). We therefore assumed that the self-luminous disturbance was in fact a detonation wave even when determination of the velocity was impossible. The irregularity of some traces, an example of which is given in Fig. 2, is taken to mean that the initiation did not take place simultaneously over the surface of the shock wave in the low density PETN pressing. This is a cause for lack of precision in measuring the depth of initiation.

Figure 3 is a graph of Depth of Initiation vs Brass Free Surface Velocity and gives some indication of the reproducibility. The corresponding shock pressures in brass are also given along the abscissa. These pressures were determined from an extrapolation of the shock Hugoniot data published by Walsh, et al (16). Their Hugoniot curve for brass is shown in the pressure/particle-velocity plane in Fig. 4 with a typical state point S indicated.

Fig. 3 Depth of Initiation vs Brass Free Surface Velocity. The depth of initiation is the distance from the original position of the brass surface to the level in the charge indicated by the position of first light on the film. Depths of initiation less than 1 mm or greater than 8 mm could not be accurately measured, and are indicated by the open-sided symbols.

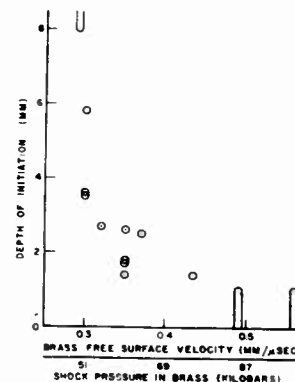


TABLE I  
Data from PETN Wedge Initiation Experiments

PETN density =  $1.0 \text{ gm/cm}^3$   
Wedge angle =  $19.5^\circ$   
PETN specific surface =  $3000 \text{ cm}^2/\text{gm}$

Shot No.	"X" in Shock Attenuator		Brass Free Surface Velocity (mm/ $\mu\text{sec}$ )	Depth of Initiation in PETN (mm)	Time of Initiation in PETN ( $\mu\text{sec}$ )
	Material	Thickness (in.)			
1	<sup>a</sup> Devcon-C	1	0.56	1	--
2	<sup>b</sup> Pentite	1	0.49	1	--
3	Lucite	1	0.43	1.4	1.25
4	Lucite	1 1/4	0.37	1.8	1.75
5	Lucite	1 1/4	0.38	1.4	1.39
6	Lucite	1 1/4	0.37	1.7	1.75
7	Lucite	1 1/2	0.37	2.5	2.53
8	Lucite	1 1/2	0.36	2.6	2.83
9	Lucite	1 1/2	0.33	2.7	3.03
10	Lucite	1 3/4	0.34	5.9	6.78
11	Lucite	1 3/4	0.33	3.6	3.91
12	Lucite	1 3/4	0.33	3.5	4.17
13	Lucite	2	0.29	8	--

<sup>a</sup>Devcon-C is an aluminum-filled epoxy resin manufactured by Devcon Corp., Danvers, Mass.

<sup>b</sup>Pentite is a plastic-bonded pentaerythritol, pressed close to theoretical density.

## DISCUSSION

The shocked state of the brass can be determined simply from the experimental results. However, defining the state of the shocked PETN is less straightforward. The PETN has been treated as a homogeneous material and the initiating shock has been assumed to move with a velocity, in the neighborhood of 1 mm/ $\mu$ sec, equal in each case to the quotient of the numbers in the last two columns in Table I. We have used what Walsh, *et al* have called the Graphical Solution of the interface equations. A more complete description of this procedure can be found in their article (16). Starting from a typical shocked state such as S in Fig. 4, subsequent state points of the expanding brass must lie along the adiabat through point S. We have used the approximation that the adiabat can be replaced by the mirror image of the Hugoniot about the line corresponding to the value of  $U_p$  at the point S. Such a curve is shown dotted in Fig. 4. From the values of shock velocity we have then constructed lines having slopes equal to  $\rho_0 U_s$  for the PETN, one of which is shown as a dashed line in Fig. 4. In order for the pressure and particle velocity to be continuous across the PETN-brass interface, the state point of the PETN for a given experiment must be at the intersection I of the two curves. Repeating this process for each experiment we arrived at a series of PETN state points which, with certain reservations, can be regarded as defining a PETN Hugoniot, shown in Fig. 5.

These reservations regarding the reality of the PETN pressure and particle-velocity arise because of the assumptions made concerning the initiating shock and because the heterogeneous PETN pressing has been treated as homogeneous for hydrodynamic purposes. These questions deserve considerable discussion and have been the subject of the special experiments described below.

## The Initiating Shock

By increasing the illumination of the surface of the wedge and eliminating the simultaneous free surface velocity measurement it has been possible to obtain records of the initiating disturbance in its travel through the PETN. Such experiments have shown that this disturbance accelerates continuously. Although the early part of the smear camera record looks almost straight in some cases, the curvature increases progressively as the point of initiation is approached. Since this is

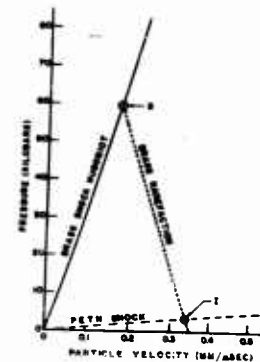


Fig. 4 Pressure vs Particle Velocity Plots for Brass and PETN. The brass Hugoniot is from Reference 16. See text.

the case, the method used in the work reported above to estimate shock velocities has yielded values too high by perhaps 10%. Thus the derived PETN pressures should be reduced approximately 10%. On the other hand, this inaccuracy is about the same magnitude as some of the other uncertainties in calculation of the pressure. The important point is not that the pressure be known with great absolute accuracy but that the fact be established that PETN can be initiated by shock pressures as low as a few kilobars.

When acceleration of the initial disturbance is taking place, chemical reaction is clearly present. It seems reasonable that the shock is essentially unsupported in the early stages when it is moving into the PETN with almost constant velocity. However, it must be admitted that this has not been proven, and that the existence of a meta-stable supported shock is still a possibility as far as the present experiments are concerned. If this is in fact the situation, the curve in Fig. 5 would be considered as a Hugoniot for partially reacted PETN, but only if the constant velocity region is considered to represent a steady state. However, different initial velocities seem to indicate that each point would represent, under these assumptions, a different degree of reaction and that Fig. 5 would then not represent a Hugoniot at all. The variation of the initial velocities do not have this implication for a shock with extremely small amount of chemical reaction, and in this case Fig. 5 could be a fairly close approximation to the Hugoniot for unreacting PETN.

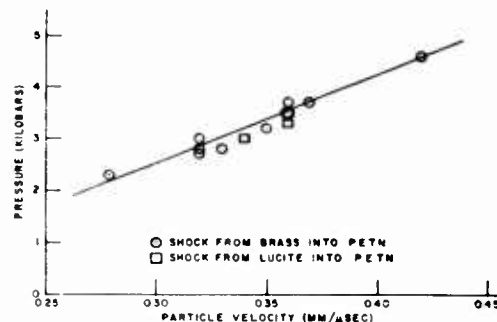


Fig. 5 PETN "Shock Hugoniot". The pressures and particle velocities were derived from measured properties in the last element of the attenuator, employing a number of assumptions whose validity is discussed in the text.

#### PETN Shock Hugoniot

There is a question as to whether it is legitimate to speak of a Hugoniot for a PETN pressing, which consists of individual PETN grains at crystal density and air spaces at very low density. The quantities  $\rho_0$  and  $U_s$ , used to arrive at the pressure and particle velocity values for the Hugoniot, are both averages. When the shock first crosses the interface between the attenuator and the explosive, it seems questionable that any small region in the PETN pressing actually exists at the pressure and particle velocity given by the point I in Fig. 4. In other words, the appropriateness of considering the pressing to be homogeneous depends on how much small scale detail is required for the purpose at hand; and consideration of initiation would seem to require details for individual grains.

For purely hydrodynamic purposes, the "average Hugoniot" of the pressing may be a very useful curve. To check this, points on the PETN Hugoniot were also determined when the PETN was shocked from a material which was hydrodynamically quite different from the brass that was used in the original experiments. The 1/2-inch-thick final attenuator element of brass was replaced by a dual element consisting of 1/2-inch of uranium and 1/2-inch of Lucite. The shock entered the PETN from the Lucite and the pressure and particle velocity in the PETN were determined from the intersection of the approximation to the Lucite (18) adiabat and the  $\rho_0 U_s$  line,  $U_s$  having been determined as before. In Fig. 5, two points from such experiments are seen to lie on the PETN Hugoniot determined from the data collected when brass was the last attenuator element. This means that the PETN Hugoniot is satisfactory for predicting shock velocities in the pressing if the hydrodynamic properties have been determined for the material from which the shock enters the PETN. A distinction has been made here between the prediction of the shock velocity (which can be checked in absolute terms by measurement) and the derivation of the corresponding pressure (which we have not measured directly).

The PETN "shock Hugoniot" in Fig. 5 is probably more accurate than the individual points. Therefore the intersections of this curve with the appropriate brass adiabats have been used to evaluate the PETN "shock pressures", which are plotted against the depths of initiation in Fig. 6. On this basis, the minimum initiating pressure of 50 kb in the brass is seen to correspond to a derived pressure of about 2.5 kb in the PETN.

There is another aspect of these experiments which could in principle be quite distinct from the hydrodynamic properties of the pressing; namely, the question of the sensitivity of the PETN when shocked from the two materials, brass and Lucite. In the microscopic sense it is clear that the impedance match is different for these two materials as the shock enters the individual PETN grains or the air spaces between them. Strictly, it could not be taken for granted that the sensitivity of the PETN would be the same for shocks from the two materials even though they eventually produced the same macroscopic average shock velocity in the pressing. However, the depths of initiation have turned out to be consistent with the hydrodynamic behavior. This is shown by the triangular points in Fig. 6.

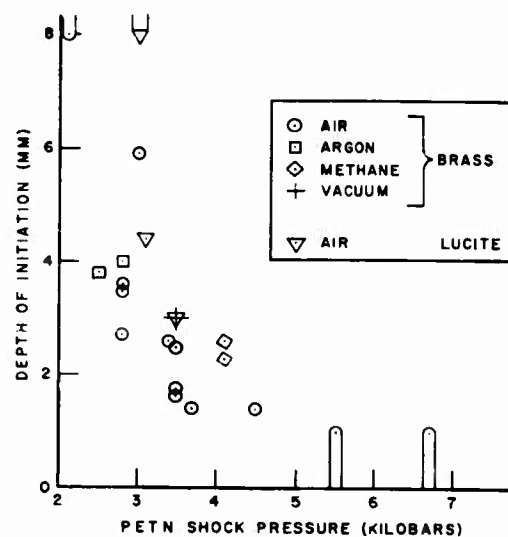


Fig. 6 Depth of Initiation vs PETN "Shock Pressure". The meaning of the pressure values is subject to the qualifications applying to the PETN Hugoniot.

In spite of the difficulties, the shock velocity in the PETN pressing can be calculated, and the initiation of the PETN will take place according to this velocity. The relative pressures, naturally, will also serve as such an index.

#### Effect of Interstitial Gases

One proposal for the mechanism of initiation of detonation involves grain-burning started by means of the compressional temperature of interstitial gases in the pressing. Compression may be considered to take place by a single shock along the Hugoniot, by a series of compressions along a curve approximating an adiabat, or even by means of a clear-cut shock reflection. Regardless of these details the temperature can be altered at least 500°C by choosing gases with widely different hydrodynamic and thermodynamic properties. In order to achieve extremes in this sort of behavior, we have evacuated wedges and replaced the air, either with argon to produce high gas temperatures, or with methane to produce low gas temperatures. The results of these tests are shown in Fig. 6, and the fact that these depths of initiation agree within experimental error with the values for air is taken as strong indication that the temperature of the interstitial gas has nothing to do with the mechanism of initiation. Temperature differences of several hundred degrees would have a profound effect on the rate of grain burning or on the rate of chemical reaction if such temperature changes could be brought to bear on these processes.

An experiment was also performed in which the pressure of the interstitial air was reduced to the range between 50 to 100 microns. The temperature of the compressed residual air in this case was not much different from that achieved at normal density but the total amount of energy available for transfer from gas to PETN was lowered by a factor of about  $10^4$ . This low-pressure shot is also shown in Fig. 6, and again demonstrates that the interstitial gases did not affect the initiation process.

#### CONCLUSIONS

By use of a special low-bulk-density PETN it has been possible to extend wedge-type initiation measurements to low-density pressings. For such pressings it is to be expected that the nature of the crystals and the properties of the interstitial gases would affect the initiation characteristics, if they are ever to be important. The experiments reported on the lack of effect of interstitial gases seem to eliminate this component from the mechanism. Further experiments need to be done to assess the importance of the properties of the solid grains.

The particular type of PETN we have used has been shown, at  $1.0 \text{ gm cm}^{-3}$  density, to be sensitive to shocks that are quite weak compared to those required for the initiation of high density explosives. The hydrodynamics of the interface between the material



used to carry the shock and the particulate explosives can apparently be treated satisfactorily by using methods developed for homogeneous materials. On this basis we arrive at a pressure of about 2 1/2 kb in the PETN pressing as the lowest pressure with which we have been able to produce initiation. In future experiments this pressure will be compared to the pressure necessary to initiate pressings in other densities. It is hoped that the changed interface conditions can be properly taken into account in this manner.

#### ACKNOWLEDGMENT

The authors wish to thank Donald Wilson for assistance in making the experiments and for preparing the illustrations. The PETN wedges were supplied by A. E. Marchand.

#### REFERENCES

1. H. Muraour, Mem. d' Artill. Fr. 12, 559 (1933).
2. H. Eyring, R. E. Powell, G. H. Duffey, and R. B. Parlin, Chem. Rev. 45, pp. 138-142 (1949).
3. M. A. Cook, D. H. Pack, L. N. Cosner, and W. A. Gey, J. Appl. Phys. 30, 1579 (1959).
4. G. P. Cachia and E. G. Whitbread, Proc. Roy. Soc. (London) A 246, 268 (1958).
5. W. R. Marlow and I. C. Skidmore, Proc. Roy. Soc. (London) A 246, 284 (1958).
6. T. E. Holland, A. W. Campbell, and M. E. Malin, J. Appl. Phys. 28, 1217 (1957).
7. A. W. Campbell, W. C. Davis, and J. R. Travis, Shock Initiation of Detonation in Liquid Explosives, this symposium.
8. A. W. Campbell, W. C. Davis, J. B. Ramsay, and J. R. Travis, Shock Initiation of Solid Explosives, this symposium.
9. J. M. Majowicz and S. J. Jacobs, Initiation to Detonation of High Explosives by Shocks, Lehigh Meeting, Fluid Dynamics Div. APS November 1957.
10. A. Michel-Levy, H. Muraour, Compt. Rend, 204, 576 (1937).
11. C. H. Winning and H. E. Edgerton, J. Soc. Mot. Pict. Engr. 59, 178 (1952).
12. R. G. Shreffler and W. E. Deal, J. Appl. Phys. 24, 44 (1953).
13. J. H. Cook, Research 1, 474 (1948).
14. B. G. Craig and W. C. Davis, to be published.
15. J. M. Walsh, M. H. Rice, Solid State Physics (Academic Press, New York and London, 1958) Vol. 6, p. 29.
16. J. M. Walsh, M. H. Rice, R. G. McQueen, E. L. Yarger, Phys. Rev. 108, 196 (1957).
17. E. Berlow, R. H. Barth and J. E. Snow, The Pentaerythritols, (Reinhold, New York, 1958), p. 57.
18. W. E. Deal and R. G. McQueen, Private Communication (1957).

THE TRANSITION FROM SHOCK WAVE TO DETONATION  
IN 60/40 RDX/TNT

E.L. Kendrew and E.G. Whitbread  
Explosives Research and Development Establishment  
Ministry of Aviation  
Waltham Abbey, England.

INTRODUCTION

In recent years an increasing amount of attention has been paid to the initiation of detonation by shock; this is important for both the design of weapons and the general understanding of sensitivity.

Hertzberg (1) was the first to observe that if a charge is detonated by a shock wave the detonation occurs at a point inside the charge and not where the shock wave entered. As the shock has a lower velocity than the detonation the concept of a 'delay' is thereby introduced, i.e. the charge takes longer to detonate than the time calculated by dividing length by detonation velocity. The concept depends on the reasonable but incorrect assumption that the detonation ought to start at the entry face. The weakness of this assumption is well illustrated by the behaviour of large, near perfect, RDX crystals which usually detonate backwards from the face by which the shock wave leaves the crystal (2).

There are at present two theories on the shock initiation of explosives. It is common to both that the shock wave initiates some reaction in that part of the charge through which it first passes; one theory (3) holds that the energy from this reaction reinforces the shock in a continuous manner, while the other theory (4) postulates that the rising temperature of the reacting material ultimately results in the production of a condition of thermal super-conductivity and a "heat-pulse" flashes through the charge, setting up a detonation when it overtakes the shock front.

It is a consequence of the first theory that the ensuing detonation will propagate only in the direction of the initial shock wave, since with a continuous build-up process the region immediately

behind the detonation zone must be greatly depleted of chemical energy, and such a region, if thick enough, would act as a barrier to a detonation propagating back into the shocked material. In the second theory however there is nothing to prevent a detonation developing in both directions at once.

In general the first theory is founded on experiments with charges of small cross section and the second with charges of larger section.

The programme, of which a part is described here, has two objects: first, to resolve this difference, and second, either (i) to study the formation and transmission of the "heat pulse" or (ii) to demonstrate the dependance of the acceleration process (and hence the so called delay time) on the initial shock pressure.

#### EXPERIMENTAL

A novel feature of the explosive charges used in this work is that in most of the experiments the shock wave passes successively through a number of thin layers of explosive each separated from its neighbours by metal foil. The purpose of this is twofold: The metal foil will prevent the flow of a "heat pulse" from layer to layer (5) and the entire assembly is an approximate but practical representation of a one-dimensional system in Lagrangian co-ordinates of mass and time (6). It is appreciated that for the latter purpose the system has obvious limitations but it is most valuable as a first step.

In future work it is intended to utilise measurements made of the movement of the interface between layers, since the particle velocity changes with pressure more than 5 times as rapidly as does wave front velocity. As discussed later this has not yet been carried out.

The basic test assembly is shown in figure 1. The "donor charge" was an explosive lens designed to give a slightly concave wave form. The "gap" always contained a large sheet of 16 g. mild steel which also acted as a shield to prevent the products of the donor charge obscuring the camera's view of the "receptor". The "gap" was made up to the necessary thickness with laminated brass (for the smallest assemblies) or with sheets of card (for the larger charges).

Three sizes of receptor charge were used: 15 x 15 x 38 mm, 50 x 50 x 150 mm and 75 x 75 x 200 mm with "donor" charges to suit. The "receptors" were usually made up as stacks of laminae each separated from its neighbours by sheets of brass foil 0.04 mm. thick and with alternate layers coloured black. The laminae were 2.5 mm thick for the smallest charges and 7.5 mm thick for the others. On occasion solid charges were used, as some

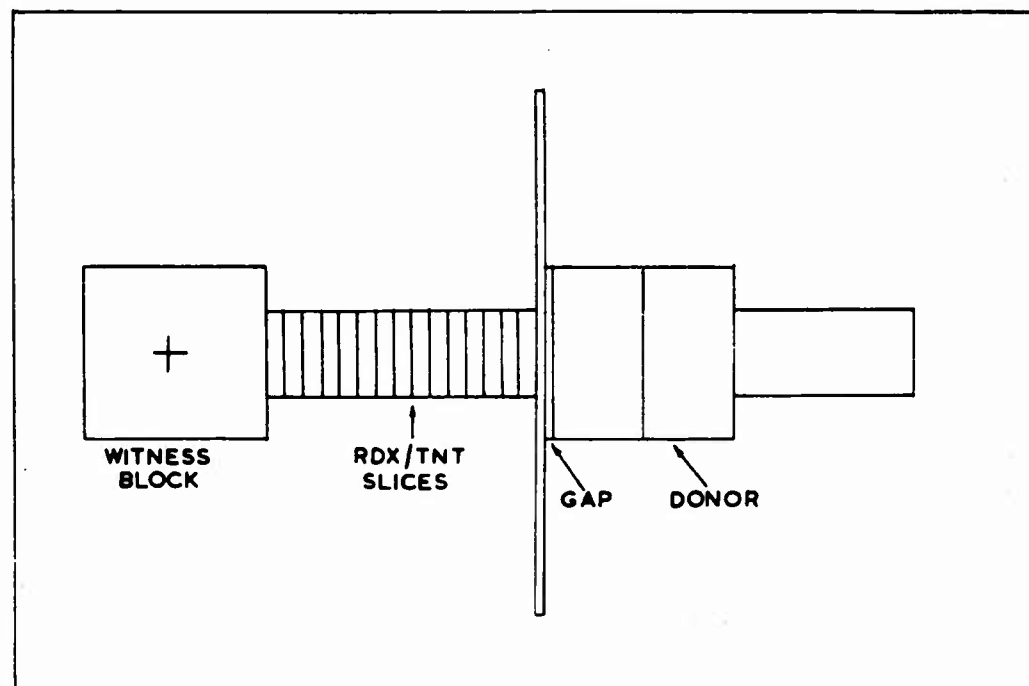


FIGURE 1

qualitative information is more easily obtained with this type.

All explosive components (with the exception of the smallest donor charges) were made from RDX/TNT Grade A, cast under a pressure of 100 p.s.i. and with controlled cooling of the moulds by hot water jackets. Selected sections were cut from the casts and machined to size by standard methods. To obtain a better surface each section of the laminated charges was hand scraped and tested on a surface plate. The charges were assembled with the least possible amount of rubber cement and under some pressure.

The smallest donor charges were machined from pressed tetryl pellets.

The experiments were photographed using a Beckman and Whitley 189 framing camera at  $1.2 \times 10^6$  and  $5 \times 10^5$  f.p.s. Kodak tri-X, developed normally, was used for the major part of the work but a few shots were taken in colour on Anscochrome for illustrative purposes. Conventional synchronisation, argon flash bomb and blast shutter techniques were used throughout.

The charges were photographed from the side, with the optical axis at right angles to the motion of the shock front. All measurements were made on the centre line of the side face.

To the present time the quantitative study has been concentrated on the smallest (15 mm square section) size of charge. Of these 56 have been fired, in 37 a detonation developed at distances from the "gap" varying from 10 mm to the full length of the charge (38 mm) and in 19 no detonation resulted.

The shock front measurements for each film were first recorded as a space-time curve and the velocities at each point taken as the tangent to the curve. The distance between the "gap" and the onset of detonation varied from shot to shot, the velocities were not therefore plotted against the distance from the "gap" but against the distance measured backwards from the point of transition from shock wave to detonation (i.e. from where the air shock becomes luminous toward the "gap"). The results may be grouped as a single relation (figure 2); as the velocities themselves are taken from smoothed curves the individual points are not marked but the braces indicate the spread of the data.

#### DISCUSSION

In previous work it had been found that a minimum shock pressure of 90 Kb was necessary to initiate RDX/TNT charges of 12.5 mm square cross section. The wave front velocity was of the order of 4000 mps. Much lower initial velocities have now been observed in the 15 mm square section charges which ultimately detonated. The difference is not yet fully explicable but must be mainly due to the fact that the measurements now put forward were made on the

surface of the charge, the previously recorded data referring to the interior. As the charge expands behind the shock front rarefaction waves move into the compressed material reducing the pressure and velocity and this reduction is immediately effective at the surface.

This has so far prevented effective use of the surface particle velocity measurements but could be overcome if the way in which the expansion takes place were properly understood.

A superficial examination of the photographs obtained so far shows a similarity to the expansion of material flowing through an orifice and subjected to the influence of the so called "simple" waves (Prandtl-Meyer expansion, ref. 6 but p 267 et seq). However an exact analysis has not yet been attempted.

On the first theory of transition, in which the shock is not reinforced until overtaken by the "heat pulse", a laminated charge of the type used in these experiments must either: (i) Detonate in the first layer, the detonation being quenched and reformed in each subsequent layer in the manner described by Cook (5) or (ii) fail, since if the heat pulse generated in the first layer does not overtake the shock wave in that layer it will be stopped by the metal foil; the shock wave will be weaker in the second layer so the heat pulse in this layer will arise later than in the first and must suffer a similar fate. Thus a laminated explosive/metal charge must detonate in the first layer or fail.

With laminated charges of all cross sections described earlier it has always been possible to obtain a transition from shock to detonation when the shock wave had traversed most of the charge. This in itself is a strong argument against the "heat pulse".

Three kinds of behaviour of the wave were found, according to the cross section of the charge used.

1. With charges of 15 mm square cross section there is a continuous acceleration from near sonic speed to detonation. The velocities in the individual shots vary considerably but all show an increase of the same form. The minimum velocity possible cannot be below sonic, and assuming this to be about 3000 m.p.s. it can be seen from figure 2 that no less than 54% of the acceleration occurs in the last 2.5 mm before detonation, 20% in the 2.5 mm before that and 10% in the previous 2.5 mm. This implies that nearly 85% of the acceleration occurs in the last 7.5 mm before detonation and only about 15% in the 12.5 mm before that.

It was not found possible to measure acceleration more than 20 mm before detonation. In those shots where the shock traversed more than 20 mm before detonation (7 out of the 56) the acceleration, if present, was too slight. A further complication was that the concave wave shape generated by the donor charge rapidly inverted,

producing spurious effects which rendered measurements in the first few millimetres useless.

In the region of gentle acceleration there is a slight change in the colour of the charge in that the yellow of the explosive becomes tinted with blue, in the region of rapid acceleration (the last three layers or so) there is a very marked colour change to deep brown. It is probable that in both cases these changes are due to chemical reaction although in the first instance (light blue) it could be due to the air shock surrounding the expanding charge.

In no case was "reverse detonation" observed. This is presumably because the layer of explosive immediately behind the detonation is too devoid of chemical energy, having supported half the acceleration within 2.5 mm.

2. With charges of 75 mm cross section the initial shock is of 3000 m.p.s. velocity, which is probably very near sonic speed, there is no measurable acceleration and the detonation develops in both directions. The velocity of the forward propagating detonation is initially above the accepted value of 7900 m.p.s. by as much as 500 m.p.s. but rapidly (within 20 mm) falls to the normal rate. The reverse wave velocity is initially about 1000 m.p.s. low and falls to a yet lower rate as the wave moves farther into the shocked region.

3. The most interesting phenomenon occurred with the intermediate size charges, i.e. of 50 mm square section. The shock wave is initially of about sonic velocity and does not accelerate until 10 mm before the transition point. When acceleration occurs it is limited to the centre of the wave (as seen on the side of the charge) which develops a thin, dark pre-detonation region followed by a detonation propagating, forward in the centre, sideways to the corners and then backwards in the corners only (fig. 3). This is exactly as if there were a short cylindrical region, in the charge centre and normal to the axis, in which the reverse detonation is inhibited. This cylinder is of such a diameter (60 mm in this instance) that it cuts into the faces of the square section charge, leaving the corners free.

An alternative possibility is that there is a critical diameter below which the reverse detonation is prohibited. But if the effective diameter is reduced asymmetrically by removing two adjacent corners at the point where transition occurs, the reverse detonation is not inhibited altogether but restricted to the two remaining corners. (fig. 4).

The most probable explanation is that the lateral rarefaction waves restrict the rapid acceleration to the central region. This will result in the wave distorting into an extremely convex

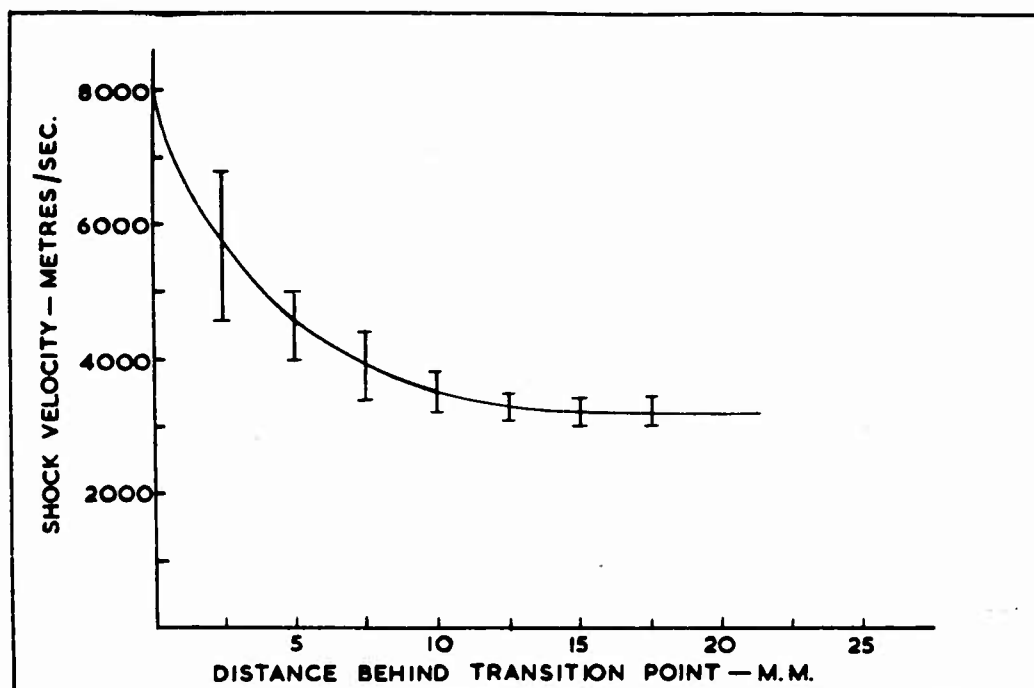


FIGURE 2

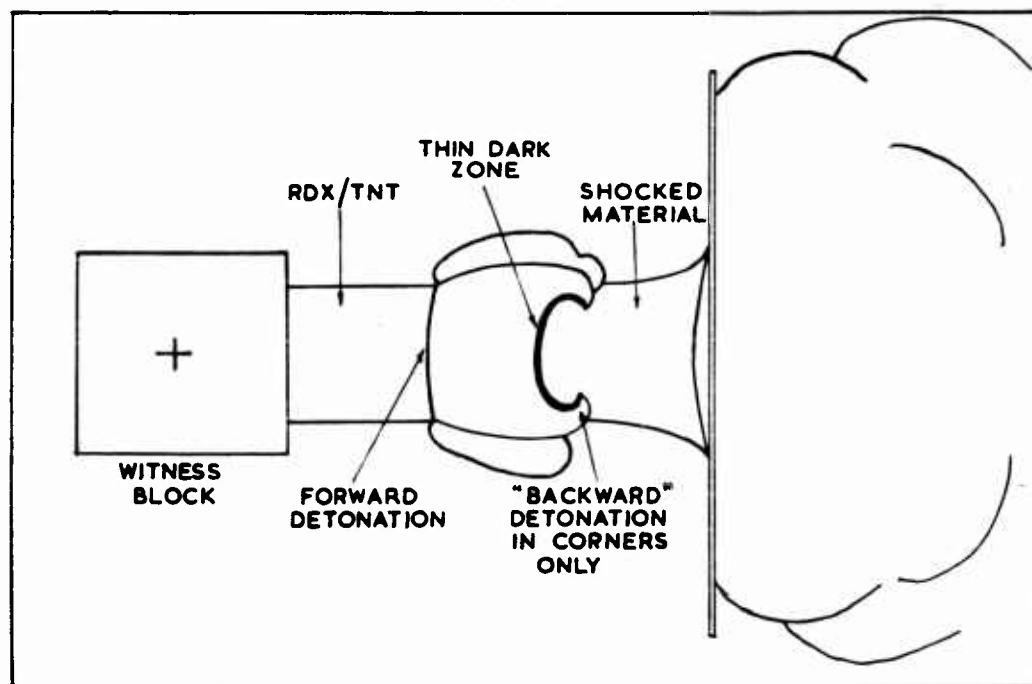


FIGURE 3



shape as transition occurs, with the result that the detonation can spread laterally into unreacted material. If the charge has a much bigger section than the central accelerating "core" the latter will not be seen at the sides until it has spread into unreacted material and a detonation is propagating in both directions. The velocities initially observed on the surface are easily explained by the geometry of such a system.

Some confirmation has been provided by an experiment in which the detonation occurs just before the end of a 50 mm square cross section charge. The detonation is seen to emerge from the centre of the end face when the shock wave in the side face is still 10 mm from the end of the charge (fig. 5). A similar result has also been obtained by Sultanoff (7).

The diameter of this accelerating "core" is, in an ideal case with rectangular pulses, the diameter at which the converging lateral rarefaction waves meet the tail of the initial pulse and will therefore be a function of charge diameter, rarefaction velocity and initial pulse length. Further work is needed to amplify this point.

#### BIBLIOGRAPHY

1. "Initiation of High Explosives" G.Hartzberg R.Walker  
Nature 161 1948 pp 647-8
2. "The Explosive Initiation of a Single Crystal of  
Cyclotrimethylene Trinitramine (RDX)" G.K. Adams J. Holden.  
E.G. Whitbread. Compte Rendu du XXXI<sup>e</sup> Congrès International  
de Chemie Industrielle - Liege Sept. 1958.
3. "The Initiation of Explosives by Shock" G.P. Cachia and  
E.G. Whitbread. Proc Roy Soc A 246 p.268 et seq.
4. "Instrumented Card-Gap or S.P.H.F. - Plate test", M.A. Cook  
D.H. Pack L.N. Cosner W.A. Gey. J. App. Phys 30 No. 10  
p.1579 et seq.
5. "The Science of High Explosives" M.A. Cook, Reinhold  
Publishing Corp. p.83-4
6. "Supersonic Flow and Shock Waves" R. Courant,  
K.O. Friedrichs. Interscience Publishers Inc. p.30.
7. "New Observations of Explosive Phenomena by Submicrosecond  
Color Photography" M. Sultanoff 85th Semi Annual Convention  
S.M.P.T.E.

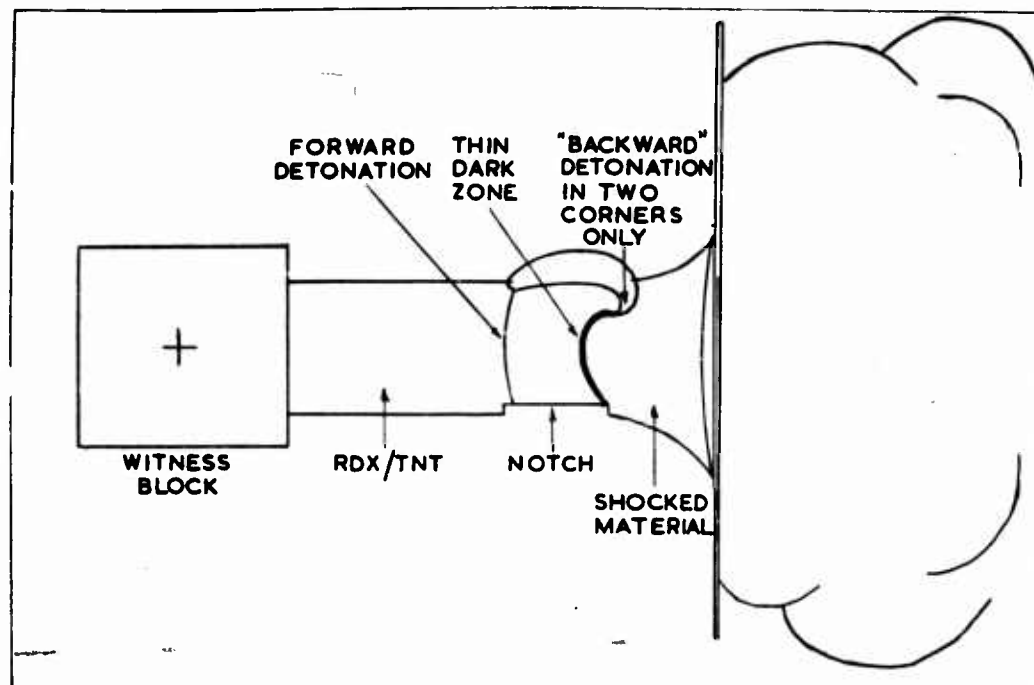


FIGURE 4

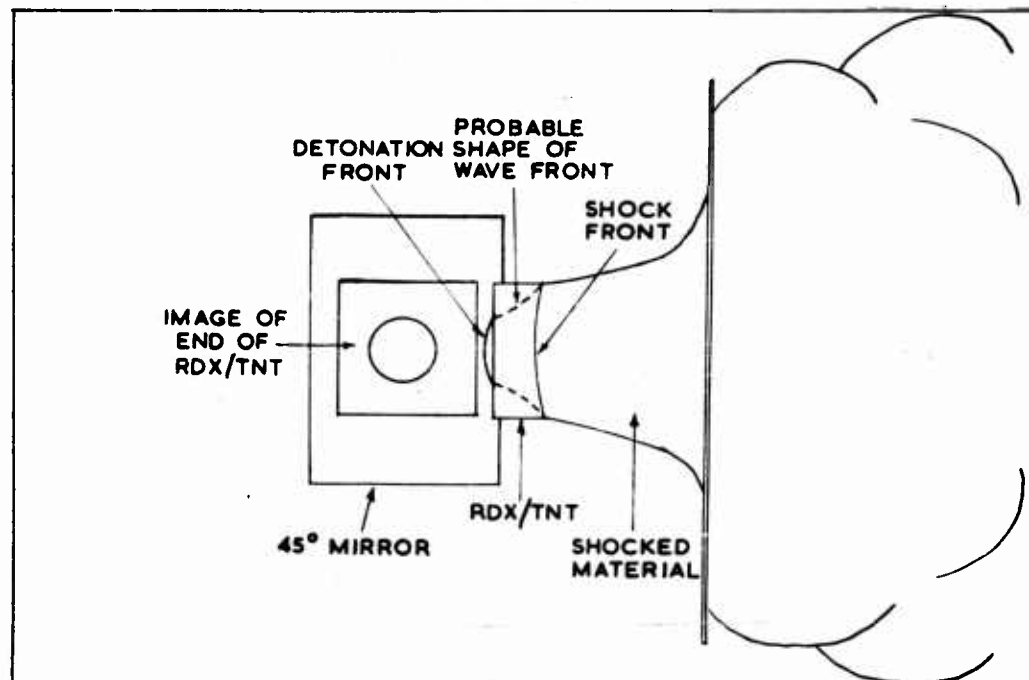


FIGURE 5

ACKNOWLEDGEMENT

The authors acknowledge with gratitude help in discussions with Mr. G.K. Adams under whose direction the work has been carried out.

ILLUSTRATION

A 16 mm film has been printed from the original high speed camera records of the experiments described.

DETERMINATION OF THE SHOCK PRESSURE  
REQUIRED TO INITIATE DETONATION OF AN ACCEPTOR  
IN THE SHOCK SENSITIVITY TEST

I. Jaffe, R. Beauregard, A. Amster  
U. S. Naval Ordnance Laboratory  
Silver Spring, Maryland

ABSTRACT: The attenuation of the velocity of a shock wave was measured in Lucite under conditions similar to those of the shock sensitivity test. Two systems, one based upon the reaction of pressure probes to the pressure pulse of the shock wave and the other a smear camera, were used to record the events. The reliability of the pressure probe in recording the events was comparable to the smear camera record of the shock for the first three inches of Lucite after which the response of the pressure probes lagged behind the camera record. With the aid of the smear camera, additional data were calculated for Lucite in the low pressure region (4-5 kbar) by measuring the shock velocity in Lucite and water. These data were used to extend the equation of state for Lucite to the region applicable to this investigation.

The shock pressure in Lucite was calculated as a function of the Lucite length from the velocity obtained experimentally and the equation of state for Lucite. This was compared to the length of the gap in the shock sensitivity tests to obtain an approximate value of the pressure required for the initiation to detonation of various explosives.

I. Introduction

Shock sensitivity tests for explosives, in which the sensitivity of an explosive is measured by interposing a gap of some inert material between a high explosive donor and the explosive under test, have been in use for a number of years. The sensitivity of the explosives were rated on an arbitrary gap scale peculiar to the conditions of the test and the inert material used for the gap. This

investigation was made to interpret the shock sensitivity test results in terms of shock pressure required to initiate the explosive. In effect, the gap distance was calibrated.

The present work was carried out on Lucite rods, since it was determined cellulose acetate (used in forming the gap) and Lucite were similar shock attenuators. The investigation consisted of extending the equation of state data of Lucite to the lower pressures in the gap and of using the data obtained to relate pressure and gap thickness for the conditions under which the gap tests are made.

The equation of state data were obtained by initiating a shock with two cylindrical tetryl pellets (each 2 inches dia. x 1 inch thick) and measuring the shock velocity as a function of distance in Lucite rods and in water (the equation of state of which is known) as it progresses from the Lucite to the water. Using the customary approximation at the Lucite-water interface, the pressure and particle velocity in Lucite before the interface may be obtained.

## II. Experimental Methods

The attenuation of the shock velocity in Lucite was determined by two different experimental techniques. One was based upon recording the passage of a pressure pulse by an electronic system, and the other used high speed photography to follow the shock front. This latter technique was used to obtain additional data to determine a more accurate curve for the equation of state of Lucite.

### A. Electronic Method Used to Measure Shock Velocity

Figure I is a schematic drawing of the experimental assembly used to measure the attenuation of a shock wave in a Lucite rod. A donor, consisting of two tetryl pellets, was initiated by a Seismo\* detonator. The detonation wave developed in the tetryl becomes a shock wave in the Lucite rod. The progress of the shock wave was followed by a series of pressure probes carefully placed in the assembly. The pressure pulse impinged on a copper tube 0.033 inches away from a copper wire. When the copper tube made contact with the copper wire, a circuit was closed and an impulse was transmitted to an oscilloscope (Tektronic No. 535). A Polaroid camera was used to make permanent records of the oscillograph tracings.

---

\* Detonators were obtained from Olin Mathieson

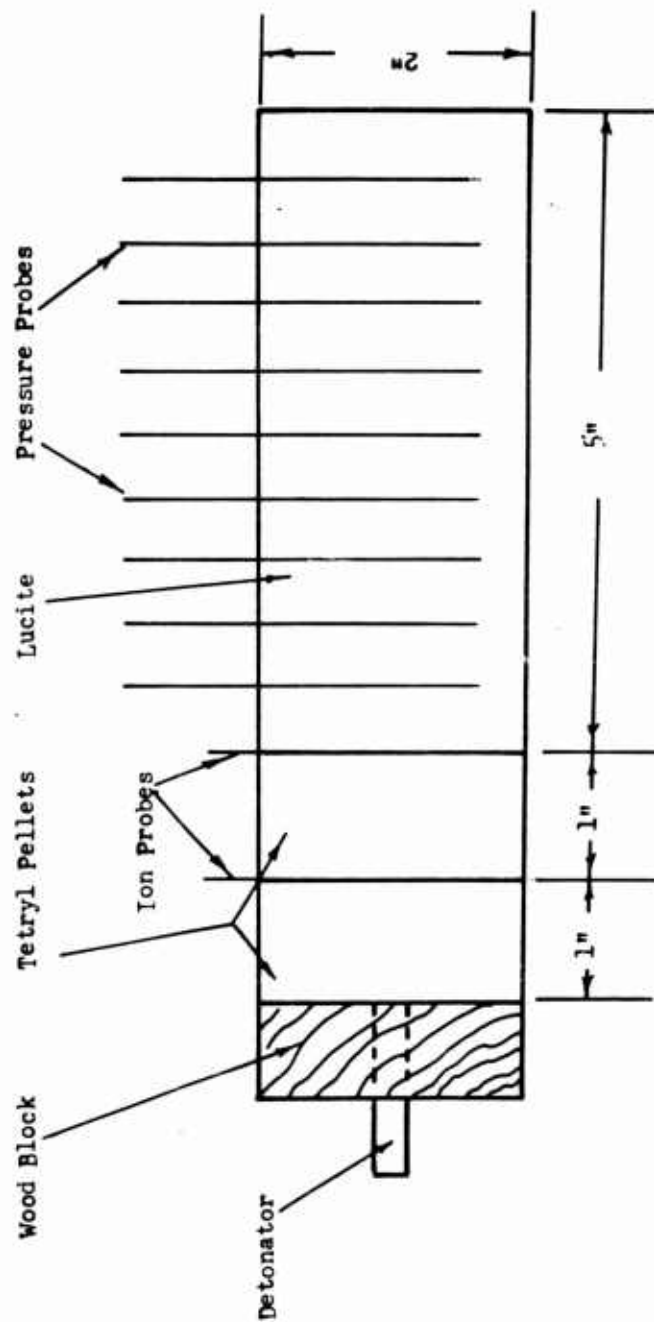


FIGURE I- Assembly for the Measurement of Shock Attenuation in Lucite

A series of holes 0.053 inches in diameter were carefully made at specified intervals in a Lucite rod. The pressure probes were inserted and the necessary leads were soldered to the probes. The tetryl pellets were securely taped to the Lucite rod. An ionization probe was inserted between the two tetryl pellets, and at the tetryl-Lucite interface. The entire ensemble was placed in the bombproof chamber where the leads were connected to the oscilloscope leads and the detonator put in place. Meanwhile a series of calibrated time marks was obtained on the oscilloscope by using a Tektronic No. 181 Time-Mark Generator. The time scale was recorded on the film just prior to the experiment.

The oscilloscope was triggered by the ionization probe placed between the two tetryl pellets. By beginning the oscilloscope sweep prior to the arrival of the detonation at the tetryl-Lucite interface, a much more definitive and precise measurement was obtained of the time of arrival of the shock in the Lucite. The arrival of the reactive shock at the tetryl-Lucite interface was recorded by the second ionization probe. The further progress of the shock wave down the Lucite rod was followed by the pressure probes. A more comprehensive discussion of the pressure probe and the electronic system used is given elsewhere (1,4).

The system contained a donor made up of two tetryl pellets, identical to those used in the shock sensitivity test at the laboratory. Cellulose acetate cards, 0.01 inches thick by 2 inches in diameter were used to build gaps less than one-half inch thick. For larger gaps, Lucite discs, one-half inch and 1 inch thick were used with the cellulose acetate cards to build the required gap. A number of charges were prepared in the exact manner used for the shock sensitivity tests and ionization probes were placed at designated positions in the Lucite-cellulose acetate gap. The gap was prepared by stacking the cards and discs in units one to two inches high. Each unit was compressed to form a compact pile and a hole was drilled in it for a pressure probe. The attenuation of the shock velocity was measured at 0.5, 1.0 and 1.5 inches and compares with the shock velocity measured in the Lucite rod.

#### B. High Speed Photography

The objects of this experiment were three-fold:

- 1) to measure the attenuation of the shock wave in Lucite by an alternate method;

2) to determine the reliability of the measurements made by the pressure probes; and

3) to obtain data which will define more precisely the equation of state of Lucite for the lower shock pressures.

Figure II is a schematic drawing which shows the arrangement of the various components. The Lucite rod was machined from a bar 2 inches x  $2\frac{1}{4}$  inches in cross section to a rod approximately  $2\frac{1}{16}$  inches in diameter with two parallel flat surfaces 2 inches apart and  $\frac{5}{8}$  inches wide. These parallel flats eliminated distortion of the light by the curved surfaces as the light passed through the Lucite rod. Pressure probes were inserted at designated points in the usual manner. The rod was supported vertically with its end submerged approximately  $\frac{1}{4}$  inch below the surface of the water contained in a small trough. A Lucite blast shield of known thickness was placed on top of the Lucite rod to prevent the products, resulting from the detonation of the tetryl pellets, from obscuring the view of the camera. Above this shield were placed the two tetryl pellets and the detonator. The ionization probe used to trigger the camera and the oscilloscope was placed at the tetryl-Lucite interface.

To record the reaction two oscilloscopes, a Tektronic No. 535 and a raster oscilloscope were used in conjunction with the smear camera. A spark was arranged to go off at the end of the reaction to provide a common point, on both the oscilloscope and the camera records, from which the time intervals could be measured and compared. The illumination for the camera was obtained from an exploding wire set behind the Lucite rod. Four experiments were performed, two using four-inch long Lucite rods and two using three-inch long Lucite rods.

### III. Results

Figure III is a typical record of the attenuation of a shock wave measured by the pressure probes in a Lucite rod using the sweep oscilloscope. The time scale is 1  $\mu$ sec per division, and can be read to  $\pm 0.5$   $\mu$ sec. The alternate positive and negative response of the pressure probes, as they were activated, made it possible to determine the position of any malfunctioning probe. Table I contains the results of the experiments performed using two tetryl pellets with the Lucite rods and the gap card units.

Of the four experiments (Expt. #5,6,7 and 8) made using the electronic system and the smear camera, only two



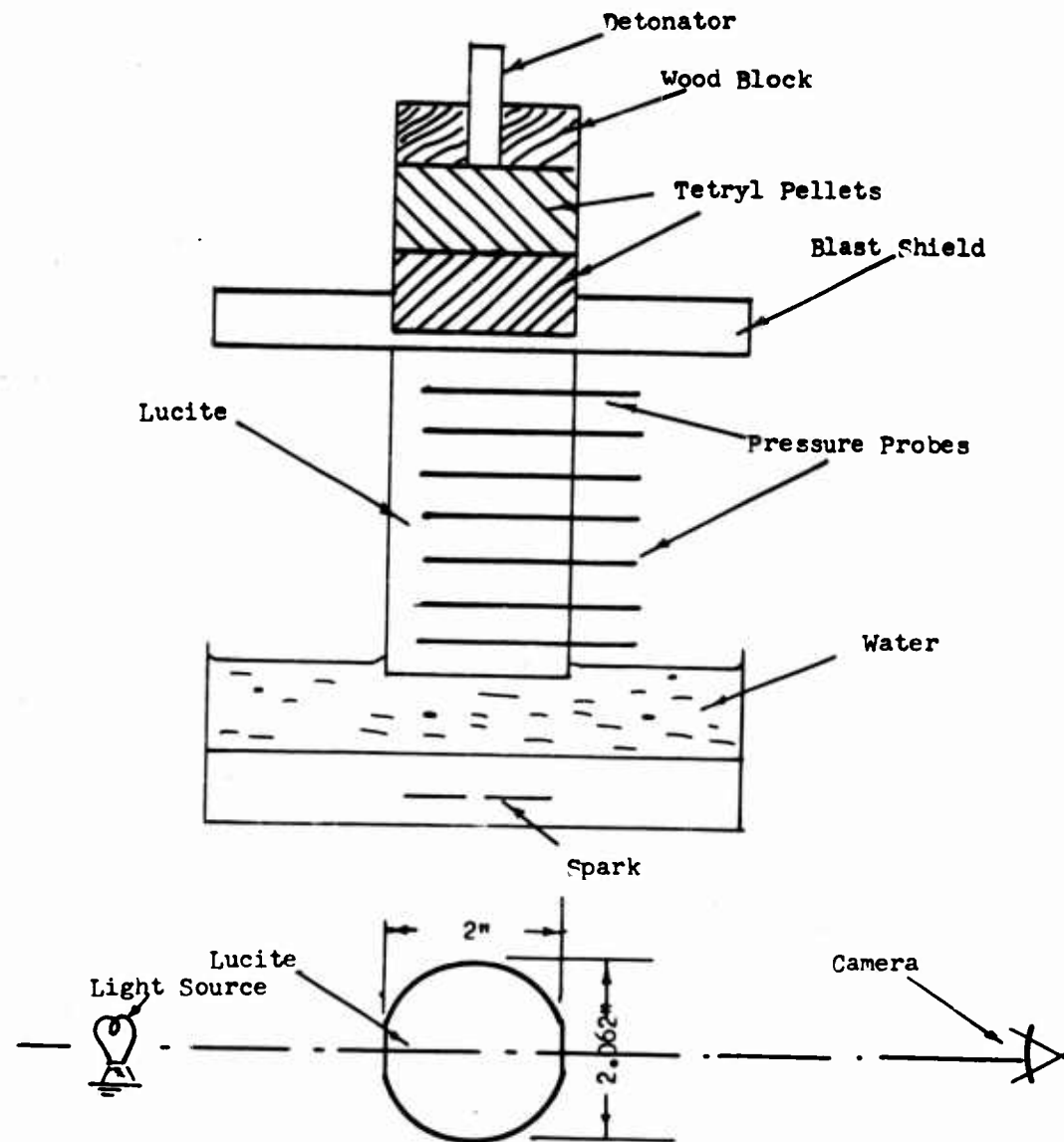


FIGURE 2- Shock Attenuation in Lucite and Water

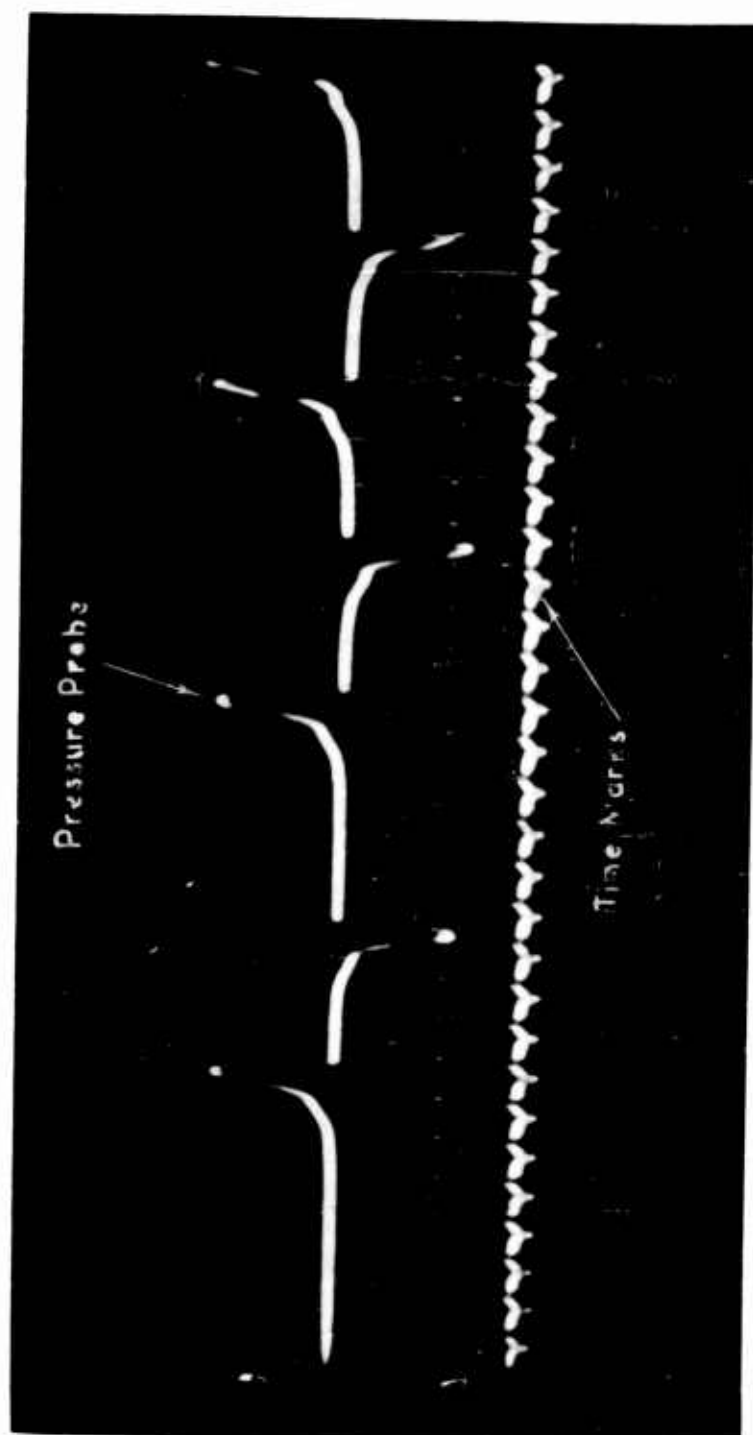


Figure 3 - Pressure probe record

TABLE I  
ATTENUATION OF SHOCK IN A LUCITE ROD (Pressure Probe)  
(Two Tetryl Pellets)

Distance of Probe		Time (Microseconds)				Mean microsec
in.	mm.	Expt.#1	Expt.#2	Expt.#3	Expt.#4	
0.5	12.7	-	-	2.5	3.0	2.8
1.0	25.4	5.2	6.0	5.5	6.2	5.7
1.5	38.1	8.6	9.6	9.2	9.5	9.2
2.0	50.8	12.0	13.5	12.8	-	12.8
2.5	63.5	16.1	17.8	17.0	17.4	17.1
3.0	76.2	20.5	-	21.1	21.4	21.0
3.5	88.9	25.1	26.5	25.2	26.0	25.7
4.0	101.6	29.7	31.0	29.6	31.1	30.4
4.5	114.3	33.7	37.0	33.7	35.5	35.0
5.0	127.0	-	-	-	-	-

ATTENUATION OF SHOCK IN GAP UNITS

0.53	13.4	2.7	-	75 - 0.01 in. acetate cards
1.00	25.4	6.1	6.0	1/2 in. Lucite disc and 75 - 0.01 in. cards
1.50	38.2	9.5	9.5	1 in. Lucite disc and 75 - 0.01 in. cards

could be used for comparison between the two systems. In experiment #7 the fiducial point was not obtained while in experiment #8 the electronic system did not respond satisfactorily. Figure IV shows the records obtained from the smear camera.

The time scale on the raster oscilloscope was 0.1 microseconds per division and could be read to  $\pm 0.02$  microseconds. The time scale for the photographic records was 1.26 mm per microsecond and could be read with a microcomparator to better than  $\pm 0.02$  microsecond. The magnification factor for the camera was determined for each experiment by measuring the distance between the probes on the film and relating this to the actual distance between probes. The same magnification factor was used to interpret distance for the shock wave in the water.

Table II contains the results obtained by the smear camera, measured from the fiducial point (spark).

#### IV. Discussion

In the hydrodynamic theory of shock waves, the conservation of momentum requires that

$$P = \rho_0 uU \quad (1)$$

where the initial pressure ( $P_0$ ) and particle velocity ( $u_0$ ) are assumed to be zero and where

$P$  = shock pressure

$\rho_0$  = initial density of the material

$u$  = particle velocity

$U$  = shock velocity.

In order to obtain the pressure at any point in a shocked homogeneous medium, it is necessary to measure the shock velocity and the particle velocity. However, if a set of data corresponding to equation (1) is known, i.e. the equation of state of the medium is known, a measurement of  $U$  vs the attenuation path length ( $X$ ) for the test geometry can be combined with the known data to give a  $P - X$  curve. Since it was desired to use the pressure probes to obtain the  $U - X$  data, their adequacy for such measurements was investigated.

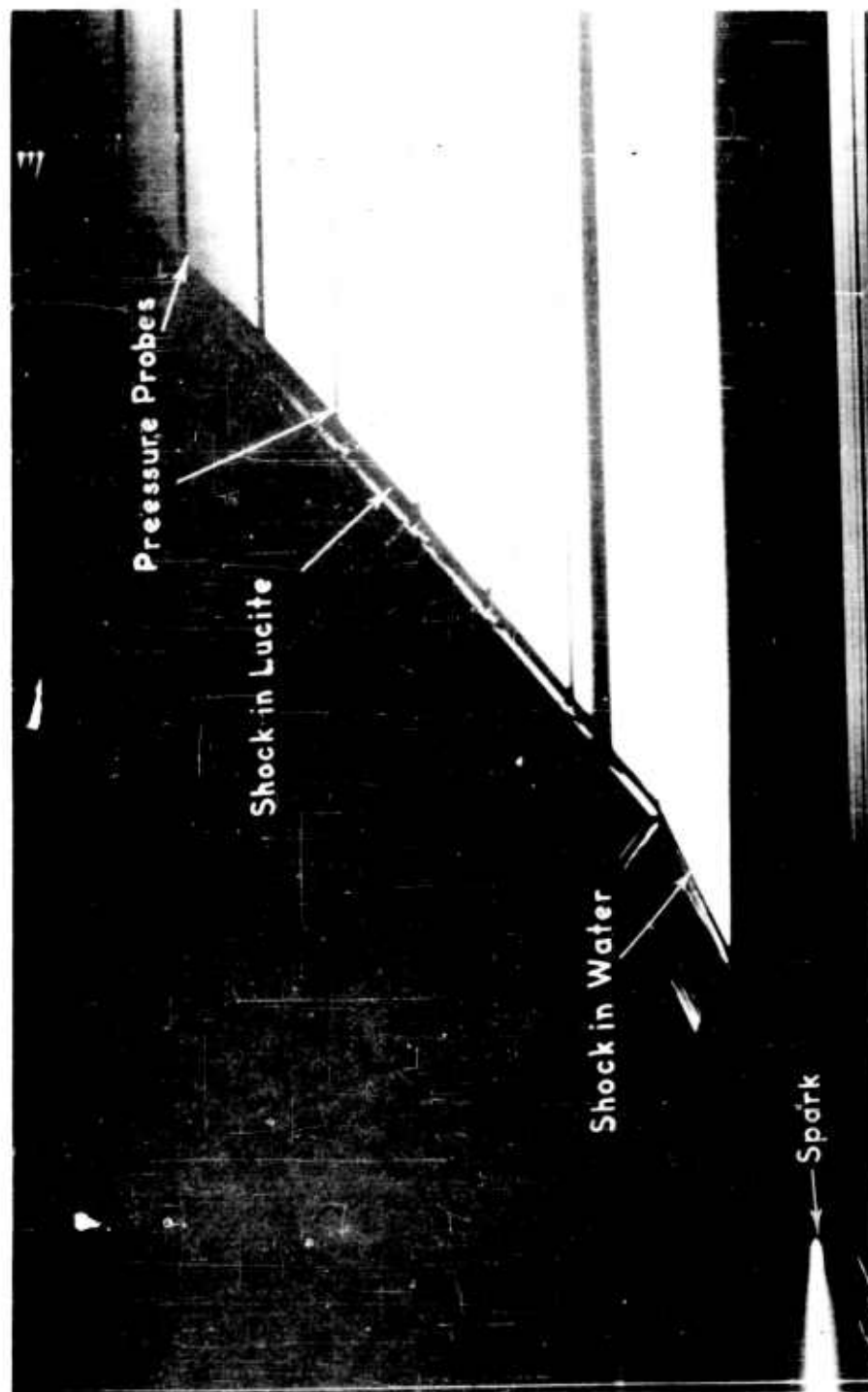


Figure 4 - Shock velocity in Lucite and water

TABLE II  
RESULTS OF EXPERIMENTS #5 AND #6 USING THE CAMERA,  
RASTER AND SWEEP OSCILLOSCOPE

Expt. #5						
Probe No.	Distance from Donor (mm)	Distance from Spark			C - S ( $\mu$ sec)	C - R ( $\mu$ sec)
		Sweep Scope S ( $\mu$ sec)	Raster Scope R ( $\mu$ sec)	Camera C ( $\mu$ sec)		
1	4.2	47.43	47.72	48.0	+ 0.6	+ 0.3
2	12.0	45.73	46.08	46.31	0.6	0.2
3	22.1	43.37	43.65	43.90	0.5	0.3
4	34.6	40.27	40.36	40.48	0.2	0.1
5	47.4	36.59	36.59	36.89	0.3	0.3
6	60.1	31.97	32.14	32.66	0.7	0.5
7	72.7	28.27	28.24	28.80	0.5	0.6
8	85.3	23.29	23.38	24.42	1.1	1.0
Spark		0	0	0		

Expt. #6						
1	4.2	46.52	47.01	-	-	-
2	12.0	45.12	45.56	44.97	- 0.1	- 0.6
3	22.1	42.32	42.77	42.77	+ 0.4	+ 0.0
4	34.6	39.25	39.61	39.61	0.4	0.0
5	47.4	35.34	35.68	35.75	0.4	0.1
6	60.1	-	-	31.74	-	-
7	72.7	26.70	27.01	27.71	0.9	0.6
8	85.3	22.50	22.74	23.56	1.1	0.8
Spark		0	0	0		

### A. Pressure Probe Reliability

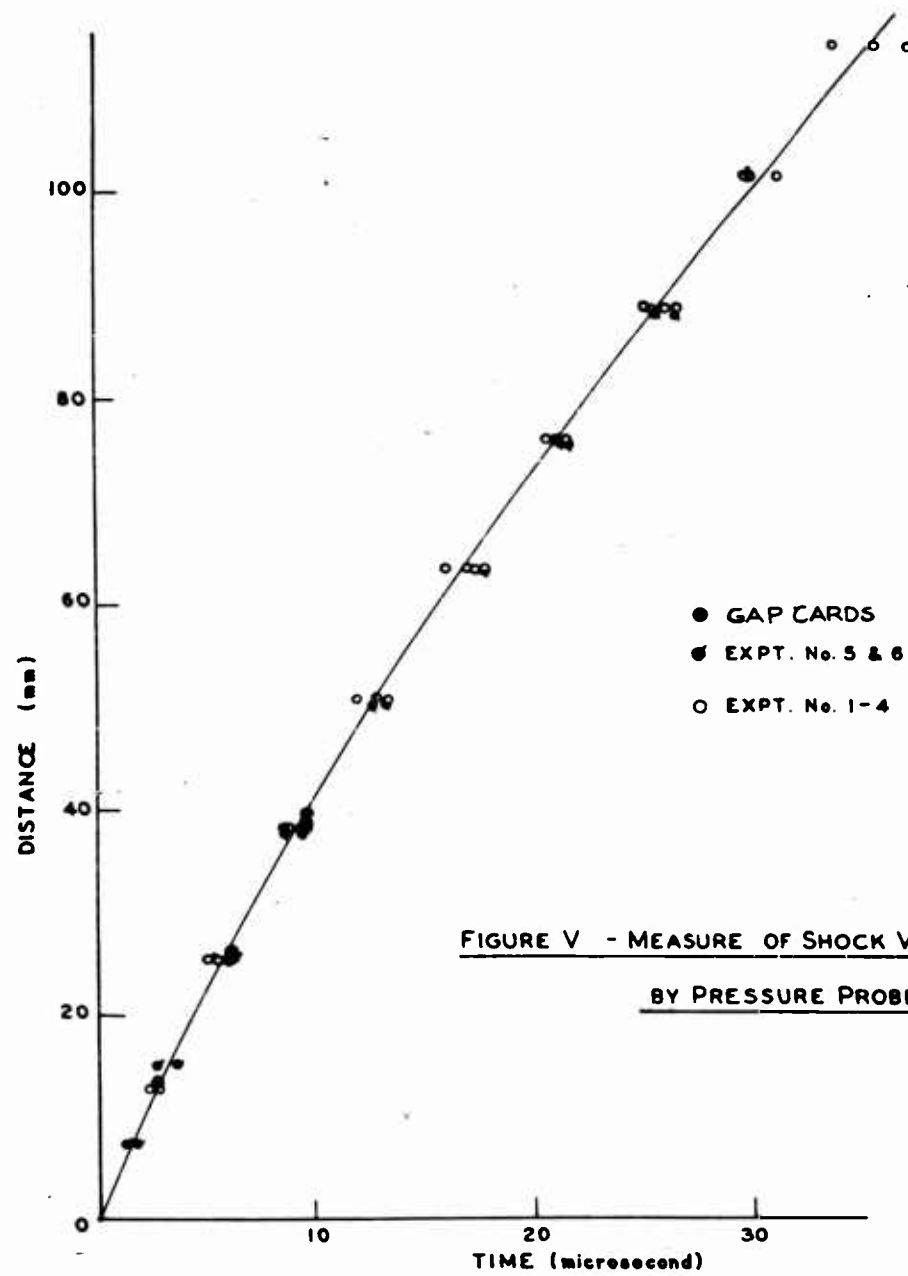
The construction of the pressure probe causes a time lag between the arrival of the shock and its recording. The distance between the bare copper wire and the outer copper tube is approximately 0.033 inches. To record the shock, the copper must travel this distance to make contact with the inner core. Moreover, the time lag should increase as the shock pressure and velocity decrease and the response of the pressure probes should fall further behind as the shock is attenuated. In Table II a comparison is made between data from the smear camera and the sweep oscilloscope (Col. 6) and between the smear camera and the raster oscilloscope (Col. 7). In all but one instance the camera did record the process before the electronic systems did. However, with the exception of probes #7 and #8, placed at a distance of 72.7 and 85.3 mm from the donor, the time lag was, on the whole, less than 0.5 microseconds. The sweep oscilloscope data were slightly higher, 0.6 microseconds.

Thus, the pressure probe may be used to interpret the shock velocity for the initial three inches of Lucite with fair accuracy and reliability. Beyond this, as the shock wave becomes more attenuated, the time lag increases. At its worst (four inches of Lucite) the divergence of the probe results from the optical results does not exceed 6%. The sensitivity of most propellants and explosives tested lie below the three inch limit. Consequently, the pressure probe measurements can be considered fairly adequate for this work.

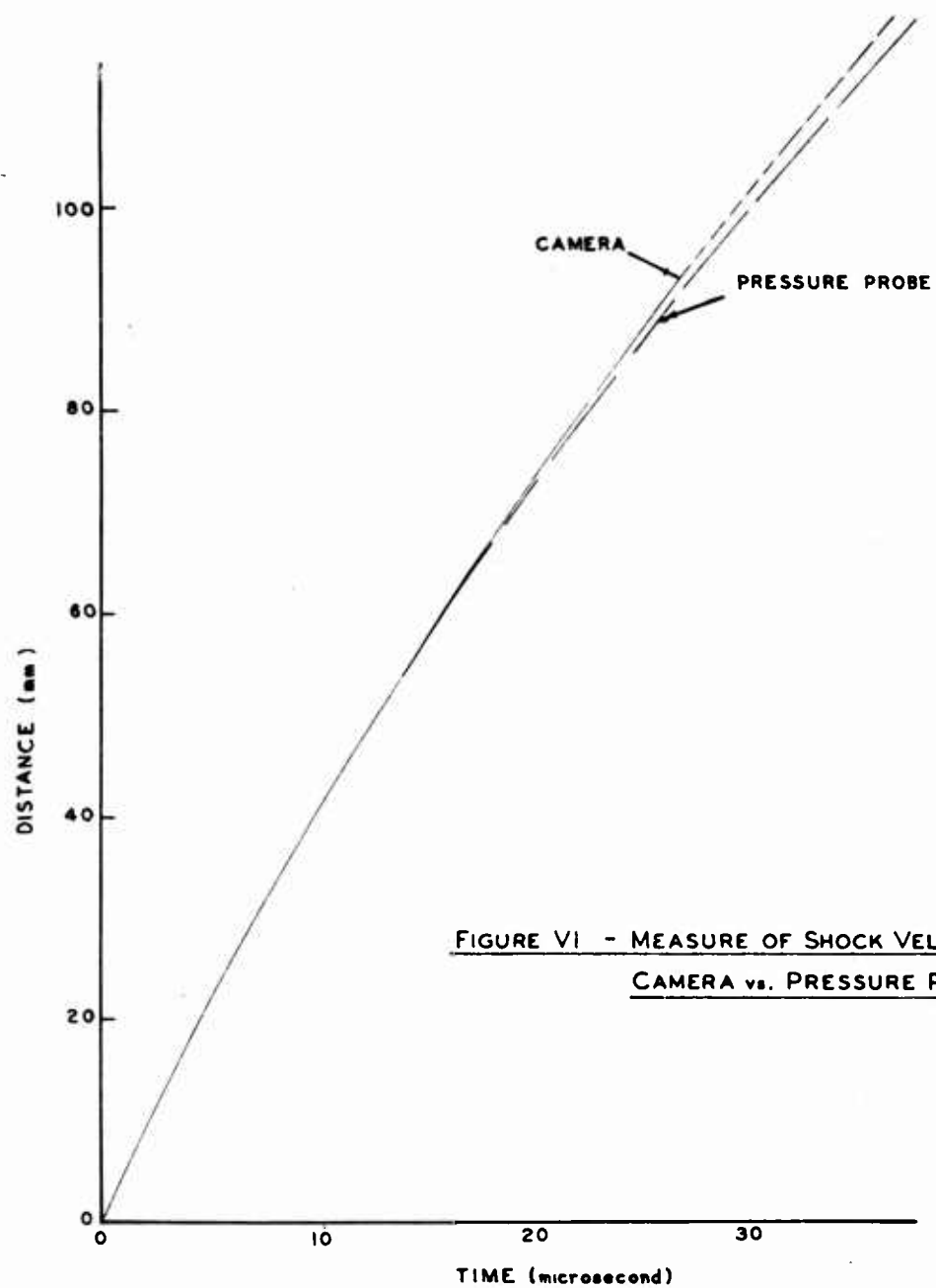
### B. Velocity vs Distance for Lucite

The results of the experiments are plotted in Figures V and VI. The data obtained with the pressure probes are plotted in Figure V. The precision of these measurements varied from a standard deviation of  $\pm 2.3\%$  to 4%. This precision includes any variation due to the probe, the position of the probe, or any variation of the Lucite or the tetryl booster. Included in this plot is the data obtained by the pressure probes placed in the gap material (see above). It is quite apparent that for the distances measured the cellulose acetate and Lucite systems are comparable.

In Figure VI, a comparison is made between the data obtained with the camera and the pressure probes. The lag of the pressure data behind the data recorded by the smear camera is quite evident after the shock was attenuated by traveling through three inches of Lucite.







## C. Pressure vs Distance for Lucite

In Figure VII the particle velocity was plotted as a function of the shock velocity from the experimental data obtained on Lucite (5), Plexiglass (6) and Perspex (7). These substances are quite similar in characteristics and it is assumed that their properties in the shock region do not differ from each other. However, the lowest shock strength obtained experimentally is at the upper end of the region critical to this investigation. Most shock sensitivity results on explosives are within the gap range of 30 to 65 mm and the maximum transmitted shock velocity obtained by the two tetryl pellets is about 4.6 mm per microsecond. The extrapolation to  $u = 0$  is difficult since the shock pressure is obtained as a product of the particle and shock velocities.

The approximate shock pressures were obtained from the usual boundary approximations (8,9),

$$\mu_L = \mu_{H_2O} \frac{(\rho_0 U)_{H_2O} + (\rho_0 U)_L}{2(\rho_0 U)_L} \quad (2)$$

where

$\mu_L$  = particle velocity in Lucite

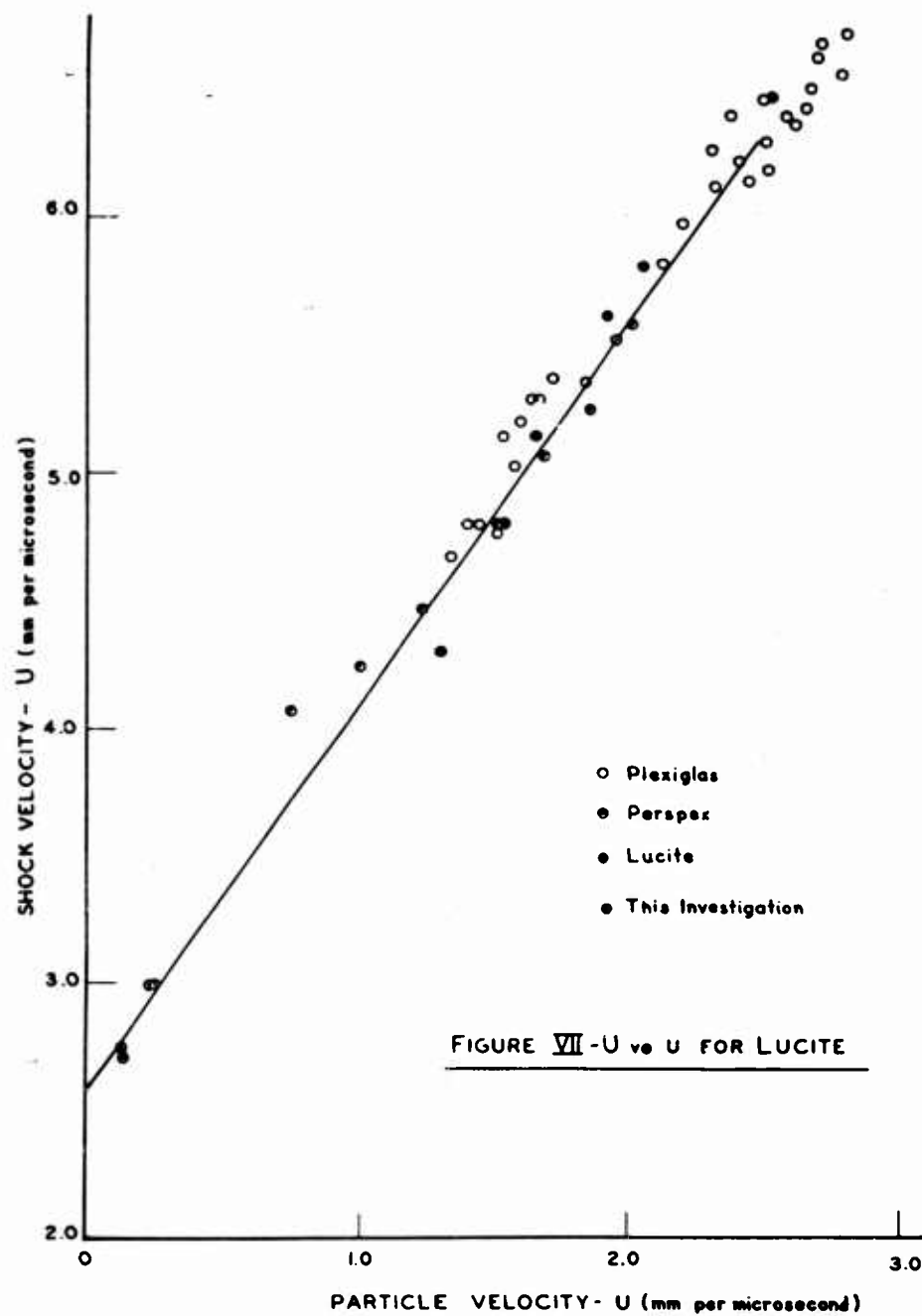
$\mu_{H_2O}$  = particle velocity in  $H_2O$

$\rho_0$  = density of Lucite or water

$U$  = shock velocity in Lucite or water

in conjunction with the experimental data obtained for the shock velocity in Lucite and water, and the particle velocity for water obtained from the literature (10). The calculated particle velocity for Lucite in Eqn. (1) yields the corresponding shock pressure.

Figure VIII is a typical plot of the results (Table II) obtained by the smear camera. The shock velocities for both Lucite and water are determined at the intersection of the respective curves which corresponds to the Lucite-water interface. Table III contains the measured shock velocities and the corresponding particle velocities calculated by Eqn. (2). Using these points for the lower pressure region and the other data already available in the higher pressure region a straight line was drawn through all the data. This curve (Fig. VII) was extrapolated to  $U = 2.59$  mm per microsecond at  $\mu = 0$ ; the



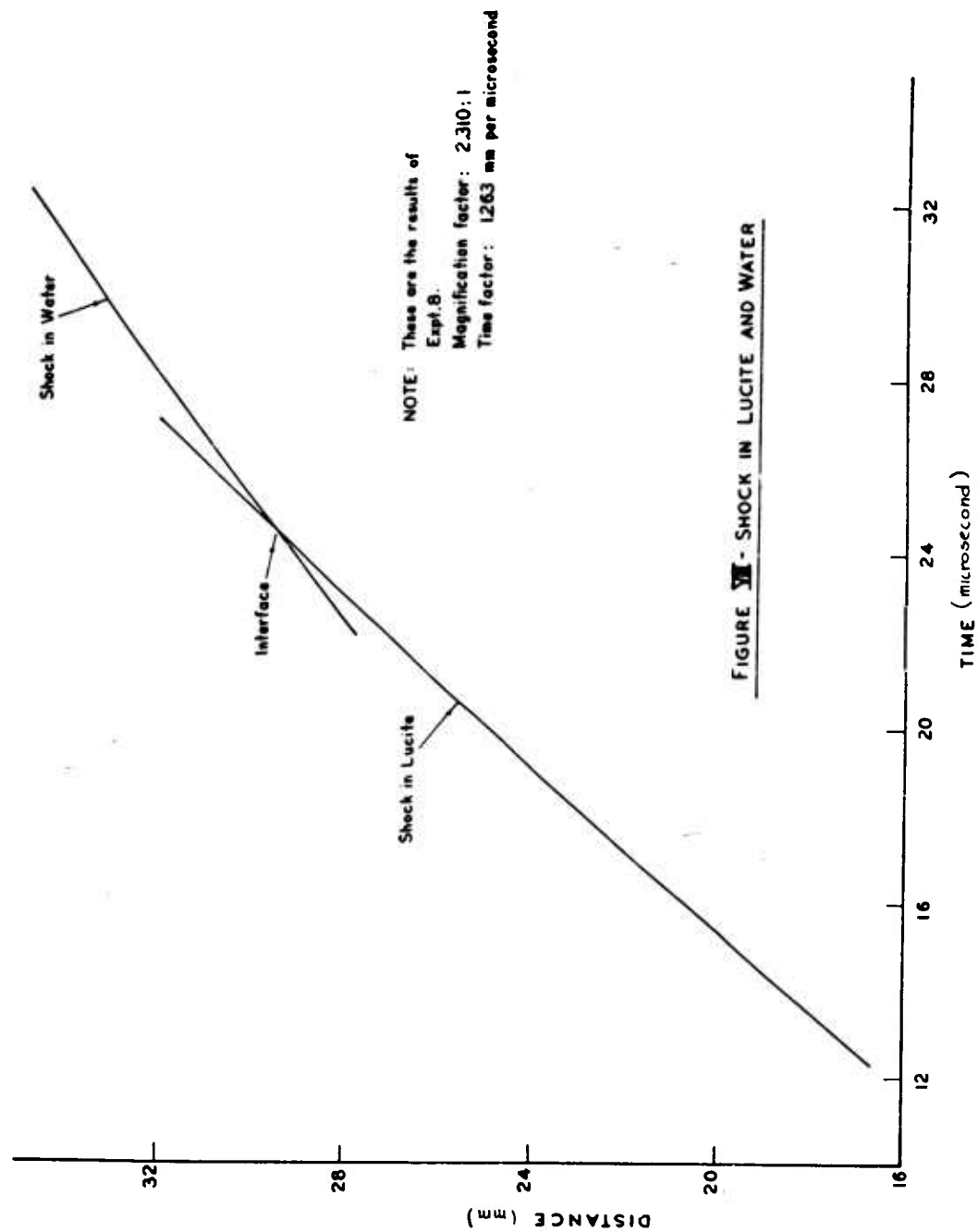


FIGURE VII - SHOCK IN LUCITE AND WATER

extrapolated value is approximately equal to the hydrodynamic sound velocity calculated as 2.44 mm per microsecond.

All the data required to develop a pressure-distance curve (P vs X) are available. From experiments 5 thru 8 a U - X curve (shock velocity vs distance, Fig. VI) was obtained for the specified geometry. In addition these experiments provided the data (Table III) required to calculate and complete the U - u curve (shock velocity vs particle velocity, Fig. VII). Using these two curves and Eqn. (1) ( $P = \rho_0 Uu$ ) it is possible to calculate P - X (pressure vs distance, Table IV) and obtain the curve in Figure IX in which the pressure appears to vary exponentially with the distance. Figure X is a plot of log P vs X and may be approximated by the equation

$$P = 105e^{-0.0358X} \quad (3)$$

These curves will allow direct interpretation of gap length in terms of shock pressure obtained at the end of the Lucite gap. While this pressure is somewhat higher than the pressure entering the acceptor because of the

---

TABLE III  
SHOCK VELOCITY IN LUCITE AND H<sub>2</sub>O, OPTICAL DATA

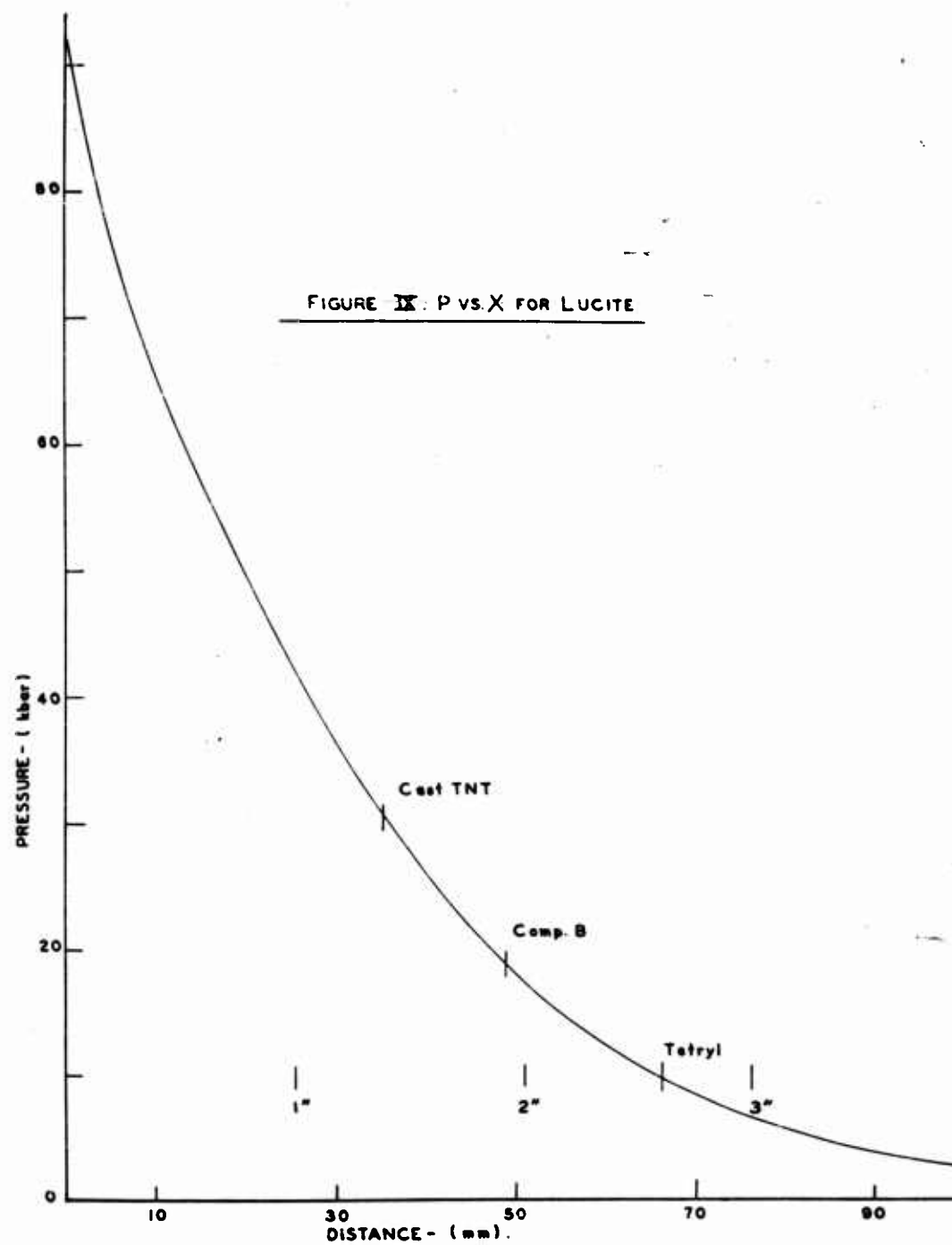
---

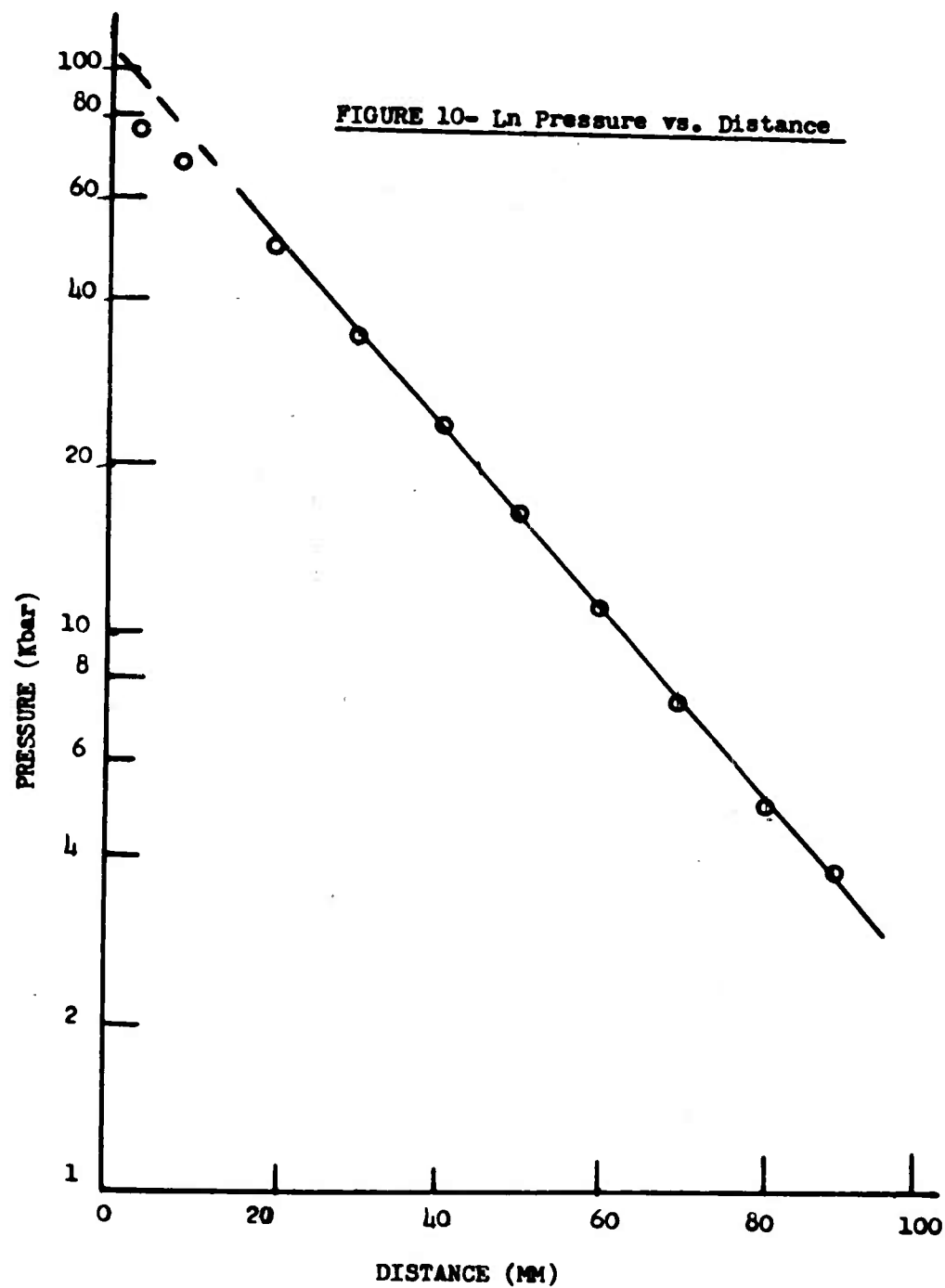
Expt.No.	Conversion Factor**	$U_L$ mm/ $\mu$ sec	$U_{H_2O}$ mm/ $\mu$ sec	$\mu_{H_2O}$ mm/ $\mu$ sec	$U_L$ (calc) mm/ $\mu$ sec
5	4.043	2.701	1.840	0.162	0.128
6	4.274	2.744	1.817	0.160	0.125
7	2.938	2.990	2.130	0.312	0.250
8	2.911	2.952	2.069	0.281	0.224

---

\*\* The conversion factor contains both the magnification factor and time factor.

---





impedance mismatch between the donor and acceptor, it is hoped that this scale of P vs X will offer additional guidance in the sensitivity work. This is especially so since the impedance of Lucite is so near the range found for most explosives. The pressures required to initiate the explosives TNT (34.5 kbar), Composition B (19 kbar) and tetryl (10 kbar) have been indicated in Figure IX.

TABLE IV  
CALCULATED PRESSURE AND DISTANCE DATA FOR LUCITE

Distance mm	Pressure Kbar
5	75.47
10	66.08
20	50.95
30	36.83
40	26.31
50	18.29
60	12.44
70	8.51
80	6.06
90	4.35
100	2.89

#### ACKNOWLEDGMENT

The authors wish to thank B. Harrell and G. Roberson for their assistance in obtaining experimental data. Also we wish to thank Dr. S. J. Jacobs, Dr. A. Macek and Dr. D. Price for the invaluable advice and criticisms offered, and B. E. Drimmer and his associates N. L. Coleburn and T. P. Liddiard for their assistance and cooperation in obtaining the necessary data for Lucite and water.



REFERENCES

1. A. B. Amster, R. L. Beauregard, G. J. Bryan, and E. K. Lawrence, NavOrd Report 5788, Detonability of Solid Propellants, I. Test Methods and Instrumentation, 3 February 1958.
2. A. B. Amster, R. L. Beauregard, and G. J. Bryan, NavOrd Report 6222, Detonability of Solid Propellants, II. Sensitivity of Some Double Base and Composite Propellants, 15 December 1958, Confidential.
3. A. B. Amster, R. L. Beauregard, G. J. Bryan, and E. K. Lawrence, NavOrd Report 6091, Current Status of the Propellant Sensitivity Program at NOL, 20 May 1958, Confidential.
4. A. B. Amster and R. L. Beauregard, Rev. Sci. Inst. 30, 942 (1959).
5. Los Alamos Scientific Laboratory, private communication.
6. N. Coleburn, Naval Ordnance Laboratory, private communication.
7. J. S. Buchanan, H. J. James, and G. W. Teague, Armament Research and Development Establishment ARDE Memorandum (MX)20/59, April 1959.
8. H. D. Mallory, NavOrd Report 1883, The Measurement of Detonation Pressures in Explosives, 5 March 1953, Confidential.
9. W. C. Holton, NavOrd Report 3968, The Detonation Pressures in Explosives as Measured by Transmitted shocks in Water, 1 December 1954, Confidential.
10. M. H. Rice and J. M. Walsh, J. Chem. Phys. 26, No. 4, 824 (1957).
11. C. B. Officer, Introduction to the Theory of Sound Transmission, McGraw-Hill Book Co., Inc., N.Y., 1958.
12. American Institute of Physics Handbook, McGraw-Hill Book Co., Inc., New York, 1957.

A COMPUTATIONAL TREATMENT OF THE TRANSITION  
FROM DEFLAGRATION TO DETONATION IN SOLIDS

C. T. Zovko and A. Macek  
U. S. Naval Ordnance Laboratory  
Silver Spring, Maryland

**ABSTRACT:** Experimental results of the study of spontaneous transition from deflagration to detonation at the Naval Ordnance Laboratory indicate that the approach to the problem can be in two stages; the first is the formation of a shock from pressure waves engendered by a confined deflagration, and the second the shock-initiation of detonation. Since a preliminary analytical treatment of the first stage, reported previously, led to promising results, a more extensive IBM-704 program has now been undertaken. Two numerical codes have been tested, a previously developed one based on the so-called "q-method" and a special one written for this program which avoids amplitude fluctuations inherent in the "q-method" and thus gives a more realistic representation of a shock wave. Representations of spontaneous shock formation obtained by the two numerical codes and by the analytical treatment are discussed and compared. The numerical methods yield the temperature as a function of time and location during growth of the shock and thus allow a study of simple chemical kinetic models. Introduction of chemical kinetics into the program gives a basis for elucidation of the second stage of the transition problem, namely shock-initiation of detonation.

While the phenomena of deflagration (slow, pressure-dependent burning) and detonation are reasonably well understood, spontaneous transition from one regime to the other is still in early exploratory stages, and it is one of the major unsolved problems in explosives technology. Gross experimental features of the phenomenon have emerged only recently (1,2,3,4,5). It appears that the onset of detonation in condensed explosives is preceded by a relatively long (up to 80  $\mu$ sec) interval of rapid burning which propagates at a fraction (1/10 to 1/5) of the steady

state detonation velocity. There is also evidence that the actual transition from rapid burning (sometimes termed "low order detonation") to steady state detonation takes place rapidly (within several microseconds) at a plane some distance ahead of the burning front.

The evidence thus far is consistent with the hypothesis that the onset of detonation is due to a shock wave which arises spontaneously as a result of deflagration, and which initiates detonation in unburnt explosive. The hypothesis was subjected to quantitative scrutiny at this Laboratory; in addition to experiments mentioned above, a preliminary theoretical treatment was carried out (6) by means of the following model:\*

A thermally initiated (slow) laminar flame progresses into a homogeneous solid explosive charge. Pressure of the hot products, because of rigid confinement, increases steeply and, in consequence, sends compression waves into unburnt explosive.

On this basis it was shown that compression waves thus formed coalesce into a shock wave within 10-15 cm from the region of thermal initiation. Since, experimentally, the typical pre-detonation distance is in the same range (6-14 cm), it appears reasonable to suppose that the theoretically computed shock is the direct cause of detonation.

While the analytical methods thus give promising results, it is very desirable to extend the treatment in two ways: first, by repeating the computation using different equation of state parameters and different shock-generating pressure pulses; and second, by calculating the energy (or temperature) as a function of time and distance. The latter computation can then, in principle, be used to study the chemical kinetics of the explosive reaction during build-up and thus elucidate the transition phenomenon. Such an extension clearly calls for machine computation. This report gives an introduction to the computational program which is now in progress.

The report consists of four parts. The first part describes the scope of the program treated so far and the equation of state used. The second and third parts describe two different numerical codes for the IBM-704 computer and compare the results from these codes with the previously obtained analytic results. The fourth part describes the shock formation, chemical kinetics and shock initiation.

---

\* Reference 6 gives the conceptual and analytical basis of the computational work described below, and it will be frequently referred to in the subsequent pages.

## SCOPE OF THE PROBLEM

## A. Hydrodynamics

As has been stated above, the approach to the problem of transition to detonation at the Naval Ordnance Laboratory has been via two stages. The first one is formation of a shock from pressure waves engendered by a confined deflagration. The second one is shock-initiation of detonation.

The shock formation problem is programmed in the following way: The difference equations for conservation of mass, momentum and energy are written down as applied to a one-dimensional flow problem. The explosive charge, which obeys an equation of state described below, is divided into  $N$  zones ( $0 < N < 500$ ). At time  $t = 0$  the pressure throughout the charge is fixed at a low but finite value ( $P(t=0) = 0.08$  kbar). At subsequent times, the near boundary is subjected to prescribed pressures increasing with time. The result is that compression waves of increasing amplitudes travel forward from the near boundary.

For a realistic description of the transition process the pressure at the near boundary must simulate the backing pressure rise in a confined deflagration. In such a case the theoretical relationship between  $P$  and  $t$ , derived in Ref. 6, is given by

$$t = K \int_{P_0}^P \frac{dP}{P(A-P)^2}, \quad (1)$$

where  $K$  and  $A$  are constants; at low pressures this is sufficiently well approximated by the exponential  $P = P_0 e^{kt}$  where  $P_0$  (i.e. pressure at  $t=0$ ) and  $k$  are experimental parameters. The exponential form, which was used previously in the analytical treatment, is used also in the machine computations. However, an indefinitely long exponential pressure increase would be unrealistic, because it would lead to unreasonably high pressures as well as to extremely high values of  $dP/dt$ . In reality, such a situation does not occur; rather, the pressure will increase until the confinement is broken and then decrease. As a crude simulation of such behavior the pressure in the computation is allowed to increase exponentially until about 10 microseconds after the estimated bursting pressure of the steel casing has been attained; thereafter, the pressure is assumed constant. The last stipulation may be at least partly justified if one assumes that the actual pressure decrease is relatively slow; it appears rather more

realistic than the other extreme, namely a discontinuous pressure drop to zero, which would cause too rapid a rear-rarefaction to set in. Thus the assumed near boundary condition is

$$\begin{aligned} P &= P_0 e^{kt} & t &\leq t(P_{\max}) \\ P &= P_{\max} & t &\geq t(P_{\max}) \end{aligned}$$

Hydrodynamically, the problem of coalescence of compression waves into a shock can be divided in two parts. In the first part the compression is isentropic and the flow is simple. The compression energy is  $E_s$  and the temperature attained,  $T_s$ , is given by  $T_s - T_0 = \frac{E_s}{C_v}$ , where  $C_v$  is heat capacity of the explosive and  $T_0$  the ambient temperature. This part was treated analytically in Ref. 6 by the method of characteristics. The method, in fact, is valid only for such simple flow (i.e. no shocks); it does not give a basis for further calculation; in particular, it cannot show where and when the shock becomes strong enough to initiate detonation.

The second part of the problem starts with the overlap of simple waves. The flow then ceases to be simple and there is an increase of entropy across the compression wave. As  $P$  and  $dP/dt$  at the near boundary increase, shock compression conditions, described by the Rankine-Hugoniot relations, may ultimately be reached at the front of the disturbance. Since the most important part of the problem is expected to be the region of shock formation, i.e. region intermediate between simple flow and shock conditions, a parameter  $\zeta$ , which measures the extent of shock nature is hereby defined such that

$$0 < \zeta = \frac{E - E_I}{E_H - E_I} < 1 \quad (2)$$

Here  $E$ ,  $E_I$  and  $E_H$  are actual (computed), isentropic and shock (Hugoniot) compression energies respectively, corresponding to a given pressure. (Since simple flow is isentropic ( $\Delta S=0$ ), an alternative parameter,  $0 < \zeta' =$

$\frac{\Delta S}{S_H} < 1$ , could be defined to measure the extent of shock nature). The two parts of the hydrodynamic problem are thus characterized by  $\zeta=0$  and  $\zeta>0$  respectively; the upper limit of the parameter,  $\zeta=1$ , corresponds to a full grown shock.

While in a condensed medium the difference, for a given pressure, in energy (and consequently in temperature) between the two modes of compression characterized by the extreme values of  $\zeta$  will not be large, the difference in chemical reaction rates should be quite considerable and may mean a difference between failure and initiation of detonation. Hence it is convenient that, in addition to pressure, another parameter specifying the energy be known.  $\zeta$  has been chosen because it gives a direct indication of deviation from simple flow conditions.

### B. Equation of State

A generalized Tait equation of state has been chosen to represent the solid explosive

$$(P + B) V - (P_0 + B) V_0 = (\gamma - 1) (E - E_0) \quad (3)$$

With appropriate values of the constants B, and  $\gamma$ , the equation gives a remarkably realistic representation of the compression of solid explosives over a wide range of pressures\*. Combined with the isentropic condition,

$$dE = -PdV, \quad (4)$$

the equation reduces to the form used in Ref. 6 (which does not include the energy):

$$P = \frac{B}{\gamma} \left( \left( \frac{V_0}{V} \right)^\gamma - 1 \right) \quad (5)$$

Explicit equations relating the various properties for isentropic compression and for shock compression on the basis of Eqn. 3 are collected in Table I.

The arbitrary parameters chosen in Ref. 6 were B = 105 kbar,  $\gamma = 3$ . The choice deserves a comment.

If Eqn. (3) is to be fitted to a set of data in a certain range of pressures, the constants B and  $\gamma$  can, in general, be assigned any convenient values. If, however, the lower limit of the range is  $P = 0$ , by virtue of the relation

$$c = v \sqrt{-\left(\frac{\partial P}{\partial v}\right)_s} = \sqrt{v(\gamma P + B)}, \quad (6)$$

---

\* The authors are indebted to Dr. S. J. Jacobs for having pointed out the promising possibilities of this extremely simple equation.

TABLE I  
SUMMARY OF ISENTROPIC AND HUGONIOT FORMS OF THE EQUATION OF STATE  
USED IN THIS REPORT

The equation of state in its ordinary form is

$$(P + B) V - (P_0 + B) V_0 = (\gamma - 1) (E - E_0).$$

<u>Isentropic</u>	<u>Hugoniot</u>
$V = V_0 \left( \frac{\gamma P_0 + B}{\gamma P + B} \right)^{\frac{1}{\gamma}}$	$V = V_0 - \frac{2V_0(P - P_0)}{(\gamma + 1)P + 2B + (\gamma - 1)P_0}$
$E - E_0 = \frac{V_0}{\gamma - 1} \left( (P + B) \frac{\gamma P_0 + B}{\gamma P + B} - (P_0 + B) \right)$	$E - E_0 = \frac{V_0 (P^2 - P_0^2)}{(\gamma + 1)P + (\gamma - 1)P_0 + 2B}$

the value of  $B$  is fixed by

$$B = \frac{C_0^2}{V_0} \quad (6')$$

This is certainly the case in the shock formation problem, where in the early stages of shock growth, the pressure is quite low. The value  $B = 105$  kbar used in Ref. 6 corresponds to an initial sonic velocity  $C_0 = 2.56$  mm/ $\mu$ sec, which is an average of the range of 2.25 - 2.85 mm/ $\mu$ sec found by Majowicz (7) for a series of explosives. Thus the value of this parameter is realistic.

There is no doubt that the value of  $\gamma = 3$ , used in Ref 6 (and by some earlier workers), is too low, because it gives an unrealistically high compressibility. The reason why the value has been used at all is twofold. First, it is a carry-over from calculations of high pressure gases, such as detonation products, in which the Eqn. 3 with  $B = 0$  and  $\gamma \approx 3$  gives reasonable results. Second, and perhaps more important, the choice of  $\gamma = 3$  lends convenient tractability to hydrodynamic equations. In particular, it allows the boundary path in the shock formation problem to be evaluated in closed form (see Ref. 8); this would be impossible for any value  $\gamma > 3$  (and probably for most non-integral values).

Figure 1 shows a comparison of the computed  $P - V$  relation for two different sets of parameters  $B$  and  $\gamma$  as well as experimental data of Majowicz and Jacobs (9). The high compressibility of a hypothetical material for which  $\gamma = 3$  is evident. The value of  $\gamma = 4.5$ , on the other hand (combined with  $B = 100$  kbar) is very realistic, and it is the current choice for the machine computations. However, since the analytical treatment exists (Ref. 6) in which the first set of values was used ( $\gamma = 3$ ,  $B = 105$ ), the preliminary computations discussed below, were run with this set of parameters for the sake of comparison.

The sonic velocity, corresponding to  $B = 100$  kbar, is 2.5 mm/ $\mu$ sec, a most reasonable value.

#### NUMERICAL SOLUTION OF HYDRODYNAMIC PROBLEMS (GENERAL)

The general hydrodynamic problem is a solution of the equations of motion, state and energy release subject to appropriate boundary conditions. The equations of motion for a one dimensional case are

$$\rho_0 \frac{\partial u}{\partial t} = - \frac{\partial P}{\partial x} \quad (\text{conservation of momentum}) \quad (7)$$



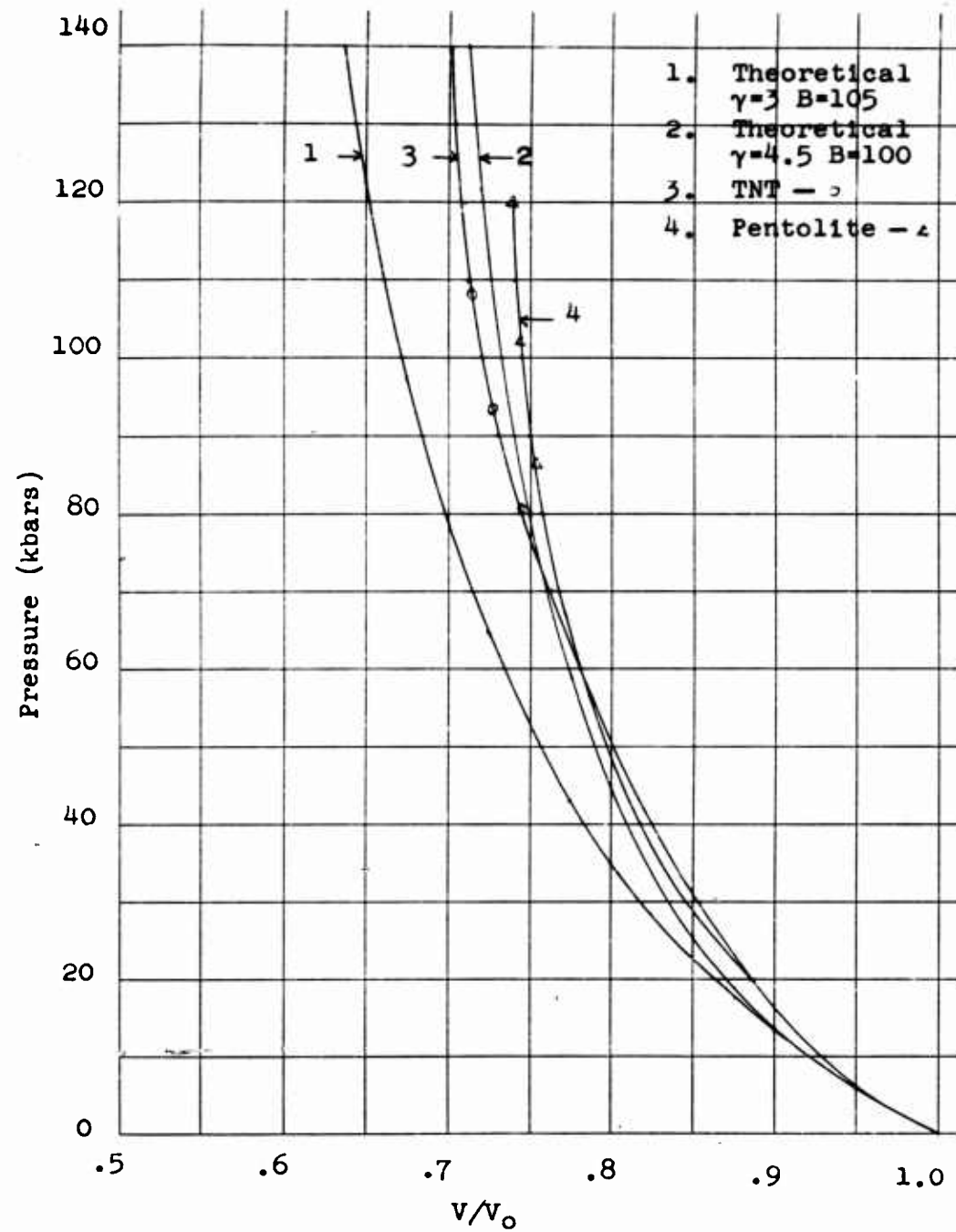


FIGURE 1 - Experimental and Theoretical Hugoniot Curves for Unreactive Explosives

$$\frac{\partial E}{\partial t} - \frac{\partial Q}{\partial t} + P \frac{\partial V}{\partial t} = 0 \quad (\text{conservation of energy}) \quad (8)$$

$$\text{and } \rho_0 \frac{\partial V}{\partial t} = \frac{\partial u}{\partial x} \quad (\text{conservation of mass}), \quad (9)$$

where

- $t$  = time
- $\rho_0$  = initial density
- $u$  = particle velocity
- $P$  = pressure
- $E$  = specific internal energy
- $Q$  = heat added per unit mass (from chemical reaction)
- $V$  = specific volume
- $X$  = distance
- $x$  = Lagrange coordinate defined by the relation

$$\frac{\partial X(x,t)}{\partial x} = \rho_0 V(x,t) .$$

The equation of state is

$$P = \Phi(E,V) . \quad (10)$$

The equation of chemical energy release is

$$\frac{\partial Q}{\partial t} = R(Q,E,V) . \quad (11)$$

One way to obtain a solution is by numerical techniques. This consists of dividing the Lagrange space coordinate ( $x$ ) into a number of equal zones and approximating the differentials in equations 7, 8, 9 and 11 by finite difference ratios. In the difference equations, the dependent variables are usually specified at the interfaces between the zones or at the centers of the zones.

The boundary conditions must specify the values of the dependent variables for all values of the Lagrangian space coordinate ( $x$ ) at time zero and for the end points ( $x = 0$  and  $x = x_{\max}$ ) at all times. Once the boundary conditions are specified the difference equations can then be solved to obtain the values of the variables at the interior points.

Most differencing schemes have the limitation that they cannot handle discontinuities. The equations of motion (Eqns. 7, 8 and 9) admit discontinuous solutions; in fact, the discontinuities are the most interesting parts of the solutions. Two methods of overcoming this difficulty will be discussed in the next section.

The time increment ( $\Delta t$ ) used cannot be chosen arbitrarily. A stability analysis (Ref. 10) of the problem will yield a maximum value of  $\Delta t$  with which reasonable results can be obtained. Stability analysis is an analysis of the history of an arbitrarily introduced error. Usually a critical value of  $\Delta t$  will be determined such that if  $\Delta t$  were to be made larger than this critical value, the error will increase, if  $\Delta t$  were to be made smaller than this critical value, the error will decrease and if  $\Delta t$  is made equal to this critical value the error will remain constant.

#### TWO SPECIFIC METHODS OF OBTAINING NUMERICAL SOLUTIONS TO HYDRODYNAMIC PROBLEMS

Two methods of handling discontinuities will be discussed in this section. They are the Richtmyer-von Neumann "q" method (Ref. 11) and the Lax method (Ref. 12). In both methods discontinuities are approximated by steep but finite slopes.

The "q" method eliminates discontinuities by the inclusion of an artificial dissipative term. Physically it can be considered as a one-dimensional viscosity. This dissipative term "q" is defined by the equation

$$q = - \frac{(K \Delta x)^2}{V} \cdot \frac{\partial u}{\partial x} \cdot \left| \frac{\partial u}{\partial x} \right|, \quad (12)$$

where  $K \Delta x$  = arbitrary constant.\*  $K \Delta x$  is approximately  $1/3$  the distance over which the shock is spread.

The term "q" is added to the pressure (P) and Eqns. (7) and (8) became respectively,

$$\rho_0 \frac{\partial u}{\partial t} = - \frac{\partial}{\partial x} (P + q) \quad \text{and} \quad (13)$$

$$\frac{\partial E}{\partial t} - \frac{\partial Q}{\partial t} + (P + q) \frac{\partial V}{\partial t} = 0 \quad (14)$$

Equation (9), which does not contain pressure, is unchanged.

The resultant set of equations (Eqns. (9), (10), (11), (13) and (14) do not have discontinuous solutions. The solutions of the modified equations and the original equations are very nearly the same except in regions where the solution of the original equations would have a discontinuity. Equations (9), (10), (11), (13) and (14) approximate the discontinuity by a smooth but steep curve.

The Hugoniot relation across a shock,

$$E_f - E_i = \frac{1}{2} (P_i + P_f) (V_i - V_f) \quad , \quad (15)$$

is not affected by the inclusion of q.

Thus the "q" method is successful in that it eliminates discontinuities and gives a good approximation to the true solution in every aspect except details of the shock.

A computer (IBM 704) program which utilizes the "q" method and a second order differencing scheme was constructed at the Naval Ordnance Laboratory by W. Walker. Some results from this code will be discussed in the next section.

Another method for handling the problem of discontinuities was devised by Lax (Ref. 12). While the "q" method involves a quasi-physical concept and a modification of the equations of motion, the Lax method does neither. Rather, it handles discontinuities by the nature of its unusual differencing scheme. The Lax scheme

---

\* Considering the arbitrary constant as the product of K and  $\Delta x$  is superfluous at this stage of the discussion. However, when the differential equations are replaced by finite difference equations the  $\Delta x$  mentioned above and the  $\Delta x$  used as the increment of the independent variable are identical. K is a dimensionless constant usually near unity.

requires that all of the differential equations be in perfect differential form, i.e.

$$A \frac{\partial Y}{\partial t} = \frac{\partial Z}{\partial x}, \quad (16)$$

where A is a constant. This differential equation is then differenced in the following way

$$\begin{aligned} \frac{A}{\Delta t} \left( Y_x^{t+\Delta t} - \frac{1}{2} (Y_{x+\Delta x}^t + Y_{x-\Delta x}^t) \right) \\ = \frac{1}{2\Delta x} (Z_{x+\Delta x}^t - Z_{x-\Delta x}^t) \end{aligned} \quad (17)$$

In so-called normal regions where  $\frac{\partial^2 Y}{\partial x^2}$  is small,

$$\frac{1}{2} (Y_{x+\Delta x}^t + Y_{x-\Delta x}^t) \approx Y_x^t \quad (18)$$

In this case the Lax difference scheme approaches an ordinary forward difference scheme. Therefore, in normal regions, the solution obtained by the Lax scheme approaches the analytic solution.

In regions where  $\frac{\partial^2 Y}{\partial x^2}$  is high (at shocks) Eqn. (18)

is not valid and the Lax scheme comes into effect. It causes any discontinuities (or other extreme changes) to be replaced by a steep but smooth change.

As mentioned earlier, the equations of motion must be in perfect differential form if the Lax scheme is to be used. The equations of conservation of mass (Eqn. (9)) and momentum (Eqn. (7)) and the equation of chemical energy release (Eqn. (11)) are already in perfect differential form. A fourth, independent, perfect differential equation must be constructed. This can be done by multiplying Eqn. (7) by  $u$ , Eqn. (8) by  $\rho_0$  and Eqn. (9) by  $-P$  and adding the results

$$\begin{aligned} \rho_0 \left( u \frac{\partial u}{\partial t} + \frac{\partial E}{\partial t} - \frac{\partial Q}{\partial t} + P \frac{\partial V}{\partial t} - P \frac{\partial V}{\partial t} \right) \\ = -u \frac{\partial P}{\partial x} - P \frac{\partial u}{\partial x} \end{aligned} \quad (19)$$

Simplifying;

$$\rho_0 \frac{\partial}{\partial t} \left( \frac{1}{2} u^2 + E - Q \right) = - \frac{\partial}{\partial x} (Pu) \quad (20)$$

One of the results of this task is a computer (IBM 704) program to solve hydrodynamic problems by the Lax method. Appendix I gives a description of this program.

#### Comparison of Analytic, "q" and Lax Methods

The general hydrodynamic problem solved numerically by the "q" and Lax methods as described above, will now be compared to the previously obtained analytic solution (6). The same equation of state and boundary conditions were used in all three calculations. Equation (3) was used as the equation of state. It was assumed that no reaction took place so  $Q(x,t)$  was set equal to zero.

The following boundary conditions were used in all three calculations

$$P(0,t) = P(0,0) e^{kt} \quad \text{for } t \leq 60 \mu\text{sec};$$

$$k = .1 \mu\text{sec}^{-1}$$

$$P(0,t) = P(0,60) \quad \text{for } t \geq 60 \mu\text{sec};$$

$$P(x_{\text{max}},t) = P(0,0)$$

$$P(x,0) = P(0,0)$$

$$u(x,0) = 0$$

$$P(0,0) = .08 \text{ kbars}$$

$V(x,0) = .6245 \text{ cc/gm}$  and  $E(x,0) = 2 \times 10^4 \text{ ergs/gm}$  were the values calculated for an adiabatic compression from .001 to .08 kbars. These boundary conditions approximate the boundary conditions realized in the experimental work.

Figure 2 compares the  $P - X$  plots at  $66 \mu\text{sec}$  obtained from the analytic, "q" and Lax methods. Except for fluctuations in the plateau, the "q" method agrees more closely with the analytic method than does the Lax method.

Figure 3 compares  $P - X$  plots at  $100 \mu\text{sec}$  obtained from the "q" and Lax methods. At this time a real solution would have a discontinuity extending slightly below the plateau. The "q" method gives a somewhat closer approximation to this discontinuity than does the Lax method. However, the "q" method gives severe fluctuations in the plateau, while the Lax method gives none.

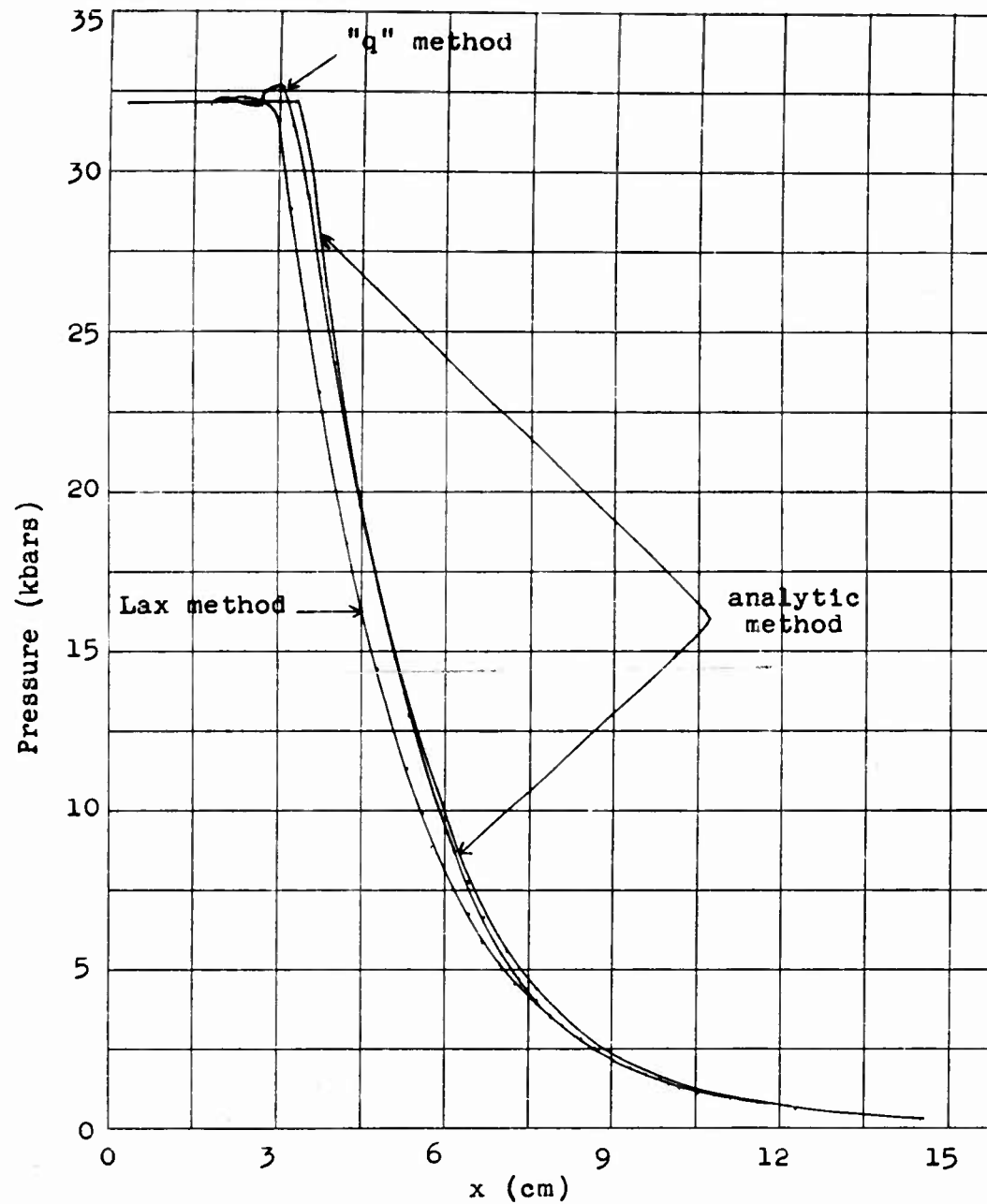


FIGURE 2

Pressure-Distance Profiles as Computed by the  
Lax, "q" and Analytic Methods

The time of the computation is 66.1  $\mu$ sec after  
the first application of pressure.

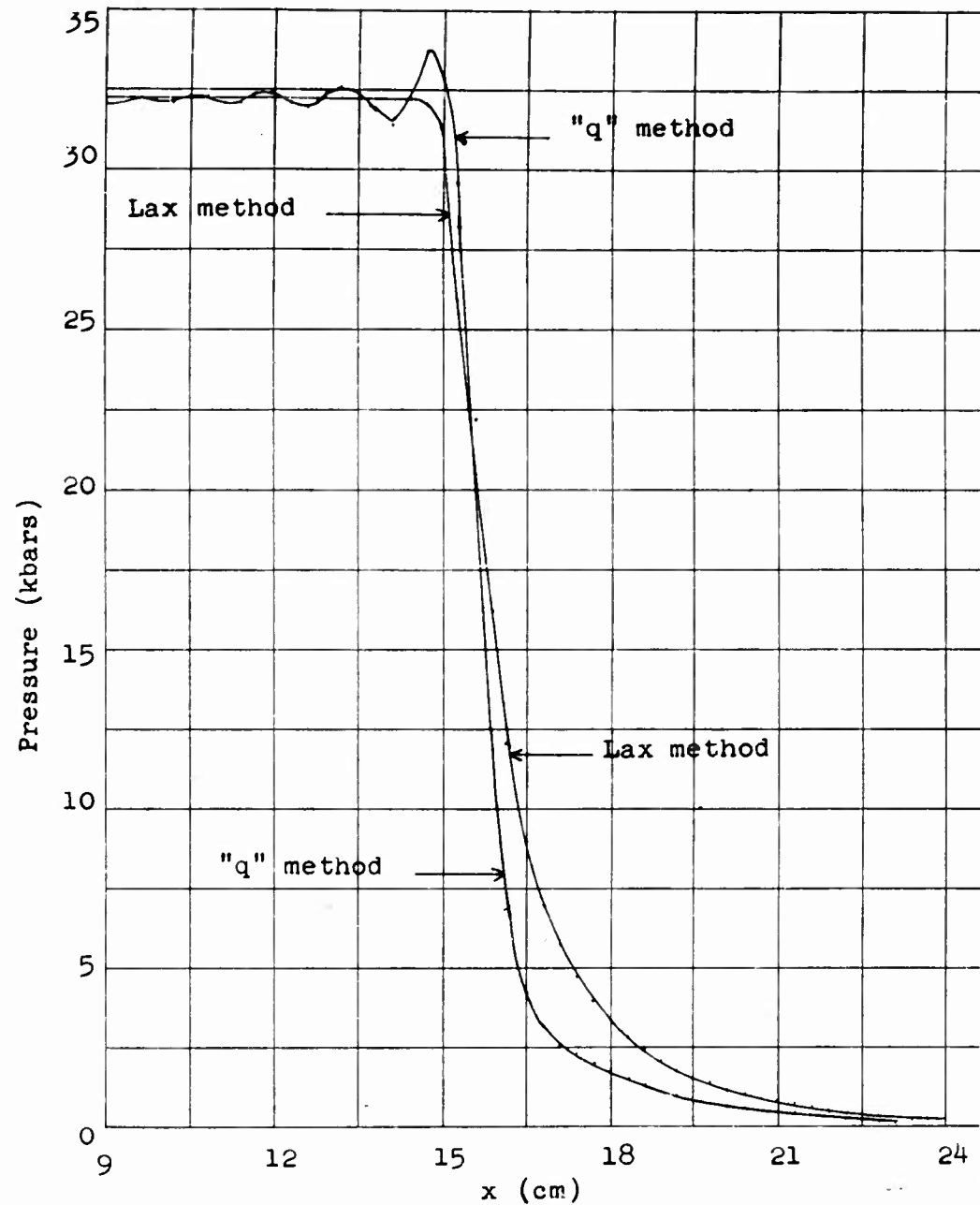


FIGURE 3

Pressure-Distance Profiles as Computed by the  
Lax and "q" Methods

The time of the computation is 100  $\mu$ sec after  
the first application of pressure.



Because of the exponential dependence of reaction rates on temperature (i.e. energy), the spurious fluctuations inherent in the "q" method render the "q" method almost useless for reaction rate studies. Therefore all further numerical work discussed in this report is based on the Lax scheme.

## SHOCK FORMATION AND INITIATION

### A. Shock Formation

The analytic solution (Ref. 6) to this problem showed that a shock had started to form at about 12 cm from the boundary at 90  $\mu$ sec. The analytic method cannot give the rate of shock growth.

The rate of growth of the shock is illustrated in Fig. 4 which gives energy-distance (or temperature-distance) profiles at several different times as computed numerically by the Lax method using the previously defined boundary conditions and equation of state. The generating pressure pulse was allowed to increase exponentially for 60  $\mu$ sec so that the maximum pressure reached was  $P_{\max} = 32.27$  kbars; thereafter the boundary pressure remained at 32.27 kbars. In Fig. 4, the upper horizontal line gives the energy that would result from a shock compression to 32.27 kbars; the lower line gives the energy that would result from an isentropic compression to 32.27 kbars. The actually computed energy has increased perceptibly above the limiting isentropic value at 72.1  $\mu$ sec, at which time the compression front is about 5.3 cm from the boundary. However, the transition from the isentropic compression to the shock compression is continuous; there is no sharp point of shock formation.

The growth of the shock is also shown in Fig. 5, in which the parameter  $\xi$  (evaluated at the compression front) is plotted against time. The figure also gives the location of the compression front as a function of time, so that the extent of the shock nature ( $\xi$ ) in the front can be read both as a function of time and distance.

### B. Shock Initiation

Figures 4 and 5 show that, assuming a chemically inert medium, the shock wave is half developed ( $\xi = .5$ ) when the compression wave has travelled about 16 cm into the charge. The next step was to see whether the temperatures generated were sufficient to start a detonation in an actual (i.e. chemically reactive) explosive, and

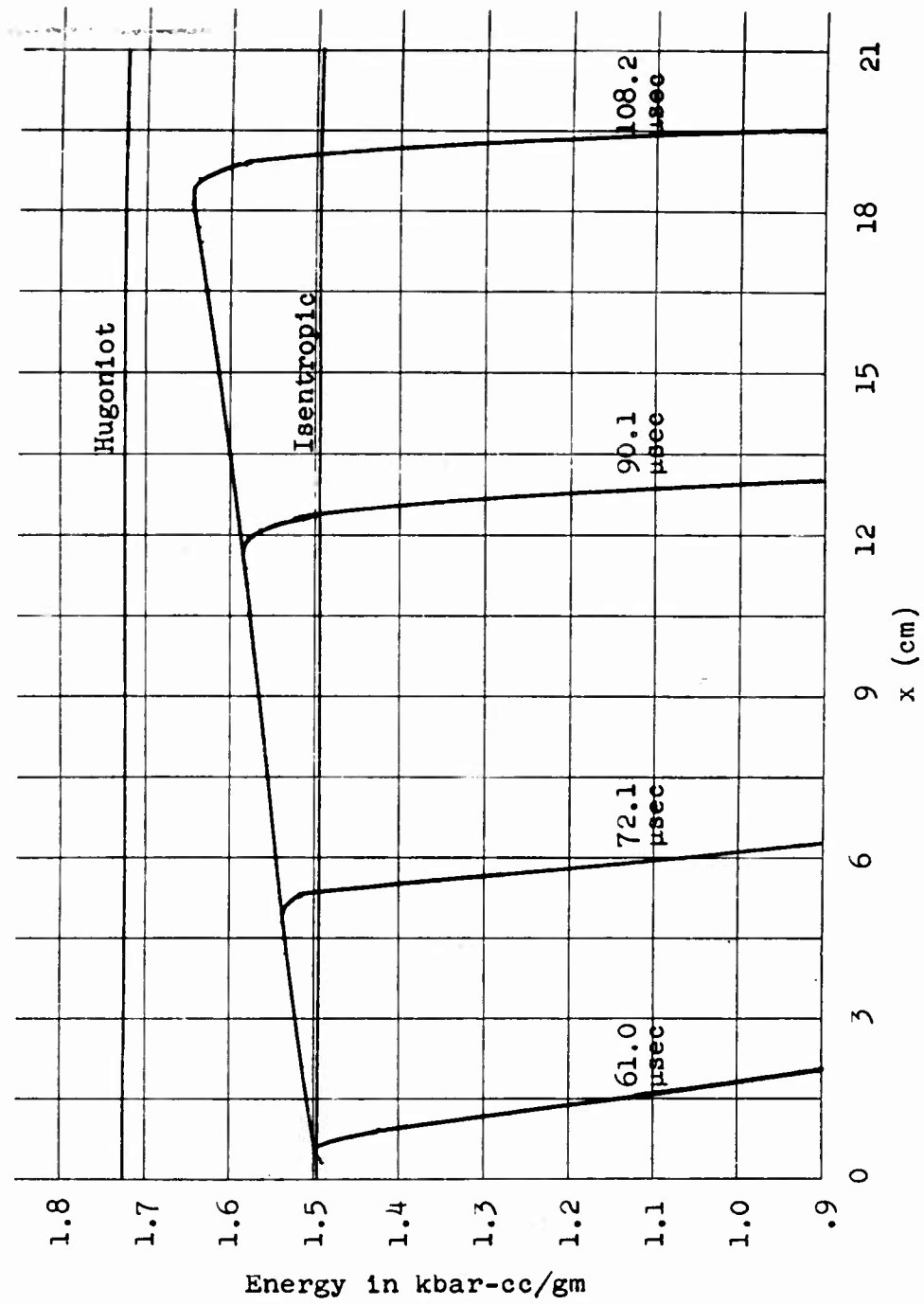
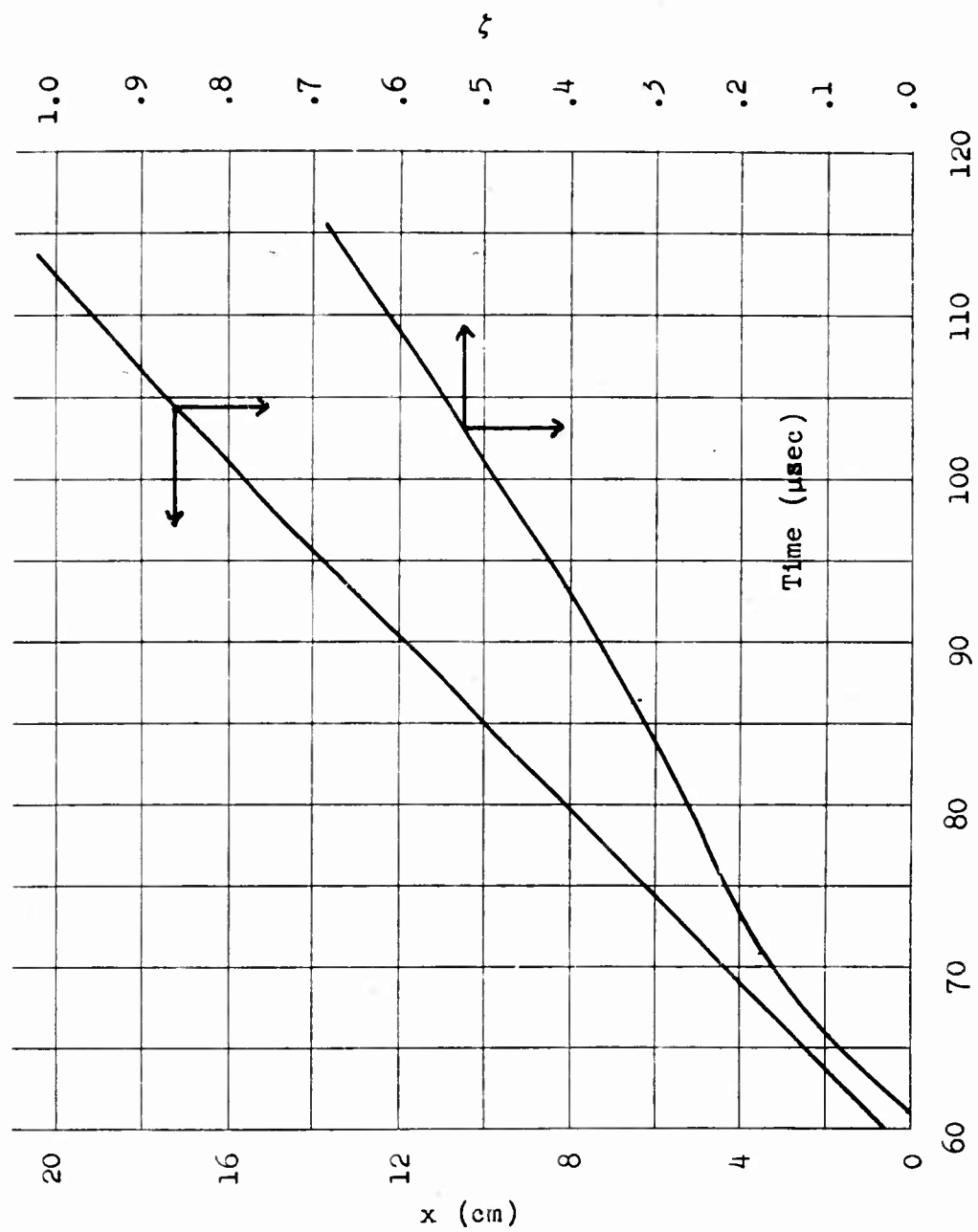


FIGURE 4 - Energy vs Distance at Several Different Times in a Non-Reactive Material

FIGURE 5 -  $x$  and  $\zeta$  vs Time

where the detonation would start. The latter point is of particular interest because, experimentally in the NOL-DDT test (Ref. 6), the detonation starts about 15 cm. into the charge.

The computed point of initiation, in general, could be located anywhere between the boundary and the wave front. As seen in Fig. 4, the layer of explosive near the compression front is at a temperature higher than that of the boundary, but its residence time at that temperature is shorter. The point at which the chemical reaction rate becomes sufficiently high to generate a detonation wave will evidently depend on the specific parameters used in the computation.

In order to see if the theoretical model agrees with the experiments, a simple first order kinetic model was used, i.e.

$$\frac{\partial F(x,t)}{\partial t} = (1 - F(x,t)) A e^{-\frac{E_a}{RT(x,t)}} \quad (21)$$

where,

$F(x,t)$  = mass fraction of burnt explosive,

$A$  = preexponential factor,

$E_a$  = activation energy,

$R$  = gas constant,

and  $T(x,t)$  = temperature.

$T(x,t)$  is defined by the equation

$$T(x,t) = T_0 + \frac{Q(x,t)}{C_v} \quad (22)$$

Since  $Q(x,t)$  is the energy liberated by the chemical reaction at a point  $(x,t)$  and  $\Delta H$  is the heat of explosion of the explosive, then

$$F(x,t) = \frac{Q(x,t)}{\Delta H} \quad (23)$$

Therefore, equation (21) can be rewritten as

$$\frac{\partial Q(x,t)}{\partial t} = \Delta H \left( 1 - \frac{Q(x,t)}{\Delta H} \right) A e^{-\frac{E_a}{RT(x,t)}} \quad (24)$$

This is the explicit form of equation (11) that was used in the following calculations. The constants in equations (22) and (24) are

$$C_v = 1.254 \times 10^7 \text{ ergs/gm}^\circ\text{C}$$

$$\Delta H = 5.016 \times 10^{10} \text{ ergs/gm}$$

$$A = 10^{14} \text{ sec}^{-1}$$

$$E_a = 35,000 \text{ cal/mole.}$$

A computer run was made using the previously discussed boundary conditions and equation (24) to compute the reaction rate. The maximum pressure was 32.27 kbars. The computed temperatures were too low to cause any appreciable reaction. The run gave results almost identical to the run represented in Fig. 4.

Figure 6 illustrates the most important result of this run. It is a plot of  $F(x,t)$  vs  $x$  at several different times. It shows that after the shock is partly developed, the greater reaction rate in the interior (due to the greater temperature increase from the partly developed shock) causes the reaction to proceed farther than it does at the boundary.

A subsequent run was made with one important change. The near boundary pressure was,

$$P(0,t) = .08 e^{kt} \text{ kbars for } t \leq 67.5 \text{ } \mu\text{sec}$$

$$k = .1 \text{ } \mu\text{sec}^{-1}$$

$$P(0,t) = .08 e^{6.75} \text{ kbars} = 68.32 \text{ kbars for}$$

$$t \geq 67.5 \text{ } \mu\text{sec}$$

The higher pressure caused the temperature (i.e. energy) to reach higher values than in the previous run. The reaction rates from these higher temperatures were great enough to cause the reaction to go to completion.\* The reaction first went to completion\* 17.7 cm in from the

\* The first order reaction assumed here would never actually go to completion, but in a numerical computation the reaction goes to completion. The error is completely negligible.

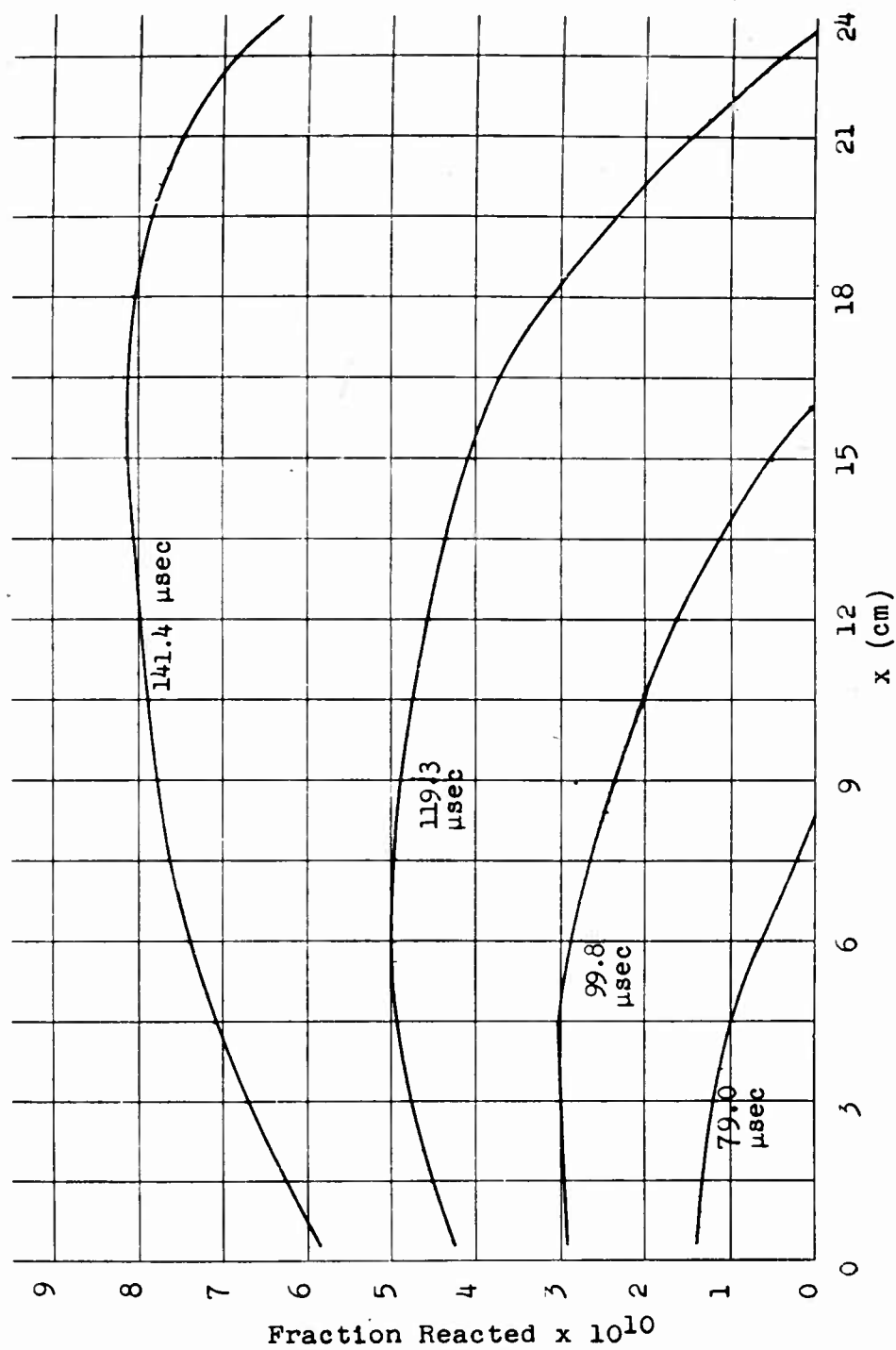


FIGURE 6 - Fraction Reacted vs Distance at Several Different Times

boundary. Figure 7 illustrates the course of the reaction. It is a plot of  $F(x,t)$  vs  $x$  at several different times.

Figure 8 is a plot of  $T(x,t)$  vs  $x$  at two different times from two different computer runs. In one run the material was assumed to be non reactive; in the other run the material was assumed to be reactive. The times chosen were slightly before and slightly after the reaction went to completion in the reactive run. The interior temperature is higher than the boundary temperature; this coupled with the exponential dependence of reaction rate on temperature caused the reaction to go to completion in the interior before it went to completion at the boundary.

Figure 9 is a plot of pressure vs  $x$  at several different times for the 68.32 kbar maximum pressure, reactive explosive calculation. It shows the development of the detonation wave.

#### DISCUSSION

Measurements and rough calculations (Ref. 6) indicate that the maximum boundary pressure attained in the NOL-DDT test is about 32 kbars. Calculations based on this maximum pressure and homogeneous first order kinetics show no appreciable reaction. This is not surprising since it is almost certain that initiation by weak stimuli (e.g. weak shocks) requires some mechanism of stress concentration (e.g. occluded grit or gas bubbles). The important result from the 32 kbar calculation was the observation that the reaction inside the charge surpassed the reaction at the boundary.

A later calculation was made based on a maximum boundary pressure of 68 kbars. This was done to compensate for the absence of stress concentrating mechanisms in the model used. This pressure was adequate to cause initiation of the explosive. The initiation started in the interior at a location comparable to the experimental results.

It was concluded from these calculations that the shock formation-shock initiation model for the transition from deflagration to detonation is essentially correct.

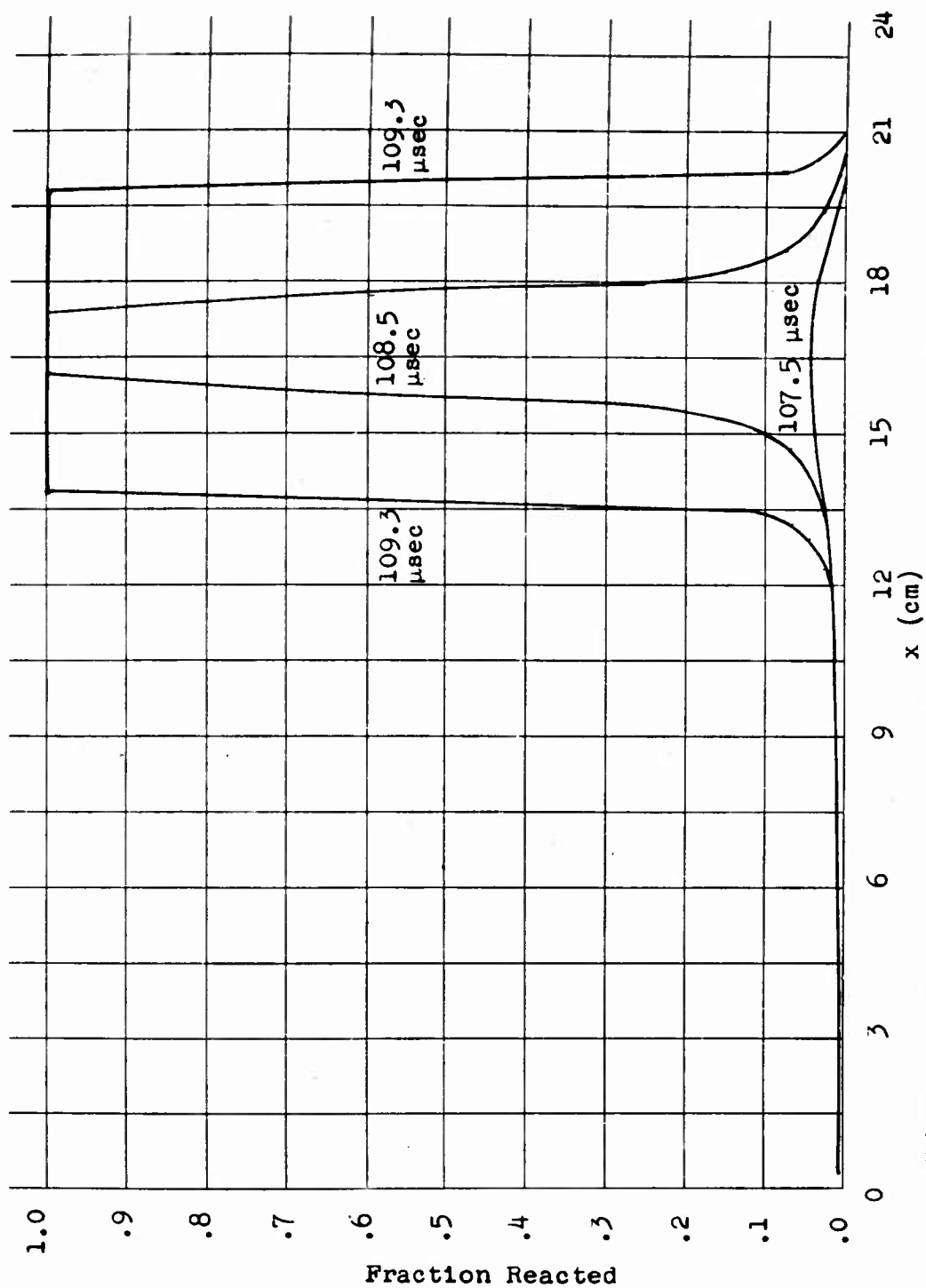


FIGURE 7 - Fraction Reacted vs Distance at Several Different Times



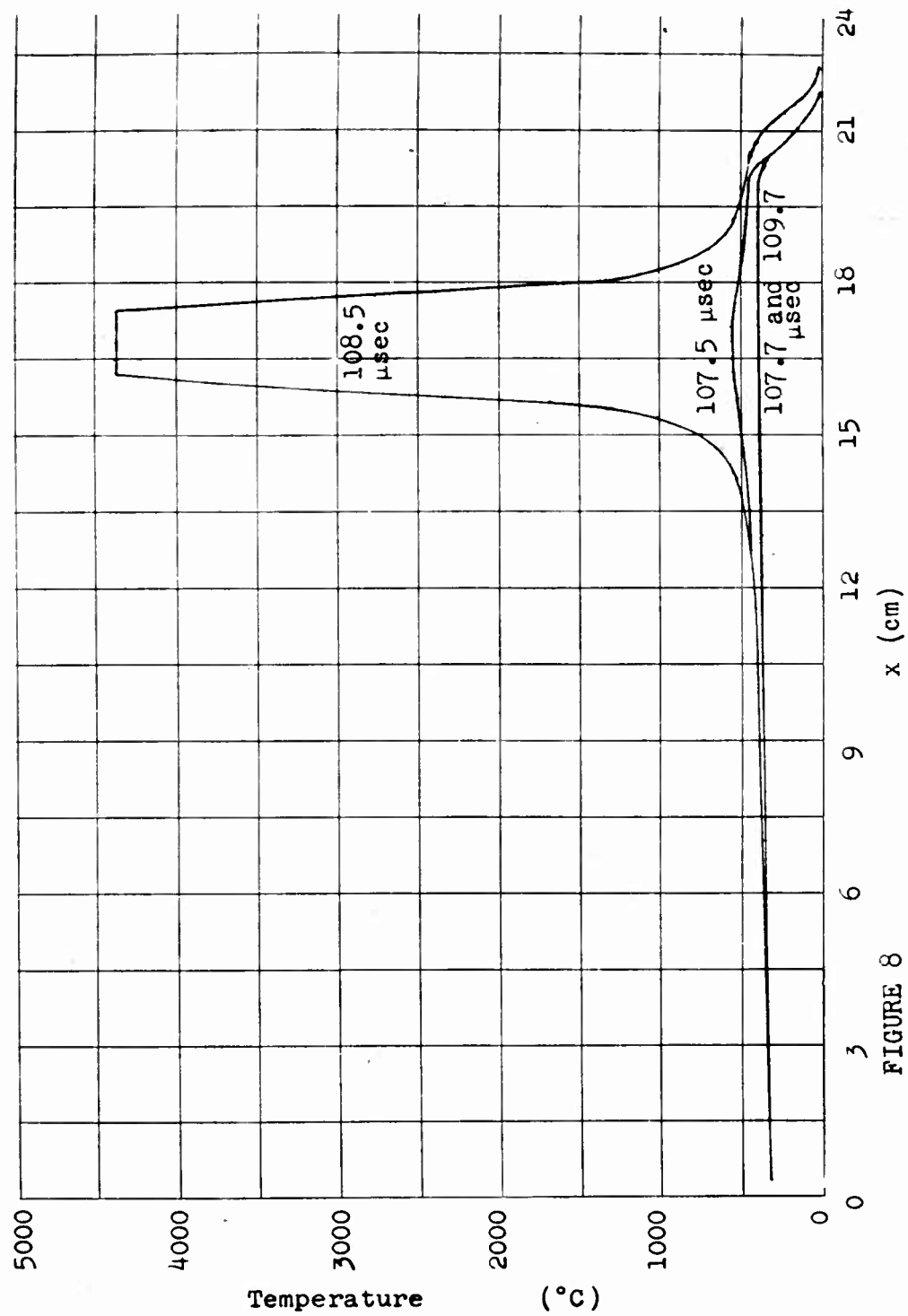


FIGURE 8  
Temperature vs Distance at Several Different Times with Reactive and Non-Reactive Materials

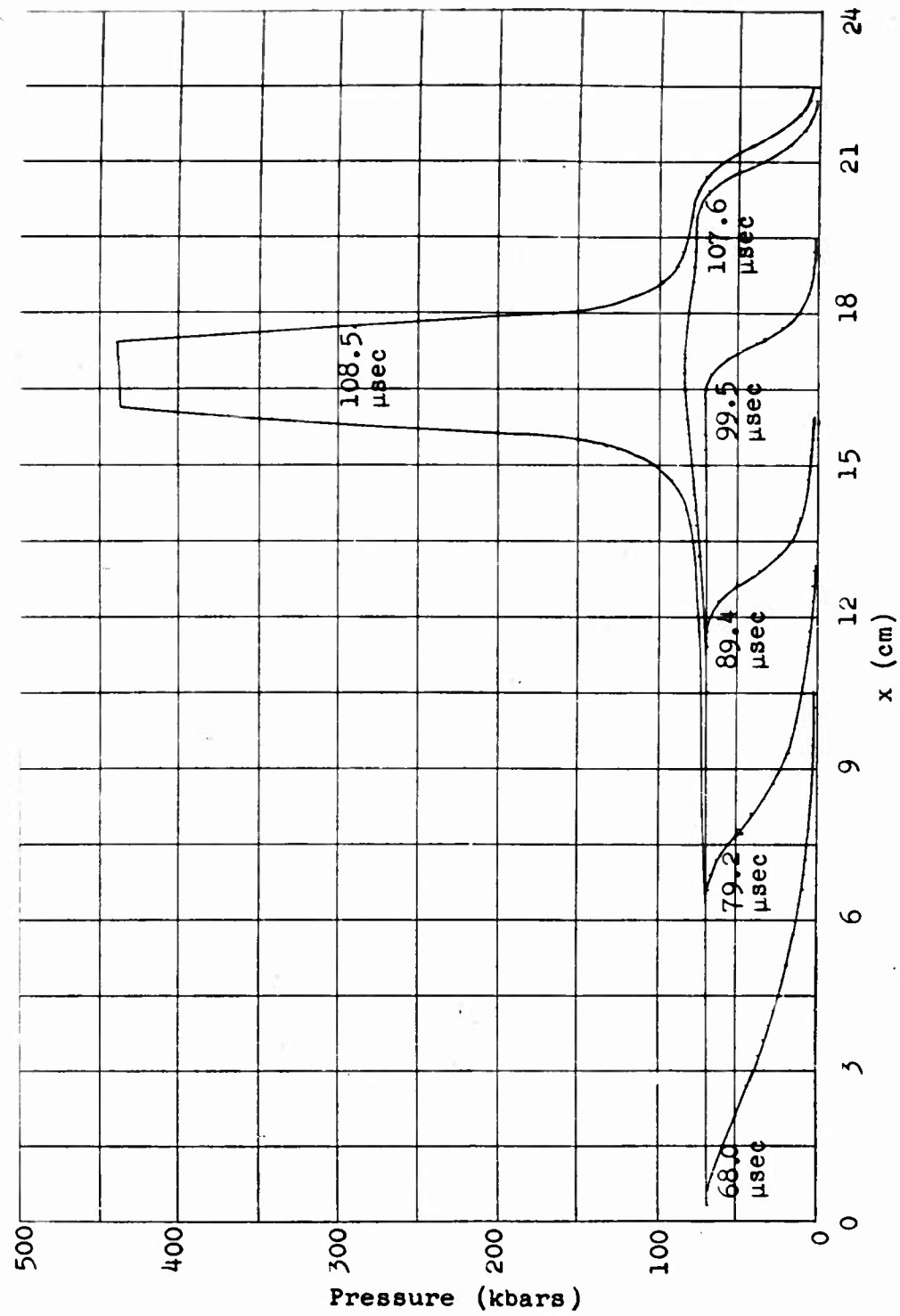


FIGURE 9 - Pressure vs Distance at Several Different Times with a Reactive Material

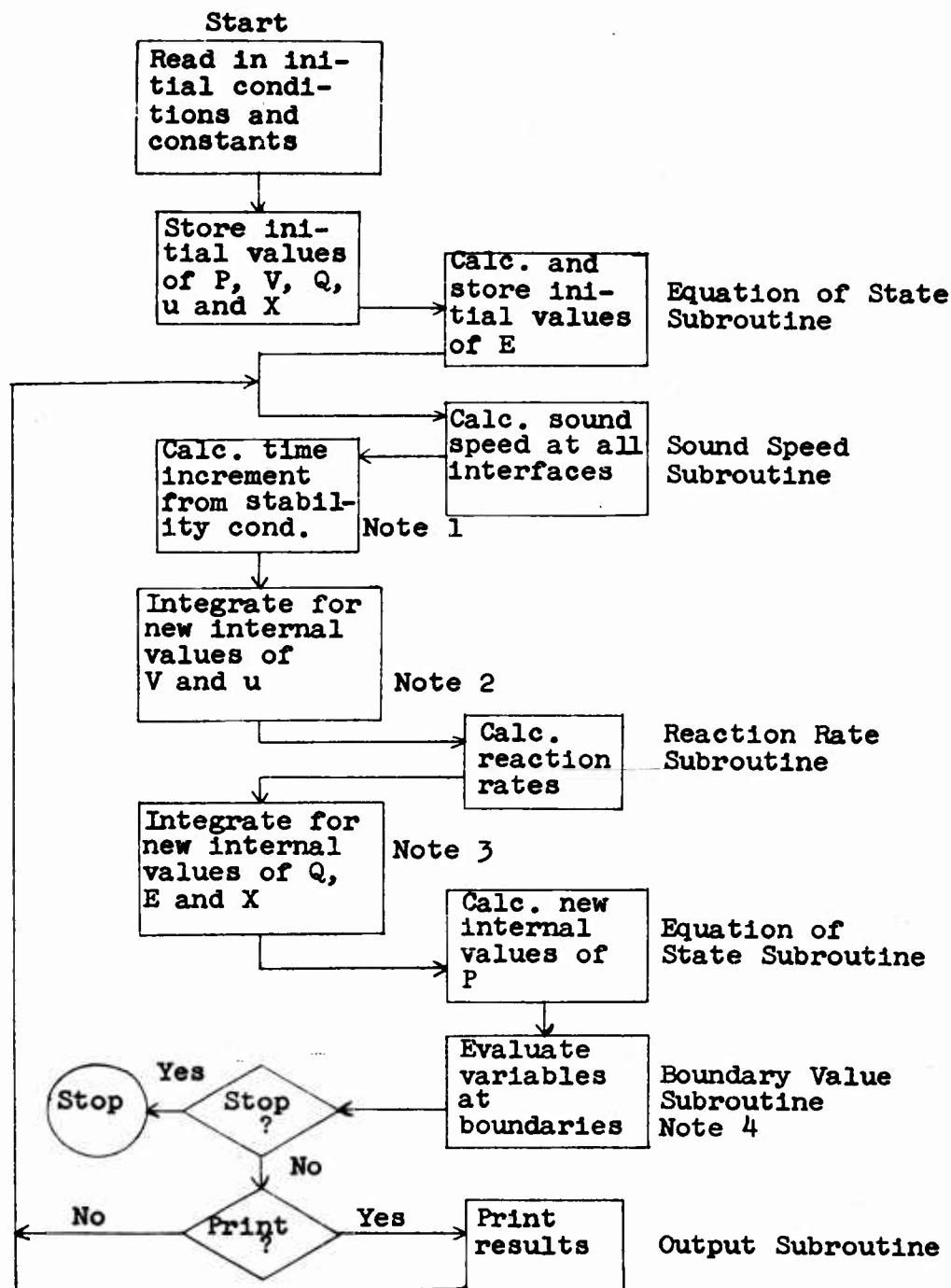


FIGURE 10. Flow Chart of Computer Program

## REFERENCES

1. F. P. Bowden and O. A. Gurton, Proc. Roy. Soc., 198A, 337 (1949); 198A, 350 (1949).
2. A. Macek and R. W. Gipson, NavOrd 5758, 1 November 1957; NavOrd 6104, 12 May 1958.
3. N. Griffiths and J. M. Groocock, ARDE Rep. (MX) 6/59. March 1959.
4. M. A. Cook, R. T. Keyes, W. S. Partridge and W. O. Ursenbach, JACS, 79, 32 (1957).
5. C. H. Winning, Proc. Roy. Soc., 246A, 288 (1958).  
(References 4 and 5 deal with initiation by relatively weak shocks, not by deflagration).
6. A. Macek, J. Chem. Phys., 31, 162 (1959).
7. J. M. Majowicz, unpublished.
8. A. Macek, NavOrd 6105, 12 May 1958.
9. J. M. Majowicz and S. J. Jacobs, NavOrd 5710, November 1957.
10. R. D. Richtmyer, "Difference Methods for Initial Value Problems", Interscience Publishers, Inc., N.Y., 1957.
11. J. von Neumann and R. D. Richtmyer, J. Appl. Phys., 21, 232 (1950).
12. P. D. Lax, Communications on Pure and Applied Math., 7, 199 (1954).

## APPENDIX I

As a part of this task a computer (IBM 704) program was constructed to solve hydrodynamic problems on the basis of the Lax scheme. The program consists of a main routine in which the equations of motion are integrated and certain other unchanging operations are performed. Calculations involving the equation of state, reaction rates, boundary conditions and stability are carried out in subroutines. Thus if any of these things must be changed, only the appropriate subroutine need be reprogrammed.

The program runs according to the flow diagram in Figure 10. The following are notes to Figure 10:

- (1) The stability analysis of this system shows that

$$\Delta t < \rho_0 \Delta x \frac{V}{C}.$$

$\Delta t$  is computed at every interface and the smallest value is used.

- (2) At this step the equations of conservation of mass and momentum are integrated. The equation of conservation of mass (Eqn. 9), when differenced according to the Lax scheme, becomes

$$\frac{\rho_0}{\Delta t} \left( v_x^{t+\Delta t} - \frac{1}{2} (v_{x+\Delta x}^t + v_{x-\Delta x}^t) \right) = \frac{1}{2\Delta x} (U_{x+\Delta x}^t - U_{x-\Delta x}^t).$$

Since the values of all of the variables are known at  $t$ , this equation can be used to evaluate  $v_x^{t+\Delta t}$ . Likewise, the equation of conservation of momentum (Eqn. 7) when differenced according to the Lax scheme becomes,

$$\frac{\rho_0}{\Delta t} \left( U_x^{t+\Delta t} - \frac{1}{2} (U_{x+\Delta x}^t + U_{x-\Delta x}^t) \right) = \frac{1}{2\Delta x} (P_{x+\Delta x}^t - P_{x-\Delta x}^t).$$

Since the values of all of the variables are known at  $t$ , this equation can be used to evaluate  $U_x^{t+\Delta t}$ .

Since  $0 < x < x_{\max}$ , the above two equations cannot be used to evaluate the variables at  $t+\Delta t$  where  $x = 0$  or  $x_{\max}$  because this would demand values of the variables at  $x$  outside the range  $0 < x < x_{\max}$ .

(3) At this step the equations of chemical energy release and conservation of energy are integrated. The equation of chemical energy release, when differenced according to the Lax scheme, becomes

$$\frac{1}{\Delta t} \left( Q_x^{t+\Delta t} - \frac{1}{2} (Q_{x+\Delta x}^t + Q_{x-\Delta x}^t) \right) = R_x^t.$$

Since the right hand side of this equation can be evaluated directly, it will not be differenced or averaged.  $R_x^t$  are evaluated in the reaction rate subroutine. Therefore, this equation can be used to evaluate  $Q_x^{t+\Delta t}$ .

(4) The values of the variables at the boundaries (i.e. at  $x=0$  and  $x=x_{\max}$ ) are computed in the boundary value subroutine. The values of the pressure  $P$  are specified by the equations,

$$P(0,t) = .08 e^{0.1t} \text{ kbar for } t \leq t_{co}$$

$$P(0,t) = .08 e^{0.1t_{co}} \text{ kbar for } t \geq t_{co}$$

$$P(x_{\max},t) = .08 \text{ kbar for all values of } t$$

The values of the other variables at the boundaries are computed from  $P(0,t)$ ,  $P(x_{\max},t)$  and equations 7, 9, 11 and 19. The Lax differencing scheme cannot be used at the boundaries because it would require values of the variables outside the range of  $0 < x < x_{\max}$ . Therefore a different differencing scheme is used. For a partial differential equation of the following general type,

$$A \left( \frac{\partial Y}{\partial t} \right) = \left( \frac{\partial Z}{\partial x} \right),$$

the following differencing scheme is used;

$$\begin{aligned} \frac{A}{2\Delta t} \left( Y_x^{t+\Delta t} - Y_x^t + Y_{x+\Delta x}^{t+\Delta t} - Y_{x+\Delta x}^t \right) \\ = \frac{1}{2\Delta x} \left( Z_{x+\Delta x}^t - Z_x^t + Z_{x+\Delta x}^{t+\Delta t} - Z_x^{t+\Delta t} \right). \end{aligned}$$

## A METHOD FOR DETERMINATION OF DETONABILITY OF PROPELLANTS AND EXPLOSIVES

S. Wachtell & C. E. McKnight  
Picatinny Arsenal  
Dover, New Jersey

### ABSTRACT

A new quantitative approach to establishing the detonability of propellants and explosives through a study of the deflagration to detonation transition (DDT) has shown promising results. Results indicate that each explosive material has a critical pressure above which the transition from deflagration to detonation will occur.

The measurement depends on the determination of burning rate as a function of pressure. By comparing the burning rates obtained in a strand burner with those obtained for large solid cylinders in a closed bomb at high pressure, a pressure is found for each explosive above which the closed bomb burning rate vs pressure curve turns sharply upward from the normal burning rate vs pressure curve obtained with the strand burner.

This deviation is believed to be the result of a crazing or surface cracking of the explosive causing a large increase in burning area. This rapid increase in burning area is considered to be the basic intermediate step in transition from deflagration to detonation.

The pressure at which this increase in burning surface begins and the rate at which it occurs can be used as the basis for a quantitative classification of the detonability of explosives.

This method has been applied to a number of explosives and propellants and the results are reported.

### INTRODUCTION

The development of new high energy solid propellants which go into the manufacture of modern missiles has reemphasized the gap in our understanding of the mechanism of transition from deflagration.

to detonation (DDT). While the number of cases in which actual transition has occurred in propellants is extremely small, the advent of larger and larger solid propellant motors with higher and higher energy propellants makes the prediction of the possibility of such an occurrence more and more urgent.

Existing test methods for evaluation of sensitivity fall into two basic categories, those involving initiation by shock and those involving thermal initiation. None of the methods give information about a property of the propellant or explosive which defines its susceptibility to undergo transition from deflagration to detonation. In this paper I will present a method by which we can quantitatively measure this property.

Kistiakowsky (1) described the following mechanism for the development of detonation in a large mass of granular or crystalline explosive ignited thermally at a localized region within the bulk:- As the explosive burns, the gases formed cannot readily escape between the explosive crystals and a pressure gradient develops. This increase in gas pressure in turn causes an increase in burning rate which in turn causes increase in pressure with constantly increasing velocity. This condition results in the formation of shock waves which are reinforced by the energy released by the burning explosive and they eventually reach an intensity where the entire energy of the reaction is used for propagation of the shock wave, and a stable detonation wave is produced. A critical size exists for each material above which this deflagration can pass over into detonation under proper conditions. Below this size the burning will first increase, and then decrease as the material is consumed.

The transition to detonation is considered to be essentially a physical process in which the linear burning rate of the bed of material increases to the rate of several thousand meters per second although the individual particles are consumed at the rate of only several hundred inches per second.

The validity of this mechanism for propellants in granular form has been demonstrated by a number of workers (2), (3). While this mechanism is applied to granular material why should it not apply as well to composite or homogeneous propellants, if the growth of a shock front can be shown (4) which is accompanied by an increasing break-up of the surface of the propellant?

The apparent non-detonability (through transition) of nitro-cellulose propellants is due to the dense surface preventing deflagration from taking place in the interstices of the materials. For composite propellant the continuous and highly elastic nature of the binder probably prevents this type of reaction. However, it has been shown (5), (6) that many highly elastic materials will undergo brittle failure when stress at very high strain rates is applied.



### GENERAL APPROACH

In the light of experience with some cannon propellants in closed bomb tests in which unexpectedly high rates of change of pressure were observed, it was considered possible that this technique might be used to demonstrate this property for rocket propellants. It had been found that when the tested lot of cannon propellant deviated from normal, the occurrence of high rates of change of pressure started at a specific pressure, which was reproducible. Since the burning rate law has been shown to hold for these propellants, a reasonable explanation is that surface cracking or crazing occurred under the pressure and thermal stress of the reaction. This increase in burning surface is believed to be the initial step in the transition from deflagration to detonation and the critical pressure and the rate at which the increase in surface area occurs can be calculated from measurements made in the closed bomb.

The calculation of linear burning rate from closed bomb measurements has been standard procedure for many years. (7), (8). From a consideration of the original geometry of a grain of material and a knowledge of the rate of change of pressure in the bomb when the grain is burned, the linear burning rate at any particular pressure can be calculated. This calculation assumes that the grain is ignited uniformly over its entire surface and always burns normal to that surface. However, if surface cracking or crazing should occur, the calculated linear burning rates will be far in excess of the value expected, and the increase in surface area can be calculated from this apparent increase in linear burning rate. A detailed discussion of these calculations is given in Appendix A.

### EXPERIMENTAL APPROACH

#### TNT

To determine whether this method would throw any light on the burning of high explosives, cylinders of TNT were prepared with diameters of 1" to 1 $\frac{1}{4}$ " and lengths of from 1" to 3". These cylinders were machined from solid blocks of TNT which had been carefully cast to make certain that they contained no voids or porosity. All the cylinders were machined from the same block and were considered to have approximately the same crystalline structure. These cylinders were placed in a standard 200cc closed bomb with a reinforced cylinder wall and fired with a small amount of Grade A5 black powder and an M1A1 Squibb. Tracings of typical oscillograms resulting from the firings are shown in Figure 1. These represent a series of firings made with cylinders of TNT at various loading densities. In the first of these is inserted a line representing the trace which should have been obtained if the cylinder of TNT had burned normally. However, in each case note that a marked deviation from normal occurred at 6000-8000 psi. In examining these tracings it must be born in mind that the standard closed bomb instrumentation produces

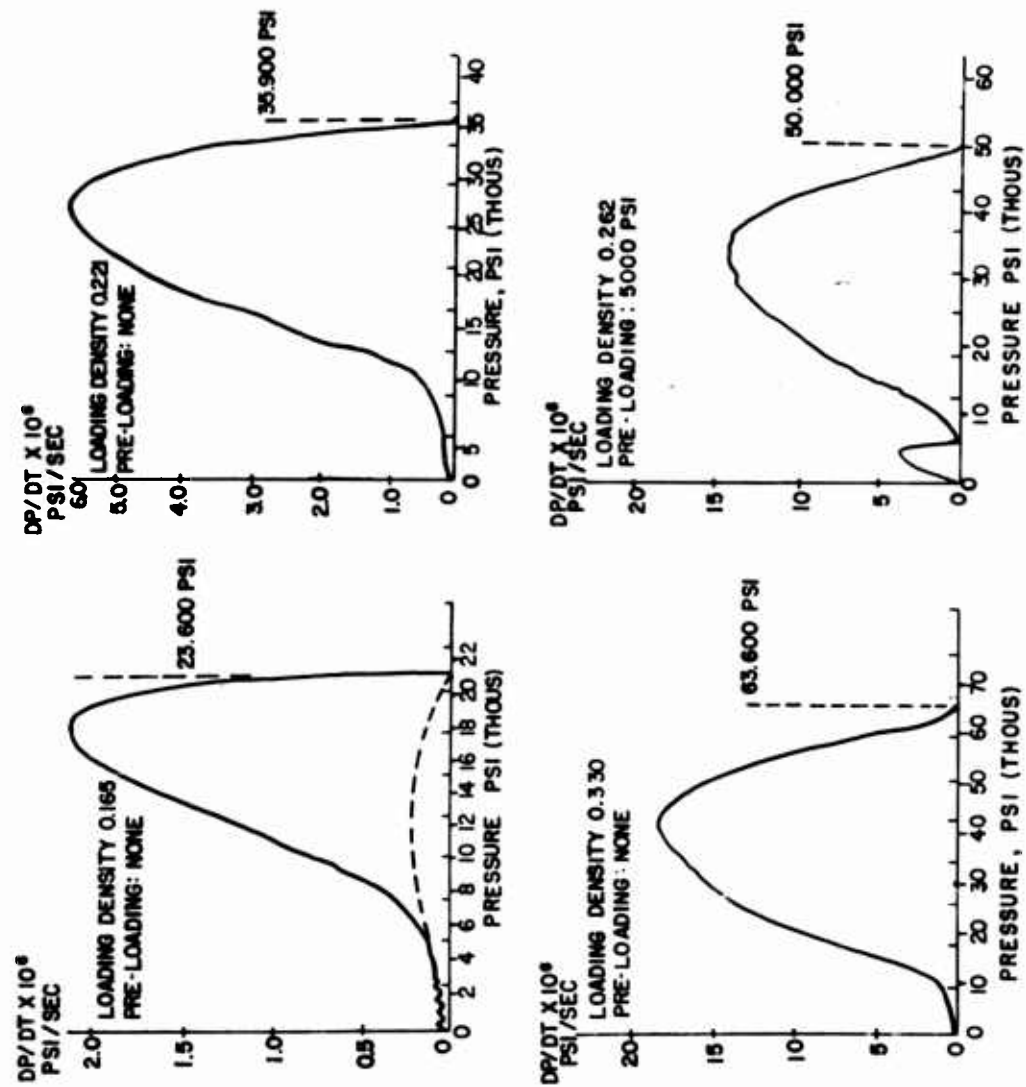


Fig. 1 - Closed bomb test TNT

an oscillogram of  $dp/dt$  vs  $P$  and that the horizontal axis represents  $P$  and the vertical axis represents rate of change of  $P$ . The scale is varied to have the trace fill the oscillogram. The calculated scales of  $P$  and  $dp/dt$  are added to the tracings.

When linear burning rates were calculated from these traces, the results shown in Figure 2 were obtained. An average line is drawn for burning rates calculated from the closed bomb test.

In order to establish the true burning rate for TNT, strands  $1/8" \times 1/8" \times 7"$  long were prepared by cutting them from a block of TNT similar to the one used previously. These were burned in a strand burner using the standard technique at pressures of from 1,000 psi to 20,000 psi. The results of these tests are included in Figure 2.

These results show that the calculated closed bomb burning rates approximately coincides with the strand burner result up to about 6,000 psi and then curves sharply upward. This "apparent" increase in burning rate is consistent with the assumption of an increase in burning surface which occurs on the cylinder due to surface crazing or cracking. Figure 3 shows a graph of the expected surface area vs pressure due to consumption of the TNT in the bomb (assuming normal burning of the grain) and the actual surface area of the crazed TNT calculated from the  $dp/dt$  of the bomb test and the actual linear burning rate of the TNT. This shows for TNT an increase in surface area of close to 20 times.

It was desired to determine whether this change in slope was strictly a pressure and thermal effect and independent of the amount of TNT burned. Therefore a technique was devised whereby a quantity of thin sheets of a very fast burning propellant was loaded into the bomb with the TNT. On ignition, this material burned quickly, giving an initial high pressure and temperature to the bomb before any appreciable burning of the TNT took place. This technique permits a larger mass of TNT to be present at higher pressure. Measurement made in this way showed no change in the pressures at which the change in slope took place in the lower part of the curve or in the slope of the middle part of the curve. However, an increase in the slope of the upper part of the burning rate curve did result. This indicates that there is possibly some minimum mass of explosive necessary to maintain the formation of increasing burning surface. Further work will be done to investigate this.

#### Composition B

Cylinders of Composition B which had been prepared in a manner similar to the TNT were then burned in the bomb at varying loading densities. In order to obtain adequate ignition of the Composition B it was necessary to use a small amount of sheet propellant as igniter. This masked that part of the curve below about 5,000 psi. However,

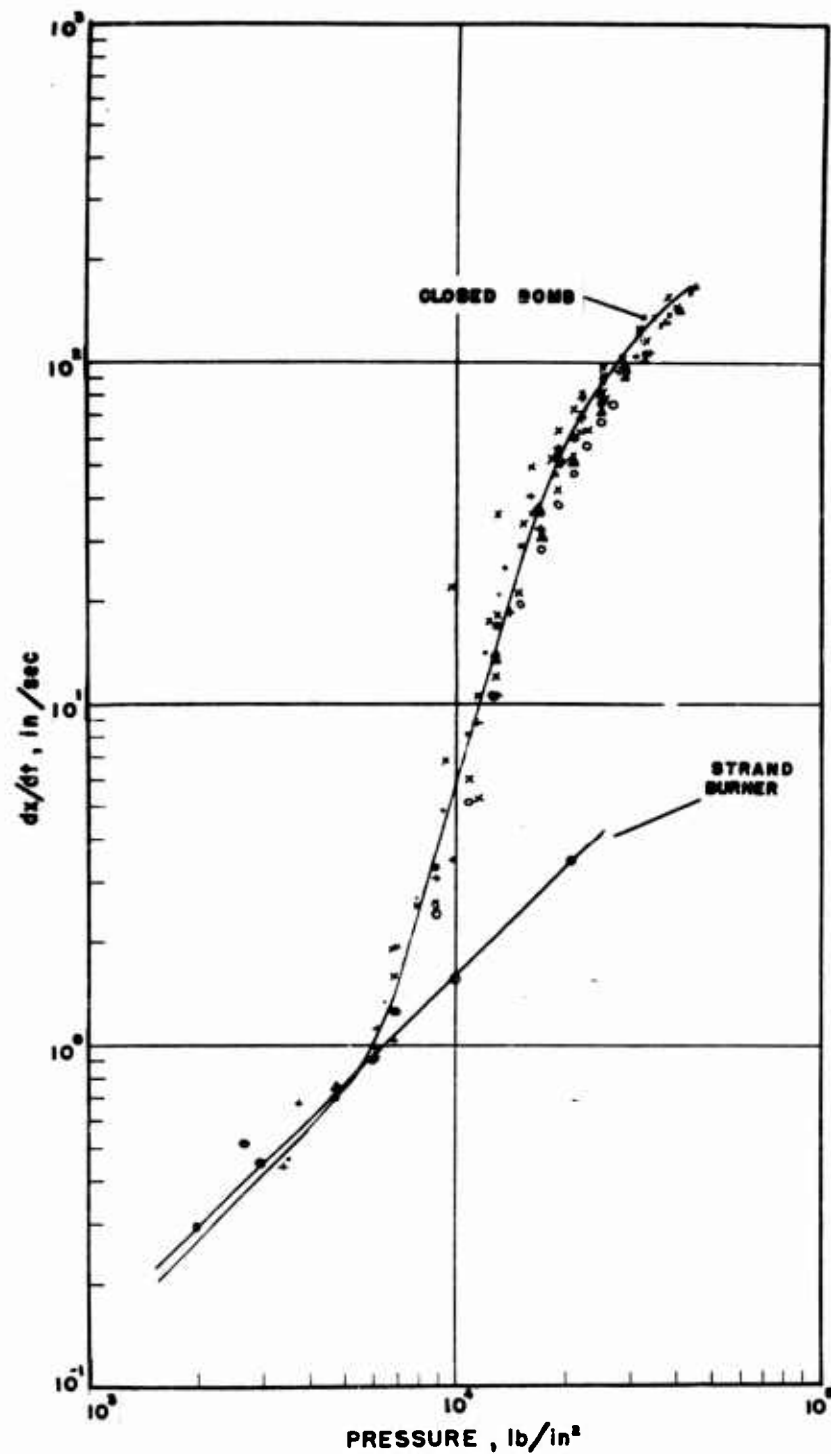


Fig. 2 - Linear burning rates of TNT obtained with closed bomb and strand burner

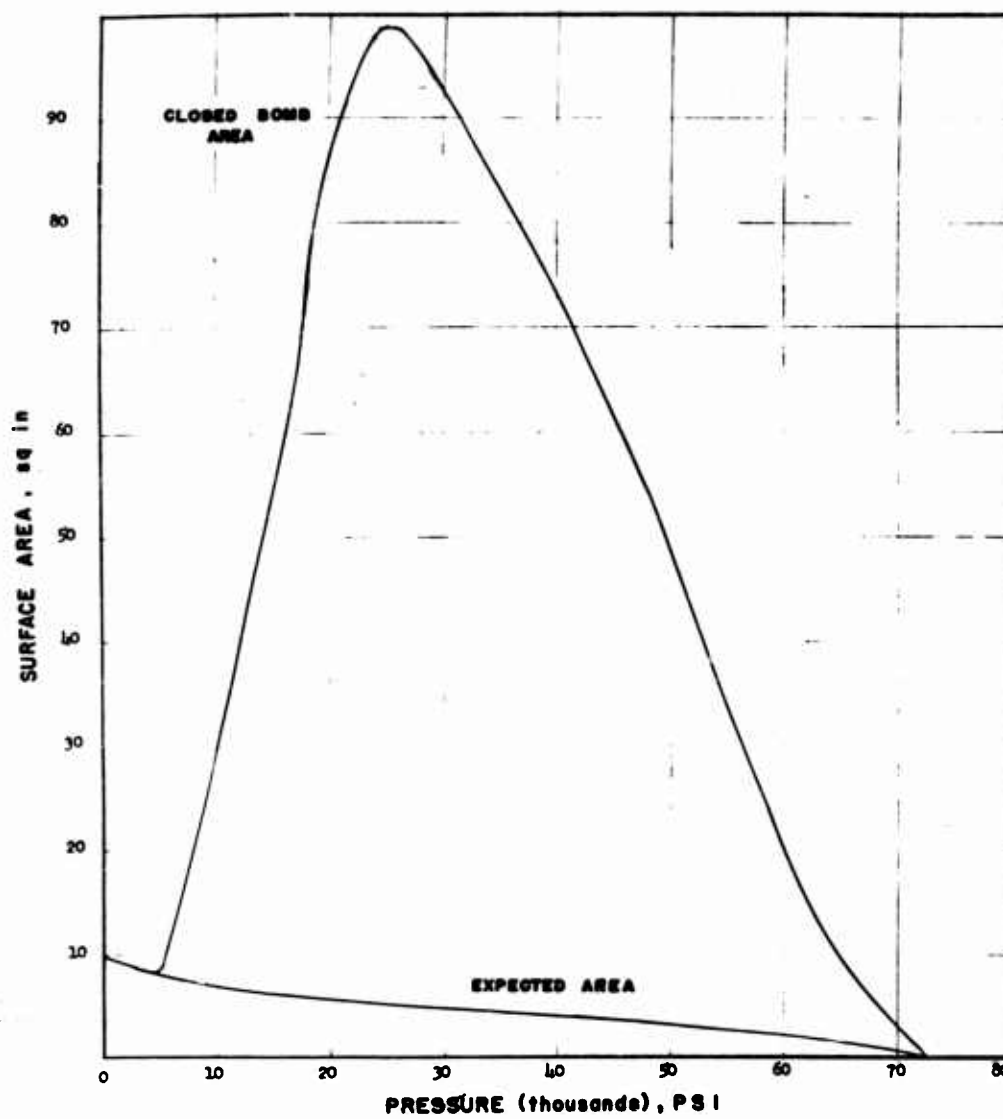


Fig. 3 - Expected surface area vs actual area obtained for TNT cylinder burned in closed bomb

strands cut from the same block of Composition B as the cylinders were burned in the strand burner to obtain the normal burning rate vs pressure curve (Figures 4 & 5). This shows that the break in the Composition B curve occurs about 4,000 - 5,000 psi. The slope of the Closed Bomb curve past the transition may be even greater than that obtained for TNT. The surface area vs pressure curves for calculated normal burning vs actual closed bomb burning of a sample of Composition B are given in (Figure 6).

#### ARP Propellant

In order to establish the applicability of this technique to high energy propellants, a sample of ARP propellant was subjected to this closed bomb test. Figure 7 shows a series of tests resulting from increasing loading densities up to about .40. When this was increased to .43 by preloading with sheet propellant, a change in slope occurred at about 35,000 - 40,000 psi similar to those which were obtained for TNT and Composition B. This was accompanied by a disintegration of one of the seals in the bomb. Unfortunately, each time conditions were used in which the transition was expected to show, the rate of pressure rise was so great that some part of the bomb seal was destroyed and the trace was lost. A bomb is being designed in which we hope to hold the pressures produced and measure transition pressures similar to those obtained for TNT and Composition B.

Figure 8 shows a plot of linear burning rate vs pressure calculated from the available data for the ARP propellant burned with and without preloading. The linear burning rates obtained with the strand burner are almost coincident with those calculated from the closed bomb at pressures of 10,000 psi and above.

#### Experimental Propellant

A sample of highly sensitive experimental propellant was then subjected to this detonability test. This material had been found to be detonable with a No. 6 blasting cap. Cylinders of different diameters were tested and pressures up to 25 thousand psi were obtained. A very sharp transition was obtained at about 15 thousand psi. Also the fall off from the maximum  $dp/dt$  begins at a much lower percentage of the maximum pressure than for the high explosive samples. Figure 9 shows a plot of the linear burning rates calculated from the closed bomb traces. The strand burner curve was extrapolated from low pressure data since strands of this material were not available for high pressure testing. Figure 10 shows the surface area relationship between expected area and actual area obtained.

A preliminary study of the data obtained for the ratio of cylinder area to actual area obtained indicates the existence of a diameter below which the continued cracking or increase in surface area stops and the explosive returns to normal burning since there is not

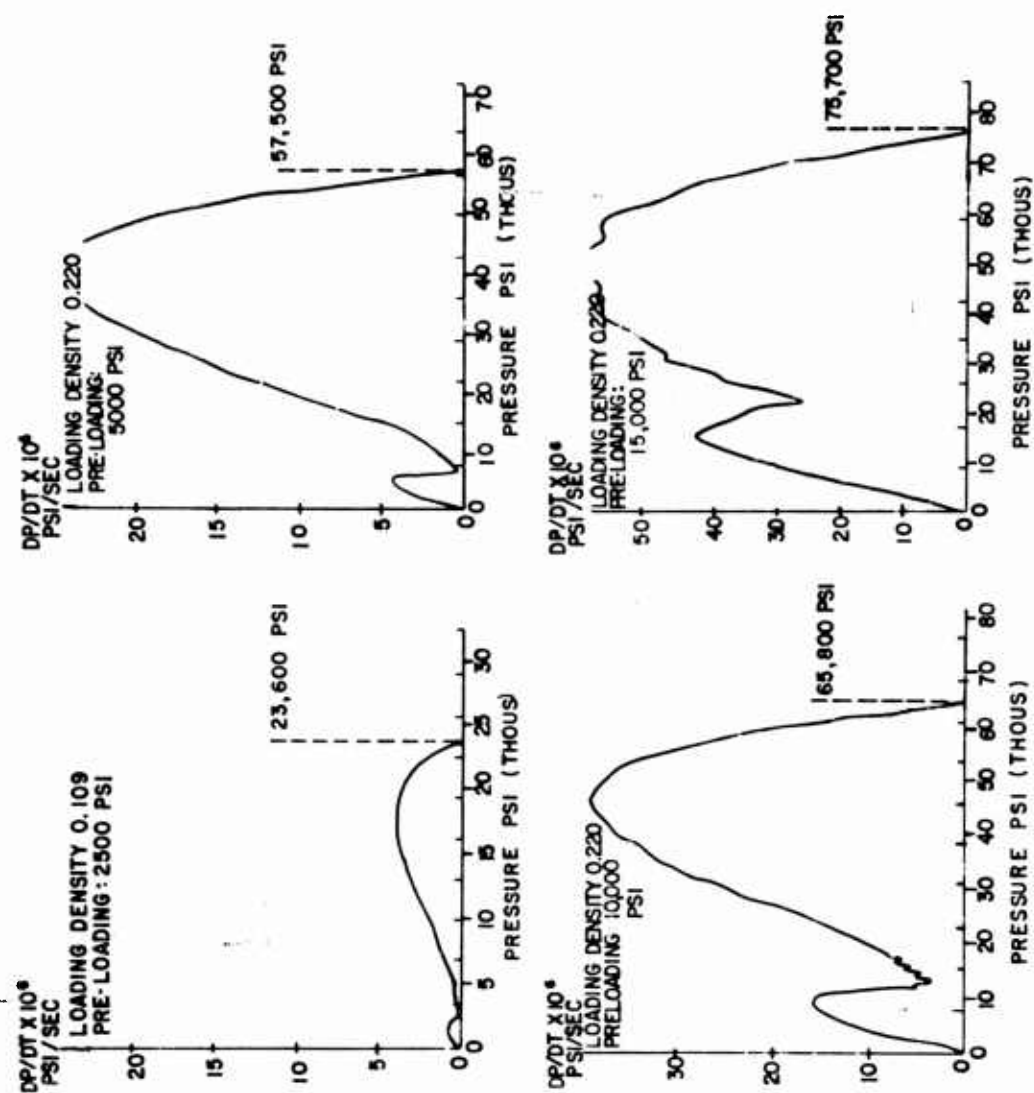


Fig. 4 - Closed bomb test composition B

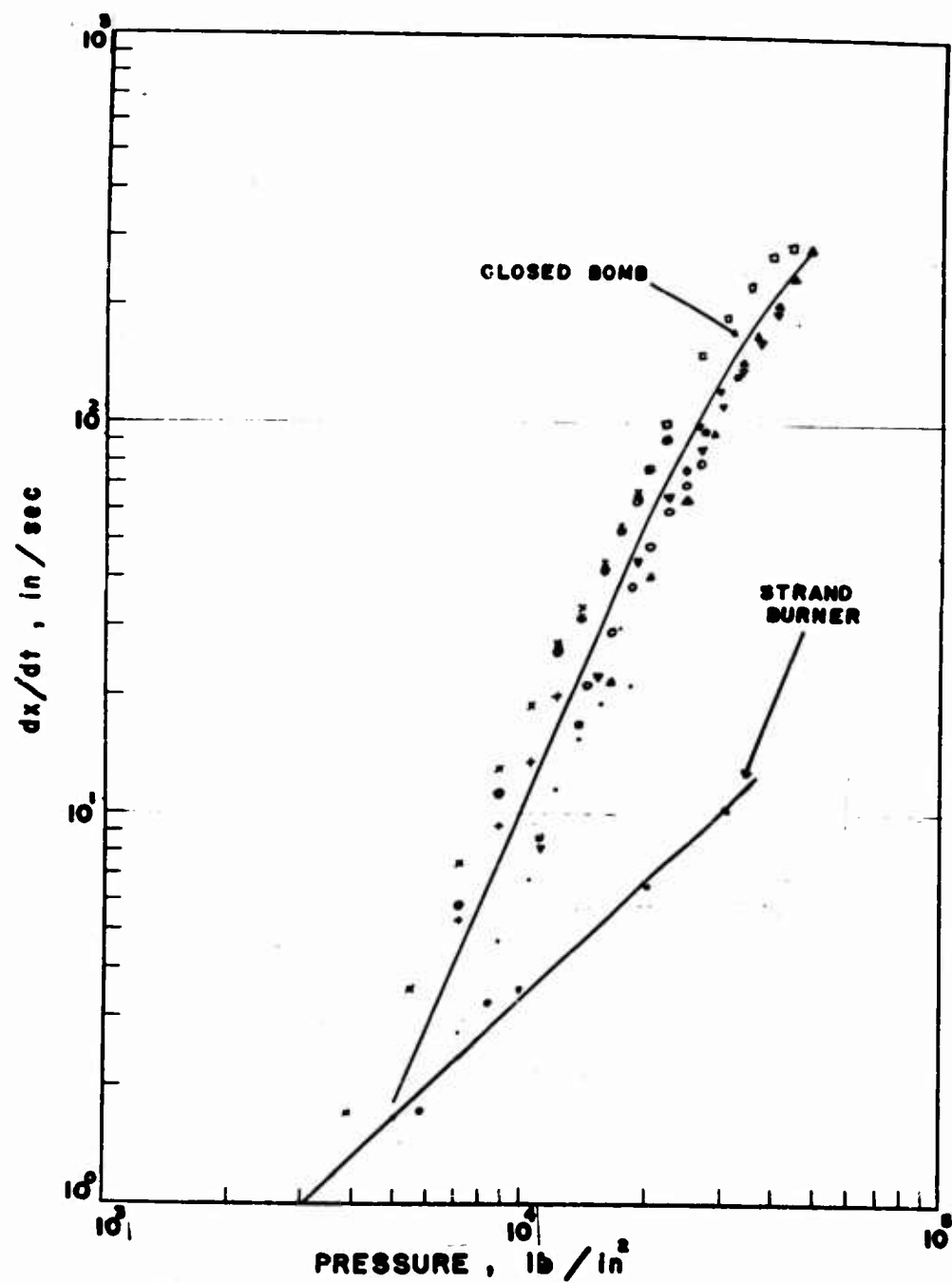


Fig. 5 - Linear burning rates of composition B obtained with closed bomb and strand burner



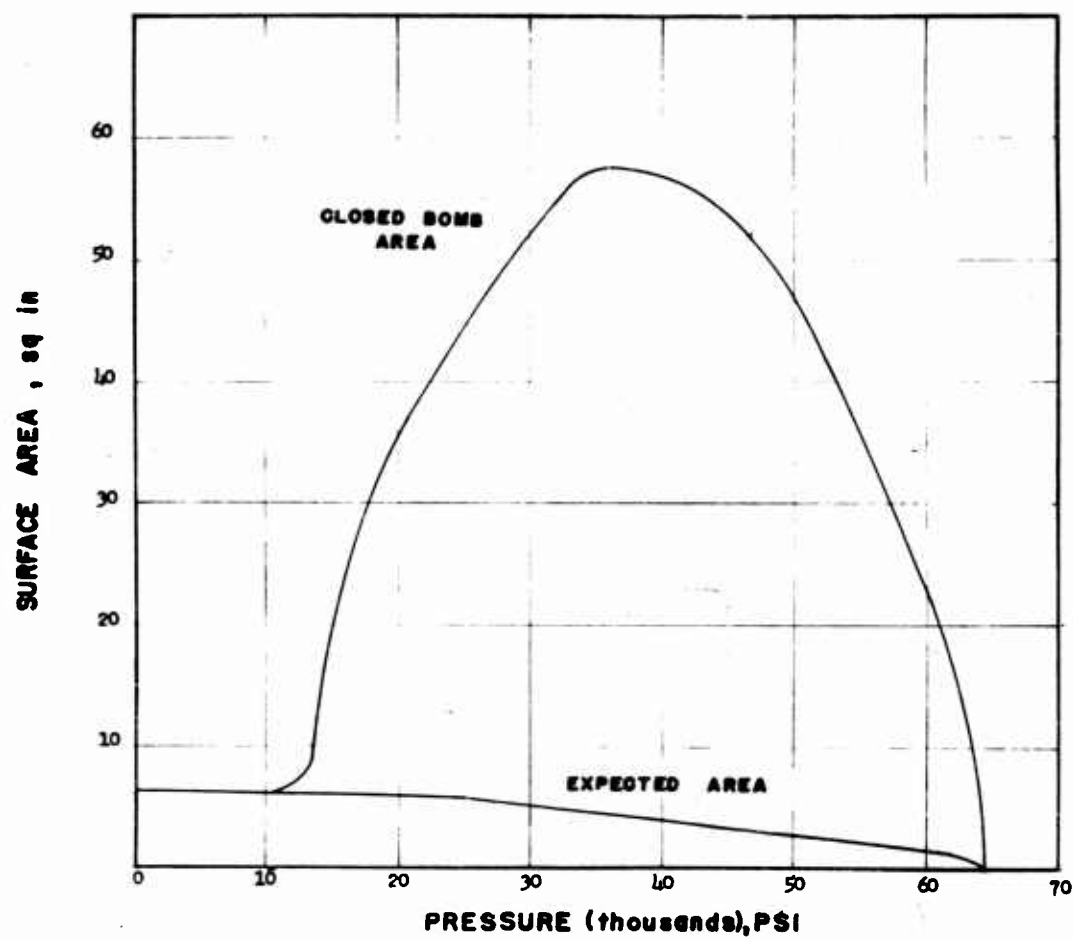


Fig. 6 - Expected surface area vs actual area obtained for composition B cylinder burned in closed bomb

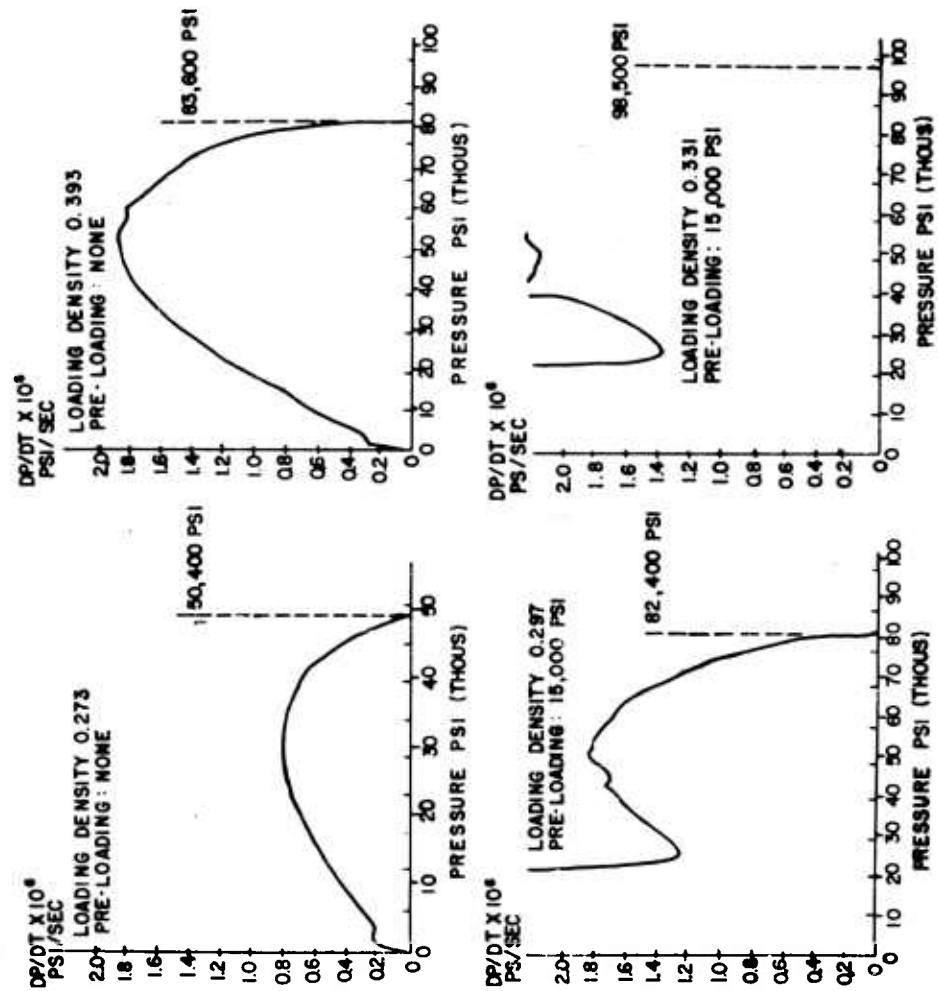


Fig. 7 - Closed bomb test ARP propellant

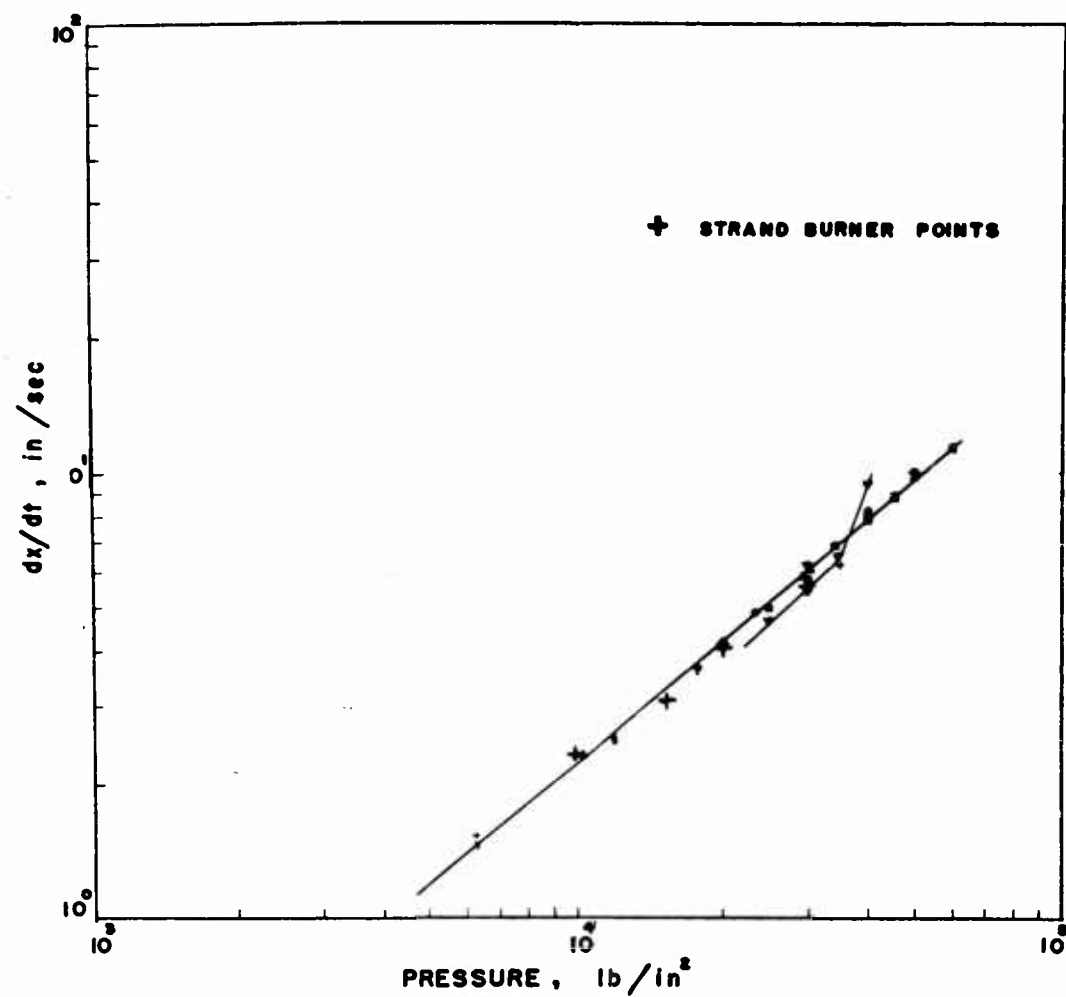


Fig. 8 - Linear burning rates of ARP propellant obtained with closed bomb and strand burner

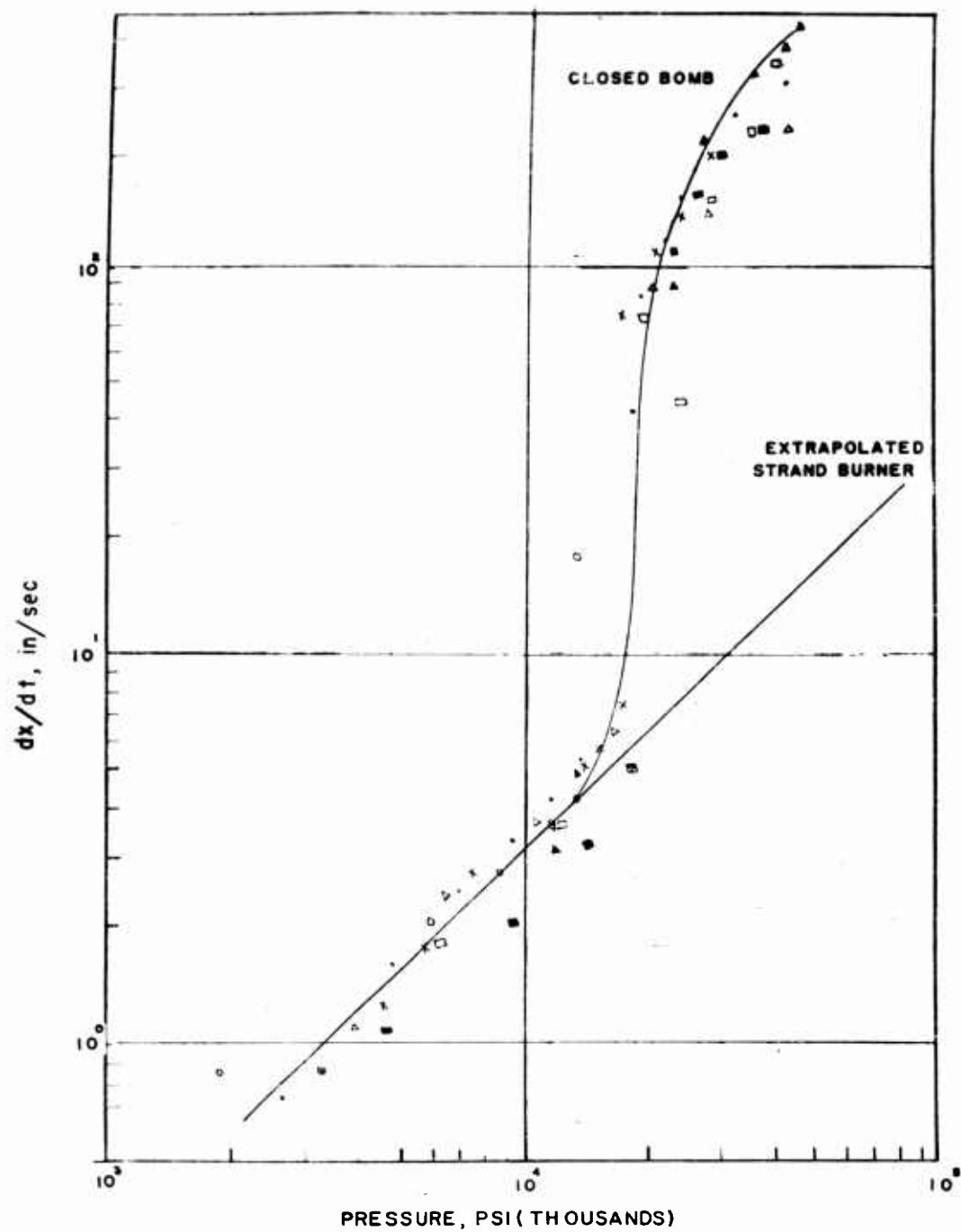


Fig. 9 - Linear burning rate of experimental propellant obtained with closed bomb

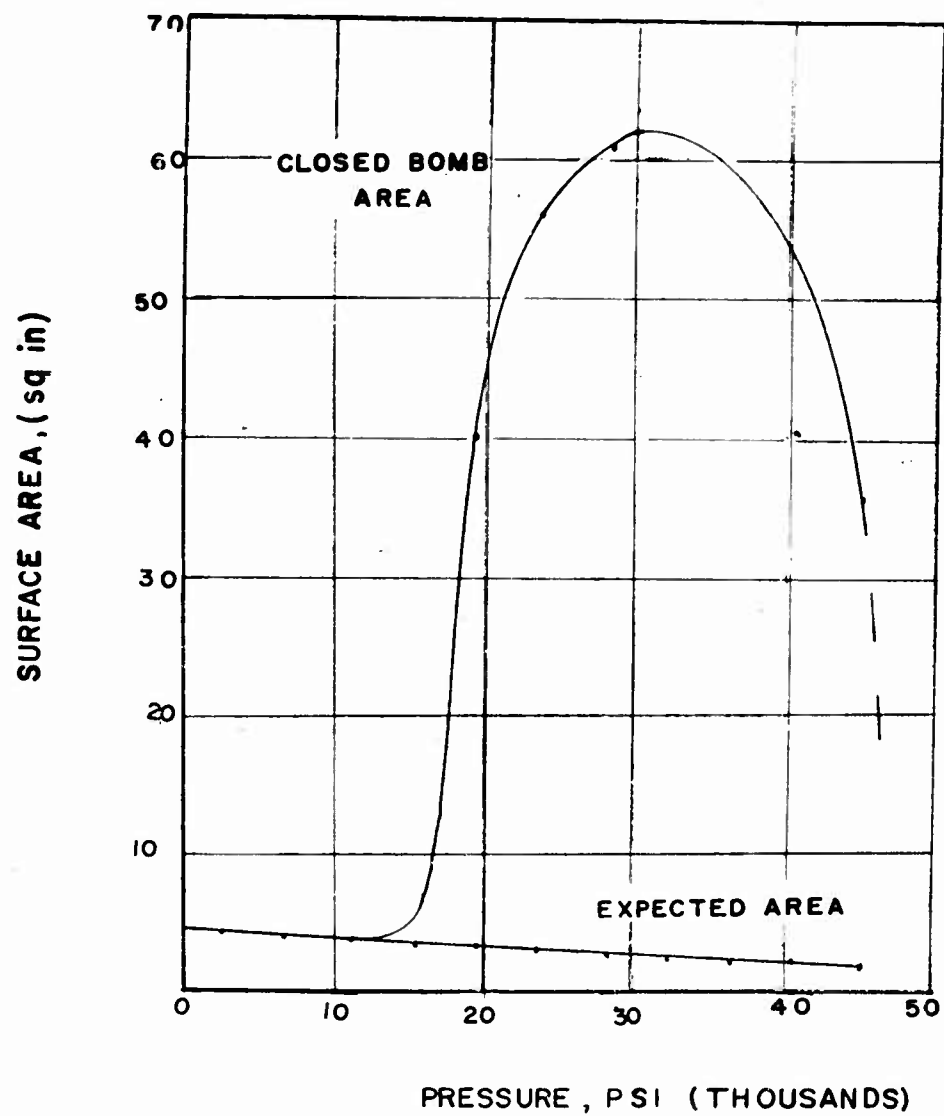


Fig. 10 - Expected surface area vs actual area obtained for experimental propellant burned in closed bomb

sufficient material available to develop a shock wave of sufficient intensity to go to stable detonation.

Figure 11 shows the ratio of surface area from closed bomb over expected surface area for the same cylinder of TNT presented in Figure 3. This shows that the ratio increased until about 35% of the grain was consumed then remained constant till about 30% of the grain was left.

An equivalent study for a Composition B cylinder in Figure 12 shows that here, the increase in surface area did not start to level off until about 70% of the grain was consumed.

The experimental propellant was tested in cylinders of different diameters and the changes in burning rate as a function of geometry were calculated. It was found that for cylinders of two different diameters, increases in surface areas were obtained down to a specific diameter which was the same for both sizes tested. This indicates the possibility that there is a minimum diameter which is characteristic of each material. This may explain the fact that in earlier work on burning of explosives in a closed bomb done by Buck, Epstein and Jacobs (Ref. 7) under the NDRC the high burning rates reported here, were not observed, since the explosives were burned in small grains.

#### CONCLUSION AND APPLICATIONS

It would appear from results of these tests that for each of the materials studied, there is a critical pressure above which the transition from deflagration to detonation can occur. This is believed to be the result of a surface cracking or crazing which increases the burning surface to a point where a shock front can form. The existence of this condition is considered necessary for DDT to occur. If sufficient explosive material were available, the shock front could reach sufficient intensity to establish a stable detonation front in the explosive.

The application of this test to explosives and propellants should give us a basis for a quantitative evaluation of these materials in terms of critical transition pressure, slope of the transition curve and minimum charge diameter. This will make it possible to classify these materials as to the severity of the conditions to which they can be subjected before the danger of DDT will exist. It will also make possible a study of the effects of temperature, porosity, particle size, crystal size and other physical variables on the detonability of existing propellants and for new materials as they are developed. It will be a valuable tool in the development of new formulations to study the effects of composition and processing modifications on the detonability of high energy materials.

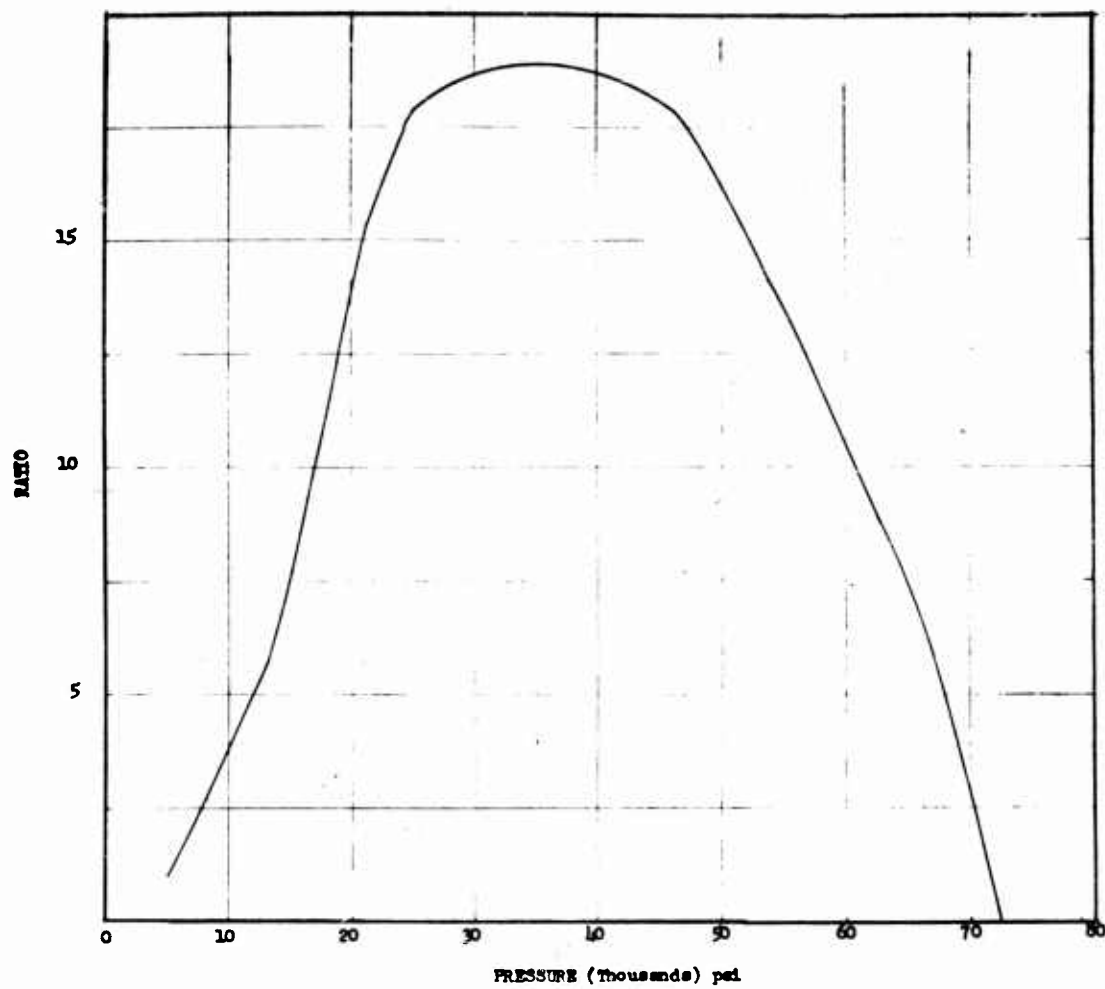


Fig. 11 - Ratio of expected area to actual area  
found for TNT cylinder

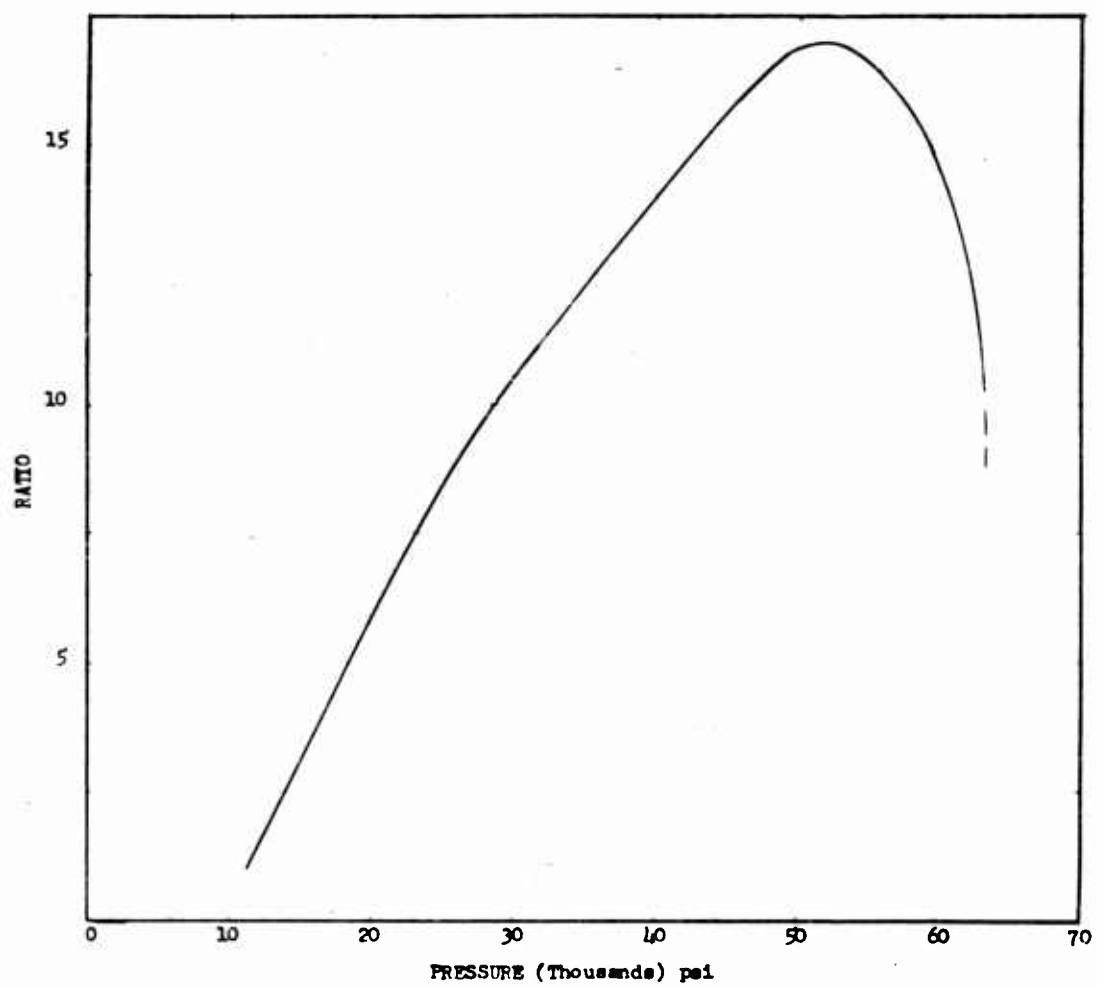


Fig. 12 - Ratio expected area to actual area found  
for composition B cylinder



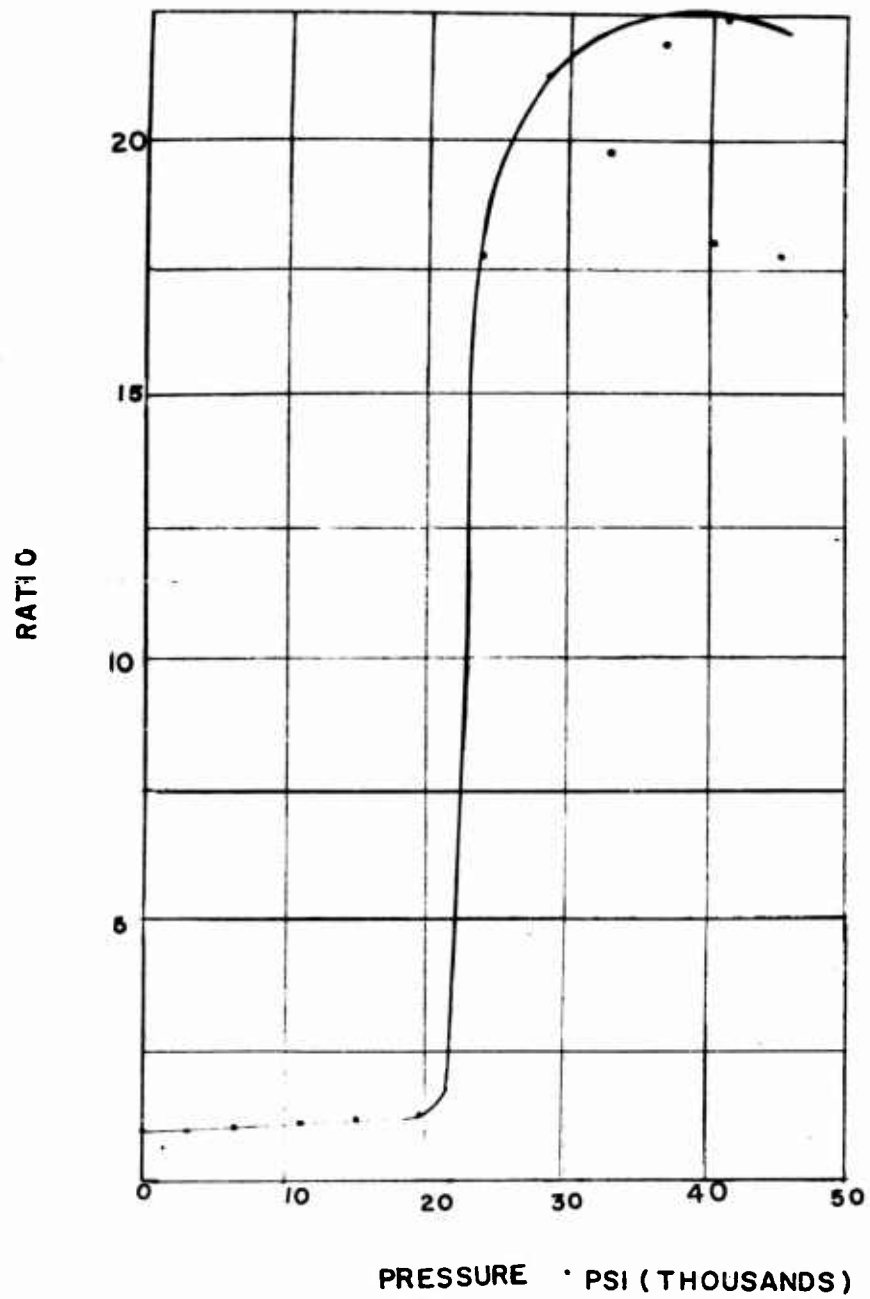


Fig. 13 - Ratio of expected area to actual area for experimental propellant

REFERENCES

1. Kistiakowsky, G.B., Initiation of Detonation in Explosives Third Symposium on Combustion Flame and Explosion Phenomena Williams and Wilkins (1949).
2. Hyndman, J.R. et al, Rohm and Haas Co. Ballistics Section Progress Report #67 October 1957.
3. Mason, C.N. et al, (U.S. Dept. of Interior, Bureau of Mines) Final Summary Report #3734. Investigation of Susceptibility to Detonation of Propellants.
4. Macek, A. (Naval Ordnance Laboratory) NAVCRD 6105, Sensitivity of Explosives VII. Transition from Slow Burning to Detonation: A Model for Shock Formation in a Deflagrating Solid. 3 Feb. 1958.
5. Jones, J.W., Sagers, D.L., and Nolan, E.J., Fracture Mechanics of Solid Propellants. Progress Report No. ELab-A-19, Feb. 16, 1959 to Feb. 15, 1960, Eastern Laboratory, E. I. du Pont de Nemours & Company (confidential).
6. Jones, J.W., Prediction of Catastrophic Rocket Motor Explosion Conditions from Broad Spectrum Mechanical Property Analysis. Preprints of Sixteenth Meeting, JANAF Solid Propellant Group, Vol 5.
7. Pallington, A.O., Weinstein, M., Method of Calculation of Interior Ballistic Properties of Propellants from Closed Bomb Data, Picatinny Arsenal Technical Report #2005 June 1954.
8. Wallace, W.F., New Formulas for Rapid Calculation of Linear Burning Rates of Solid Propellants. Picatinny Arsenal Technical Report #2488, April 1958.

APPENDIX A

## 1. Linear Burning Rate

## A. Theory

The linear burning rate is the rate at which the burning surface of a propellant recedes in a direction normal to the flame front.

If  $dx$  be the distance burning proceeds during anytime interval  $dt$ , then  $dx/dt$  is the linear burning rate.

By assuming that all surfaces of the burning propellant burn at the same rate and by using a known geometry the linear burning rate can be deduced from the mass rate of burning. By the assumption of a suitable equation of state the mass rate of burning can be deduced from the rate of change in pressure surrounding the burning propellant in a closed vessel.

For particles of known shape, such as perforated or solid cylinders the closed bomb fitted with a rapid response pressure gage is suitable experimental apparatus for determining the linear rate of burning of propellants or explosives at any pressure.

The apparatus produces an oscillographic trace of piezo-originated voltages as measures of the rate of change of pressure,  $dp/dt$  and pressure,  $P$ . Sample traces are shown in Figure 7. The rate of change of pressure is calculated from the ordinate voltage  $V_x$ , and the pressure from the abscissa,  $V_y$ , after appropriate calibration and determination of gage constants.

$$P = K_g C_x V_x + K_1 \quad (1)$$

$$dp/dt = \frac{K_g V_y}{R} \quad (2)$$

The maximum pressure (at the end of burning) can be used to measure the combined temperature and gas molecular weight function, thus completing an expression for the equation of state in terms of  $Z$ , the weight fraction burned, and  $p_i$  the pressure due to prepressurizing and igniter, if any, where  $K_g$ ,  $C_x$  and  $K_1$  are equipment constants:

$$P_{\max} = K_g C_x V_{x\max} + K_1 \quad (3)$$

$$P = p_i + Z \frac{\left(1 - \left(\frac{m_1}{m_0}\right) a_1 + a\right) D_0}{1 - \left(b + \frac{m_1}{m_0} a_1 + (a-b) Z\right) D_0} (P_{\max} - p_i) \quad (4)$$

To simplify calculations the term  $(m_1/m_0) a_1$  is considered negligible because of the relatively small quantity involved in  $m_1$ , the mass of igniter and prepressurizing materials.

The geometry for solid cylinders of propellant or explosives burning on all surfaces is stated in terms of fraction burned,  $Z$ , and dimension remaining,  $(d-2x)$  and  $(h-2x)$ , at anytime:

$$Z = 1 - \frac{(d-2x)^2 (h-2x)}{d^2 h} \quad (5)$$

The derivative,  $dp/dZ$ , may be found from equation (4) and the derivative  $dZ/dx$  from equation (5):

$$dp/dZ = f_1(Z) \quad (6)$$

$$dZ/dx = f_2(x) \quad (7)$$

The linear burning rate can be calculated from equations (2), (6) and (7):

$$dx/dt = \frac{dp/dt}{(dp/dZ)(dZ/dx)} \quad (8)$$

#### B. Calculation Method

The equations (4) through (8) have, in principle, been rearranged by Wallace (8) to a form suitable for direct solution. The solution was made in terms of the surface area ( $S_x$ ) at any value of  $x$ . With slight modifications, the equations of Wallace were used to convert the closed bomb data to linear burning rates.

The equations used for this solution for a solid cylinder are listed below. These equations were programmed for solution in an IBM 650 computer.

$$K6 = (d-h)^2 / 1.5 hd^2 \quad (9)$$

$$K5 = 27 hd^2 / 2 (d-h)^3 \quad (10)$$

$$B = (P_{\max} - p_i) (1-aD) / (a-b)D \quad (11)$$

$$C = (1-bD) / (a-b)D \quad (12)$$

$$Z = \frac{(P-p_i) (1-bD)}{(P_{\max} - p_i) (1-aD) + (P-p_i) (a-b)D} \quad (13)$$

$$E = 1 + K5 (1-Z) \quad (14)$$

$$\text{If } E < 1 \\ \phi = \cos^{-1} E \quad (15)$$

$$S_x/V_o = [1 - 2 \cos(60^\circ + 2/3 \phi)] K_6 \quad (16)$$

$$\text{If } E \geq 1 \quad (17)$$

$$S_x/V_o = \left\{ \left[ E + (E^2 - 1)^{1/2} \right]^{1/3} + \left[ E - (E^2 - 1)^{1/2} \right]^{1/3} \right\}^2 - 1 \quad K_6$$

$$dx/dt = \frac{dp/dt}{\frac{B}{C} (1 + \frac{P}{B})^2 \frac{S_x}{V_o}} \quad (18)$$

In these equations certain special cases had to be recognized to allow for discontinuities introduced by algebraic and trigonometric solutions. When diameter exactly equals length, a discontinuity arises in Eq (9) for  $K_6$ . An increment of 0.01 inch is therefore added to one dimension for this special case. If the quantity  $E$  is less than unity a cosine procedure is used (Eq 15); if equal to or greater than unity a cube-root procedure is used (Eq 17). Either procedure leads to  $S_x/V_o$  which is then used in the final equation (Eq 18) with the experimentally observed  $dp/dt$  to calculate the linear burning rate  $dx/dt$ .

## II. Equivalent Surface Areas.

### A. Theory

When linear burning rates are found from closed bomb data from single cylinders of propellant or explosive using the solid cylinder geometry as described above the results compare well with strand burner results below a certain characteristic pressure. At other pressures the burning rate so calculated must be regarded as an "apparent" burning rate because it deviates a great deal from strand burner results.

This suggests that the general configuration may be cylindrical, but the surface may be full of cracks or breaking into small pieces, with the strand burning rate governing the reaction for each burning particle. Combining experimentally determined rate of pressure rise,  $dp/dt$ , and pressure,  $P$ , with strand burning rates,  $dx/dt$ , permits solving for a surface area,  $S_x$ , will reflect the abnormally high mass rate of burning.

Thus  $P$ ,  $dp/dt$ , and  $P_{max}$  are found as before (Eq 1,2,3). The equation of state showing total pressure as function of fraction burned is also applicable (Eq 4). Likewise the fraction burned is related to the burning cylinder dimensions by (Eq 5) for a smooth cylinder. In (Eq 8, and 18), however, the predicted linear burning

rate  $dx/dt = aP^n$  would be used. Then from (Eq 18) the equivalent area  $S_x$  is found representing surface area of cracks and convolutions on the surface of a rough cylinder. The equivalent areas are found to proceed through a maximum before reaching zero during burning.

## AUTHOR INDEX

Note: Pages 1 - 325 appear in Volume 1.

Allison, F.E.	112	Kendrew, E.L.	
Amster, A.	584	Keyes, R.T.	150,
Austing, J.L.	396	Kirkham, J.	
Aziz, A.K.	205		
		Ling, R.C.	
Bean, C.M.	1		
Beauregard, R.	584	Macek, A.	
Bernstein, D.	88	Mason, C.M.	
Boyle, V.M.	520	McKnight, C.E.	
		Moore, D.B.	
Cachia, G.P.	1	Muller, G.M.	
Campbell, A.W.	469,499		
Chaiken, R.F.	305	Napadensky, H.S.	
Clay, R.B.	150		
Cook, M.A.	150,184,357	Orlow, T.	
Davis, W.C.	469,499	Paszek, J.	
Deal, W.E.	386	Placese, D.	
		Porter, S.J.	
Enig, J.W.	534		
Erikson, T.A.	24	Ramsay, J.B.	
Erkman, J.O.	253	Rinehart, J.S.	
Funk, A.G.	184	Sadwin, L.D.	
		Savitt, J.	309,
Gibson, F.C.	436	Seay, G.E.	
		Seely, L.B., Jr.	
Hauver, G.E.	241	Shupe, O.K.	
Hayes, B.	139	Smith, L.C.	
Hess, W.R.	42	Sternberg, H.M.	
Hurwitz, H.	205	Stresau, R.H.	309,
		Sultanoff, M.	
		Summers, C.R.	
Jaffe, I.	584		
James, E., Jr.	327	Taylor, B.C.	
Jameson, R.L.	120	Taylor, J.W.	
Joyner, T.B.	50	Travis, J.R.	

**UNCLASSIFIED**

**UNCLASSIFIED**